MASARYKOVA UNIVERZITA

Lékařská fakulta

MR zobrazení tenzoru difuze centrálního nervového systému

Habilitační práce

MUDr. Miloš Keřkovský, Ph.D.

Brno 2019

MUNI
MED

Obsah

1. Úvod

Zobrazení magnetickou rezonancí (MR) je v současnosti dobře etablovanou zobrazovací metodou, která je standardní součástí diagnostiky nejrůznějších onemocnění centrálního nervového systému (CNS). Tato modalita je oceňována zejména pro excelentní kontrastní rozlišení, neinvazivitu a absenci zátěže pacientů ionizujícím zářením. Možnosti zobrazení pomocí MR jsou velmi široké a heterogenní, neboť tato metoda umožňuje využití velkého množství zobrazovacích sekvencí, z nichž každá nabízí jiné charakteristiky výsledného obrazu vyšetřovaných tkání z hlediska kontrastu a prostorového rozlišení.

Jakkoliv je však metoda MR již od svých počátků inovativní a technicky vyspělá, v některých oblastech zobrazovací diagnostiky při využití konvenčních sekvencí již naráží na limity svých možností. Jednou z těchto oblastí je zobrazení bílé hmoty mozku či míchy, která se při použití konvenčních technik jeví fyziologicky jako poměrně homogenní tkáň bez možnosti diferenciace dalších detailů její vnitřní struktury (1). Bílá hmota mozková je přitom, jak známo, složitá vysoce strukturálně organizovaná tkáň s anatomicky definovatelnými nervovými drahami různého průběhu; zobrazení této struktury za fyziologických i patologických podmínek stále představuje určitou výzvu pro zobrazovací metody.

Jednou z nejnadějnějších metod, která se v posledních letech na tomto poli výrazně prosazuje, je technika zobrazení tenzoru difuze (diffusion tensor imaging, DTI), jejíž technické základy byly popsány v roce 1994 (2). Tato metoda umožňuje in-vivo vizualizaci průběhu nervových drah pomocí pokročilých metod analýzy anizotropie difuzivity (traktografie) (3), v mnoha odborných studiích se též ukázalo, že tato technika skýtá obrovský potenciál pro diagnostiku nejrůznějších onemocnění a poskytuje nový pohled na ultrastrukturální patologické změny zejména v rámci bílé hmoty mozku či míchy (1; 4; 5). Práce na tomto tématu nicméně zdaleka není ukončená; hlavní proudy výzkumu v této oblasti se v současnosti zaobírají využitím DTI v diagnostice jednotlivých onemocnění nervového systému a aplikovatelností této metody v klinické praxi. Poměrně často jsou diskutována i témata reprodukovatelnosti měření, redukce artefaktů či využití různých technik analýzy obrazových dat (6; 7).

Těmto výše uvedeným tématům je věnována i tato habilitační práce, která je koncipována jako soubor komentovaných publikací. U sedmi z těchto prací je autor této práce prvním autorem a u jedné ze tří uvedených spoluautorských publikací je autorem korespondenčním.

2. Seznam původních publikací autora

I. Dostál M, Keřkovský M, Koriťáková E, Němcová E, Stulík J, Staňková M, Bernard V. Analysis of diffusion tensor measurements of the human cervical spinal cord based on semiautomatic segmentation of the white and gray matter. J Magn Reson Imaging 2018;48:1217-1227.

II. Keřkovský M, Stulík J, Obhlídalová I, Praksová P, Bednařík J, Dostál M, Kuhn M, A. Šprláková-Puková A, Mechl M. Moderní techniky MR zobrazení u roztroušené sklerózy. Cesk Slov Neurol N 2017;80:647-657

III. Hüttlova J, Kikinis Z, Kerkovsky M, Bouix S, Vu MA, Makris N, Shenton M, Kasparek T. Abnormalities in myelination of the superior cerebellar peduncle in patients with schizophrenia and deficits in movement sequencing. Cerebellum 2014;13:415-424.

IV. Keřkovský M, Stulík J, Dostál M, Kuhn M, Lošák J, Praksová P, Hulová M, Bednařík J, Šprláková-Puková A, Mechl M. Structural and functional MRI correlates of T2 hyperintensities of brain white matter in young neurologically asymptomatic adults. EurRadiol 2019;29:7027-7036.

V. Keřkovský M, Šprláková-Puková A, Kašpárek T, Fadrus P, Mechl M, Válek V. Diffusion tensor imaging – současné možnosti MR zobrazení bílé hmoty mozku. Cesk Slov Neurol N 2010;73/106:136–142.

VI. Keřkovský M, Šprláková-Puková A, Bednařík J, Smrčka M, Mechl M. Význam MR zobrazení difuze míchy v diferenciální diagnostice míšních lézí. Cesk Slov Neurol N 2013;76/109:477-481.

VII. Keřkovský M, Zitterbartová J, Pour L, Šprláková-Puková A, Mechl M. Diffusion Tensor Imaging in Radiation-Induced Myelopathy. J Neuroimaging 2015;25:836-840.

VIII. Kerkovsky M, Bednarík J, Dušek L, Sprláková-Puková A, Urbánek I, Mechl M, Válek V, Kadanka Z. Magnetic resonance diffusion tensor imaging in patients with cervical spondylotic spinal cord compression: correlations between clinical and electrophysiological findings. Spine (Phila Pa 1976). 2012;37:48-56.

2. Seznam původních publikací autora

IX. Kadaňka Z Jr, Adamová B, Keřkovský M, Kadaňka Z, Dušek L, Jurová B, Vlčkova E, Bednařík J. Predictors of symptomatic myelopathy in degenerative cervical spinal cord compression. Brain Behav 2017;7:e00797.

X. Keřkovský M, Bednařík J, Jurová B, Dušek L, Kadaňka Z, Kadaňka Z Jr, Němec M, Kovaľová I, Šprláková-Puková A, Mechl M. Spinal Cord MR Diffusion Properties in Patients with Degenerative Cervical Cord Compression. J Neuroimaging 2017;27:149-157.

3. Technické aspekty DTI

3.1. Zobrazení difuze

Pod pojmem difuze se rozumí náhodný pohyb molekul vody ve tkáni označovaný jako tzv. Brownův pohyb. Tento jev může za určitých podmínek ovlivnit intenzitu signálu sekvencí spinového i gradientního echa MR zobrazení. Zobrazení difuze umožňuje využití symetrických magnetických gradientů, které ve voxelech se stacionárními protony (nízkou difuzivitou) způsobí rozfázování a opětovné zfázování precese spinů, takže nedojde k žádnému úbytku signálu. Oproti tomu ve voxelech s vysokou mírou difuzivity molekul vody dojde pouze k neúplnému zfázování precese, což ve výsledku vede k poklesu intenzity signálu (8).

V současnosti je většina difuzně vážených sekvencí založena na Stejskal-Tannerově technice (9; 10). Tato využívá umístění dvou časově zcela symetrických pulzů gradientů magnetického pole okolo radiofrekvenčního 180° pulzu spinového echa. Senzitivita sekvence vůči difuzi může být upravena amplitudou a časovým trváním zmiňovaných gradientů. Parametr sekvence definující míru difuzního vážení se označuje jako tzv. b faktor, který je funkcí amplitudy, trvání a prostorové distribuce gradientních pulzů (11). Hodnoty b faktoru se v praxi obvykle pohybují v rozmezí 0-1000 s/mm^2. V praxi se dnes nejčastěji využívá sekvencí typu „single-shot" (SSh), kde je použit pouze jeden excitační (90°) radiofrekvenční pulz a poté je nabrán celý k-prostor technikou echo-planárního zobrazení (EPI) (12). Výhodou tohoto řešení je především vysoká rychlost akvizice dat, nevýhodou může být naopak vysoká citlivost sekvence vůči susceptibilním artefaktům nebo nízký poměr signál/šum (13).

3.2. Anizotropie difuze

Významným jevem v souvislosti se základními principy techniky DTI je tzv. anizotropie difuze. Jedná se o závislost míry difuzivity na směru použitého magnetického gradientu, která je v prostředí vysoce strukturálně organizované tkáně bílé hmoty mozku či míchy dána skutečností, že difuze molekul vody probíhá snadněji podél dlouhé osy nervových svazků než

ve směru příčném. Tuto směrovou závislost můžeme blíže ozřejmit pomocí opakované aplikace gradientu magnetického pole v několika různých směrech (typicky v 6 až 64). Vektory vyjadřující míru difuzivity v jednotlivých směrech jsou potom využity pro matematickou konstrukci 3D elipsoidu, jehož tvar a orientace charakterizuje anizotropii difuze v jednotlivých voxelech (14). Tvar elipsoidu může být popsán pomocí tří hodnot (λ1, λ2 a λ3), které reprezentují velikost tří jeho hlavních os a jsou označovány jako tzv. vlastní vektory (eigen vektory). Z těchto parametrů je možné vypočíst celou řadu skalárních veličin, pomocí kterých je možné kvantifikovat různé aspekty difuzivity. Často používanými parametry jsou frakční anizotropie (FA), která udává relativní míru anizotropie v daném voxelu (0-1), a hodnota střední difuzivity (mean diffusivity, MD), která vyjadřuje celkovou míru difuzivity nezávislé na anizotropii difuze (11). Další pokročilejší možností zpracování DTI dat je tzv. traktografie (fiber-tracking). Tato technika je založena na „stopování" převládajícího směru difuze za předpokladu, že tento odpovídá skutečnému směru průběhu nervových traktů (15). Umožňuje tak virtuální rekonstrukci průběhu jednotlivých nervových drah s možností jejich projekce do základních strukturálních obrazů konvenčních MR sekvencí.

3.3. Metody analýzy dat

V otázce metodiky analýzy obrazových dat DTI obecně existuje celá řada přístupů. Za nejjednodušší lze považovat měření parametrů difuzivity v rámci manuálně definovaných oblastí zájmu (region of interest, ROI) ve zvolených oblastech mozku či míchy. Nevýhodu tohoto postupu mohou představovat nepřesnosti v umístění ROI a následné zkreslení výsledů. S tímto problémem se snaží vypořádat některé automatizované techniky analýzy DTI dat, které jsou již dobře etablovány zejména v oblasti DTI zobrazení mozku. Jednou z často využívaných metod je TBSS (tract-based spatial statistics) založená na platformě FSL (Functional MRI of the Brain Software Library). Tato metoda umožňuje automatizovanou analýzu skalárních parametrů difuzivity bílé hmoty v celém měřeném objemu mozku a je vhodná zejména pro „voxel-based" statistické porovnání různých skupin zkoumaných subjektů (16).

V případě zobrazení míchy existuje relativně méně možností výpočetní analýzy obrazových dat, nezbytnou součástí takových postupů je segmentace obrazů míchy v obrazech MR a registrace s daty DTI. V této oblasti bylo popsáno několik technik použitelných při segmentaci celé míchy nebo separátní segmentaci šedé a bílé hmoty míšní (17). Kromě manuální segmentace zkušeným operátorem, která je často používána jako zlatý standard pro porovnání s pokročilejšími metodami, lze využít kupříkladu intenzitně založených segmentačních metod využívajících prahování intenzity signálu jednotlivých tkání (18) nebo deformačních metod, které jsou založené na postupné deformaci uzavřené křivky s cílem minimalizovat její energii na základě modelu vnějších a vnitřních sil (19). K pokročilejším technikám se řadí klasifikační a atlasové metody, které jsou založeny na prostorové registraci segmentovaného obrazu a standardizované předlohy (20). V poslední době jsou stále častěji využívány pokročilé metody segmentací využívající metod strojového učení a neuronových (21).

V současnosti jsou nicméně stále hledány robustní a reprodukovatelné metodické přístupy zahrnující co nejpřesnější segmentaci šedé a bílé hmoty míchy, registraci s DTI daty a statistické vyhodnocení parametrů difuzivity. Touto problematikou se zabývá metodicky zaměřená publikace **I. (Dostál et al., J Magn Reson Imaging 2018)**, ve které je představen ucelený postup pro analýzu dat DTI zobrazení krční míchy. V této práci je aplikována semiautomatická klasifikační metoda využívající prvků strojového učení (ITK-SNAP) pro segmentaci šedé a bílé hmoty míchy ve strukturálních T2 vážených obrazech s následnou registrací získaných segmentačních masek s daty DTI. Uvedená metoda je zde podrobena důkladné analýze hodnotící její přesnost a reprodukovatelnost včetně dopadu na variabilitu měřených skalárních parametrů DTI a je v těchto aspektech porovnána s výsledky segmentací založených na lépe etablované atlasové metodě Spinal Cord Toolbox (SCT). Shoda jednotlivých segmentačních masek mezi porovnávanými skupinami byla kvantifikována pomocí parametrů Diceho koeficientu a Hausdorffovy vzdálenosti. Získaná data byla podrobena statistické analýze hodnotící vzájemnou míru shody jednotlivých segmentačních technik a intra- i inter-observer variabilitu segmentací provedených pomocí jednotlivých metod.

Jedním z hlavních výsledků této studie je průkaz lepší shody klasifikační metody se zlatým standardem manuální segmentace v porovnání se SCT, naopak nebyly zjištěny významné

rozdíly v měřených hodnotách FA míchy mezi oběma semiautomatickými segmentačními metodami.

Silnou stránkou této studie je zejména kombinace pokročilých metod segmentace MR obrazů míchy s následnou analýzou DTI dat, takže je možné uvedenou metodu na základě získaných výsledků nabídnout jako jeden z možných komplexních metodických přístupů k analýze difuzivity krční míchy. Autor této habilitační práce je korespondenčním autorem uvedené publikace, podílel se velkou měrou na celkové koncepci studie, na akvizici dat i jejich analýzách.

4. Výzkumné a klinické aplikace DTI

Jak bylo zmíněno výše, vysoce organizovaná mikrostruktura normální bílé hmoty CNS je příčinou výrazné anizotropie difuze v této tkáni. Ukazuje se, že různé patologické změny v bílé hmotě často vedou ke snížení anizotropie při patologickém nárůstu difuzivity molekul vody napříč nervovými trakty, což je možné detekovat pomocí DTI; senzitivita této techniky byla v tomto smyslu mnohokráte potvrzena, včetně experimentů na zvířecích modelech (22). Zejména index FA je v současnosti považován za parametr vysoce senzitivní vůči narušení integrity bílé hmoty a je také jedním z nejčastěji sledovaných parametrů ve studiích využívajících DTI zobrazení (4). Někteří autoři též poukazují na skutečnost, že při podrobnější analýze směrové charakteristiky difuzivity je možné odlišit poškození bílé hmoty na podkladě axonální dezintegrace, kdy dochází zejména ke snížení podélné difuzivity (λ1) od demyelinizace, kdy je zvýšena difuzivita příčná (23). Na skalární parametry difuzivity je proto možné nahlížet jako na cenné biomarkery, které mohou přispět je zpřesnění MR diagnostiky u nejrůznějších onemocnění mozku či míchy. Přidanou hodnotou je možnost jejich kvantifikace, což může dále přispět k objektivnějšímu zhodnocení ultrastrukturálních patologických změn v postižené tkáni.

4.1. Zobrazení mozku

Jednou z oblastí, kde je technika DTI v poslední době hojně využívána je výzkum a diagnostika roztroušené sklerózy (RS). Existují důkazy o korelaci parametrů difuzivity s histopatologickými nálezy demyelinizace a axonální dezintegrace (24). Abnormality difuzních parametrů byly zjištěny v rámci demyelinizačních T2 hyperintenzních plak v porovnání s normálně vyhlížející bílou hmotou (NAWM) (25) a patrně nejpozoruhodnější je skutečnost, že změny difuzivity lze prokázat i v rámci samotné NAWM i NAGM (šedá hmota normálního vzhledu) v porovnání se zdravými jedinci (26). DTI lze tak vnímat jako citlivější metodu pro detekci patologických změn u pacientů s RS v porovnání s konvenčními technikami MR zobrazení. Této problematice je mimo jiné věnována přehledová práce **II. (Keřkovský et al., Cesk Slov Neurol N 2017)**, která shrnuje vícero moderních technik zobrazení MR, které jsou využitelné v diagnostice RS. V rámci této práce jsou publikována i vlastní data autora

dokumentující diagnostický význam DTI zobrazení mozku u pacientů s klinicky izolovaným syndromem, u kterých byly nalezeny významné změny parametrů difuzivity (FA a MD) v rozsáhlých oblastech bílé hmoty mozkové v porovnání s kontrolní skupinou pomocí metody TBSS a následné voxel-based statistické analýzy.

Jako příklad další skupiny onemocnění, kde lze DTI využít jako citlivý detektor patologických změn v bílé hmotě mozkové, jsou onemocnění psychiatrická. Tato technika byla aplikována kupříkladu v řadě prací dokumentujících změny difuzivity bílé hmoty mozku u pacientů se schizofrenií, což poskytuje nový náhled na patofyziologii tohoto onemocnění a podporuje teorii patologické konektivity bílé hmoty mozkové jako jeden z významných faktorů vzniku tohoto onemocnění (27; 28). Jedním z výstupů spolupráce autora této habilitační práce s kolegy z oboru psychiatrie je publikace **III. (Hüttlova et al., Cerebellum 2014).** V této práci jsou porovnávány parametry difuzivity v průběhu vybraných rekonstruovaných nervových drah (kortikospinální dráhy a horních mozečkových pedunklů) mezi zdravými kontrolami a podskupinami pacientů se schizofrenií lišícími se klinickým nálezem motorických abnormalit dle skóre NES (Neurological Evaluation Scale). Statistickou analýzou byly nalezeny významné změny difuzivity v průběhu pravostranné kortikospinální dráhy u pacientů bez zjištěné poruchy motoriky. Naopak u pacientů s prokázanou alterací sekvencování pohybů byly zjištěny změny difuzních parametrů v oblasti levého horního mozečkového pedunklu. Tato zjištění mohou přispět k pochopení patogeneze motorických abnormalit u pacientů se schizofrenií. Na této publikaci se autor podílel po stránce akvizice MR dat v rámci širšího projektu zahrnujícího krom DTI i funkční MR zobrazení zaměřené na hodnocení abnormalit motorických funkcí u souboru pacientů se schizofrenií.

Metoda DTI byla v řadě studií použita též ke studiu bílé hmoty mozkové u zdravých subjektů. Příkladem mohou být závěry několika autorů poukazující na změny difuzivity bílé hmoty v korelaci s věkem nebo pohlavím zkoumaných subjektů (29; 30; 31). Do této skupiny studií lze zařadit i recentní publikaci **IV. (Keřkovský et al., EurRadiol 2019)**, ve které jsou hledány koreláty v obrazech DTI a dalších pokročilých modalit MR zobrazení s mírou výskytu náhodně nalezených T2 hyperintenzních ložisek v bílé hmotě mozkové u kohorty mladých neurologicky asymptomatických subjektů. V této práci byl kvantifikován výskyt těchto ložisek za pomocí segmentace se stanovením jejich počtu a objemu. Finální analýza dat zahrnovala jednak porovnání difuzních parametrů měřených v rámci ložisek s průměrnými hodnotami

NAWM, parametry počtu a objemu lézí byly dále korelovány s difuzními parametry měřenými v celé bílé hmotě mozkové za pomocí TBSS analýzy. Na základě výše uvedené ROI analýzy jsme zjistili signifikantně vyšší hodnoty MD v porovnání s difuzivitou měřenou v rámci NAWM, na druhou stranu však nebyla prokázána korelace objemu ani počtu ložisek se skalárními parametry difuzivity bílé hmoty pomocí TBSS. Tato skutečnost proto naznačuje, že ultrastrukturální abnormality jsou u těchto asymptomatických jedinců limitovány pouze na lokalitu samotných T2 hyperintenzních ložisek a nepostihují rozsáhlejší oblasti ostatní bílé hmoty. Z dalších modalit zkoumaných v této publikaci byly dále nalezeny signifikantní změny funkční konektivity mezi několika oblastmi mozku v korelaci s narůstajícím objemem a počtem ložisek. V závěru práce je diskutován význam těchto výsledků pro budoucí studie zahrnující hodnocení kohort asymptomatických subjektů, u nichž výskyt T2 hyperintenzit v bílé hmotě mozku může mít vliv na zkoumané parametry pokročilých technik MR zobrazení.

Jednou z klinicky orientovaných aplikací DTI je využití této techniky pro předoperační zobrazení traktů bílé hmoty mozku u pacientů s mozkovými tumory před plánovanou resekcí. Využívána je zejména deterministická traktografie, kterou je možné použít pro rekonstrukci různých drah v závislosti na lokalizaci tumoru. Tato technika umožňuje zobrazení prostorového vztahu určité dráhy k patologické lézi, případně odlišení jejího odtlačení tumorem od přímé infiltrace a destrukce (32). Spolehlivost této techniky byla potvrzena v řadě prací, které prokazují dobrou korelaci peroperační subkortikální stimulace motorických i jiných drah bílé hmoty s průběhem drah rekonstruovaných pomocí DTI (33; 34). Obrazy rekonstruovaných drah je možné integrovat do systému stereotaktické neuronavigace, což umožňuje neurochirurgovi získat lepší představu, v jakém prostorovém vztahu se příslušná dráha nalézá v operačním poli ve vztahu k tumoru (35). Poměrně častým předmětem zájmu předoperačního DTI vyšetření je kortikospinální dráha, která je jedním z nejdůležitějších traktů z hlediska možného peroperačního poškození a následného vzniku funkčního neurologického deficitu. Při zpracování může být výhodou integrace dat funkční MR mapující motorický kortex pro správné a specifické umístění oblastí zájmu použitých pro rekonstrukci dráhy (36). Někteří autoři poukazují na výhody současného využití traktografie kortikospinální dráhy se zmiňovanou technikou peroperační elektrické stimulace za účelem minimalizace funkčního deficitu při operacích tumorů v motorických elokventních oblastech

(37). Ukázka výsledků předpoperační traktografie je zahrnuta v publikaci **V. (Keřkovský et al., Cesk Slov Neurol N 2010)**. V této přehledové práci jsou dále shrnuty technické aspekty DTI a různé možnosti klinického či výzkumného využití této metody pro zobrazení mozku s prezentací vlastních zkušeností autora s touto technikou.

4.2. Zobrazení krční míchy

Lze říci, že v oblasti páteře a míchy je realizace DTI vyšetření stále určitou výzvou, což mimo jiné dokumentuje fakt, že počet studií zabývajících se tímto tématem je výrazně menší v porovnání se zobrazením difuze mozku. Důvod je možno spatřovat patrně ve větším riziku zatížení obrazů artefakty podmíněných nehomogenitami magnetického pole v oblasti páteře, obecně horším poměrem signál/šum a zároveň potřebou vysokého rozlišení pro podrobnější zobrazení relativně malého objemu míchy. Méně časté je též rozšíření vhodných sekvencí, které navíc obvykle vyžadují velkou míru optimalizace (38).

Přesto lze konstatovat, že DTI zobrazení míchy je prakticky proveditelné a je využitelné mimo jiné pro bližší charakteristiku nejrůznějších míšních ložiskových lézí, kde je konvenční MR diagnostika obecně obtížná vzhledem k často nespecifickým nálezům. DTI vyšetření v této oblasti může přispět jak kvantifikací skalárních parametrů difuzivity, tak rekonstrukcí míšních drah pomocí traktografie (39). Za klinicky významnou lze považovat zejména detekci akutní míšní ischémie pomocí vizualizace restrikce difuzivity v rámci ischemického míšního ložiska (38). Jiní autoři poukazují na potenciál DTI v otázce bližší charakteristiky míšních tumorů či vlivu expanzivní léze na průběh nervových traktů míchy (40; 41). Obdobně jako v případě analýzy difuzivity mozkové tkáně i v případě zobrazení míchy platí, že pomocí kvantifikace skalárních parametrů anizotropní difuze lze s vysokou citlivostí detekovat ultrastrukturální změny míšní tkáně u nejrůznějších neurologických onemocnění jako je idiopatická transverzální myelitida (42), amyotrofická laterální skleróza (43) nebo roztroušená skleróza (44).

Zkušenosti autora této práce s využitím techniky DTI pro MR diagnostiku různých míšních lézí tumorózní i netumorózní etiologie jsou shrnuty v článku **VI. (Keřkovský et al. Cesk Slov Neurol N 2013).** V této práci je retrospektivně analyzován soubor 11 pacientů s nálezem

ložiskové míšní léze různé etiologie, u nichž bylo provedeno DWI nebo DTI zobrazení míchy. Hodnocení zahrnovalo kvantifikaci difuzních parametrů a v případě DTI i rekonstrukce míšních drah pomocí traktografie, diskutován je zde význam těchto nálezů pro odlišení jednotlivých míšních patologií. V této práci je poukázáno mimo jiné na nálezy restrikce difuze v rámci ložisek míšní ischémie a roztlačení nervových drah míchy u pacientů s míšním ependymomem. V této souvislosti je třeba konstatovat, že nálezy patologických změn míchy tumorózní i netumorózní povahy jsou při konvenčním MR zobrazení mnohdy nespecifické, takže se při hodnocení často nevyhneme neurčitým závěrům, které v daném časovém okamžiku neumožňují zahájení specifické léčby (45). Přídatné informace, které poskytují nové techniky MR zobrazení včetně DTI jsou proto z klinického pohledu velmi cenné.

Nález DTI zobrazení u pacienta s radiační myelopatií byl publikován podrobněji jako kazuistické sdělení **VII. (Keřkovský et al., J Neuroimaging 2015)**. V této práci je popsáno zejména ve své době unikátní in-vivo pozorování ischemických změn s restrikcí difuzivity v postiženém segmentu míchy v korelaci s patofyziologickým konceptem vaskulárního podílu na nekrotizujících patologických změnách míšní tkáně u pacientů s radiační myelopatií (46).

Zbývající tři publikace jsou věnovány problematice využití DTI u pacientů s degenerativní cervikální myelopatií (DCM). Tato diagnóza představuje určitý problém pro konvenční MR diagnostiku s ohledem na skutečnost, že individuální tolerance míchy vůči kompresi je poměrně variabilní (47), a z toho vyplývající častou diskrepanci mezi mírou míšní komprese a klinickou manifestací myelopatie (48). Tuto skutečnost dokládá též relativně častý výskyt náhodných nálezů degenerativní míšní komprese u asymptomatických jedinců (49).

Potenciál DTI lze v této oblasti spatřovat v detekci změn difuzivity vzniklých v důsledku strukturálních abnormalit navozených míšní kompresí, které by případně umožnily detekovat incipientní změny v rámci kompresivní myelopatie citlivěji než konvenční techniky MR zobrazení a korelovaly lépe s klinickým obrazem. Výsledky jedné z prvních studií zabývajících se touto problematikou byly publikovány v práci **VIII. (Kerkovský et al. Spine 2012).** V této prospektivní studii zahrnující 52 pacientů s míšní kompresí a 11 zdravých kontrol byly hodnoceny parametry difuzivity krční míchy v místě maximální komprese a v referenční etáži bez komprese (C2/3), zaznamenány byly též morfologické parametry kvantifikující míru degenerativní spinální stenózy. Statistickým porovnáním skupiny všech pacientů s kontrolní

skupinou byl prokázán signifikantní pokles hodnoty FA míchy v místě míšní komprese u pacientů v porovnání s referenčním měřením u kontrolní skupiny. Tyto změny byly prokázány jak u podskupiny symptomatických pacientů, tak i u pacientů bez známek klinicky manifestní myelopatie, nicméně při přímém porovnání těchto podskupin byl pokles FA u symptomatických pacientů signifikantně výraznější v porovnání s asymptomatickou skupinou. Statisticky významný byl též nárůst hodnot aparentního difuzního koeficientu (ADC) u symptomatických pacientů. Naproti tomu morfologické parametry (průměr páteřního kanálu a plocha míchy) nebyly schopny spolehlivě odlišit symptomatické a asymptomatické pacienty, DTI parametry vykazovaly též vyšší prediktivní hodnotu při následné ROC analýze v porovnání s nálezem abnormalit zjištěných při elektrofyziologickém vyšetření. Z těchto dat vyplývá, že kvantifikace DTI parametrů koreluje s klinickým obrazem myelopatie lépe než nálezy konvenčního MR zobrazení i elektrofyziologického vyšetření. K obdobným závěrům došli další autoři v následujících publikacích (50; 51), v poslední době je poukazováno též na možný potenciál DTI v otázce predikce pooperačního klinického vývoje u pacientů s DCM (52). Aplikace této metody by tak mohla pomoci v přesnější identifikaci pacientů, kteří by mohli profitovat z indikace operační dekomprese páteřního kanálu.

Horkým tématem v oblasti DCM je též otázka predikce rozvoje symptomatické myelopatie u pacientů s asymptomatickou míšní kompresí. Touto problematikou se zabývá publikace **IX. (Kadaňka Z Jr et al., Brain Behav 2017)**, kde figuruje autor této habilitační práce coby spoluautor zajišťující akvizici MR dat, měření morfologických parametrů i analýzu dat DTI. Tato prospektivní observační studie hodnotí kohortu 112 pacientů, u kterých je korelována řada klinických i MR parametrů s rozvojem klinicky symptomatické cervikální myelopatie ve sledovaném období minimálně dvou let. Rozvoj myelopatie byl významně asociován s několika klinickými parametry (např. radikulopatie), s elektrofyziologickými nálezy a s morfologickými parametry měřenými na konvenčních MR obrazech jako je předozadní průměr páteřního kanálu nebo plocha míchy, nicméně prediktivní hodnota DTI prokázána nebyla.

V poslední přiložené publikaci **X. (Keřkovský M et al. J Neuroimaging 2017)** je poukázáno na multifaktoriální povahu změn difuzivity u pacientů s DCM. V této práci jsou zkoumány DTI nálezy u skupiny 130 pacientů s degenerativní kompresí krční míchy a 71 zdravých kontrol.

Hlavním cílem práce bylo zjistit, do jaké míry hodnoty FA a ADC krční míchy ovlivňují krom její komprese další faktory, jako je pohlaví a věk pacientů nebo etáž krční páteře, ve které jsou uvedené parametry měřeny. Ve skupině pacientů s míšní kompresí byly zjištěny signifikantní korelace obou difuzních parametrů s klinickou manifestací myelopatie a také s měřenými morfologickými parametry kvantifikujícími míru spinální stenózy a míšní komprese, což je v souladu s našimi dřívějšími závěry. Dále však byla zjištěna i statisticky významná závislost obou měřených parametrů na etáži ve skupině zdravých kontrol, významná korelace hodnot FA s věkem ve skupině pacientů s míšní kompresí a vliv pohlaví subjektů na ADC hodnoty u pacientů i kontrolní skupiny. Tyto závěry mohou být významné z hlediska interpretace nálezů DTI u jednotlivých pacientů s DCM a pro stanovení normativních hodnot.

Na základě našeho zkoumání využití DTI u pacientů s DCM lze říci, že DTI je metoda schopná velmi citlivé detekce ultrastrukturálních změn krční míchy spojených s projevy klinicky symptomatické myelopatie. Tato skutečnost může mít význam například v klinicky nejasných případech, kdy je otázkou míra významnosti přítomné míšní komprese. Při interpretaci absolutních měřených hodnot skalárních parametrů difuze je však třeba zohlednit další faktory, jako je věk a pohlaví subjektů nebo etáž, ve které jsou změny difuzivity míchy zkoumány; v tomto ohledu bude třeba dalších studií za účelem získání komplexnějších normativních dat. Prediktivní hodnota DTI v otázce budoucího rozvoje myelopatie prozatím dle našich zkušeností není dostatečně robustní, určitý potenciál však v tomto ohledu mohou skýtat novější slibné techniky akvizice a analýzy obrazových dat založené na principech difuzního MR zobrazení jako je např. NODDI (neurite orientation dispersion and density imaging) (53) nebo DKI (diffusion kurtosis imaging) (54) .

5. Závěr

V této habilitační práci jsou shrnuty výzkumné zkušenosti autora s jednou z pokročilých technik MR, kterou je DTI zobrazení aplikované v oblasti CNS. V publikacích je dokumentován ve shodě se světovou odbornou literaturou velký potenciál této metody, která je u řady onemocnění citlivější v otázce detekce ultrastrukturálních patologických změn tkání mozku či míchy než konvenční techniky MR zobrazení. Tato metoda proto představuje nejenom cenný výzkumný nástroj, který může přispět k detailnějšímu pochopení patofyziologie řady onemocnění, nýbrž i významnou diagnostickou modalitu, která může nabídnout kvantitativní biomarkery v podobě skalárních parametrů difuzivity využitelné pro primární diagnostiku nebo predikci klinického vývoje u jednotlivých pacientů. K dosažení tohoto cíle je třeba rozsáhlého výzkumného úsilí ve smyslu podrobného a reprodukovatelného zhodnocení diagnostické výtěžnosti této metody u jednotlivých onemocnění, k čemuž se snaží přispět i autor touto prací.

6. Seznam použité literatury

1. Dong Q, Welsh RC, Chenevert TL, Carlos RC, Maly-Sundgren P, Gomez-Hassan DM et al. Clinical applications of diffusion tensor imaging. J Magn Reson Imaging 2004;19:6–18.

2. Basser PJ, Mattiello J, LeBihan D. MR diffusion tensor spectroscopy and imaging. . Biophys J 1994;66:259-267.

3. Essayed WI, Zhang F, Unadkat P, Cosgrove GR, Golby AJ, O'Donnell LJ. White matter tractography for neurosurgical planning: A topography-based review of the current state of the art. Neuroimage Clin 2017;15:659-672.

4. Assaf Y, Pasternak O. Diffusion tensor imaging (DTI)-based white matter mapping in brain research: a review. J Mol Neurosci 2008;34:51-56.

5. Thurnher MM, Law M. Diffusion-weighted imaging, diffusion-tensor imaging, and fiber tractography of the spinal cord. Magn Reson Imaging Clin N Am 2009;17:225-244.

6. Jovicich J, Marizzoni M, Bosch B, Bartrés-Faz D, Arnold J, Benninghoff J et al. Multisite longitudinal reliability of tract-based spatial statistics in diffusion tensor imaging of healthy elderly subjects. Neuroimage 2014;101:390-403.

7. Higaki T, Nakamura Y, Tatsugami F, Kaichi Y, Akagi M, Akiyama Y et al. Introduction to the Technical Aspects of Computed Diffusion-weighted Imaging for Radiologists. Radiographics 2018;38:1131-1144.

8. D., Le Bihan. Molecular diffusion, tissue microdynamics and microstructure. NMR Biomed 1995;8:375-386.

9. Le Bihan D, Breton E, Lallemand D, Grenier P, Cabanis E, Laval-Jeantet M. MR imaging of intravoxel incoherent motions: application to diffusion and perfusion in neurologic disorders. Radiology 1986;161:401-407.

10. Stejskal EO, Tanner JE. Spin diffusion measurements: spin echoes in the presence of a time-dependent field gradient. J Chem Phys 1965;42:288-292.

11. Mukherjee P, Berman JI, Chung SW, Hess CP, Henry RG. Diffusion tensor MR imaging and fiber tractography: theoretic underpinnings. AJNR Am J Neuroradiol 2008;29:632-641.

12. Turner R, Le Bihan D, Maier J, Vavrek R, Hedges LK, Pekar J. Echo-planar imaging of intravoxel incoherent motion. Radiology 1990;177:407-414.

13. DG., Mitchell. MRI Principles. Saunders, Philadelphia 1999:201-202.

14. Basser PJ, Pajevic S, Pierpaoli C, Duda J, Aldroubi A. In vivo fiber tractography using DT-MRI data. Magn Reson Med 2000;44:625-632.

15. Conturo TE, Lori NF, Cull TS, Akbudak E, Snyder AZ, Shimony JS et al. Tracking neuronal fiber pathways in the living human brain. Proc Natl Acad Sci U S A 1999;96:10422-10427.

16. Smith SM, Jenkinson M, Johansen-Berg H, Rueckert D, Nichols TE, Mackay CE et al. Tract-based spatial statistics: voxelwise analysis of multi-subject diffusion data. Neuroimage 2006;31:1487-505.

17. De Leener B, Taso M, Cohen-Adad J, Callot V. Segmentation of the human spinal cord. MAGMA 2016;29:125-153.

18. J., Rogowska. Chapter 5 - Overview and Fundamentals of Medical Image Segmentation. [autor knihy] ed. Handbook of Medical Image Processing and Analysis (Second Edition). Burlington: Academic Press In: Bankman IN a 2009:73-90.

19. Kass M, Witkin A, Terzopoulos D. Snakes: Active contour models. Int J Comput Vis 1988;1:321-331.

20. Wachinger C, Golland P. Atlas-Based Under-Segmentation. Med Image Comput Comput Assist Interv 2014;17:315-322.

21. Gros C, De Leener B, Badji A, Maranzano J, Eden D, Dupont SM et al. Automatic segmentation of the spinal cord and intramedullary multiple sclerosis lesions with convolutional neural networks. Neuroimage 2019;184:901-915.

22. Harsan LA, Poulet P, Guignard B, Steibel J, Parizel N, de Sousa PL et al. Brain dysmyelination and recovery assessment by noninvasive in vivo diffusion tensor magnetic resonance imaging. J Neurosci Res 2006;83:392-402.

23. Song SK, Sun SW, Ju WK, Lin SJ, Cross AH, Neufeld AH. Diffusion tensor imaging detects and differentiates axon and myelin degeneration in mouse optic nerve after retinal ischemia. Neuroimage 2003;20:1714-1722.

24. Mottershead JP, Schmierer K, Clemence M, Thornton JS, Scaravilli F, Barker GJ et al. High field MRI correlates of myelin content and axonal density in multiple sclerosis--a post-mortem study of the spinal cord. J Neurol 2003;250:1293-1301.

25. Filippi M, Iannucci G, Cercignani M, Assunta Rocca M, Pratesi A, Comi G. A quantitative study of water diffusion in multiple sclerosis lesions and normal-appearing white matter using echo-planar imaging. Arch Neurol 2000;57:1017-1021.

26. Yu CS, Lin FC, Liu Y, Duan Y, Lei H, Li KC. Histogram analysis of diffusion measures in clinically isolated syndromes and relapsing-remitting multiple sclerosis. Eur J Radiol 2008;68:328-334.

27. Arat HE, Chouinard VA, Cohen BM, Lewandowski KE, Öngür D. Diffusion tensor imaging in first degree relatives of schizophrenia and bipolar disorder patients. Schizophr Res 2015;161:329-339.

28. Kubicki M, McCarley R, Westin CF, Park HJ, Maier S, Kikinis R et al. A review of diffusion tensor imaging studies in schizophrenia. J Psychiatr Res 2007;41:15-30.

29. Gunning-Dixon FM, Brickman AM, Cheng JC, Alexopoulos GS. Aging of cerebral white matter: a review of MRI findings. Int J Geriatr Psychiatry 2009;24:109–117.

30. Sullivan EV, Rohlfing T, Pfefferbaum A. Quantitative fiber tracking of lateral and interhemispheric white matter systems in normal aging: relations to timed performance. Neurobiol Aging 2010;31:464-481.

31. Takao H, Hayashi N, Ohtomo K. Sex dimorphism in the white matter: fractional anisotropy and brain size. J Magn Reson Imaging 2014;39:917-923.

32. Wei CW1, Guo G, Mikulis DJ. Tumor effects on cerebral white matter as characterized by diffusion tensor tractography. Can J Neurol Sci 2007;34:62-68.

33. Bello L, Gambini A, Castellano A, Carrabba G, Acerbi F, Fava E et al. Motor and language DTI Fiber Tracking combined with intraoperative subcortical mapping for surgical removal of gliomas. Neuroimage 2008;39:369-382.

34. Berman JI, Berger MS, Chung SW, Nagarajan SS, Henry RG. Accuracy of diffusion tensor magnetic resonance imaging tractography assessed using intraoperative subcortical stimulation mapping and magnetic source imaging. J Neurosurg 2007;107:488-494.

35. Neumann E, Svoboda T, Fadrus P, Keřkovský M, Šprláková-Puková A. Využití traktografie začleněné do neuronavigace při operacích intraaxiálních tumorů mozku uložených v těsné blízkosti kortikospinální dráhy. Cesk Slov Neurol N 2011;74/107: 675–680.

36. Smits M, Vernooij MW, Wielopolski PA, Vincent AJ, Houston GC, van der Lugt A. Incorporating functional MR imaging into diffusion tensor tractography in the preoperative assessment of the corticospinal tract in patients with brain tumors. AJNR Am J Neuroradiol 2007;28:1354-1361.

37. Mikuni N, Okada T, Enatsu R, Miki Y, Hanakawa T, Urayama S et al. Clinical impact of integrated functional neuronavigation and subcortical electrical stimulation to preserve motor function during resection of brain tumors. J Neurosurg 2007;106:593-598.

38. Thurnher MM, Bammer R. Diffusion-weighted MR imaging (DWI) in spinal cord ischemia. Neuroradiology 2006;48:795-801.

39. Vargas MI, Delavelle J, Jlassi H, Rilliet B, Viallon M, Becker CD et al. Clinical applications of diffusion tensor tractography of the spinal cord. Neuroradiology 2008;50:25-29.

40. Ducreux D, Fillard P, Facon D, Ozanne A, Lepeintre JF, Renoux J et al. Diffusion tensor magnetic resonance imaging and fiber tracking in spinal cord lesions: current and future indications. Neuroimaging Clin N Am 2007;17:137-147.

41. Ducreux D, Lepeintre JF, Fillard P, Loureiro C, Tadié M, Lasjaunias P. MR diffusion tensor imaging and fiber tracking in 5 spinal cord astrocytomas. AJNR Am J Neuroradiol 2006;27:214-216.

42. Lee JW, Park KS, Kim JH, Choi JY, Hong SH, Park SH et al. Diffusion tensor imaging in idiopathic acute transverse myelitis. AJR Am J Roentgenol 2008;191:52-57.

43. Budrewicz S, Szewczyk P, Bladowska J, Podemski R, Koziorowska-Gawron E, Ejma M et al. The possible meaning of fractional anisotropy measurement of the cervical spinal cord in correct diagnosis of amyotrophic lateral sclerosis. Neurol Sci 2016;37:417-421.

44. Hesseltine SM, Law M, Babb J, Rad M, Lopez S, Ge Y et al. Diffusion tensor imaging in multiple sclerosis: assessment of regional differences in the axial plane within normal-appearing cervical spinal cord. AJNR Am J Neuroradiol 2006;27:1189-1193.

45. Smrčka M, Šprláková A, Smrčka V, Keřkovský M. Problematika indikace operační léčby u intramedulárních lézí. Cesk Slov Neurol N 2010; 73/106:393–397.

46. Okada S, Okeda R. Pathology of radiation myelopathy. Neuropathology 2001;21:247-265.

47. al-Mefty O, Harkey HL, Marawi I, Haines DE, Peeler DF, Wilner HI et al. Experimental chronic compressive cervical myelopathy. J Neurosurg 1993;79:550-61.

48. Kadanka Z, Kerkovsky M, Bednarik J, Jarkovsky J. Cross-sectional transverse area and hyperintensities on magnetic resonance imaging in relation to the clinical picture in cervical spondylotic myelopathy. Spine (Phila Pa 1976) 2007;32:2573-2577.

49. Kovalova I, Kerkovsky M, Kadanka Z, Kadanka Z Jr, Nemec M, Jurova B et al. Prevalence and Imaging Characteristics of Nonmyelopathic and Myelopathic Spondylotic Cervical Cord Compression. Spine (Phila Pa 1976) 2016;41:1908-1916.

50. Rajasekaran S, Yerramshetty JS, Chittode VS, Kanna RM, Balamurali G, Shetty AP. The assessment of neuronal status in normal and cervical spondylotic myelopathy using diffusion tensor imaging. Spine (Phila Pa 1976) 2014;39:1183-1189.

51. Yoo WK, Kim TH, Hai DM, Sundaram S, Yang YM, Park MS et al. Correlation of magnetic resonance diffusion tensor imaging and clinical findings of cervical myelopathy. Spine J 2013;13:867-876.

52. Rindler RS, Chokshi FH, Malcolm JG, Eshraghi SR, Mossa-Basha M, Chu JK et al. Spinal Diffusion Tensor Imaging in Evaluation of Preoperative and Postoperative Severity of Cervical Spondylotic Myelopathy: Systematic Review of Literature. World Neurosurg 2017;99:150-158.

53. Ma X, Han X, Jiang W, Wang J, Zhang Z, Li G, Zhang J, Cheng X, Chen H, Guo H, Tian W. A Follow-up Study of Postoperative DCM Patients Using Diffusion MRI with DTI and NODDI. Spine 2018;43:E898-E904.

54. Li D, Wang X. Application value of diffusional kurtosis imaging (DKI) in evaluating microstructural changes in the spinal cord of patients with early cervical spondylotic myelopathy. Clin Neurol Neurosurg 2017;156:71-76.

7. Abstract

MR diffusion tensor imaging of the central nervous system

Diffusion tensor imaging (DTI) is a relatively novel MRI technique which has recently demonstrated a great potential for the imaging of central nervous system (CNS). This method can detect subtle ultrastructural changes within brain and spinal cord tissues using the measurements of various diffusion scalar parameters. However, a lot of research effort is to be made to introduce DTI as a routine clinically applicable tool as it is necessary to develop well-reproducible methods of data acquisition and analysis and objectively evaluate the diagnostic power of this method in various clinical settings.

The author of this work summarizes his experience with the research applications of DTI in neuroimaging as a collection of ten research papers published within past nine years. Most of the presented studies focus on DTI of the spinal cord emphasizing the issue of degenerative cervical spinal cord compression. DTI applied in this field proved as a promising diagnostic tool closely correlating with the clinical manifestation of myelopathy. Other cited studies deal with different topics comprising neuroimaging in schizophrenia or investigation of the structural and functional correlates of asymptomatic brain white matter hyperintensities in healthy subjects. One methodically oriented study focuses on the advanced techniques of the cervical cord DTI data analysis, a few of the papers review technical aspects and state-of-the-art clinical applications of DTI.

This work presents DTI as a valuable modern diagnostic tool, which provides clinically relevant results in various areas in compliance with up-to-date literature data, and further contributes to the current state of knowledge.

8. Originály původních publikací autora

Analysis of Diffusion Tensor Measurements of the Human Cervical Spinal Cord Based on Semiautomatic Segmentation of the White and Gray Matter

Marek Dostál, MS,[1,2] Miloš Keřkovský, PhD,[2]* Eva Koriťáková, PhD,[3]

Eva Němcová, MD,[2] Jakub Stulík, MD,[2] Monika Staňková, MD,[2] and

Vladan Bernard, PhD[1]

Background: Segmentation of the gray and white matter (GM, WM) of the human spinal cord in MRI images as well as the analysis of spinal cord diffusivity are challenging. When appropriately segmented, diffusion tensor imaging (DTI) of the spinal cord might be beneficial in the diagnosis and prognosis of several diseases.

Purpose: To evaluate the applicability of a semiautomatic algorithm provided by ITK-SNAP in classification mode (CLASS) for segmenting cervical spinal cord GM, WM in MRI images and analyzing DTI parameters.

Study Type: Prospective.

Subjects: Twenty healthy volunteers.

Sequences: 1.5T, turbo spin echo, fast field echo, single-shot echo planar imaging.

Assessment: Three raters segmented the tissues by manual, CLASS, and atlas-based methods (Spinal Cord Toolbox, SCT) on T_2-weighted and DTI images. Masks were quantified by similarity and distance metrics, then analyzed for repeatability and mutual comparability. Masks created over T_2 images were registered into diffusion space and fractional anisotropy (FA) values were statistically evaluated for dependency on method, rater, or tissue.

Statistical Tests: t-test, analysis of variance (ANOVA), coefficient of variation, Dice coefficient, Hausdorff distance.

Results: CLASS segmentation reached better agreement with manual segmentation than did SCT ($P < 0.001$). Intra- and interobserver repeatability of SCT was better for GM and WM (both $P < 0.001$) but comparable with CLASS in entire spinal cord segmentation ($P = 0.17$ and $P = 0.07$, respectively). While FA values of whole spinal cord were not influenced by choice of segmentation method, both semiautomatic methods yielded lower FA values ($P < 0.005$) for GM than did the manual technique (mean differences 0.02 and 0.04 for SCT and CLASS, respectively). Repeatability of FA values for all methods was sufficient, with mostly less than 2% variance.

Data Conclusion: The presented semiautomatic method in combination with the proposed approach to data registration and analyses of spinal cord diffusivity can potentially be used as an alternative to atlas-based segmentation.

Level of Evidence: 1

Technical Efficacy: Stage 2

Using such conventional magnetic resonance imaging (MRI) techniques as T_1- and T_2-weighted images, radiologists are able to discern gray matter (GM), white matter (WM), and cerebrospinal fluid (CSF). These conventional methods are insufficient, however, for imaging WM's internal structure.[1] WM is an organized fibrous structure that results in water diffusion becoming anisotropic and with preferred diffusion along the direction of the fibers. One

TABLE 1. Imaging Protocol

Type	Orientation	TR [msec]	TE [msec]	FOV [mm]	Matrix	Slice thickness [mm]	Other information
T_1-w	Sagittal	400	7.8	255×255×33	528×528	3.3	TSE, Avg = 4
T_2-w	Sagittal	3,500	120	255×255×33	528×528	3.3	TSE, Avg = 8
T_2-w[a]	Axial	334	9.21	170×170×56	432×432	4	FFE, Avg = 4
DTI[a]	Axial	3,200	92.3	170×170×56	192×192	4	SS EPI, 1 b = 0, 15 dir (b = 800s/mm^2), Avg = 6

T1-weighted (T1-w), T2-weighted (T2-w), diffusion tensor imaging (DTI), repetition time (TR), echo time (TE), field of view (FOV), turbo spin echo (TSE), fast field echo (FFE), single shot echo planar imaging (SS EPI), average (Avg).
[a]Performed in two separate continuing acquisitions from C1 to C3/C4 and from C3/C4 to C7 with emphasis on maximal perpendicularity to the spinal cord and while being attentive to minimizing gap or mutual overlap of these FOVs. T2-w and DTI had the same center of FOV (Fig. 1).

method currently used for assessing the quality of WM's internal structure is diffusion tensor imaging (DTI). In pathological states, WM fibers are degraded, thereby disturbing their structural integrity and resulting in more isotropic water diffusion (decrease in anisotropy). DTI is used, for example, in studies of brain tumors, multiple sclerosis (MS), epilepsy, ischemic stroke, as well as tumors and other lesions of the spinal cord.[2]

A necessary and frequently crucial step in analyzing DTI images of the central nervous system is segmentation of WM, GM, and CSF. There exist many methods for segmenting brain images,[3] but there are far fewer methods for spinal cord segmentation.[4] Most of these methods segment the entire spinal cord (ESC) and CSF at various levels of automation (semiautomatic or fully automatic) and from various image modalities (T$_1$, T$_2$, DTI, and others).[5–11] Only a few methods are able to segment not just the ESC but also WM and GM.[7,9,12–19]

The main objective of this study was to evaluate the possibilities for using a semiautomatic segmentation method (CLASS) based on a semisupervised machine-learning technique implemented in ITK-SNAP[20–24] for segmentation of MRI data of the cervical spinal cord and to utilize this technique for analyzing diffusion parameters of different spinal cord tissues.

Materials and Methods

The study group consisted of 20 volunteers (16 women and 4 men) aged 23 to 40 years (mean age of 28.05 and standard deviation of 4.6 years) in whom no pathological spinal cord changes were found by an experienced neuroradiologist (M.K.). All volunteers signed informed consent agreements to participate in the study, which was approved by the University Hospital's Ethics Committee.

MRI data were acquired using a 1.5T MR (Philips Achieva, Best, Netherlands) with a 16-channel head and cervical coil. The scanning protocol is shown in Table 1. T$_2$-weighted fast field echo and DTI sequences had the same geometry covering in two parts

spinal cord segments C1–C3/C4 and C3/C4–C7, while taking into consideration the overlap of areas around the C3/C4 disc and the best perpendicularity to the spinal cord of both parts (Fig. 1).

The first step in data analysis was to join upper and lower T$_2$ and DTI images into the same space orientation. Coordinates of the spinal canal were manually set on the two images (upper and lower), rigid registration was performed, and one image of the entire uninterrupted cervical spine was created. Based on sagittal images, only axial slices ranging from the level of the posterior arch of C1 to the cranial endplate of the C7 vertebral body were used for all other steps. Functional MRI of the Brain Software Library (FSL) was used for processing all images,[25] ITK-SNAP v. 3.4 for manual and CLASS segmentation[20,23,24] (http://www.
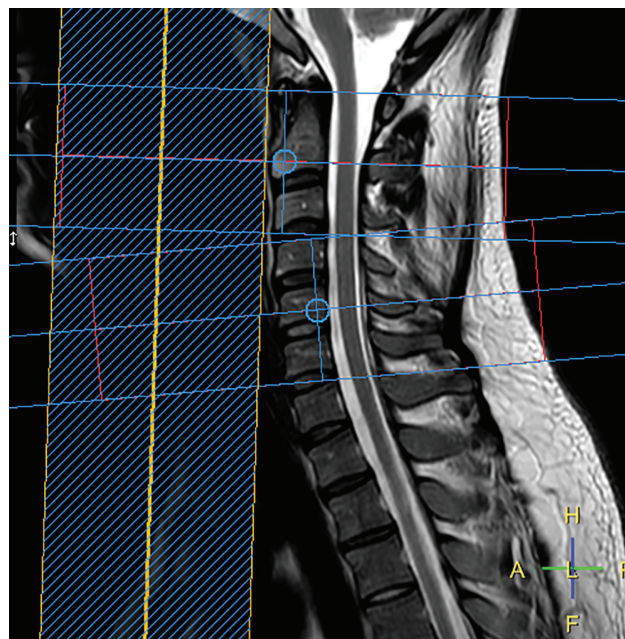
FIGURE 1: Example of T$_2$-weighted fast field echo and DTI sequences planning on the T$_2$-weighted image in sagittal plane. Axial T$_2$ and DTI sequences had the same geometry covering in two parts spinal cord segments C1–C3/C4 and C3/C4–C7, while taking into consideration the overlap of areas around the C3/C4 disc and the best perpendicularity to the spinal cord of both parts.

itksnap.org/pmwiki/pmwiki.php) and Spinal Cord Toolbox (SCT)[26] (https://sourceforge.net/projects/spinalcordtoolbox/) as a representative of atlas-based segmentation methods.

All segmentations were done by three raters and three methods, as shown below. Rater 1 (M.D.) trained segmentations with ITK-SNAP for at least 20 hours. Raters 2 (E.N.) and 3 (J.S.), both with 5 years of practice in radiology, trained for 3 hours and 1 hour, respectively. Rater 1's manual segmentations were supervised by a neuroradiologist with more than 12 years of MRI practice (M.K.) and were regarded as a reference standard. All raters are coauthors of this article.

Manual segmentation of the ESC, GM, and WM on T_2 images was performed independently by three raters using ITK-SNAP software for the entire group and then three more times on seven randomly selected subjects (two men and five women) at minimum 2-day intervals between these assessments. Only ESC was manually segmented on DTI (FA) images in the same design as T_2 images. During manual segmentation, raters paid attention to the best possible tissue separation to minimize the contamination with CSF. T_2 images were registered into DTI space by identical matrix. The center of gravity of each slice of the binary mask was calculated for both T_2 and DTI masks, and the centers of gravity of both images were registered by a simple 2D translation algorithm. Then 3D non-rigid registration was applied. Each step of the registration was repeated for GM and WM binary masks using exactly the same registration matrices as were calculated when ESC was registered. This method enables determination of FA values for ESC, GM, and WM.

ESC segmentation by SCT (sct_propseg algorithms) was performed in three different initialization settings with constant parameters (radius 4; detect-n 4; detect-gap 4; nbiter 200; max-area 120; max-deformation 2.5; min-contrast 50). The first setting was in default mode, which is fully automated (Default); the second was in three-point mode, wherein raters manually set three points within the central canal of the spinal cord on three different axial slices (3 Point); and the third was in CenterLine mode, where raters manually marked the position of the spinal cord central canal by one voxel on all axial slices (CenterLine). WM and GM were segmented using the sct_segment_graymatter algorithm under default settings, and the threshold of the obtained probabilistic tissue masks was set to 0.5.

ESC segmentation by ITK-SNAP was performed by a classification method (CLASS), which consists of three steps. The first step (presegmentation) includes manual labeling of voxels of two or more different classes (in our case this means ESC as the first class and the nearest surrounding like CSF or vertebrae as the second class) on three slices (second, middle, and penultimate). Special care was taken to avoid contamination of the ESC area with voxels of surrounding tissues at the borderline zone to decrease the partial volume effect. These manually defined volumes were subsequently used as a training set for classification of the tissues within an individual subject. Based on this training the contextual information about intensity of neighboring voxels and coordinates of voxels from multiple image layers were derived. These data, which allow for correctly classifying structures without marked image contrast due to their different texture, are used as an input for a random forest classifier[21] and geodesic active contour method.[27,28] The contour represents closed surface, which is evolving according to partial differential equation, where internal forces (derived from contour's geometry) and external forces (given by the image information) affect the contour evolution. For more mathematical background concerning the methods used, see Yushkevich et al,[20] Yushkevich and Gerig,[23] Yushkevich et al,[24] and Caselles et al.[27] The number of trees (100 trees) as well as tree depth (50 trees) was constant for each run. An output of the presegmentation step is "speed image," which is a product of the speed function as one component of evolving force. Its value is close to 0 at the edges of intensity in the input image or close to 1 in regions where intensity is homogeneous. The second step initializes the segmentation by manual placement of the seed points over the spinal cord area on every even-numbered slice. In the last step (evolution), the user sets the weights from the active contour equation, which affects the expansivity and smoothness of segmentation masks, and iteratively runs the evolution. The number of iteration steps varied around 100, and each iteration took around 30 seconds to complete.

Several preprocessing steps were performed before segmenting GM and WM by ITK-SNAP. The ratio of GM and WM areas on axial scans is ~20:80,[29,30] and the signal intensity of GM is higher than that of WM on T_2-weighted images. We therefore assumed that 20% of ESC voxels with the highest intensity corresponded mainly in GM. Voxels with extremely high and low intensity were "homogenized" by applying an upper threshold and threshold, respectively (Eq. 1):

$$I_{new} = \begin{cases} I_{Q15} & I \leq I_{Q15} \\ I & I_{Q15} < I < I_{Q90} \\ I_{Q90} & I \geq I_{Q90} \end{cases} \quad (1)$$

where I_{new} is the voxel value after homogenization; I_{Q15} and I_{Q90} are values of the 15% and 90% intensity quartiles, respectively; and I is the current value of the given voxel. This step ensured that 15% of the least intensive and 10% of the most intensive voxels have the same respective intensity values (ie, they are homogenous). Subsequently, all voxels were modified according to the formula:

$$I_{new} = \left(\frac{I - I_{Q82.5}}{10} \right)^2 \quad (2)$$

where I_{new} is the calculated voxel value, $I_{Q82.5}$ is the value of the 82.5% intensity quartile, and I is the current value of the given voxel. This step ensured that the intensity of voxels with a large probability of being GMs is close to zero and all others have higher values (ie, the background has a value equal to zero). This step makes segmentation easier because the algorithm does not need to recognize three different tissues (WM, GM, background) with similar intensities but only two tissues (WM, the rest) (Fig. 2B).

The segmentation of GM and WM was similar to that of ESC. Raters manually segmented GM, WM, and also a small area of background around ESC on three slices of the original T_2 image. The algorithm, however, uses the information from both images (original T_2 and the modified one, which was described in a previous paragraph) as a teaching feature. Iterated segmentation was done afterwards, and the GM and background masks were
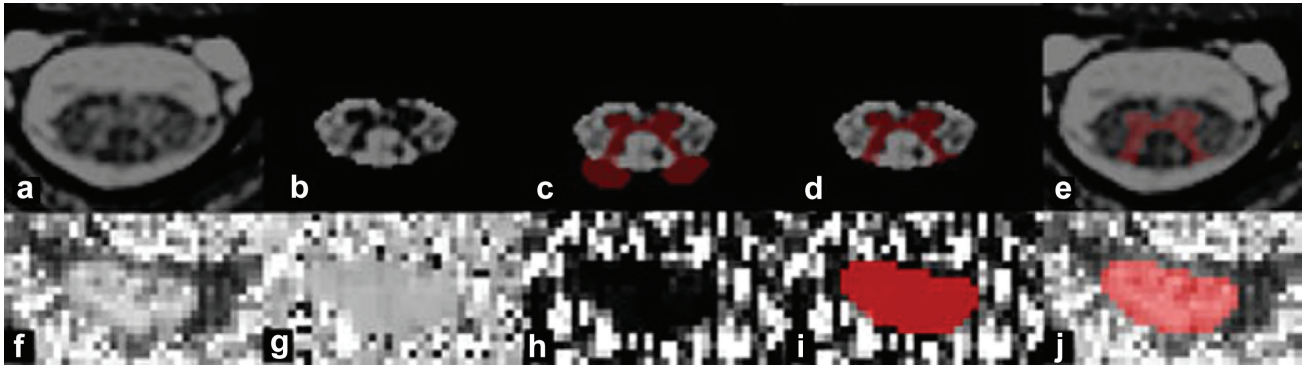
FIGURE 2: Original T_2 image of spinal cord (A), preprocessed image before GM segmentation by ITK-SNAP (B), result of segmentation by classification algorithm for two tissues (C), final GM segmentation on preprocessed image (D), and on original image (E). FA image of spinal cord in different subjects (F), projection image of the main diffusion tensor vector onto the x-axis (G), squared projection image of the main diffusion tensor onto the x-axis (H), final entire spine cord segmentation on image H (I), and on FA image (J) with good result including blurred area.

obtained (Fig. 2C). Only voxels included within the ESC mask were considered to be GM, however (Fig. 2D). ESC voxels, which are not classified as GM, represent WM. WM and GM masks were registered into the DTI space in the same way as described for the manual segmentation method.

When preprocessing DTI data, we applied eddy current correction (FSL) and diffusion tensor was fitted by dtifit script (FSL) for upper and lower images. After that, both parts of the cervical spinal cord were connected with the same transformation matrix as in the case of the T_2 image, and thus a whole cervical spinal cord DTI image was created. For manual segmentation, an image of FA values was used (Fig. 2F). The FA image and squared projection image of the main diffusion tensor vector (MDTV) onto the x-axis (marked by FSL as V_1) were used for segmenting ESC and CSF using the CLASS method.

The original V_1 image (Fig. 2G) was squared to remove the negative sign and sharpen edges between ESC and CSF (Fig. 2H). Raters manually segmented ECS on the FA image, while the CLASS algorithm uses both FA and V_1 images for teaching, which improves the segmentation accuracy. The segmentation mask was shown in parallel on both the FA and V_1 images (Fig. 2I,J) for visual examination.

Two metrics were used to verify segmentation agreement: similarity and distance. The 3D Dice coefficient (DC) was used to represent the similarity metric:

$$DC = \frac{2(S_1 \cap S_2)}{|S_1| + |S_2|} \quad (3)$$

where S_1 and S_2 are counts of voxels acquired by segmentations 1 and 2, respectively. The numerator denotes double the number of voxels which have both segmentations in common, and the denominator delineates the total combined voxel count of the two segmentations. The result ranges from 0 to 1, where 1 indicates identical segmentation and 0 indicates absolutely different segmentation. The DC coefficient is highly sensitive to the total number of voxels, which has a larger impact on evaluations of small structures like GM than on large structures.[31]

The distance metric is described by the Hausdorff distance (HD):

$$HD = \max\left(h(A, B), h(B, A)\right) \qquad h(A, B) = \max_{a \in A} \min_{b \in B} \|a - b\| \quad (4)$$

where h(A,B) is the direct Hausdorff distance between finite point sets A and B and $\|a - b\|$ is the Euclidean distance of two points a and b from point sets A and B, respectively.[32] HD is expressed in millimeters and describes maximal imprecision of the two segmentations. Both metrics were performed using EvaluateSegmentation script.[31]

The first step in evaluating the segmentations was a mutual comparison of the CLASS and SCT methods (in three different modes) with manual segmentation of the most experienced (gold standard) operator for ESC segmented on the T_2 image. The two best modalities, SCT CenterLine mode and CLASS method, were then statistically evaluated and compared with manual segmentation in more detail for both image contrasts (T_2 and FA) and for different tissues (WM and GM). Furthermore, intra- and interobserver repeatability were evaluated for segmentation of all tissues using manual and both semiautomatic segmentation techniques (SCT, CLASS). Finally, the influences of rater and segmentation method on FA values of different spinal cord tissues and their repeatability were appraised.

For evaluating intraobserver repeatability, images of seven randomly chosen subjects were segmented four times by all three raters using different methods: manual segmentation, SCT (CenterLine), and CLASS. Masks obtained by a single rater from a single subject using a particular segmentation method were paired off in all possible combinations, representing six independent pairs (combination number $\binom{4}{2} = 6$). For each method, 126 DC and HD were calculated (seven subjects, three raters, six combinations) and mutually evaluated by t-test separately for every tissue.

In the case of interobserver repeatability, masks obtained by segmentation in all 20 subjects by all three raters were paired off in all three possible combinations. All in all, we obtained 60 DC and HD for every method and tissue.

Binary masks of ESC, GM, and WM created based on images of 20 subjects by CLASS and manual segmentation methods were registered into the DTI space. Because SCT masks were
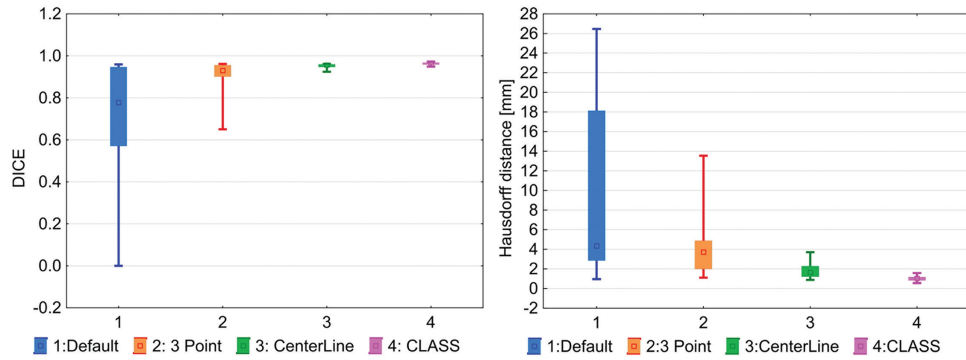
FIGURE 3: Mutual comparison of four semiautomatic segmentations of entire spinal cord on T$_2$-w image with manual segmentation represented by 3D Dice coefficient and Hausdorff distance on box-and-whisker plots (min, 25% quartile, median, 75% quartile, max). Boxes of different colors represent agreement of different semiautomatic methods with manual segmentation from the perspective of 3D Dice coefficient and Hausdorff distance values. Default: Spinal Cord Toolbox (SCT) in Default mode, 3 Point: SCT three-point initialization method, CenterLine: SCT CenterLine method, and CLASS: ITK-SNAP classification method.

generated directly in DTI space, they did not need registration. Analysis of variance (ANOVA) was used to compare how application of different segmentation methods performed by various raters impacts FA values of different tissues. Factorial ANOVA was performed with FA values as dependent variables and with raters, methods, and tissues as categorical factors.

FA's intraobserver repeatability was verified on seven subjects, each segmented four times by three raters and three methods. An intraobserver coefficient of variation (CoV) was calculated based on four median FA values of the same subject, method, and rater. In the case of interrepeatability, median FA values obtained from 20 subjects, three raters, and three methods without repetition were used. Inter-CoV was calculated based on three median FA values for the same subject, method, and different rater. CoV values of different methods for individual tissues were mutually compared using *t*-tests.

Statistics

Student's *t*-test was used for statistical comparison of different segmentation methods quantified by DC and HD values as well as for comparison of repeated segmentations in terms of inter- and intraobserver repeatability evaluations. ANOVA and Tukey's posthoc test were used to compare FA values of various tissues obtained by different methods and raters and CoV was used to quantify the repeatability of FA values obtained by means of different segmentation techniques.

$$CoV(x) = SD(x)\bar{x} \qquad (5)$$

CoV is a ratio of the standard deviation (SD) of quantity x and the mean value of this quantity ($\bar{x}$). It is expressed as a percentage. The lower the value, the better is the consistency.

Statistical tests were computed using Statistica 12 (StatSoft, Tulsa, OK) software, graphs were created with the same software, DC and HD were performed using EvaluateSegmentation script[31] and for all statistical tests the significance level was set to 0.05.

Results

Mutual Comparison of the Methods

Rater 1 segmented the ESC of all 20 subjects by all five methods (manually, CLASS, and SCT in three different settings). DC and HD were calculated for semiautomated

methods compared to manual segmentation (Fig. 3). Based on these results, and inasmuch as the other two modes corresponded unsatisfactorily with manual segmentation, for further segmentations we used SCT only in the CenterLine mode.

A detailed comparison of the two most promising semiautomatic methods with manual segmentation done by Rater 1 was determined for ESC segmented on T$_2$ and FA images and for GM and WM segmented on T$_2$ images in all 20 subjects. CLASS segmentation performed by a skilled rater generally resulted in statistically significantly more masks being similar to manual segmentation than did SCT segmentation in CenterLine mode for both T$_2$ and FA images (Fig. 4).

Intraobserver Repeatability

This section evaluates the consistency of different segmentation methods repeated by the same rater on the same subject (Table 2). For ESC and WM segmentation, both semiautomated methods are more consistent than is manual segmentation performed by all raters (Fig. 5). This is demonstrated by the significantly higher DC values and lower HD values achieved by the semiautomatic methods as compared to the manual method. In the case of GM segmentation, semiautomated methods also yielded higher DC values, while CLASS also produced higher HD values than both manual and SCT. In nine cases, the SCT method segmented ESC on the FA image inaccurately, thereby resulting in lower DC and higher HD values (outliers in Fig. 5).

Interobserver Repeatability

The consistency of segmentation methods across different raters is shown here (Table 2). In the case of ESC segmentation, both semiautomated methods produce more consistent results across raters (Fig. 6). SCT is the most consistent method for GM and WM segmentation across raters. The CLASS method is slightly poorer than manual segmentation for WM and poorer when GM is segmented.
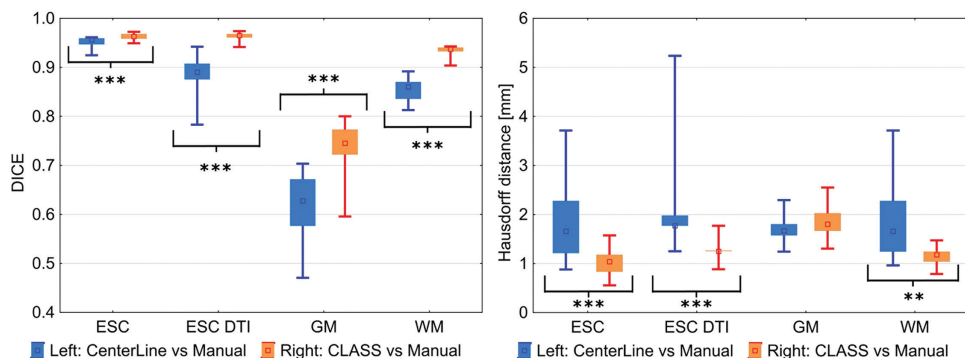
FIGURE 4: Comparison of entire spinal cord (ESC) segmented on T_2 data, ESC on DTI data, gray (GM) and white matter (WM) segmented on T_2 data in all 20 subjects is represented by 3D Dice coefficient and Hausdorff distance on box-and-whisker plots (min, 25% quartile, median, 75% quartile, max). The blue boxes represent a comparison of the Spinal Cord Toolbox (SCT) method with the CenterLine seed mask against manual segmentation as the gold standard. The orange boxes compare ITK-SNAP classification method (CLASS) with manual segmentation. A t-test was performed to evaluate statistical differences between agreements of different methods. $**P < 0.001$ and $***P < 0.0001$. The pair with no asterisk do not differ statistically ($P > 0.05$).

TABLE 2. Overview of Intra- and Interrepeatability of Three Segmentation Methods and Four Different Segmentations Described by 3D Dice Similarity Coefficient and Hausdorff Distance

		Median DICE (IQR)				Median HD [mm] (IQR)			
		ESC	ESC DTI	GM	WM	ESC	ESC DTI	GM	WM
Intrarepeatability	Man	96.5(2.0)	96.6(2.3)	80.3(8.9)	91.9(5.1)	0.79(0.3)	0.89(0.4)	1.15(0.4)	0.88(0.2)
	SCT	98.7(0.7)	99.0(0.4)	87.3(4.5)	95.9(1.6)	0.96(0.4)	0.89(0)	0.96(0.4)	0.96(0.4)
	CLASS	99.0(1.2)	97.6(2.1)	82.3(17.3)	95.9(2.9)	0.56(0.5)	0.89(0.4)	1.55(1.4)	0.92(0.3)
Interrepeatability	Man	95(2.1)	95.5(1.7)	70.1(6.5)	86.8(3.1)	0.88(0.2)	1.25(0.4)	1.62(0.3)	0.96(0.2)
	SCT	98.7(0.9)	98.8(0.8)	87(5.8)	95.8(1.6)	0.96(0.9)	0.88(0.4)	1.04(0.4)	0.96(0.6)
	CLASS	98.7(1.3)	96.7(2.4)	65.4(19.3)	87.5(3.5)	0.57(0.3)	0.88(0.4)	2.56(1.1)	1.18(0.2)

The interquartile range represents the distance between the 25% and 75% quartiles. Manual method (Man), Spinal Cord Toolbox in CenterLine mode (SCT), ITK-SNAP in classification mode (CLASS), entire spinal cord (ESC), gray (GM), white matter (WM), entire spinal cord segmented in DTI data (ESC DTI), 3D Dice similarity coefficient (DICE), Hausdorff distance (HD), and interquartile range (IQR).
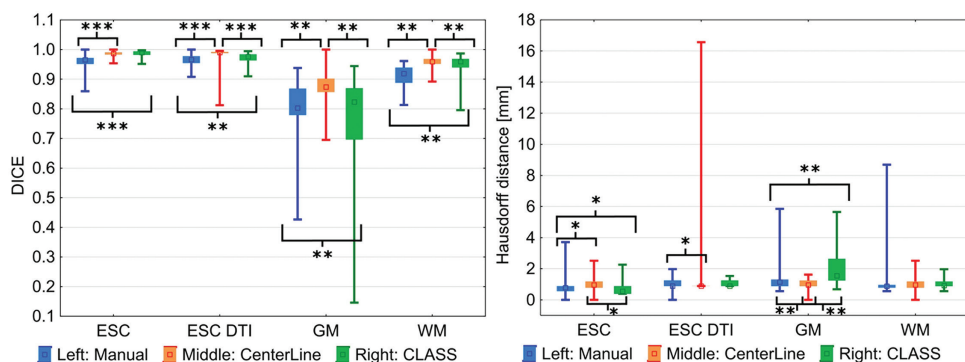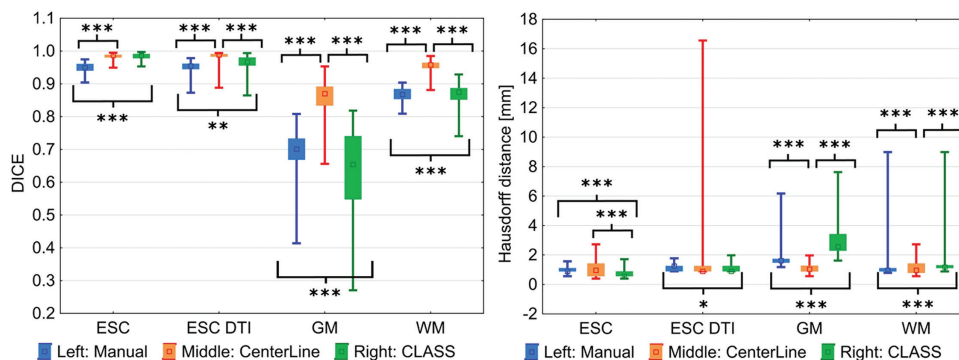

FIGURE 5: Intrarepeatability of three segmentation methods performed by three raters, four times on seven subjects and three tissues (entire spinal cord on T_2-w [ESC] and on DTI [ESC DTI], gray [GM] and white matter [WM]). All possible pair-combinations of segmented masks were created, and 1134 3D Dice coefficients (DICE) and Hausdorff distances (HD) were calculated. Box-and-whisker plots show the results (min, 25% quartile, median, 75% quartile, max) and each box represents 126 coefficients. Blue boxes represent intrarepeatability of manual segmentation; orange boxes show results of Spinal Cord Toolbox (SCT) method with CenterLine seed mask; and green boxes represent ITK-SNAP classification method (CLASS). A t-test was performed to evaluate statistical differences between agreements of different methods. $*P < 0.01$, $**P < 0.001$, and $***P < 0.0001$. Pairs with no asterisk did not differ significantly ($P > 0.05$).

FIGURE 6: Interrepeatability of three segmentation methods performed by three raters on 20 subjects and four tissues (entire spinal cord on T$_2$-w [ESC] and DTI [ESC DTI], gray [GM] and white matter [WM]). All possible pair combinations of segmented masks were created and 720 3D Dice coefficients (DICE) and Hausdorff distances were calculated. Box-and-whisker plots show results (min, 25% quartile, median, 75% quartile, max), and each box is assembled from 60 coefficients. Blue boxes represent interrepeatability of manual segmentation; orange boxes show results of the Spinal Cord Toolbox (SCT) method with CenterLine seed mask; and green boxes indicate the ITK-SNAP classification method (CLASS). A *t*-test was performed to evaluate statistical differences between agreements of different methods. *$P < 0.01$, **$P < 0.001$, and ***$P < 0.0001$. Pairs with no asterisk did not differ significantly ($P > 0.05$).
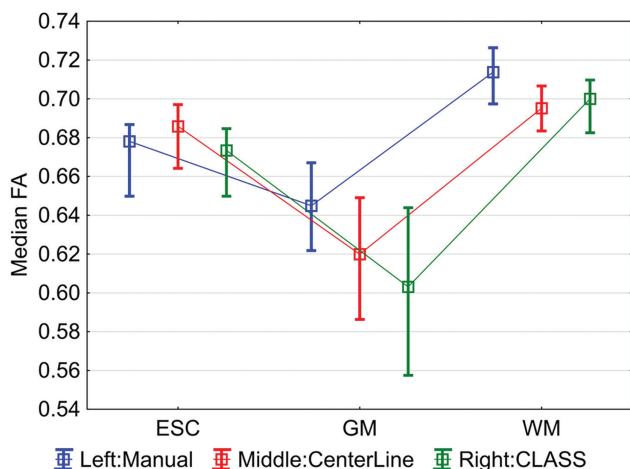
FIGURE 7: Tukey's post-hoc test of method–tissue interaction term shows significantly higher median FA value obtained by manual segmentation of gray matter (GM) in comparison with both semiautomated methods ($P < 0.005$). FA value differences equal 0.02 (CenterLine) and 0.04 (CLASS). Boxes indicate median FA values and whiskers mark the 25% and 75% quartiles. The FA values of entire spinal cord (ESC) and white matter (WM) are not significantly dependent on segmentation method or rater.

Evaluation of FA Values

We showed no dependence of FA values on rater ($F[2,513] = 0.22$, $P = 0.806$), but the effects of method, tissue, and their interaction term are statistically significant ($F[2,513] = 13.68$, $P < 0.0001$; $F[2,513] = 198.49$, $P < 0.0001$; and $F[4,513] = 5.92$, $P < 0.005$, respectively). No other effect was statistically significant. Tukey's post-hoc test was performed on the method–tissue interaction term (Fig. 7) and shows that the manual segmentation of GM was significantly different from both other methods ($P < 0.005$). Divergence between median FA values of manual and semiautomated methods were equal to 0.02 (CenterLine) and 0.04 (CLASS). The semiautomated methods show very good agreement for all tissues.

Repeatability of FA values for all methods was sufficient, with mostly less than 2% variance. SCT produced the most consistent results and the repeatability of the manual method was similar to that of the CLASS method (Table 3).

TABLE 3. Median Values of Coefficient of Variation Describe Intrarepeatability of Three Segmentation Methods on Three Tissues Done by Three Different Raters in Four Repetitions on Seven Subjects and Interrepeatability on 20 Subjects Without Repetition

	CoV [%] Intrarepeatability (IQR)				CoV [%] Interrepeatability (IQR)		
Tissue\Method	Manual	CenterLine	CLASS	Tissue\Method	Manual	CenterLine	CLASS
ESC	1.4(0.5)[@]	0.1(0.04)	1(0.6)[@]	ESC	2.2(1.7)[*]	0.1(0.1)	1.3(1.5)[*]
WM	1(0.7)	0.1(0.04)	0.4(0.2)	WM	1.3(1.2)[+]	0.1(0.2)	1.6(1.0)[+]
GM	1.2(0.4)	0.2(0.3)	1.8(1.1)	GM	1.8(1.2)	0.4(0.3)	3.8(3.4)

Paired CoV values marked with *, + , and @ symbols are not significantly different (*t*-test, $P > 0.05$); other pairs are significantly different ($P < 0.05$). Coefficient of variation (CoV), entire spinal cord (ESC), gray matter (GM), white matter (WM), Spinal Cord Toolbox segmentation in CenterLine mode (CenterLine), ITK-SNAP in classification mode (CLASS), interquartile range (IQR).

Discussion

In this article we introduced the application of ITK-SNAP segmentation in classification mode on the structural and DTI MRI data of cervical spinal cord. Requirements for this method included a capability for accurate segmentation of the ESC area, separate segmentation of WM and GM from T_2-weighted images, as well as segmentation of the ESC area from DTI images and differentiation of its contours from CSF. We focused on the clinical applicability and employment of the method for analysis of the diffusion parameters of spinal cord.

There exist several approaches to spinal cord segmentation. Basically, three main groups of segmentation methods further divided into various subgroups can be differentiated.[4] In older studies, there generally predominated use of intensity-based methods such as thresholding, edge detection, or intensity-based classifiers.[31,33–35] Other authors used surface-based segmentation like active contour or deformable models[8,10,17,36,37] and the last main group adopted such image-based methods as graph-cut, atlas deformation, or classifiers.[7,15,16] From the perspective of this classification we may consider ITK-SNAP as a hybrid method using some of the components from all three of these groups due to its employment of active contour algorithms, random forest classifier, and texture information about intensity and voxel coordinates. This approach has the advantage that it does not use atlas deformable algorithms. That makes this method more personalized, eliminates the risk of misregistration, and may also make it more accurate in specific pathological conditions when the spine is deformed or abnormal, eg, in case of severe spinal cord compression. Work-flow of the segmentation in ITK-SNAP also enables easy separate segmentation of the visible spinal cord lesions, which can further be used for separate analysis of diffusion parameters within these areas. On the other hand, this method may be more sensitive to image quality compared to atlas-based models and could yield poorer results in situations where the contrast- or signal-to-noise ratio is poor. In such conditions even an experienced radiologist may find it difficult to perform manual segmentation and the use of an atlas-based method may be beneficial.

ITK-SNAP was introduced as a general segmentation tool with a user-friendly interface and was originally evaluated on segmentation of caudate nucleus.[20] Since that time, its use has been reported in more than 1700 articles.[24] The first classification method based on random forests is available from ITK_SNAP v. 3.2 (January 2015) without implementation of texture information. This additional technique was added into v. 3.4 (January 2016) and it allows advanced learning methods such as multimodal segmentation, whereby learning algorithms take information from several different images for better classification.[23,24] As far as we are aware, these semiautomatic techniques have not yet been systematically evaluated for the segmentation of human spinal cord.

Older studies[33,34,36,37] and studies dealing with DTI[11,13,35] mostly use MR with 1.5T induction, taking advantage of lower susceptibility artifacts in DTI acquisition. Of the aforementioned studies, the CLASS method presented in this article achieves the most accurate results in segmenting the entire spinal cord from a T_2 image. The more recent studies and studies dealing with WM and GM segmentation[5,7,9,14–19,38] use mostly MR with 3T induction. T_2-weighted images from such MR devices have better signal-to-noise ratios, and thus the contrast between GM and WM is sharper and the segmentation is more accurate. This may be an advantage especially in examining lower cervical spine, where the image quality is usually poorer than in the case of upper cervical segments. On the other hand, DTI data are more affected by susceptibility artifacts. Our presented method is therefore not the most accurate in segmenting GM and WM, but it is still among the most accurate methods published to date.

It should be noted, however, that the comparison of different segmentation methods based on DC and HD coefficients with literature data is complicated due to the varying acquisition parameters and image quality. Therefore, using the same dataset, we decided to perform direct comparison of the newly applied CLASS method with the better-established and commonly published SCT technique. A similar approach was used in a study by Prados et al,[38] who compared the capabilities of different segmentation methods on dedicated MR data. That study provides a broader overview of different up-to-date techniques. The methods generally reached median DC values for GM segmentation between 0.6 and 0.85 and median HD values ranged from 1.5 to 7 mm in comparison to manual segmentation. Compared to this, the benefit of our study may be seen especially in the extension of the segmentations also on the DTI data to connect anatomical information with diffusion. Thus, we can introduce a comprehensive and clinically usable methodological approach of cervical cord DTI data analysis. In any case, the CLASS method may merit further evaluation as part of the ongoing GM segmentation challenge project[38] in order to be compared with more techniques than just SCT.

Some publications[10,14,15,18,33,36,37] quantify segmentation repeatability by comparing areas or volumes of segmentation masks or on the basis of various derived coefficients (coefficient of variation or intraclass correlation coefficients [ICC]). We do not consider such approaches to be optimal for quantifying the segmentation method, because congruence of areas or volumes does not automatically imply congruent segmentations. Therefore, we believe it is more suitable to use a similarity metric (Dice coefficient, Jaccard

coefficient, global consistency error, or the like) together with a distance metric (such as Hausdorff distance or Mahalanobis distance), which correlate mutually as little as possible and thus do not yield redundant information.[31]

As for DTI data analysis, we evaluated the reproducibility and influence of different segmentation techniques on FA, which we chose as a representative scalar parameter quantifying anisotropic diffusion. FA values measured within ESC and WM appeared to be very consistent among different raters and methods, as ANOVA analysis revealed no significant differences. Some inconsistency was observed in the case of FA values of GM, where manual segmentations provided slightly, but statistically significantly, higher FA values as compared to both semiautomatic methods. Given that FA of normal GM is physiologically lower than that of WM,[39] the higher FA values of GM measured within the masks of manual segmentation may be attributed to incorrect inclusion of a greater number of WM voxels by less experienced raters. From this perspective, measurement of lower GM FA by both semiautomatic methods may be considered more plausible.

To measure FA within WM and GM, we used a technique of 2D registration of segmentations on T_2 and FA images using a spinal cord contour as a landmark. Due to the large variability in spinal cord curvature, lack of unambiguous landmarks, and small dimensions, affine or nonrigid 3D registration is almost impossible.[5] Therefore, we had to apply 2D rigid registration for the entire spinal cord contour segmented from particular axial scans and applied the resulting transformation matrix on the masks of individual tissues. For the lowest possible deviations of T_2 and DTI images, emphasis was given to congruence of their geometric acquisition parameters. Visual examination was also performed by overlapping the images along the z-axis in the sagittal plane. Perpendicularity of axial sections is necessary for maximizing contrast between WM and GM in a T_2 image and minimizing the partial volume effect in a DTI image.[40] The acquisition was therefore divided into two parts, with emphasis on maximum perpendicularity of the individual sections and avoiding mutual overlap of these acquisitions.

The technique described above did not reveal significant differences of measured FA values for GM, WM, and ESC between the CLASS and CenterLine SCT methods. This result indicates that our approach may provide a functional alternative to a more established atlas-based technique for quantifying diffusion parameters. Both methods revealed statistically significant differences in FA between WM and GM. This supports the accuracy of the measurements, as it is difficult to establish the gold standard of WM and GM segmentations in DTI data by visual control due to comparatively low contrast and resolution.

The inter- and intraobserver variability of FA expressed by CoV was generally low among all techniques, which denotes the generally good reproducibility of this biomarker. However, the variability of FA measured using the CenterLine method showed the lowest rate. Minor manual input combined with the atlas-based technique is probably the reason for similarly better agreement of the segmentation masks themselves between different raters and repeated measurements compared to the CLASS method.

This work has several limitations that originate in part from the intention to examine the clinical applicability of the method. One of those limitations is the setting of fixed SCT parameters, which may influence the results. We decided on a constant setting in order to maximize the benefits of the automatic method with relatively minimal input from the operator. Moreover, the degree to which a common user will comprehend all of the parameters may not be sufficiently high to enable precise optimization of all parameters for individual segmentations. As discussed above, the use of a 1.5T magnetic field could constitute another limitation.

The time aspect and labor intensity could also play a role in determining the practical applicability of this method. The mean duration of segmentation in one subject by rater MD performed on seven subjects was estimated at 635 seconds for SCT and 644 seconds for the CLASS method. Although the segmentation of all spinal cord tissues (with visual inspection of each segmentation mask, but without any postprocessing or manual corrections of segmentation masks) by SCT requires less time than does the CLASS method; the difference is not so great as one might expect when considering the higher degree of automatization in the case of SCT. This may be caused by the need for extra checking of the particular steps in SCT processing, which are done automatically by the CLASS method during the segmentation procedures. Moreover, creating CenterLine masks for T_2 and FA images in SCT is quite time-consuming. Although there can be no doubt that the CLASS method is more laborious than is SCT, as it uses more manual input from the operator, this disadvantage may be offset in part by creating scripts to increase the efficiency of the method. On the other hand, when the segmentation is not sufficiently accurate, the CLASS method allows straightforward and prompt manual correction immediately after the iteration step. That is in contrast to SCT, which requires setting up appropriate threshold values for cutting off less probable voxels of GM and WM, and uses an additional software tool to make the appropriate corrections manually. In order more objectively to evaluate the performance of the two semiautomatic techniques in this study, however, no manual corrections to either CLASS or SCT segmentations were made.

Although another potential limitation may be seen in the relatively low number of subjects, the power of statistical analyses evaluating the accuracy of segmentations was generally sufficient due to multiple repetitions by several operators. As the machine-learning algorithm implemented in the CLASS method is individually based, the total number of subjects analyzed is not really relevant from this perspective. Inasmuch as spine curvature is relatively variable, however, a larger study group could cover a wider spectrum of anatomical configurations and potentially provide more precise results.

The choice as to the number of voxels marked for the learning algorithm could also constitute a source of some inaccuracy. In this study, we used information from three defined slices at upper, middle, and lower cervical levels. This number of slices was set empirically based on preliminary testing, and it was chosen as the best compromise between accuracy and the time needed for processing. Nevertheless, in patients with severe spinal deformity or alteration of the spinal cord signal intensity, it may be beneficial to provide a higher number of teaching masks or to place them at different spinal cord segments to achieve the best results from the semiautomatic segmentation. Inasmuch as the algorithm uses voxel coordinates and intensity of neighboring voxels as a teaching feature, a small spinal cord lesion or mild compression at the level of the teaching masks should not have substantial negative impact on the resulting segmentation, but the performance of the CLASS technique in such pathological conditions is yet to be established.

To conclude, the ITK-SNAP semiautomatic segmentation technique using machine learning is exploitable for the segmentation of a human cervical spinal cord in structural and DTI MRI data and constitutes a convenient alternative to an atlas-based segmentation method. While SCT provides rather more reproducible segmentations, the CLASS technique, on the other hand, revealed better agreement of segmentation masks with manual segmentation by the most experienced rater. Furthermore, the introduced technique for registration of DTI and T_2 images appears to be applicable for measurements of diffusion scalar parameters within different tissues of the spinal cord, thus providing results corresponding to those of a more established atlas-based technique used by SCT.

Acknowledgments

References

1. Dong Q, Welsh RC, Chenevert TL, et al. Clinical applications of diffusion tensor imaging. J Magn Reson Imaging 2004;19:6–18.

2. Lerner A, Mogensen MA, Kim PE, Shiroishi MS, Hwang DH, Law M. Clinical applications of diffusion tensor imaging. World Neurosurg 2014;82:96–109.

3. Balafar MA, Ramli AR, Saripan MI, Mashohor S. Review of brain MRI image segmentation methods. Artif Intell Rev 2010;33:261–274.

4. Leener BD, Taso M, Cohen-Adad J, Callot V. Segmentation of the human spinal cord. Magn Reson Mater Phys Biol Med 2016;29:125–153.

5. Asman AJ, Bryan FW, Smith SA, Reich DS, Landman BA. Groupwise multi-atlas segmentation of the spinal cord's internal structure. Med Image Anal 2014;18:460–471.

6. Chen M, Carass A, Cuzzocreo J, Bazin P-L, Reich DS, Prince JL. Topology preserving automatic segmentation of the spinal cord in magnetic resonance images. IEEE 2011:1737–1740.

7. Chen M, Carass A, Oh J, et al. Automatic magnetic resonance spinal cord segmentation with topology constraints for variable fields of view. NeuroImage 2013;83:1051–1062.

8. De Leener B, Kadoury S, Cohen-Adad J. Robust, accurate and fast automatic segmentation of the spinal cord. NeuroImage 2014;98:528–536.

9. El Mendili M-M, Chen R, Tiret B, et al. Fast and accurate semi-automated segmentation method of spinal cord MR images at 3T applied to the construction of a cervical spinal cord template. PLoS One 2015;10:e0122224.

10. Horsfield MA, Sala S, Neema M, et al. Rapid semi-automatic segmentation of the spinal cord from magnetic resonance images: Application in multiple sclerosis. NeuroImage 2010;50:446–455.

11. Tang L, Wen Y, Zhou Z, von Deneen KM, Huang D, Ma L. Reduced field-of-view DTI segmentation of cervical spine tissue. Magn Reson Imaging 2013;31:1507–1514.

12. Asman AJ, Smith SA, Reich DS, Landman BA. Robust GM/WM segmentation of the spinal cord with iterative non-local statistical fusion. Med Image Comput Comput-Assist Interv MICCAI Int Conf Med Image Comput Comput-Assist Interv 2013;16(Pt 1):759–767.

13. Ellingson BM, Ulmer JL, Schmit BD. Gray and white matter delineation in the human spinal cord using diffusion tensor imaging and fuzzy logic. Acad Radiol 2007;14:847–858.

14. Yiannakas MC, Kearney H, Samson RS, et al. Feasibility of grey matter and white matter segmentation of the upper cervical cord in vivo: A pilot study with application to magnetisation transfer measurements. NeuroImage 2012;63:1054–1059.

15. Bergo FPG, França MC, Chevis CF, Cendes F. SpineSeg: A segmentation and measurement tool for evaluation of spinal cord atrophy. In: 2012 7th Iber Conf Inf Syst Technol CISTI; 2012:1–4.

16. Fonov VS, Le Troter A, Taso M, et al. Framework for integrated MRI average of the spinal cord white and gray matter: The MNI–Poly–AMU template. NeuroImage 2014;102:817–827.

17. Koh J, Scott PD, Chaudhary V, Dhillon G. An automatic segmentation method of the spinal canal from clinical MR images based on an attention model and an active contour model. In: 2011 IEEE Int Symp Biomed Imaging Nano Macro; 2011:1467–1471.

18. Taso M, Le Troter A, Sdika M, et al. A reliable spatially normalized template of the human spinal cord — Applications to automated white matter/gray matter segmentation and tensor-based morphometry (TBM) mapping of gray matter alterations occurring with age. NeuroImage 2015;117:20–28.

19. Yiannakas MC, Mustafa AM, De Leener B, et al. Fully automated segmentation of the cervical cord from T1-weighted MRI using PropSeg: Application to multiple sclerosis. NeuroImage Clin 2016;10:71–77.

20. Yushkevich PA, Piven J, Hazlett HC, et al. User-guided 3D active contour segmentation of anatomical structures: Significantly improved efficiency and reliability. NeuroImage 2006;31:1116–1128.

21. Breiman L. Random forests. Mach Learn 2001;45:5–32.

22. Criminisi A, Shotton J. Semi-supervised classification forests. In: Decis For Comput Vis Med Image Anal. Criminisi A, Shotton J (eds.).

Advances in Computer Vision and Pattern Recognition. London: Springer; 2013:95–107.

23. Yushkevich PA, Gerig G. ITK-SNAP: An intractive medical image segmentation tool to meet the need for expert-guided segmentation of complex medical images. IEEE Pulse 2017;8:54–57.

24. Yushkevich PA, Gao Y, Gerig G. ITK-SNAP: An interactive tool for semi-automatic segmentation of multi-modality biomedical images. In: 2016 38th Annu Int Conf IEEE Eng Med Biol Soc EMBC; 2016: 3342–3345.

25. Jenkinson M, Beckmann CF, Behrens TEJ, Woolrich MW, Smith SM. FSL. NeuroImage 2012;62:782–790.

26. De Leener B, Lévy S, Dupont SM, et al. SCT: Spinal Cord Toolbox, an open-source software for processing spinal cord MRI data. NeuroImage 2017;145(Pt A):24–43.

27. Caselles V, Kimmel R, Sapiro G. Geodesic active contours. Int J Comput Vis 1997;22:61–79.

28. Zhu SC, Yuille A. Region competition: unifying snakes, region growing, and Bayes/MDL for multiband image segmentation. IEEE Trans Pattern Anal Mach Intell 1996;18:884–900.

29. Goto N, Otsuka N. Development and anatomy of the spinal cord. Neuropathology 1997;17:25–31.

30. Fradet L, Arnoux P-J, Ranjeva J-P, Petit Y, Callot V. Morphometrics of the entire human spinal cord and spinal canal measured from in vivo high-resolution anatomical magnetic resonance imaging. Spine 2014; 39:E262–E269.

31. Taha AA, Hanbury A. Metrics for evaluating 3D medical image segmentation: analysis, selection, and tool. BMC Med Imaging 2015;15: 29.

32. Taha AA, Hanbury A. An efficient algorithm for calculating the exact Hausdorff distance. IEEE Trans Pattern Anal Mach Intell 2015;37: 2153–2163.

33. Losseff NA, Webb SL, O'Riordan JI, et al. Spinal cord atrophy and disability in multiple sclerosis. Brain 1996;119:701–708.

34. Tench CR, Morgan PS, Constantinescu CS. Measurement of cervical spinal cord cross-sectional area by MRI using edge detection and partial volume correction. J Magn Reson Imaging 2005;21:197–203.

35. Zivadinov R, Banas AC, Yella V, Abdelrahman N, Weinstock-Guttman B, Dwyer MG. Comparison of three different methods for measurement of cervical cord atrophy in multiple sclerosis. Am J Neuroradiol 2008;29:319–325.

36. Coulon O, Hickman SJ, Parker GJ, Barker GJ, Miller DH, Arridge SR. Quantification of spinal cord atrophy from magnetic resonance images via a B-spline active surface model. Magn Reson Med 2002; 47:1176–1185.

37. Van Uitert R, Bitter I, Butman JA. Semi-automatic spinal cord segmentation and quantification. CARS 2005: Computer Assisted Radiology and SurgeryProceedings of the 19th International Congress and Exhibition. Int Congr Ser 2005;1281:224–229.

38. Prados F, Ashburner J, Blaiotta C, et al. Spinal cord grey matter segmentation challenge. NeuroImage 2017;152(Supplement C):312–329.

39. Feldman HM, Yeatman JD, Lee ES, Barde LHF, Gaman-Bean S. Diffusion tensor imaging: a review for pediatric researchers and clinicians. J Dev Behav Pediatr JDBP 2010;31:346–356.

40. Ellingson BM, Cohen-Adad J. Chapter 3.1. Diffusion-weighted imaging of the spinal cord. In: Quant MRI Spinal Cord. San Diego: Academic Press; 2014:123–145.

Moderní techniky MR zobrazení u roztroušené sklerózy

State-of-the-Art MRI Techniques for Multiple Sclerosis

Souhrn

Magnetická rezonance (MR) je v současnosti klíčovou součástí diagnostiky roztroušené sklerózy. Kromě konvenčních technik založených na hodnocení počtu a lokalizace viditelných lézí mozku a míchy zaznamenáváme v posledních letech rychlý rozvoj nových technik MR zobrazení, které poskytují nové kvantitativní biomarkery lépe charakterizující patologické strukturální změny tkání centrálního nervového systému vzniklé v důsledku demyelinizačního onemocnění. V tomto článku jsou shrnuty nové trendy v MR diagnostice roztroušené sklerózy po stránce technických základů jednotlivých metod, možností analýzy dat i jejich praktického využití.

Abstract

Magnetic resonance imaging (MRI) is currently a key component of multiple sclerosis diagnostics. In addition to conventional techniques, based on the evaluation of the number and localization of visible brain and spinal cord lesions, in recent years we have seen a rapid development of new MRI techniques providing new quantitative biomarkers which better characterize pathological structural changes in central nervous system tissues occurring due to a demyelinating disease. This article summarizes new trends in MRI diagnostics of multiple sclerosis in terms of the technical foundations of different methods, possibilities for data analysis and their practical use.

M. Keřkovský[1], J. Stulík[1],
I. Obhlídalová[2], P. Praksová[2],
J. Bednařík[2], M. Dostál[1,3],
M. Kuhn[4–6], A. Šprláková-Puková[1],
M. Mechl[1]

[1] Klinika radiologie a nukleární medicíny LF MU a FN Brno
[2] Neurologická klinika LF MU a FN Brno
[3] Biofyzikální ústav, LF MU a FN Brno
[4] Psychiatrická klinika LF MU a FN Brno
[5] Institut biostatistiky a analýz, LF MU, Brno
[6] Behaviorální a sociální neurovědy, CEITEC – Středoevropský technologický institut MU

✉
MUDr. Miloš Keřkovský, Ph.D.
Klinika radiologie
a nukleární medicíny
LF MU a FN Brno
Jihlavská 20
625 00 Brno
e-mail: kerkovsky.milos@fnbrno.cz

Úvod

Roztroušená skleróza (RS) představuje chronické zánětlivé onemocnění centrálního nervového systému (CNS), které je z patomorfologického hlediska charakterizováno přítomností zánětlivé infiltrace, demyelinizace, axonálního poškození a gliózy v různých 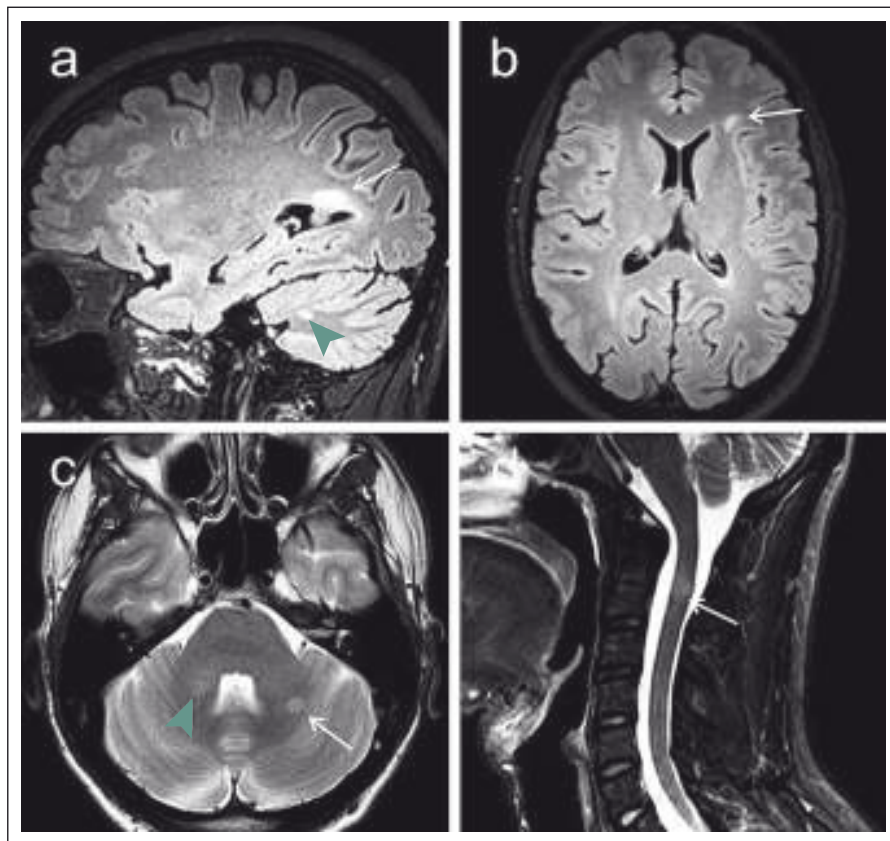oblastech CNS. Predilekčně jsou postiženy zrakové nervy, mozkový kmen, mozeček, dále periventrikulární a subkortikální bílá hmota mozkových hemisfér [1]. Je též známo, že patologický proces u pacientů s RS není limitován pouze na bílou hmotu, nýbrž postihuje často i oblasti kortikální a hluboké subkortikální šedé hmoty mozku [2]

Magnetická rezonance (MR) hraje v současnosti klíčovou roli v diagnostice RS. MR diagnostika je založena především na využití T2 vážených sekvencí a zobrazení FLAIR (fluid attenuated inversion recovery), pomocí kterých lze detekovat hyperintenzní léze mozku či míchy. Ukazuje se však, že konvenční techniky MR zobrazení neumožňují zcela komplexní náhled na patofyziologické procesy v rámci RS. Tyto limitace lze dokumentovat např. poměrně chabou korelací MR nálezů s klinickou symptomatikou a diskrepancí mezi MR zobrazením a histopatologickými nálezy [3,4]. Dále je známo, že konvenční techniky MR mají relativně omezené možnosti detekce lézí šedé hmoty a difuzních změn v bílé hmotě [5]. V posledních letech se začínají využívat nejrůznější nové techniky MR zobrazení, jejichž rozvoj je spjat s celkovým vývojem MR technologie a které nabízejí komplexnější náhled na strukturální poškození CNS v rámci RS. U některých technik je nespornou výhodou možnost kvantifikace nejrůznějších parametrů, které se mohou stát cennými biomarkery v diagnostice a sledování vývoje demyelinizačního onemocnění. V dalších odstavcích pojednáme o vybraných technikách MR zobrazování z hlediska základů techniky a analýzy získaných dat i možností praktického využití u pacientů s RS.

Obr. 1. MR vyšetření na 3T přístroji u 29letého pacienta s klinickým obrazem klinicky izolovaného syndromu (CIS).

Obr. 1a) 3D sekvence FLAIR (fluid attenuated inversion recovery) v sagitální rovině s nálezem periventrikulárního ložiska při trigonu pravé postranní komory (šipka) a dalšího drobnějšího ložiska mozečku (zelená šipka).

Obr. 1b) Rekonstrukce FLAIR obrazu v axiální rovině znázorňující subkortikální lézi vlevo frontálně (šipka).

Obr. 1c) T2 vážený obraz v axiální rovině s nálezem ložiska v levé mozečkové hemisféře (šipka) a v pravém mozečkovém pedunklu (zelená šipka).

Obr. 1d) STIR (short-tau inversion recovery) zobrazení krční míchy v sagitální rovině, šipka označuje míšní ložisko v etáži C2. Ložiska mozečku byla detekována nově v porovnání s minulým vyšetřením, nález tak splňuje kritéria diseminace v prostoru i v čase, což značí progresi CIS do klinicky definitivní roztroušené sklerózy.

Fig. 1. MRI examination on a 3T device in a 29-year-old patient with a clinically isolated syndrome (CIS) clinical image.

Fig. 1a) Fluid attenuated inversion recovery (FLAIR) 3D sequence in the sagittal plane indicating a periventricular plaque near the trigone of the right lateral chamber (arrow) and another smaller plaque of the cerebellum (green arrow).

Fig. 1b) Reconstruction of the FLAIR image in the axial plane showing the subcortical lesion in the left frontal lobe (arrow).

Fig. 1c) T2-weighted image in the axial plane indicating a plaque in the left cerebellar hemisphere (arrow) and in the right cerebellar peduncle (green arrow).

Fig. 1d) STIR (short-tau inversion recovery) imaging of the spinal cord in the sagittal plane, arrow marking the spinal cord plaque at the level of C2. Cerebellar plaques were newly detected in comparison to the previous examination, and the finding thus fulfils the criteria of dissemination in space and time indicating the progression of CIS into clinically definitive multiple sclerosis.

Konvenční techniky

Detekce T2 hyperintenzních ložisek je základem konvenčního radiologického hodnocení MR vyšetření u pacientů s RS nebo s klinicky izolovaným syndromem (CIS), který představuje iniciální stadium demyelinizačního onemocnění [6]. Z hlediska diferenciální diagnostiky a predikce vývoje CIS do klinicky definitivní RS je zásadní zejména zhodnocení počtu a lokalizace ložisek, případně jejich postkontrastního sycení a dynamiky MR nálezu v čase. Tyto atributy jsou součástí původních tzv. McDonaldových kritérií, aktuálně v poslední revizi z roku 2010 s následným upřesněním doporučeními skupiny MAGNIMS pro radiologická diagnostická MR kritéria z 2016 (obr. 1) [7].

I v oblasti těchto tzv. konvenčních technik však dochází k určitému vývoji, v této souvis-

losti je významná zejména otázka senzitivity detekce ložisek. V oblasti zobrazení míchy je kromě T2 zobrazení k dispozici již běžně využívána sekvence STIR (short-tau inversion recovery), která disponuje lepším kontrastním rozlišením demyelinizačních lézí v porovnání s T2 váženým obrazem, a usnadňuje tak jejich detekci [8]. Zejména na 3T MR přístrojích lze s výhodou využít též nové techniky 3D zobrazení sekvencí FLAIR, které disponují vyšší senzitivitou pro detekci demyelinizačních ložisek bílé hmoty mozkové [9].

Další zajímavou možností je zobrazení „double inversion recovery" (DIR). Tato sekvence pomocí dvou inverzních pulzů potlačuje zároveň signál mozkomíšního moku i bílé hmoty mozkové, čímž zvyšuje kontrast mezi bílou hmotou a kortexem [10]. Bylo prokázáno, že tato sekvence vykazuje vyšší senzitivitu pro detekci lézí v bílé hmotě oproti T2 a FLAIR vzhledem k vyššímu kontrastu ložisek vůči okolí, umožňuje též lepší detekci lézí infratentoriálních (obr. 2) [11]. Další výhodou techniky DIR je lepší detekce intrakortikálních lézí [12]. Již delší dobu je z histopatologických studií známo, že kortikální postižení je součástí patofyziologie tohoto onemocnění [13] a pomocí techniky DIR byly kortikální léze prokázány řadou autorů, a to i v nejčasnějších stadiích onemocnění [14] nebo u pacientů bez viditelných lézí v bílé hmotě [15]. Někteří autoři též poukazují na signifikantní korelace počtu kortikálních lézí s tíží kognitivního deficitu u pacientů s RS [16] nebo na korelace s mírou fyzické disability [14].

Na hranici konvenčních technik MR zobrazení lze řadit susceptibilně vážené zobrazení (susceptibility-weighted imaging, SWI). Susceptibilitou označujeme fyzikální vlastnost, která charakterizuje míru magnetizace určitého materiálu v magnetickém poli [17]. Celkovou susceptibilitu mozkové tkáně určuje převážně podíl diamagnetické vody ve tkáni, přítomnost paramagnetického železa, stupeň oxygenace krve v kapilárách a vénách a v neposlední řadě zastoupení diamagnetických složek myelinu [18]. Jednou ze zajímavých možností této techniky je zobrazení centrální venuly v rámci demyelinizačních lézí (obr. 3), což umožňují silně paramagnetické vlastnosti deoxyhemoglobinu v těchto žilních strukturách [19]. Histopatologické studie potvrzují perivenózní lokalizaci demyelinizačních plak [20], v souladu s tím řada studií pomocí SWI zobrazení prokázala přítomnost centrální vény u většiny demyelinizačních ložisek u pacientů s RS
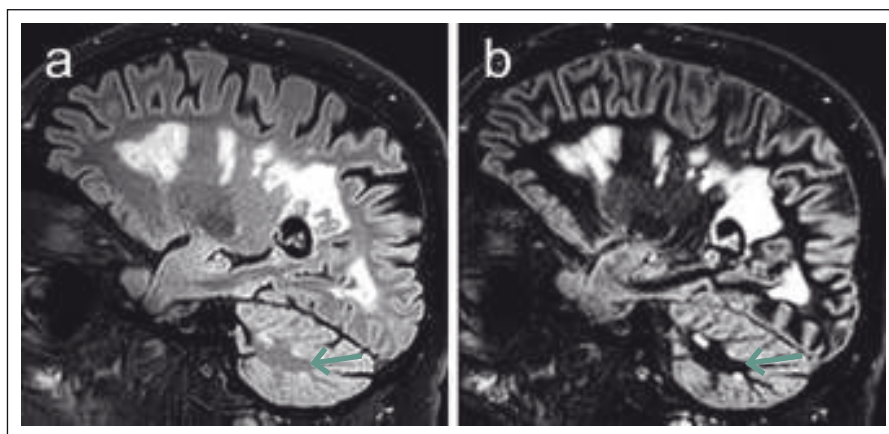
Obr. 2. Srovnání sekvencí 3D FLAIR (fluid attenuated inversion recovery) (a) a DIR (double inversion recovery) (b) u pacienta s pokročilým postižením v rámci roztroušené sklerózy. Obraz DIR disponuje zřetelně lepším kontrastním rozlišením demyelinizačních lézí vzhledem k potlačení signálu normální bílé hmoty. Lépe jsou detekovatelná zejména drobná ložiska mozečku (šipky).
Fig. 2. Comparison of 3D FLAIR (fluid attenuated inversion recovery) (a) and DIR (double inversion recovery) (b). Sequences in a patient with advanced multiple sclerosis disability. The DIR image shows a markedly better contrast resolution of demyelinating lesions due to suppression of the signal of normal white matter. In particular, small cerebellar plaques are better detected (arrows).
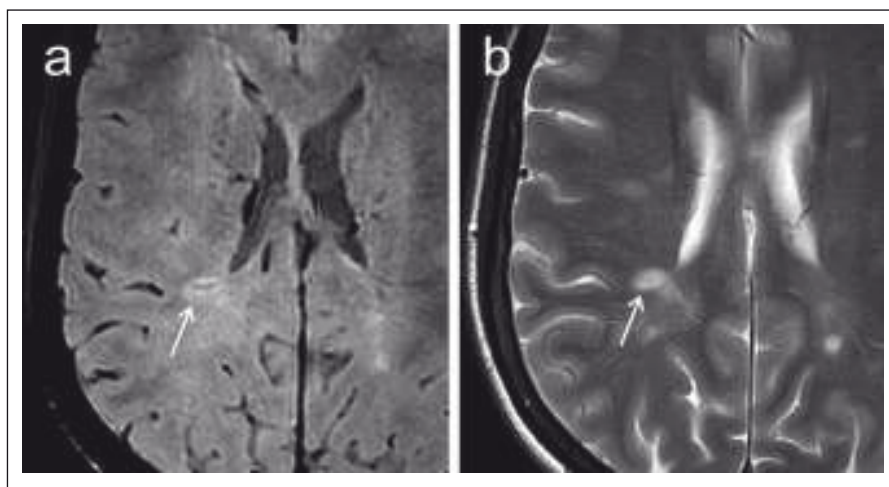
Obr. 3. Porovnání sekvence SWI (susceptibility-weighted imaging) (a) a konvenčního T2 váženého obrazu (b) v axiální rovině u pacientky s roztroušenou sklerózou.
SWI umožňuje zobrazit centrální venulu v rámci periventrikulárního demyelinizačního ložiska (označeno šipkami) v podobě jemného hypointenzního proužku. V T2 obraze centrální venula prakticky není detekovatelná.
Fig. 3. Comparison of the SWI (susceptibility-weighted imaging) (a) sequence and a conventional T2-weighted image (b) in the axial plane in a patient with multiple sclerosis.
SWI allows for displaying the central venule within the periventricular demyelination plaque (marked with arrows) in the form of a tiny hypointense band. In the T2 image the central venule is practically undetectable.

v porovnání s významně menším zastoupením tohoto nálezu u ložisek odlišné etiologie [21,22]. Autoři Tallantyre et al udávají 80% výskyt perivenulárních ložisek ze všech hodnocených T2 hyperintenzních lézí u skupiny

pacientů s RS oproti 19 % u kontrolní skupiny subjektů s T2 hyperintenzními ložisky jiné etiologie. Jako hraniční hodnota pro odlišení pacientů s RS je zde uváděno 40 % perivenulárně lokalizovaných lézí [22]. V další
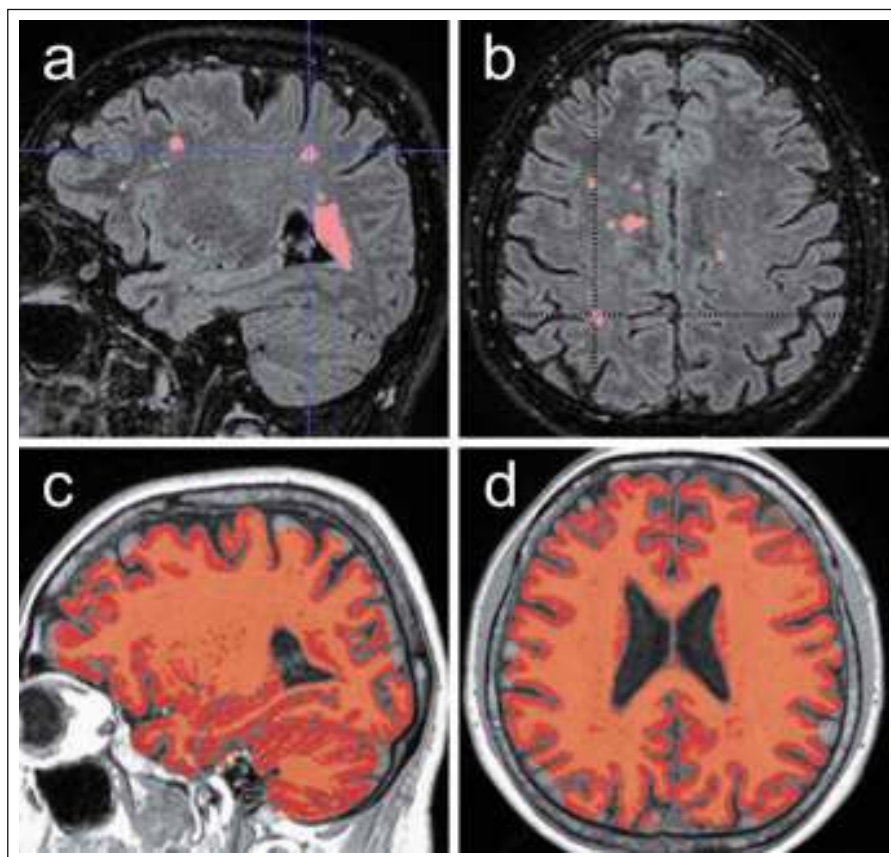
Obr. 4. Ukázka automatizovaného měření objemu T2 hyperintenzních lézí a měření objemu celého mozku.

Obr. 4a, b) Maska segmentace lézí v bílé hmotě mozkové na podkladě rekonstrukce 3D FLAIR (fluid attenuated inversion recovery) zobrazení v sagitální (a) a transverzální (b) rovině. Pro segmentaci je využito několika nástrojů platformy FSL umožňující separátní segmentaci šedé a bílé hmoty mozkové. Za pomocí registrace s normalizovaným obrazem bílé hmoty jsou segmentovány hyperintenzní léze se stanovením jejich celkového objemu [27].

Obr. 4c, d) Maska segmentace celého objemu mozku pomocí aplikace SIENAX. Tento algoritmus vyvinutý pro platformu FSL umožňuje automatizovanou segmentaci celého objemu mozku normalizovaného na velikost hlavy, dále separátní segmentaci a změření objemu šedé a bílé hmoty a objemu kompartmentu mozkomíšního moku [28].

Fig. 4. Demonstration of automated volume measurement of T2 hyperintense lesions and volume measurement of the entire brain.

Fig. 4a, b) Mask of lesion segmentation in white brain matter on the basis of a reconstructed 3D FLAIR (fluid attenuated inversion recovery) display in the sagittal (a) and transversal (b) planes. Several instruments of the FSL platform are used for segmentation, enabling separate segmentation of grey and white brain matter. Using registration with a normalized white matter image, hyperintense lesions are segmented and their total volume is determined [27].

Fig. 4c, d) Segmentation mask of the entire brain volume using the SIENAX application. This algorithm developed for the FSL platform enables automated segmentation of the entire brain volume normalized to head size as well as separate segmentation and measurement of the volume of grey and white matter and volume of the cerebrospinal fluid compartment [28].

práci autorů Kilsdonk et al je dokumentován relativně menší rozdíl v zastoupení lézí s centrální venulou u pacientů s RS (74 %) oproti pacientům s ložisky vaskulární etiologie (47 %). Při stanovení cut-off hodnoty

52 % však při společném hodnocení celkového počtu ložisek a přítomnosti centrální venuly bylo stále možné odlišit jednotlivé etiologicky různé skupiny pacientů se senzitivitou a specificitou 88 % [23]. SWI tak skýtá

určitý potenciál pro odlišení demyelinizačních lézí od ložisek odlišné etiologie, což lze považovat v rámci diagnostiky RS za obecný problém. Zároveň je však třeba říci, že specificita tohoto biomarkeru není doposud zcela ověřena a byla studována jen ve vztahu k omezenému množství patologických stavů mimo RS. Jeho spolehlivost proto musí být ještě ověřena [24]. Praktickému využití této techniky též příliš nepřispívá skutečnost, že je v současnosti doménou převážně experimentálních „high-field" MR přístrojů [25].

Další známkou, kterou lze pozorovat na sekvencích typu SWI, jsou plošné hypointenzity v rámci demyelinizačních lézí nebo jemný hypointenzní lem v periferii ložisek. Tyto nálezy jsou též některými autory uváděny jako relativně specifické pro CIS nebo RS v porovnání s jinými druhy neurologických onemocnění [23,26], ačkoli patofyziologický podklad tohoto jevu není doposud zcela objasněn; zvažován je zejména podíl depozit metabolitů železa, případně i role volných radikálů ve spojitosti se zánětlivým procesem [27].

Volumometrie

V souvislosti s nástupem nových léčebných preparátů jsou vyvíjeny velké snahy najít spolehlivé prognostické markery, pomocí nichž by bylo možné individuálně predikovat budoucí průběh a aktivitu choroby. Jako slibné se v této souvislosti jeví zejména měření počtu a objemu T2 hyperintenzních lézí a kvantifikace stupně mozkové atrofie (obr. 4). Výhodou těchto technik jsou obvykle semiautomatizované postupy a skutečnost, že jsou jako zdrojová data využity konvenční sekvence MR zobrazení, které jsou zároveň použity pro běžné radiologické hodnocení. Pro validní volumometrickou analýzu však i tyto konvenční sekvence musí splňovat určité náležitosti, a to zejména dostatečné prostorové rozlišení; pro účely hodnocení mozkové atrofie je obvykle využívána 3D T1 sekvence gradientního echa s velikostí voxelu kolem 1 mm³. Pro kvantifikaci T2 hyperintenzních lézí lze s výhodou využít 3D FLAIR sekvence turbo-spinového echa s variabilní hodnotou sklápěcího úhlu disponující obdobně vysokým rozlišením [28]. MR protokoly používané pro diagnostiku RS je tedy třeba do určité míry optimalizovat, aby data bylo možné použít pro validní měření objemu. Zejména pro účely longitudinálního sledování vývoje onemocnění u individuálních pacientů je pro dosažení co nejkonzistentnějších výsledků třeba

zdůraznit také potřebu standardizace zobrazovací diagnostiky. Jedná se o provádění kontrolních vyšetření pokud možno na stejném MR přístroji za pomoci standardního diagnostického protokolu a provádění analýz obrazových dat při použití stále stejných softwarových nástrojů. Již v počátku onemocnění může zjištění počtu případně objemu hyperintenzních ložisek v T2 obraze pomoci v odhadu pacientovy prognózy. Samotná přítomnost T2 hyperintenzních ložisek v počátku onemocnění s sebou nese riziko konverze CIS do klinicky definitivní RS v dlouhodobém horizontu v 60–80 % oproti 20% riziku konverze při negativním vstupním MR nálezu [6]. Řada autorů však udává též asociaci počtu a celkového objemu T2 hyperintenzních ložisek detekovaných v počátku onemocnění se zvýšeným rizikem pozdější konverze do klinicky definitivní RS [29].

Podle starších studií při dalším sledování koreluje počet a objem lézí s vývojem dlouhodobé disability již relativně méně. Tento jev je označován jako klinicko-radiologický paradox [30]. Další longitudinální studie nicméně prokázaly korelaci zhoršení klinického stavu v delším časovém období s vyšším počtem a objemem ložisek detekovaných v několika prvních letech onemocnění [31]. Někteří autoři poukazují též na význam objemu T2 hyperintenzních ložisek na vstupním MR vyšetření z hlediska rozvoje krátkodobé disability se zhoršením skóre EDSS (Expanded Disability Status Scale) [32,33]. Dalším parametrem, který lze pomocí výpočetní analýzy obrazu kvantifikovat z konvenčních technik T1 3D zobrazení, je míra mozkové atrofie. Progresivní ztráta objemu mozkové tkáně je obvyklým rysem RS, za níž stojí zejména ztráta myelinu a oligodendrocytů a v neposlední řadě i ztráta neuronů a neuroglie šedé hmoty mozkové [34,35]. Již v roce 1999 autoři Dastidar et al prokázali korelaci objemu kompartmentu mozkomíšního moku vyjadřujícího stupeň atrofie s klinickým skóre EDSS [36]. Mozková atrofie bývá též považována za poměrně časnou známku RS a její vývoj v prvním roce je významným prediktivním faktorem pro budoucí zhoršení [37]. Autoři Minneboo et al poukazují na význam míry atrofie mozku pro predikci vývoje klinického postižení v prvních letech onemocnění RS [32].

Je však třeba se zmínit o tom, že měřené změny objemu mozku nemusí být dány pouze skutečnou atrofií podmíněnou ztrátou mozkové tkáně. V několika studiích byl pozorován pokles objemu mozku přede-

vším v prvním roce imunomodulační léčby oproti kontrolním skupinám. Naopak v druhém a třetím roce byl pozorován protektivní efekt léčby v podobě redukce ztráty objemu mozku [38]; obdobné změny byly patrny též u pacientů léčených natalizumabem [39]. Tento jev, označovaný jako „pseudoatrofie", by mohl být spojen s ústupem edému mozkové tkáně v úvodu léčby a je třeba s ním počítat při interpretaci výsledků studií zkoumajících protektivní účinky léčby u pacientů s RS [40].

Je též známo, že jednotlivé oblasti mozku mohou atrofovat různou rychlostí; např. atrofie corpus callosum, thalamu, hypothalamu, putamen, nucleus caudatus či mozkového kmene se ukázala jako významný prediktor konverze CIS do klinicky definitivní RS [41,42]. Za významné lze považovat zejména změny objemu thalamů a kalózního tělesa. Řada autorů uvádí silné korelace atrofizace thalamu s klinickou progresí onemocnění [43]. Autoři Vaněčková et al udávají atrofii kalózního tělesa v průběhu prvního roku onemocnění jako významný prediktor rozvoje pozdější disability. Pro kvantifikaci je zde využito jednoduché a v praxi aplikovatelné měření plochy kalózního tělesa na sagitálních MR obrazech [44]. Klinický význam atrofie v ostatních zmiňovaných oblastech je třeba ještě ověřit [43].

Regionální změny objemu mozku je obecně možné kvantifikovat pomocí různých více či méně automatizovaných technik. Jako příklad lze uvést volně dostupné softwarové nástroje VBM (voxel-based morphometry) platformy SPM (statistical parametric mapping) [45]. Obdobná je situace v případě volumometrické analýzy celkového objemu mozku, jako příklad automatizovaného řešení umožňujícího stanovení celkového objemu mozku, objemu šedé a bílé hmoty a objemu kompartmentu mozkomíšního moku můžeme uvést software SIENAX [46].

Z výše uvedeného je zřejmé, že kvantifikace počtu a objemu T2 hyperintenzních lézí i měření mozkové atrofie je cenný nástroj umožňující predikovat klinický vývoj u pacientů s RS a sledovat odpověď na léčbu. Tyto techniky tak mají reálnou šanci prosadit se v praxi a stát se standardní součástí MR diagnostiky u pacientů s RS. Většímu praktickému rozšíření těchto metod doposud brání zejména nutnost použití externích softwarových aplikací, což zvyšuje časovou náročnost a celkově v praxi komplikuje hodnocení. Byla by proto žádoucí širší implementace vysoce

automatizovaných softwarových nástrojů do komerčních aplikací využívaných pro rutinní hodnocení MR vyšetření.

Zobrazení difuze

Jako difuze se označuje náhodný pohyb molekul vody ve tkáni označovaný jako tzv. Brownův pohyb. Citlivosti sekvencí spinového i gradientního echa MR zobrazení vůči tomuto jevu lze docílit použitím přídatného magnetického gradientu, jehož charakteristiku (zejm. amplitudu a časový průběh) vyjadřuje tzv. b faktor [47]. Míru difuzivity molekul vody ve tkáni se dá vyjádřit číselně hodnotou ADC (apparent diffusion coefficient). K výpočtu ADC mapy je třeba dvou měření s různou hodnotou b faktoru.

Je známo, že v rámci demyelinizačních lézí dochází ke změnám difuzivity. Autoři Christiansen et al publikovali již v roce 1993 práci analyzující ADC hodnoty u malé skupiny pacientů s RS s nálezem signifikantně vyšších ADC hodnot chronických demyelinizačních lézí v porovnání s normálně vyhlížející bílou hmotou (normal appearing white matter; NAWM), ale též zvýšení ADC hodnot u akutních plak [48]. Obdobně Yurtsever et al udávají zvýšení ADC hodnot u aktivních lézí v porovnání s NAWM [49]. Novější údaje však poukazují na skutečnost, že difuzivita akutních demyelinizačních lézí se rapidně mění zejména v prvních 10 dnech od ataky. Autoři Eisele et al popisují obraz restrikce difuze se snížením ADC hodnot u akutních lézí v rozmezí 0–7 dní od vzniku klinických obtíží, pseudonormalizaci ADC hodnot v 7.–10. dni a zvýšení ADC hodnot v rozmezí 10 dní až 4 týdnů (obr. 5) [50]. Lze tak říci, že změny difuzivity patří do obrazu RS a z pohledu neuroradiologa tak mohou mít určitý význam v diferenciální diagnostice tohoto onemocnění. V neposlední řadě můžeme uvést též změny difuzivity u ložisek progresivní multifokální leukoencefalopatie (PML), která je možnou komplikací u pacientů s RS léčených biologickou léčbou [51].

Technika zobrazení tenzoru difuze (diffusion tensor imaging; DTI) je postavena na principech difuzního MR zobrazení. Klíčovým prvkem je zde však detekce směrové závislosti difuzivity molekul vody ve tkáni v závislosti na směru použitého magnetického gradientu, tzv. anizotropie difuzivity [52]. Tuto směrovou závislost lze charakterizovat pomocí opakovaných měření s proměnnou orientací směru magnetického gradientu. Konečným výsledkem je matematická konstrukce 3D elipsoidu, jehož tvar a orientace
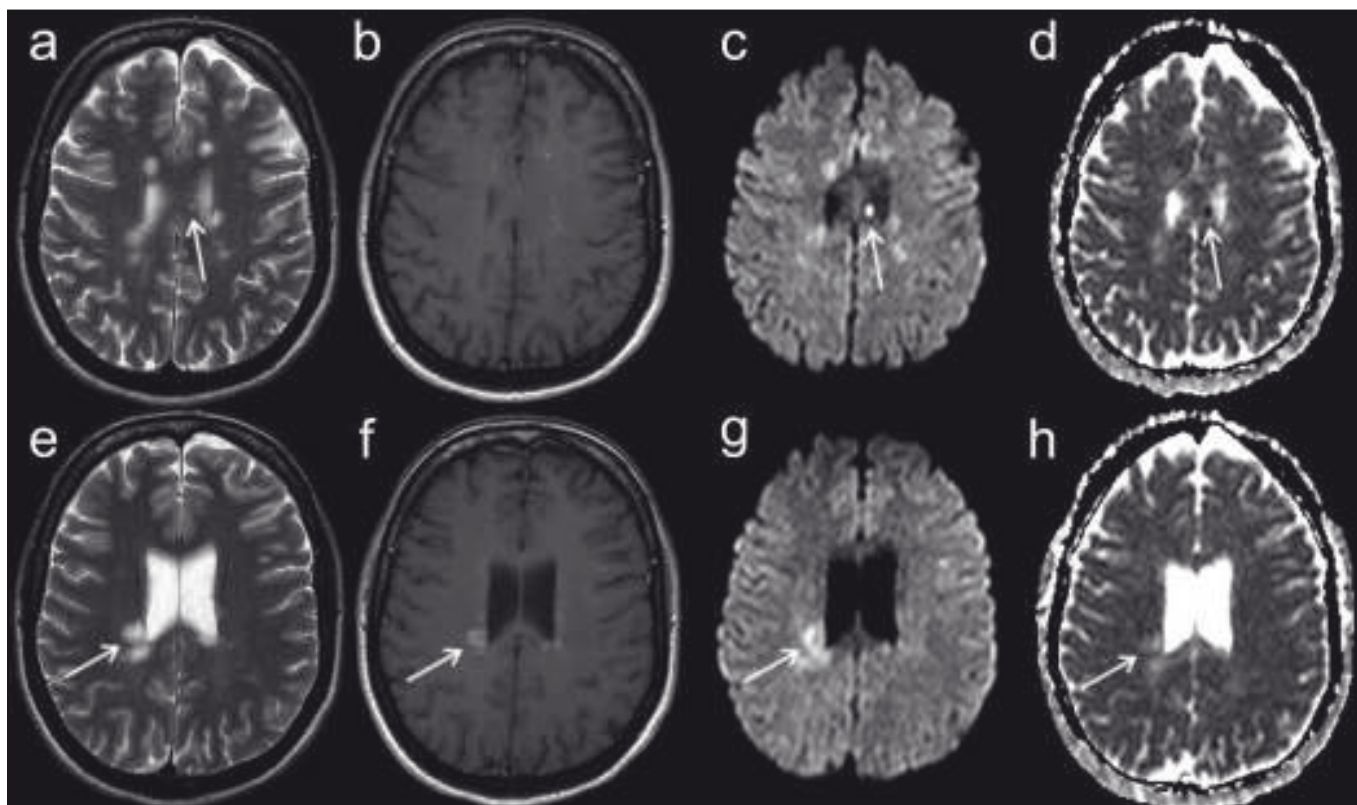
Obr. 5. MR vyšetření pacientky ve věku 39 let s přibližně 8denní anamnézou parestezií končetin.

Obr. 5a, e) T2 vážený obraz.

Obr. 5b, f) T1 obraz po aplikaci kontrastní látky.

Obr. 5c, g) Izotropní zobrazení difuze (b = 1 000 s/mm²).

Obr. 5d, h) Mapa ADC (apparent diffusion coefficient).

MR nález má charakter demyelinizačního onemocnění, splňuje kritéria diseminace v prostoru i v čase. Šipkami jsou označena ložiska s různou mírou difuzivity, u nichž lze proto usuzovat na různé stáří. Drobné ložisko kalózního tělesa (a–d) se postkontrastně nesytí, vykazuje však výraznou restrikci difuze se snížením hodnoty ADC; dle literárních údajů lze odhadovat stáří ložiska na méně než 7 dní. Naopak ložisko vpravo periventrikulárně (e–h) se již postkontrastně sytí a ADC hodnoty jsou zvýšené, tato léze vznikla patrně o několik dní dříve [50].

Fig. 5. MRI examination in a 39-year-old female patient with approximately eight-day history of limb paraesthesia.

Fig. 5a, e) T2-weighted image.

Fig. 5b, f) T1 image after administration of contrast medium.

Fig. 5c, g) Isotropic diffusion-weighted imaging (b = 1,000 sqmm).

Fig. 5d, h) ADC (apparent diffusion coefficient) map.

MRI finding has the character of a demyelinating disease and fulfils the criteria of dissemination in space and time. Arrows indicate plaques with various degrees of diffusivity in which various ages can thus be inferred. A small plaque of a callous body (a–d) does not enhance after contrast medium administration, but does demonstrate substantial restriction of diffusion by decreasing the ADC value. According to the literature, its age can be estimated as less than 7 days. On the other hand, the plaque on the right periventricular (e–h) enhances after contrast medium administration and ADC values are increased. This lesion apparently had formed several days earlier [50].

charakterizují anizotropii difuze v jednotlivých voxelech. Tvar elipsoidu může být popsán pomocí tří hodnot, které reprezentují velikost tří jeho hlavních os. Z těchto parametrů se dá vypočíst několik skalárních veličin, z nichž prakticky nejvýznamnější jsou hodnoty frakční anizotropie (FA) udávající relativní míru anizotropie v daném voxelu a střední difuzivita (mean diffusivity; MD) či ADC, jež vyjadřují celkovou míru difuzivity nezávislé na anizotropii difuze [47].

Bylo zjištěno, že pomocí kvantifikace uvedených skalárních parametrů lze citlivě detekovat strukturální patologii tkání CNS u nejrůznějších onemocnění; zejména index FA je v současnosti považován za parametr senzitivní k narušení integrity bílé hmoty a je také jedním z nejčastěji sledovaných parametrů ve studiích využívajících DTI zobrazení [53]. V minulosti byla publikována celá řada studií využívajících DTI pro detekci patologických změn mozku či míchy u pacientů s RS.

Existují např. důkazy o korelaci parametrů difuzivity s histopatologickými nálezy demyelinizace a axonální dezintegrace [54]. Tyto patologické změny vedou k nárůstu difuzivity napříč nervovými trakty způsobujícímu mimo jiné pokles hodnot parametru FA v důsledku snížené anizotropie difuzivity. V souladu s tím je zjištění, že dochází k signifikantní změně skalárních parametrů difuzivity v rámci T2 hyperintenzních ložisek v porovnání s NAWM [55]. Patrně nejpozo-
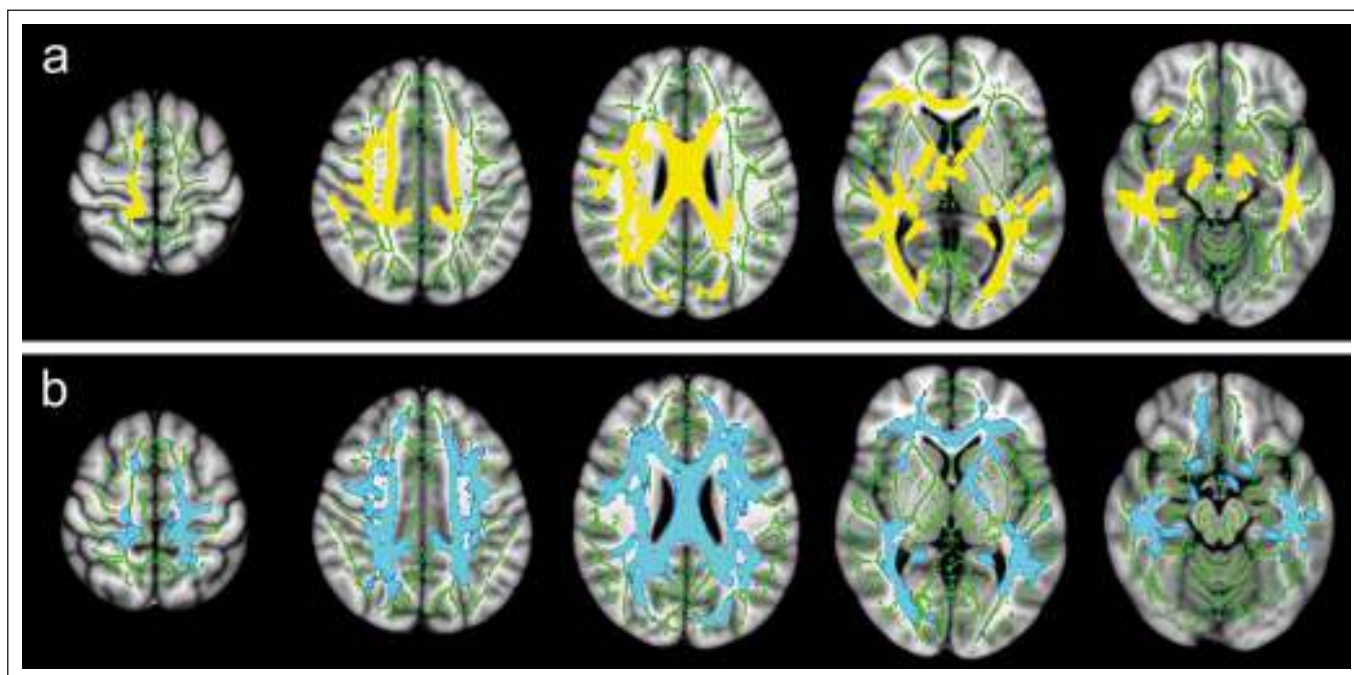
Obr. 6. Statistické „voxel-based" porovnání hodnot frakční anizotropie (FA) (a) a střední difuzivity (MD) (b) mezi skupinou 35 pacientů s klinicky izolovaným syndromem a skupinou 32 zdravých dobrovolníků pomocí aplikace TBSS (Tract-Based Spatial Statistics).
Byly nalezeny rozsáhlé oblasti bílé hmoty se statisticky významným ($p < 0,05$) snížením hodnot FA (žlutě) a zvýšením hodnot MD (modře) u pacientů v porovnání s dobrovolníky. Zelenou barvou je znázorněn průměrný skeleton hlavních traktů bílé hmoty, na který jsou v průběhu zpracování projektovány hodnoty FA a MD jednotlivých subjektů.
Fig. 6. Statistical "voxel-based" comparison of fractional anisotropy (FA) (a) and mean diffusivity (MD) (b) values between a group of 35 patients with clinically isolated syndrome and a group of 32 healthy volunteers using a TBSS (tract-based spatial statistics) application.
Large areas of white matter with statistically significant ($p < 0.05$) decrease in FA values (yellow) and increase in MD values (blue) were recorded in patients as compared to volunteers. Green colour marks the average skeleton of the main tracts of white matter upon which the FA and MD values of the individual subjects are projected during processing.

ruhodnější je skutečnost, že lze prokázat změny difuzivity i v rámci samotné NAWM i NAGM (šedá hmota normálního vzhledu) v poměru se zdravými jedinci [56]. DTI je tak možno vnímat jako citlivější metodu pro detekci patologických změn u pacientů s RS v porovnání s konvenčními technikami MR zobrazení. Někteří autoři poukazují též na korelaci změn difuzivity mozku s tíží klinického postižení např. po stránce motorických [57] či kognitivních [58] funkcí. Technika DTI byla v minulých letech aplikována úspěšně i pro zobrazení míchy u pacientů s RS, kdy byla prokázána korelace parametrů DTI s tíží klinického postižení [59] a obdobně jako v případě mozku je poukazováno na abnormality FA v oblastech míchy bez patologického nálezu na konvenčních sekvencích [60].

Existuje celá řada přístupů k metodice analýzy dat DTI. Za nejjednodušší lze považovat měření parametrů difuzivity v rámci manuálně definovaných oblastí zájmu (region of interest; ROI) ve zvolených oblastech mozku či míchy. Nevýhodu tohoto postupu mohou představovat nepřesnosti v umístění ROI a následné zkreslení výsledků. S tímto problémem se snaží vypořádat některé automatizované techniky analýzy DTI dat, jako je např. TBSS (tract-based spatial statistics). Tato metoda umožňuje analýzu difuzivity v celém měřeném objemu a je vhodná zejména pro skupinové statistické zpracování (obr. 6). Je zde využito nelineární registrace map FA následované konstrukcí skeletonu hlavních traktů bílé hmoty a projekcí voxelů jednotlivých subjektů na tento skeleton. Tím je minimalizováno nechtěné zahrnutí voxelů šedé hmoty do analýzy [61]. V případě zobrazení míchy existuje relativně méně možností výpočetní analýzy obrazových dat. I zde však již bylo popsáno několik technik využívajících semiautomatické či automatické postupy při segmentaci celé míchy nebo šedé a bílé hmoty [62], které mohou být využity i v rámci vyhodnocení difuzních parametrů (obr. 7).

Závěrem této části je třeba poznamenat, že DTI je stále spíše v pozici výzkumné aplikace než prakticky používaného diagnostického nástroje. Jednou z limitací, které brání většímu rozšíření této techniky, je poměrně velká časová náročnost DTI sekvencí. Dalším a patrně významnějším problémem je obecný nedostatek standardizace po stránce vlastní akvizice dat a jejich následné softwarové analýzy. Doposud není zcela vyřešena otázka reprodukovatelnosti měřených skalárních parametrů difuzivity při vyšetřeních na různých přístrojích [63] nebo s nastavením různých akvizičních parametrů [64], což komplikuje porovnávání výsledků různých studií a stanovení obecněji platných prahových hodnot.

Zobrazení magnetizačního transferu

Zobrazení magnetizačního transferu (magnetization transfer imaging; MTI) představuje další metodu, která jde za hranice konvenčních technik MR zobrazení a umožňuje detekovat diskrétní patologické změny tkáně mozku či míchy, k nimž dochází v rámci demyelinizačního onemocnění. Tato technika využívá odlišností v chování volných protonů obsažených v molekulách vody v po-
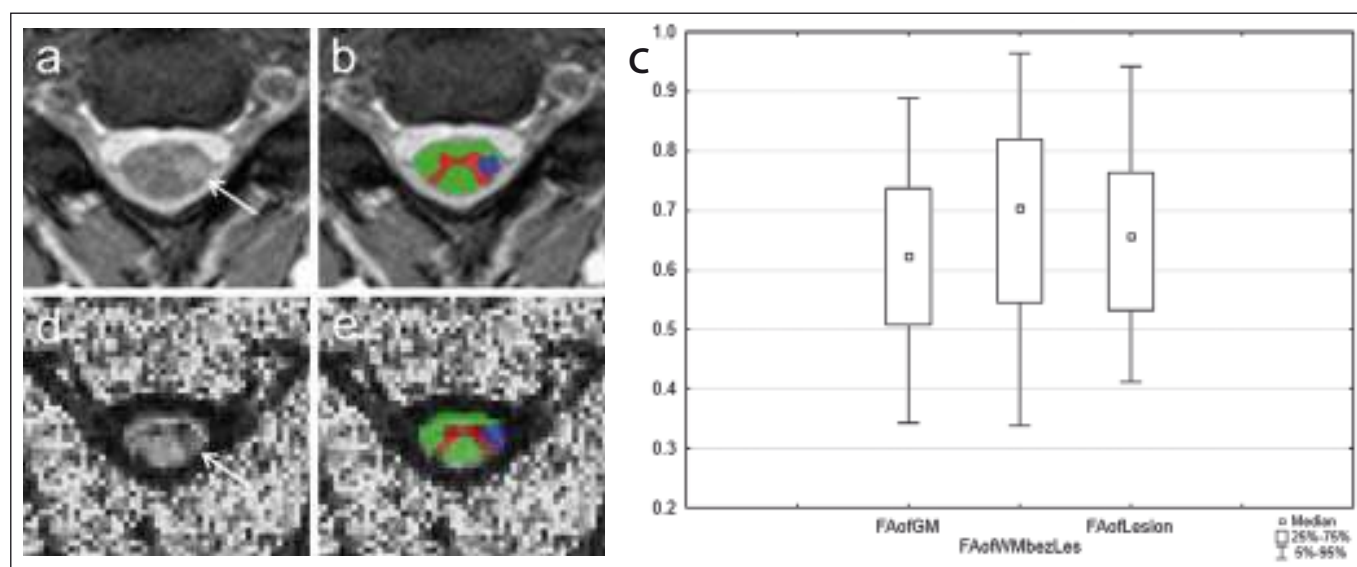
Obr. 7. MR vyšetření u pacienta s roztroušenou sklerózou s hyperintenzním míšním ložiskem patrným na axiálním T2 váženém obraze gradientního echa (šipka na panelu a). Léze je sledovatelná i v obraze zobrazení tenzorů difuze v podobě snížení intenzity signálu na mapě frakční anizotropie (FA) (d).

Obr. 7b, e) Ukázka semiautomatické segmentace bílé hmoty (zeleně), šedé hmoty (červeně) a patologického ložiska (modře) pomocí aplikace ITK-SNAP. Po registraci segmentačních masek mezi T2 a FA obrazem lze kvantifikovat hodnoty FA v jednotlivých tkáních.

Obr. 7c) Rozdíly mezi šedou a bílou hmotou a hyperintenzními ložisky je možné jednoduše graficky vyjádřit pomocí krabicového grafu.

Fig. 7. MRI examination in a patient with multiple sclerosis with a hyperintense spinal cord plaque apparent on the axial T2-weighted image of gradient echo (arrow on panel a). The lesion is perceptible also in the diffusion tensor imaging image in the form of reduced signal intensity on the fractional anisotropy (FA) map (d).

Fig. 7b, e) Demonstration of semi-automatic segmentation of white matter (green), grey matter (red), and pathological plaque (blue) using the ITK-SNAP application. After registering the segmentation masks between T2 and FA images, FA values in the individual tissues can be quantified.

Fig. 7c) Differences between grey and white matter and hyperintense lesions can easily be expressed in a box plot.

rovnání s vázanými protony, u kterých v důsledku magnetických interakcí s okolními makromolekulami dochází k velmi rychlému rozfázování magnetizace a jsou proto charakterizovány velmi krátkými T2 časy. V případě, že jsou vázané protony saturovány pomocí zvláštního saturačního radiofrekvenčního pulzu („off-resonance"), dojde k výměně magnetizace (magnetizačnímu transferu) mezi těmito protony a protony volnými, což ovlivní magnetizaci volných protonů [65]. Tento jev vede k viditelnému snížení intenzity signálu v MR obraze, existují však i možnosti jeho kvantifikace. Patrně nejčastěji používaný a nejjednodušší způsob je využití indexu MTR (magnetization transfer ratio), který představuje relativní rozdíl mezi dvěma měřeními, z nichž pouze u jednoho z nich je aplikován zmiňovaný „off-resonance" saturační pulz. MTR tak nepřímo odráží míru zastoupení makromolekul ve tkáni a umožňuje mimo jiné detekovat ztrátu myelinu a v menší míře axonální dezintegraci [66]. Na využití MTI v diagnostice RS lze nahlížet jako na určitou paralelu DTI.

Byla prokázána redukce MTR akutních i chronických demyelinizačních lézí [67], obdobně jako u DTI byla i v případě MTI zaměřena pozornost na změny v rámci NAWM i NAGM s průkazem signifikantní redukce MTR u nejrůznějších fenotypů RS vč. nejčasnějších klinických stadií [68]. Abnormality MTR též dle některých autorů korelují s délkou trvání onemocnění a s tíží klinického postižení [68,69].

MR spektroskopie
MR spektroskopie je analytická metoda umožňující detekci a kvantifikaci různých sloučenin ve tkáni. K získání MR spektra je možno využít jádra různých prvků, v klinické praxi se však nejčastěji používá jádro vodíku [70]. V praxi se obvykle uplatňuje jedna ze dvou základních technik spektroskopického zobrazení. První z nich je tzv. single-voxel spektroskopie (SVS), která zobrazuje spektrum metabolitů z jediného předem definovaného voxelu. Druhou možností je spektrální akvizice z více voxelů širší oblasti mozku označovaná někdy jako

„magnetic resonance spectroscopy imaging" (MRSI) nebo „chemical shift imaging". Pomocí obou zmiňovaných technik lze detekovat koncentraci nejrůznějších metabolitů v mozkové tkáni, jako jsou např. tuky, aminokyseliny (zejm. alanin, glutamin), laktát, N-acetylaspartát (NAA), kreatin (Cr), a myo-inositol [71].

Pro potřeby diagnostiky pacientů s RS se nejčastěji užívá detekce a kvantifikace NAA, resp. poměru NAA/Cr, dále cholinu, laktátu a myo-inositolu. NAA je obsažen v mitochondriích neuronů, v axonech a dendritech, jeho pokles proto nastává při jejich poškození či zániku. Ke snížení jeho koncentrace ale může dojít i relativně při edému či přechodně při omezení neuronální funkce. Pokles NAA je patrný zejména v akutní fázi onemocnění (obr. 8), během remise potom může docházet k jeho částečné normalizaci. Cholin je za normálních okolností vázán v buněčných membránách, k nárůstu detekovatelné volné porce dochází při rozpadu buněk. K tomu může docházet např. při zánětu, tedy i v pří-
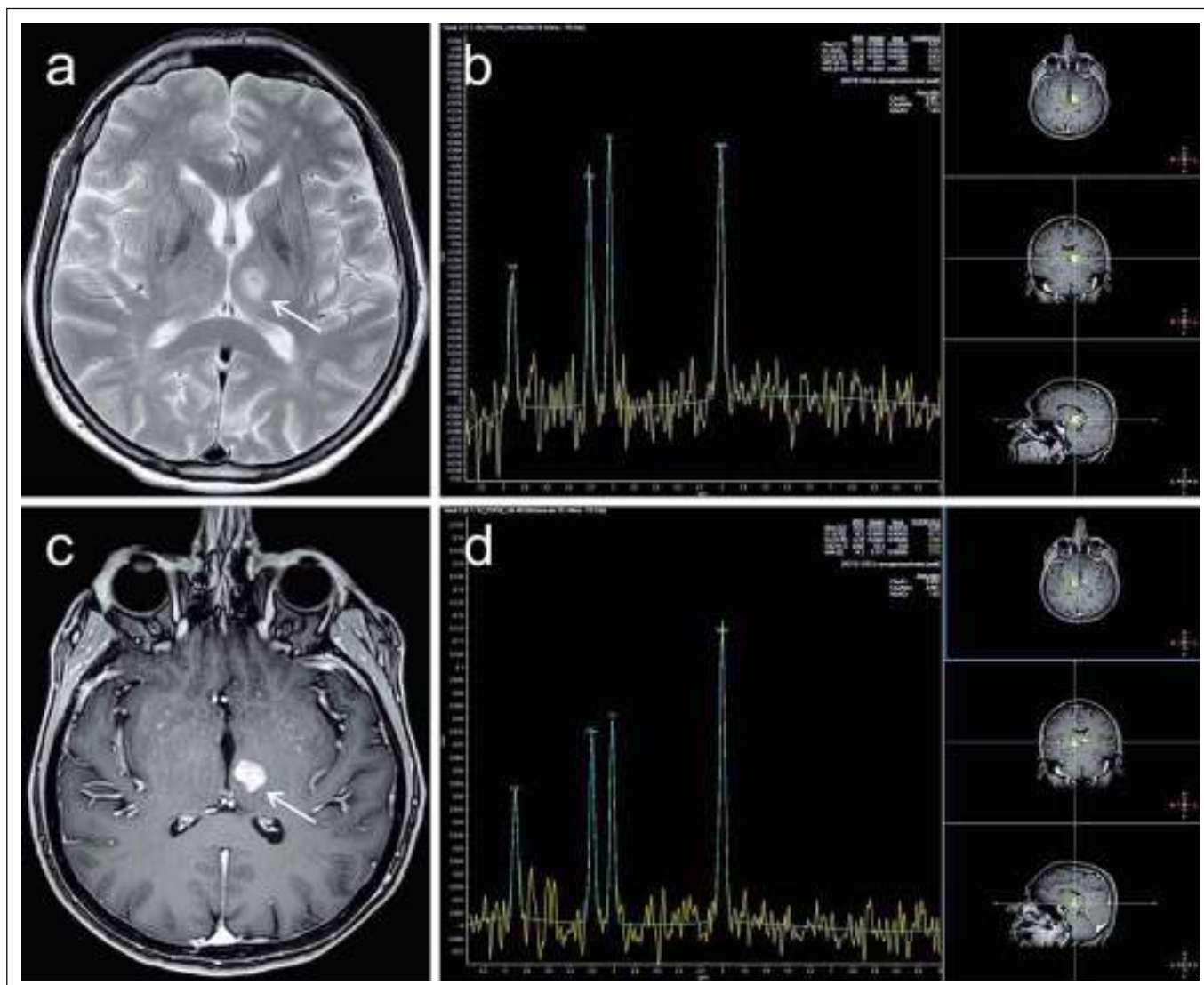
Obr. 8. MR vyšetření pacientky ve věku 67 let léčené pro roztroušenou sklerózu od roku 1991 indikované pro zhoršení pravostranné hemiparézy s přechodnou afázii. Pro upřesnění diferenciální diagnózy atypického ložiska levého thalamu (označeno šipkami) bylo provedeno též spektroskopické vyšetření technikou „single-voxel".

Léze má převážně vysoký signál v T2 obraze (a), postkontrastně se intenzivně sytí prakticky v celém objemu (c). Spektroskopie v oblasti ložiska (b) prokazuje relativní snížení koncentrace N-acetylaspartátu (NAA) vůči kreatinu (Cr) (NAA/Cr = 1,24) v porovnání s normálním spektrem získaným při kontrolním měření v oblasti kontralaterálního thalamu (NAA/Cr = 1,62) (d).

Absence elevace koncentrace cholinu svědčí proti tumoróznímu původu ložiska, jako nejpravděpodobnější etiologie je označena aktivní demyelinizační plaka. V korelaci s tím došlo na kontrolním vyšetření za 2 týdny k významné regresi T2 hyperintenzity i postkontrastního sycení.

Fig. 8. MRI examination in a 67-year-old female patient treated for multiple sclerosis since 1991, indicated for deterioration of right-side hemiparesis with transient aphasia. To increase the accuracy of differential diagnosis of an atypical focal lesion of the left thalamus (marked with arrows) a spectroscopic "single-voxel" examination was also performed.

The lesion has predominantly a high signal in the T2 image (a) and enhanced practically in its entire volume after contrast medium administration (c). Spectroscopy in the area of the lesion (b) demonstrates a relative decrease in N-acetylaspartate (NAA) to creatine (Cr) ratio (NAA/Cr = 1.24) in comparison to the normal spectrum obtained in a control measurement in the area of the contralateral thalamus (NAA/Cr = 1.62) (d). Absence of an elevated choline concentration reduces the probability that the lesion is of tumorous origin. Active demyelinating plaque is marked as the most probable aetiology. In correlation with this, at a follow-up examination 2 weeks later, a substantial regression of T2 hyperintensity and post-contrast enhancement occurred.

padě akutní fáze RS. Obdobně v akutní fázi RS pozorujeme nárůst hodnot laktátu následkem zvýšené anaerobní glykolýzy v terénu zánětu. Bylo zjištěno, že nárůst hodnot

myoinositolu je spojen s vyšší metabolickou či proliferační aktivitou astrocytů v plakách RS na rozdíl od lézí bílé hmoty jiné etiologie [72].

Výsledky studií vč. metaanalýz nejsou zatím jednotné. Přesto naznačují, že by pokles koncentrace NAA mohl být markerem predikce klinického postižení pacientů s RS,

a to zejména u již léčených pacientů vzhledem k jeho částečné normalizaci v průběhu terapie [71,73]. Detekce sníženého obsahu NAA a zároveň zvýšených hodnot cholinu a laktátu se jeví jako potenciální marker akutního postižení bílé hmoty časově předcházející korelát v konvenčním obraze MR [72].

Závěr

Přestože konvenční radiologické hodnocení přítomnosti viditelných lézí mozku a míchy zůstává doposud hlavním nástrojem v oblasti MR diagnostiky RS, existuje nepřeberné množství důkazů o novějších technikách, jako jsou např. DTI, MTI či spektroskopie, které umožňují přesněji detekovat patologické změny tkání CNS. Tyto techniky proto mají potenciál stát se cenným nástrojem v rámci diferenciální diagnostiky v iniciálních stadiích demyelinizačního onemocnění a v dalším průběhu objektivním markerem či prediktorem klinického vývoje a odpovědi na léčbu. Určitou nevýhodou těchto technik jsou nároky na skenovací čas (zejm. DTI a spektroskopie) a obecným problémem výše diskutovaných metod je doposud nedostatek standardizace akvizičních protokolů a v některých případech i omezená reprodukovatelnost měřených dat mezi různými MR přístroji [63]. Dalším aspektem, který do určité míry brání většímu praktickému rozšíření těchto metod, je nejednotnost technik softwarové analýzy naměřených dat a poměrně malá míra implementace automatizovaných technik analýzy obrazu do komerčního softwarového vybavení dodávaného hlavními výrobci MR přístrojů. Budoucí výzkum by proto měl být zaměřen na tyto otázky úzce spojené s technikou vyšetření a na hledání nových dobře reprodukovatelných a kvantifikovatelných parametrů. Půjde-li vývoj tímto směrem, lze v budoucnu očekávat inkorporaci hodnocení těchto nových biomarkerů v rámci standardní diagnostiky u pacientů s RS.

Literatura

1. Confavreux C, Vukusic S, Moreau T, et al. Relapses and progression of disability in multiple sclerosis. N Engl J Med 2000;343(20):1430–8. doi: 10.1056/NEJM200011163432001.
2. Calabrese M, Favaretto A, Martini V, et al. Grey matter lesions in MS: from histology to clinical implications. Prion 2013;7(1):20–7. doi: 10.4161/pri.22580.
3. Filippi M, Agosta F. Imaging biomarkers in multiple sclerosis. J Magn Reson Imaging 2010;31(4):770–88. doi: 10.1002/jmri.22102.
4. van Waesberghe JH, Kamphorst W, De Groot CJ, et al. Axonal loss in multiple sclerosis lesions: magnetic resonance imaging insights into substrates of disability. Ann Neurol 1999;46(5):747–54.
5. Bakshi R, Thompson AJ, Rocca MA, et al. MRI in multiple sclerosis: current status and future prospects. Lancet Neurol 2008;7(7):615–25. doi: 10.1016/S1474-4422(08)70137-6.
6. Miller DH, Chard DT, Ciccarelli O. Clinically isolated syndromes. Lancet Neurol 2012;11(2):157–69. doi: 10.1016/S1474-4422(11)70274-5.
7. Filippi M, Rocca MA, Ciccarelli O, et al. MRI criteria for the diagnosis of multiple sclerosis: MAGNIMS consensus guidelines. Lancet Neurol 2016;15(3):292–303. doi: 10.1016/S1474-4422(15)00393-2.
8. Nayak NB, Salah R, Huang JC, et al. A comparison of sagittal short T1 inversion recovery and T2-weighted FSE sequences for detection of multiple sclerosis spinal cord lesions. Acta Neurol Scand 2014;129(3):198-203. doi: 10.1111/ane.12168.
9. Patzig M, Burke M, Brückmann H, et al. Comparison of 3D cube FLAIR with 2D FLAIR for multiple sclerosis imaging at 3 Tesla. Rofo 2014;186(5):484–8. doi: 10.1055/s-0033-1355896.
10. Redpath TW, Smith FW. Technical note: use of a double inversion recovery pulse sequence to image selectively grey or white brain matter. Br J Radiol 1994;67(804):1258–63. doi: 10.1259/0007-1285-67-804-1258.
11. Wattjes MP, Lutterbey GG, Gieseke J, et al. Double inversion recovery brain imaging at 3T: diagnostic value in the detection of multiple sclerosis lesions. Am J Neuroradiol 2007;28(1):54–9.
12. Geurts JJ, Pouwels PJ, Uitdehaag BM, et al. Intracortical lesions in multiple sclerosis: improved detection with 3D double inversion-recovery MR imaging. Radiology 2005;236(1):254–60. doi: 10.1148/radiol.2361040450.
13. Bø L, Vedeler CA, Nyland HI, et al. Subpial demyelination in the cerebral cortex of multiple sclerosis patients. J Neuropathol Exp Neurol 2003;62(7):723–32.
14. Calabrese M, De Stefano N, Atzori M, et al. Detection of cortical inflammatory lesions by double inversion recovery magnetic resonance imaging in patients with multiple sclerosis. Arch Neurol 2007;64(10):1416–22. doi: 10.1001/archneur.64.10.1416.
15. Calabrese M, Gallo P. Magnetic resonance evidence of cortical onset of multiple sclerosis. Mult Scler 2009;15(8):933–41. doi: 10.1177/1352458509106510.
16. Rinaldi F, Calabrese M, Grossi P, et al. Cortical lesions and cognitive impairment in multiple sclerosis. Neurol Sci 2010;31(Suppl 2):S235–7. doi: 10.1007/s10072-010-0368-4.
17. Liu C, Li W, Tong KA, et al. Susceptibility-weighted imaging and quantitative susceptibility mapping in the brain. J Magn Reson Imaging 2015;42(1):23–41. doi: 10.1002/jmri.24768.
18. Schenck JF. The role of magnetic susceptibility in magnetic resonance imaging: MRI magnetic compatibility of the first and second kinds. Med Phys 1996;23(6):815–50. doi: 10.1118/1.597854.
19. Haacke EM, Mittal S, Wu Z, et al. Susceptibility-weighted imaging: technical aspects and clinical applications, part 1. Am J Neuroradiol 2009;30(1):19–30. doi: 10.3174/ajnr.A1400.
20. Fog T. On the vessel-plaque relationships in the brain in multiple sclerosis. Acta Neurol Scand Suppl 1964;40(Suppl 10):9–15.
21. Mistry N, Dixon J, Tallantyre E, et al. Central veins in brain lesions visualized with high-field magnetic resonance imaging: a pathologically specific diagnostic biomarker for inflammatory demyelination in the brain. JAMA Neurol 2013;70(5):623–8. doi: 10.1001/jamaneurol.2013.1405.
22. Tallantyre EC, Dixon JE, Donaldson I, et al. Ultra-high-field imaging distinguishes MS lesions from asymptomatic white matter lesions. Neurology 2011;76(6):534–9. doi: 10.1212/WNL.0b013e31820b7630.
23. Kilsdonk ID, Wattjes MP, Lopez-Soriano A, et al. Improved differentiation between MS and vascular brain lesions using FLAIR* at 7 Tesla. Eur Radiol 2014;24(4):841–9. doi: 10.1007/s00330-013-3080-y.
24. Enzinger C, Barkhof F, Ciccarelli O, et al. Nonconventional MRI and microstructural cerebral changes in multiple sclerosis. Nat Rev Neurol 2015;11(12):676–86. doi: 10.1038/nrneurol.2015.194.
25. Tallantyre EC, Morgan PS, Dixon JE, et al. A comparison of 3T and 7T in the detection of small parenchymal veins within MS lesions. Invest Radiol 2009;44(9):491–4. doi: 10.1097/RLI.0b013e3181b4c144.
26. Kelly JE, Mar S, D'Angelo G, et al. Susceptibility-weighted imaging helps to discriminate pediatric multiple sclerosis from acute disseminated encephalomyelitis. Pediatr Neurol 2015;52(1):36–41. doi: 10.1016/j.pediatrneurol.2014.10.014.
27. Absinta M, Sati P, Gaitán MI, et al. Seven-tesla phase imaging of acute multiple sclerosis lesions: a new window into the inflammatory process. Ann Neurol 2013;74(5):669–78. doi: 10.1002/ana.23959.
28. Wetter NC, Hubbard EA, Motl RW, et al. Fully automated open-source lesion mapping of T2-FLAIR images with FSL correlates with clinical disability in MS. Brain Behav 2016;6(3):e00440. doi: 10.1002/brb3.440.
29. Odenthal C, Coulthard A. The prognostic utility of MRI in clinically isolated syndrome: a literature review. AJNR Am J Neuroradiol 2015;36(3):425–31. doi: 10.3174/ajnr.A3954.
30. Barkhof F. The clinico-radiological paradox in multiple sclerosis revisited. Curr Opin Neurol 2002;15(3):239–45.
31. Rudick RA, Lee JC, Simon J, et al. Significance of T2 lesions in multiple sclerosis: A 13-year longitudinal study. Ann Neurol 2006;60(2):236–42. doi: 10.1002/ana.20883.
32. Minneboo A, Jasperse B, Barkhof F, et al. Predicting short-term disability progression in early multiple sclerosis: added value of MRI parameters. J Neurol Neurosurg Psychiatry 2008;79(8):917–23. doi: 10.1136/jnnp.2007.124123.
33. Gauthier SA, Mandel M, Guttmann CR, et al. Predicting short-term disability in multiple sclerosis. Neurology 2007;68(24):2059–65. doi: 10.1212/01.wnl.0000264890.97479.b1.
34. De Stefano N, Arnold DL. Towards a better understanding of pseudoatrophy in the brain of multiple sclerosis patients. Mult Scler 2015;21(6):675–6. doi: 10.1177/1352458514564494.
35. Filippi M, Rocca MA, Barkhof F, et al. Association between pathological and MRI findings in multiple sclerosis. Lancet Neurol 2012;11(4):349–60. doi: 10.1016/S1474-4422(12)70003-0.
36. Dastidar P, Heinonen T, Lehtimäki T, et al. Volumes of brain atrophy and plaques correlated with neurological disability in secondary progressive multiple sclerosis. J Neurol Sci 1999;165(1):36–42.
37. Vaněčková M, Seidl Z, Krásenský J, et al. Naše zkušenosti s MR monitorováním pacientů s roztroušenou sklerózou v klinické praxi. Cesk Slov Neurol N 2010;73/106(4):716–20.
38. Zivadinov R, Stosic M, Cox JL, et al. The place of conventional MRI and newly emerging MRI techniques in monitoring different aspects of treatment outcome. J Neurol 2008;255(Suppl 1):61–74. doi: 10.1007/s00415-008-1009-1.
39. Miller DH, Soon D, Fernando KT, et al. MRI outcomes in a placebo-controlled trial of natalizumab in relapsing MS. Neurology 2007;68(17):1390–401. doi: 10.1212/01.wnl.0000260064.77700.fd.
40. Koudriavtseva T, Mainero C. Brain Atrophy as a Measure of Neuroprotective Drug Effects in Multiple Sclerosis: Influence of Inflammation. Front Hum Neurosci 2016;10:226. doi: 10.3389/fnhum.2016.00226.

41. Henry RG, Shieh M, Okuda DT, et al. Regional grey matter atrophy in clinically isolated syndromes at presentation. J Neurol Neurosurg Psychiatry 2008;79(11):1236–44. doi: 10.1136/jnnp.2007.134825.

42. Kalincik T, Vaneckova M, Tyblova M, et al. Volumetric MRI markers and predictors of disease activity in early multiple sclerosis: a longitudinal cohort study. PLoS One 2012;7(11):e50101. doi: 10.1371/journal.pone.0050101.

43. Kaunzner UW, Gauthier SA. MRI in the assessment and monitoring of multiple sclerosis: an update on best practice. Ther Adv Neurol Disord 2017;10(6):247–61. doi: 10.1177/1756285617708911.

44. Vaneckova M, Kalincik T, Krasensky J, et al. Corpus callosum atrophy – a simple predictor of multiple sclerosis progression: a longitudinal 9-year study. Eur Neurol 2012;68(1):23–7. doi: 10.1159/000337683.

45. Mechelli A, Price CJ, Friston KJ, et al. Voxel-based morphometry of the human brain: Methods and applications. Current Medical Imaging Reviews 2005;1(2):105–13.

46. Smith SM, Zhang Y, Jenkinson M, et al. Accurate, robust, and automated longitudinal and cross-sectional brain change analysis. Neuroimage 2002;17(1):479–89.

47. Mukherjee P, Berman JI, Chung SW, et al. Diffusion tensor MR imaging and fiber tractography: theoretic underpinnings. Am J Neuroradiol 2008;29(4):632–41. doi: 10.3174/ajnr.A1051.

48. Christiansen P, Gideon P, Thomsen C, et al. Increased water self-diffusion in chronic plaques and in apparently normal white matter in patients with multiple sclerosis. Acta Neurol Scand 1993;87(3):195–9.

49. Yurtsever I, Hakyemez B, Taskapilioglu O, et al. The contribution of diffusion-weighted MR imaging in multiple sclerosis during acute attack. Eur J Radiol 2008;65(3):421–6. doi: 10.1016/j.ejrad.2007.05.002.

50. Eisele P, Szabo K, Griebe M, et al. Reduced diffusion in a subset of acute MS lesions: a serial multiparametric MRI study. AJNR Am J Neuroradiol 2012;33(7):1369–73. doi: 10.3174/ajnr.A2975.

51. Vaněčková M, Seidl Z, Čáp F, et al. Návrh bezpečnostní MR monitorace u pacientů s roztroušenou sklerózou léčených natalizumabem. Cesk Slov Neurol N 2016;79(6):663–9.

52. Basser PJ, Mattiello J, LeBihan D. MR diffusion tensor spectroscopy and imaging. Biophys J 1994;66:259–67. doi: 10.1016/S0006-3495(94)80775-1.

53. Assaf Y, Pasternak O. Diffusion tensor imaging (DTI)--based white matter mapping in brain research: a review. J Mol Neurosci 2008;34(1):51–61. doi: 10.1007/s12031-007-0029-0.

54. Mottershead JP, Schmierer K, Clemence M, et al. High field MRI correlates of myelin content and axonal density in multiple sclerosis – a post-mortem study of the spinal cord. J Neurol 2003;250(11):1293–301. doi: 10.1007/s00415-003-0192-3.

55. Filippi M, Iannucci G, Cercignani M, et al. A quantitative study of water diffusion in multiple sclerosis lesions and normal-appearing white matter using echo-planar imaging. Arch Neurol 2000;57(7):1017–21.

56. Yu CS, Lin FC, Liu Y, et al. Histogram analysis of diffusion measures in clinically isolated syndromes and relapsing-remitting multiple sclerosis. Eur J Radiol 2008;68(2):328–34. doi: 10.1016/j.ejrad.2007.08.036.

57. Hubbard EA, Wetter NC, Sutton BP, et al. Diffusion tensor imaging of the corticospinal tract and walking performance in multiple sclerosis. J Neurol Sci 2016;363:225–31. doi: 10.1016/j.jns.2016.02.044.

58. Meijer KA, Muhlert N, Cercignani M, et al. White matter tract abnormalities are associated with cognitive dysfunction in secondary progressive multiple sclerosis. Mult Scler 2016;22(11):1429–37. doi: 10.1177/1352458515622694.

59. Valsasina P, Rocca MA, Agosta F, et al. Mean diffusivity and fractional anisotropy histogram analysis of the cervical cord in MS patients. Neuroimage 2005;26(3):822–8. doi: 10.1016/j.neuroimage.2005.02.033.

60. Hesseltine SM, Law M, Babb J, et al. Diffusion tensor imaging in multiple sclerosis: assessment of regional differences in the axial plane within normal-appearing cervical spinal cord. Am J Neuroradiol 2006;27(6):1189–93.

61. Smith SM, Jenkinson M, Johansen-Berg H, et al. Tract-based spatial statistics: voxelwise analysis of multi-subject diffusion data. Neuroimage 2006;31(4):1487–505. doi: 10.1016/j.neuroimage.2006.02.024.

62. De Leener B, Taso M, Cohen-Adad J, et al. Segmentation of the human spinal cord. MAGMA 2016;29(2):125–53. doi: 10.1007/s10334-015-0507-2.

63. Kivrak AS, Paksoy Y, Erol C, et al. Comparison of apparent diffusion coefficient values among different MRI platforms: a multicenter phantom study. Diagn Interv Radiol 2013;19(6):433–7. doi: 10.5152/dir.2013.13034.

64. Santarelli X, Garbin G, Ukmar M, et al. Dependence of the fractional anisotropy in cervical spine from the number of diffusion gradients, repeated acquisition and voxel size. Magn Reson Imaging 2010;28(1):70–6. doi: 10.1016/j.mri.2009.05.046.

65. Henkelman RM, Stanisz GJ, Graham SJ. Magnetization transfer in MRI: a review. NMR Biomed 2001;14(2):57–64.

66. Schmierer K, Scaravilli F, Altmann DR, et al. Magnetization transfer ratio and myelin in postmortem multiple sclerosis brain. Ann Neurol 2004;56(3):407–15. doi: 10.1002/ana.20202.

67. Ropele S, Fazekas F. Magnetization transfer MR imaging in multiple sclerosis. Neuroimaging Clin N Am 2009;19(1):27–36. doi: 10.1016/j.nic.2008.09.004.

68. Filippi M, Rocca MA. Magnetization transfer magnetic resonance imaging of the brain, spinal cord, and optic nerve. Neurotherapeutics 2007;4(3):401–13. doi: 10.1016/j.nurt.2007.03.002.

69. Hayton T, Furby J, Smith KJ, et al. Grey matter magnetization transfer ratio independently correlates with neurological deficit in secondary progressive multiple sclerosis. J Neurol 2009;256(3):427–35. doi: 10.1007/s00415-009-0110-4.

70. Bertholdo D, Watcharakorn A, Castillo M. Brain proton magnetic resonance spectroscopy: introduction and overview. Neuroimaging Clin N Am 2013;23(3):359–80. doi: 10.1016/j.nic.2012.10.002.

71. Aboul-Enein F. MR Spectroscopy in Multiple Sclerosis – A New Piece of the Puzzle or Just a New Puzzle In: Kim DH et al, eds. Magnetic Resonance Spectroscopy. Rijeka (Croatia): InTech 2012:48–72.

72. Ge Y. Multiple sclerosis: the role of MR imaging. AJNR Am J Neuroradiol 2006;27(6):1165–76.

73. Llufriu S, Kornak J, Ratiney H, et al. Magnetic resonance spectroscopy markers of disease progression in multiple sclerosis. JAMA Neurol 2014;71(7):840–7. doi: 10.1001/jamaneurol.2014.895.

ORIGINAL PAPER

Abnormalities in Myelination of the Superior Cerebellar Peduncle in Patients with Schizophrenia and Deficits in Movement Sequencing

Jitka Hüttlova · Zora Kikinis · Milos Kerkovsky ·
Sylvain Bouix · Mai-Anh Vu · Nikos Makris ·
Martha Shenton · Tomas Kasparek

Abstract Deficits in the execution of a sequence of movements are common in schizophrenia. Previous studies reported reduced functional activity in the motor cortex and cerebellum in schizophrenic patients with deficits in movement sequencing. The corticospinal tract (CST) and superior cerebellar peduncle (SCP) are fiber tracts that are involved in movement sequencing. However, the integrity of these tracts has not been evaluated in schizophrenic patients with respect to the performance of movement sequencing yet. Diffusion tensor magnetic resonance images (DT-MRI) were acquired from 24 patients with schizophrenia and 23 matched control subjects. Tractography was applied to reconstruct the CST and SCP and DT-MRI-specific parameters such as fractional anisotropy (FA) and radial diffusivity (RD) were reported. The patient group was further subdivided based on the score of sequencing of complex motor acts subscale of the Neurological Evaluation Scale into those with deficits in sequencing motor acts, the SQ^{abn} group ($n=7$), and those with normal performance, the SQ^{norm} group ($n=17$). Schizophrenia patients of the SQ^{norm} subgroup had significantly reduced FA and increased RD values in the right CST in comparison to the control group; the SQ^{abn} subgroup did not differ from the controls. However, the SQ^{abn} subgroup showed impaired integrity of the left SCP, whereas the SQ^{norm} subgroup did not. Abnormalities in the right CST in the SQ^{norm} and in the left SCP in SQ^{abn} groups suggest that the patients with SQ^{abn}

Jitka Hüttlova and Zora Kikinis, both authors, contributed equally to this work.

J. Hüttlova · T. Kasparek (✉)
Department of Psychiatry, Masaryk University and University Hospital Brno, Jihlavska 20, 625 00 Brno, Czech Republic
e-mail: tomas.kasparek@centrum.cz

J. Hüttlova · T. Kasparek
Behavioral and Social Neuroscience Research Group,
CEITEC-Central European Institute of Technology, Masaryk University, Zerotinovo nam. 9, 601 77 Brno, Czech Republic

Z. Kikinis · S. Bouix · M.-A. Vu · N. Makris · M. Shenton
Psychiatry Neuroimaging Laboratory, Department of Psychiatry, Brigham and Women's Hospital, Harvard Medical School, 1249 Boylston St., Boston, MA 02215, USA

M. Kerkovsky
Department of Imaging Methods, Masaryk University and University Hospital Brno, Jihlavska 20, 625 00 Brno, Czech Republic

N. Makris
Psychiatry and Neurology Departments, Massachusetts General Hospital, Harvard Medical School, 149 Thirteenth Street, Charlestown, MA 02129, USA

M. Shenton
Surgical Planning Laboratory, Department of Radiology, Brigham and Women's Hospital, Harvard Medical School, 1249 Boylston St., Boston, MA 02215, USA

M. Shenton
Clinical Neuroscience Division, Laboratory of Neuroscience, Department of Psychiatry, VA Boston Healthcare System, Harvard Medical School Brockton, 940 Belmont Street, Brockton, MA 02301, USA

represent subgroups with distinct deficits. Moreover, these results demonstrate the involvement of the SCP in the pathogenesis of movement sequencing in schizophrenia.

Introduction

Patients with schizophrenia often have difficulties executing simple repetitive movements, like tapping a rhythm with their hands, or clenching the fist and forming a ring with two fingers in a consecutive manner [1]. These subtle motor deficits are assessed as deficits of sequencing of complex motor acts (the performance of consecutive movements over a period of time) and are a part of the clinical battery tests for neurological soft signs (NSS) [2]. NSS are divided into sequencing of complex motor acts (the performance of consecutive movements over a period of time), motor coordination (the performance of several movements at the same time), and sensory integration (integration of multimodal sensory information). In schizophrenia, sequencing of motor acts is the most frequent impairment assessed by NSS and is present in about 30 % of patients [1]. NSS can be found in non-schizophrenics, but they are more prevalent in schizophrenic patients [1], in subjects at high risk for developing schizophrenia [3, 4], and in antipsychotic-naive first-episode schizophrenic patients [5–8]. NSS is independent of antipsychotic medication or extrapyramidal side effects [5, 9], and so, it has been suggested that these symptoms reflect the basic neurobiology of schizophrenia [10].

Functional neuroimaging studies in schizophrenics with NSS demonstrated a relationship between motor sequencing tasks and the activation of a variety of regions in the brain [11–14]. Using functional magnetic resonance imaging (fMRI), we published on differences in functional connectivity between patients with deficits in sequencing motor acts (SQ^{abn}) and patients with preserved abilities in movement sequencing (SQ^{norm}) [13]. The SQ^{abn} patients showed reduced functional connectivity between the motor cortex and cerebellum, suggesting that the connection between the motor cortex and cerebellum plays a crucial role in executing movement sequences and that this connection is impaired in patients with deficits in sequencing complex motor acts. Cortico-cerebellar connections are important as the cerebellum is not only involved in movement but also in cognitive processes, such as processing and coordinating information [15, 16]. Cognitive processes are often impaired in patients with schizophrenia, and the hypothesis of cognitive dysmetria suggests that these deficits are linked to abnormal connectivity of the cerebellum and the neocortex [11]. The neocortex and cerebellum are connected by the cortico-ponto-cerebello-thalamo-cortical loop (CPCTC-loop) [17–20]. The superior cerebellar peduncle (SCP) is the main efferent fiber leaving the cerebellum and is a component of the CPCTC-loop. Apart of the CPCTC-loop, a second major fiber tract of interest here is the corticospinal tract (CST), which originates in the motor neocortex and is involved in the execution of movement.

The involvement of the cerebellum in the pathology of schizophrenia was not only explored by fMRI studies, but also by volumetric methods and by spectroscopic imaging. Magnetic resonance imaging (MRI) studies reported smaller cerebellar volumes in schizophrenia patients, mainly in the vermis [21, 22] and in the corpus medullare [23]. Additionally, proton magnetic resonance spectroscopic imaging (1H-MRSI) showed decreased level of NAA (N-acetyl-aspartate), a putative neuronal/axonal marker, in the anterior cerebellar vermis in patients with schizophrenia [24]. These studies further support cerebellar dysfunction in pathophysiology of schizophrenia.

The development of the tractography method allows now the reconstruction of specific brain white matter fiber tracts using diffusion tensor magnetic resonance images (DT-MRI) [25–27]. DT-MRI provides a quantitative output of measures such as fractional anisotropy (FA), mean diffusivity (MD), axial diffusivity (AD), and radial diffusivity (RD). FA is a measure of the directionality of water diffusion [28] and has higher values in the white matter (WM) regions with many parallel axons [29]. AD is defined as water diffusion in the direction of the axon and RD as water diffusion orthogonal to the axon, whereas MD describes overall water diffusivity. DT-MRI measures are very sensitive to uncover changes in the white matter in vivo in human subjects, but are not specific in order to describe the biological changes at the cellular level. Interpretation of changes of water diffusivity in biological tissues is based on animal experiments where DT-MRI was acquired and histology performed. In the experiment on mice, damage to the axon resulted in decreased FA and AD, whereas demyelination of the axon resulted in decreased FA and increased RD [30, 31]. Findings from DT-MRI of decreased FA, increased RD, and unchanged AD in patients diagnosed with schizophrenia suggest demyelination of axons in this disease [32–37] and are in accordance with the hypothesis of dysfunctional oligodendrocytes and subsequent abnormal myelination [38–43].

In this study, we follow up on the findings of lower connectivity between the motor cortex and the cerebellum in the SQ^{abn} group in the fMRI study [13] and explore the fiber tracts connecting these regions. We have focused to examine WM integrity of the CST and the SCP, the two major fiber tracts involved in motor execution and planning, in patients with schizophrenia (with and without movement sequencing abnormalities) and matched healthy controls. We anticipate to find changes in WM of the SCP in the SQ^{abn} group that will

correlate to the scores of the sequencing movement test. Based on previously reported changes in Diffusion Tensor Imaging (DTI) measures and demyelination of fiber tracts in schizophrenia patients, we expected to find reduced FA and increased RD in fiber tracts with abnormal WM integrity.

Methods

Subjects

Twenty-four schizophrenic patients and 23 healthy controls matched for age, gender, and handedness participated in this study (Table 1). Patients were recruited from the Department of Psychiatry, Brno, Czech Republic, and were diagnosed with schizophrenia ($n=21$) or schizoaffective disorder ($n=3$) according to DSM-IV criteria and the Mini-International Neuropsychiatric Interview (M.I.N.I.) [44]. Clinical characteristics of the sample are shown in Table 2. All subjects were treated with atypical antipsychotics; none of the subjects had a history of head injury, psychoactive substance dependence, or neurological or systemic illness that might affect imaging measures. Some patients with schizophrenia had neurological soft sign abnormalities, but did not suffer from any neurological disease. There were also no signs of neurological dysfunction during the basic physical and neurological examination.

Healthy controls were recruited from hospital staff and from the general community. They were screened to rule out psychiatric disorders using the M.I.N.I. Exclusion criteria for healthy subjects included a family history of axis I psychiatric conditions, head injury, psychoactive substance dependence, or neurological or systemic illness affecting MRI examination.

The local ethics committee approved the study protocol and procedures. After a complete description of the study, written informed consent was obtained from each subject.

Behavioral Examination

Movement sequencing performance was assessed on the subscale of the NSS using the Neurological Evaluation Scale (NES) [2]. The NES consists of 26 items divided into four subscales: sequencing of complex motor acts (NSS-SQ), motor coordination (NSS-MC), sensory integration (NSS-SI), and "other" (NSS-O). Each item is rated on a scale of 0 to 2 (0=relatively normal, 1=some disruption, 2=major disruption). Patients with schizophrenia were categorized into two subgroups based on the NSS-SQ score. The SQ subscale assesses the ability to perform a sequence of movements using the "fist-ring test" (rapid alternation between clenching the fist and forming a ring using the thumb and forefinger), "fist-edge-palm test" (tapping the desk using the fist, edge of the hand, and palm of the hand), "rhythm tapping test" (reproduction of several rhythms), and the "Ozeretski test" (both hands are placed on the table, one palm down, one palm up, and the subject is asked to simultaneously alternate the position of the hands). Patients with a NSS-SQ score higher than 2 (at least one major disruption) were classified as SQ^{abn}, while patients with a NSS-SQ score ≤ 2 were classified as SQ^{norm}.

Extrapyramidal side effects of antipsychotic medication were evaluated using the Barnes Akathisia Scale (BAS) [45], the Simpson-Angus Scale (SAS) [46], and the Abnormal Involuntary Movement Scale (AIMS) [47].

Magnetic Resonance Imaging and Image Preprocessing

Subjects were scanned using a Philips Achieva 1.5T scanner. Diffusion-weighted images of the whole brain were obtained using an echo-planar imaging single-shot (EPI SSh) DTI sequence: TR 21 s, TE 62 ms, flip angle 90°, voxel size $2\times 2\times 2$ mm, and FOV $224\times 224\times 140$ mm. The magnetic gradient with b-factor 1,000 s/mm2 was applied in 32 directions and b0 image was acquired. For the DTI data acquisition, we

Table 1 Demographic characteristics of patients with schizophrenia and healthy controls

Variable	Patients ($n=24$)	Controls ($n=23$)	Statistical analysis, patients × controls	Patients SQ^{abn} ($n=7$)	Statistical analysis, patients SQ^{abn} × controls	Patients SQ^{norm} ($n=17$)	Statistical analysis, patients SQ^{norm} × controls
Age (years±SD)	32.75 (±9.67)	30.83 (±8.19)	$t=-0.73$; $p=0.47$	36.86 (±6.64)	$t=-1.77$; $p=0.09$	31.06 (±10.37)	$t=-0.08$; $p=0.94$
Gender M/F (n, %)	11 (45 %)/13 (54 %)	11 (48 %)/12 (52 %)	$x^2=0.002$; df=1; $p=0.89$	3 (43 %)/4 (57 %)	$x^2=0.05$; df=1; $p=0.82$	8 (47 %)/9 (53 %)	$x^2=0.00$; df=1; $p=0.96$
Handedness-right handed (n, %)	24 (100 %)	23 (100 %)	–	7 (100 %)	–	17 (100 %)	–

All subjects were right-handed as evaluated by the Neurological Evaluation Scale (NES) 11 subscale for handedness

M male, F female

Table 2 Clinical and pharmacological characteristics of patients with and without movement sequencing abnormalities

Variable	Patients ($n=24$)	Patients SQ^{abn} ($n=7$)	Patients SQ^{norm} ($n=17$)	Statistical analysis, patients $SQ^{abn} \times SQ^{norm}$
Duration of illness (years±SD)	9.70 (±7.64)	13.80 (±7.19)	7.81 (±7.43)	$t=-1.59$; $p=0.13$
Number of episodes	4.21 (±1.98)	5.71 (±1.25)	3.59 (±1.91)	$t=-2.70$; $p=0.01$
Antipsychotic dose (CPZ eq.)	364.50 (±203.14)	360.64 (±195.78)	366.09 (±211.98)	$t=0.06$; $p=0.95$
BAS	0.67 (±1.93)	0.57 (±1.13)	0.71 (±2.20)	$t=0.15$; $p=0.88$
AIMS	0.00	0.00	0.00	–
SAS	1.21 (±1.25)	1.71 (±1.50)	1.00 (±1.12)	$t=-1.29$; $p=0.21$
NSS-SQ (±SD)	2.17 (±2.12)	4.86 (±1.57)	1.06 (±1.03)	$t=-7.04$; $p=0.00$
NSS-SI (±SD)	0.88 (±1.36)	0.29 (±0.76)	1.12 (±1.51)	$t=1.39$; $p=0.18$
NSS-MC (±SD)	0.17 (±0.48)	0.43 (±0.79)	0.06 (±0.24)	$t=-1.79$; $p=0.09$
NSS-O (±SD)	0.75 (±1.30)	0.29 (±0.76)	0.94 (±1.43)	$t=1.14$; $p=0.27$

NSS-T neurological soft signs, total score; *NSS-SQ* NSS, sequencing of complex motor acts; *NSS-SI* NSS, sensory integration; *NSS-MC* NSS, motor; *NSS-T* neurological soft signs, total score; *NSS-SQ* NSS, sequencing of complex motor acts; *NSS-SI* NSS, sensory integration; *NSS-MC* NSS, motor coordination; *NSS-O* NSS, others; *CPZ eq.* chlorpromazine equivalents in mg; *BAS* Barnes Akathisia Scale; *SAS* Simpson-Angus Scale; *AIMS* Abnormal Involuntary Movement Scale

used parallel acquisition technique (SENSE) with reduction factor $p=2$. DICOM data were converted to nrrd files to estimate tensors using the least squares method [48, 49]. Tensor estimation and the following tractography were performed using the 3D Slicer software version 3.6.4-beta (http://www.slicer.org/) [50, 51].

Regions of Interest and Tractography

Diffusion tensor imaging (DTI) data was used to perform region of interest (ROI)-based tractography of the CST and the SCP. Individual ROIs were selected based on the Human White Matter Atlas [52]. ROIs were drawn on color by orientation FA maps. ROIs were overinclusive to prevent the size of the ROI being a limiting factor of the tractography analysis. Tracts were delineated via streamline tractography, which was based on Runge-Kutta protocol [25]. The tracts were reconstructed in a three-dimensional view (Fig. 1) and checked visually for consistency with respect to neuroanatomy, and stray fibers were removed by additional exclusion ROIs. Finally, mean values of FA, MD, AD, and RD were calculated for each tract.

ROIs of the CST The superior inclusion ROI was drawn in the most superior axial slice where the CST is surrounded by the middle cerebellar peduncle and the transverse pontine fibers. The CST runs in the superior-inferior direction, whereas the cerebellar fibers cross the hemispheres. The second inclusion ROI was placed at the most inferior axial slice where the CST are surrounded by the middle cerebellar peduncle and the transverse pontine fibers. To exclude stray tracts crossing the hemisphere, an exclusion ROI was drawn on the midsagittal slice over the corpus callosum (see Supplementary Material a).

ROIs of the SCP The first inclusion ROI was placed at the decussation of the SCP, which appears as a circular red dot surrounded by green voxels on color by orientation FA maps in coronal slices. The ROI was drawn over the red and green area on the two most posterior slices where the decussation was visible. The second inclusion ROI drawn after tracts were seeded from the first ROI. This preliminary tract included the left and right SCP and the medial lemniscus and corticopontocerebellar fibers. Viewing this preliminary tract and the axial slices, we navigated through axial slices inferiorly until the SCP and medial lemniscus separated and then drew an ROI posterior to each of the ventricles to include the left and the right SCP separately. The corticopontocerebellar fibers protrude beyond the thalamus and were excluded by drawing an extensive exclusion ROI in the axial slice above the thalamus (see Supplementary Material b).

Assessment of Reliability of Measures Two raters (J.H. and Z.K.) blind to the diagnosis performed the reliability of the tractography by drawing ROIs manually on a subset of ten images for the SCP and 15 images for the CST. The intraclass correlation coefficient of the FA values were 0.90 (right SCP), 0.97 (left SCP), 0.93 (right CST), and 0.92 (left CST). After the reliability of the method was established, one rater (J.H.) drew ROIs for all the cases.

Statistical Analysis

Statistical analysis was performed using STATISTICA software, version 10 (www.statsoft.com). Descriptive statistics, followed by normality testing using the one-sample Kolmogorov-Smirnov test, were performed, and no significant excursions from normal distribution were detected. Group differences between patients with schizophrenia and

Fig. 1 Reconstruction of the SCP and the CST: tracts of the superior cerebellar peduncle (SCP, *colored pink*), the corticospinal tract (CST, *colored blue*) were reconstructed from DT-MRI using tractography and are viewed from the right (a), respectively, from the posterior (b). The panels c through f show the SCP and the CST tracts from three randomly chosen subjects to demonstrate the reproducibility of the tract's reconstructions. Panel c and d show the tracts reconstructed for the same subject performed each by a different rater. The background is the FA image of the brain of a subject. *A* anterior, *L* left, *P* posterior, *R* right
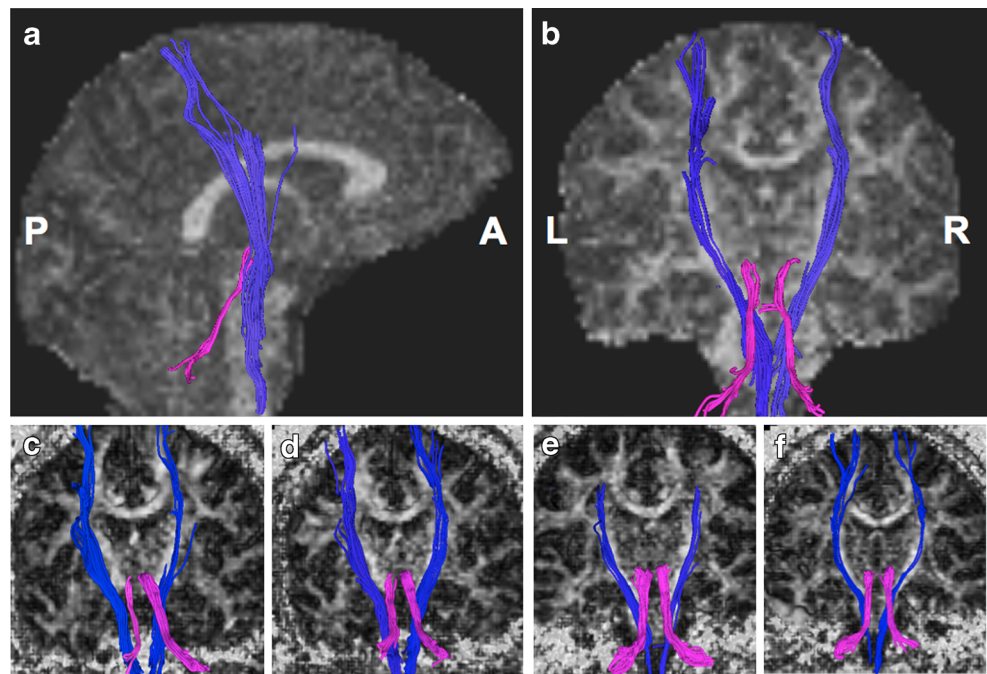
healthy controls in diffusion parameters were tested using a two-tailed two-sample *t* test. The effect of movement sequencing abnormalities was analyzed using one-way Analysis of Variance (ANOVA) with group as a factor (SQ^{norm} patients, SQ^{abn} patients, healthy controls). Between-group differences were tested using post hoc Fisher LSD tests. The confounding effects of demographic and clinical parameters were analyzed using Pearson correlations between the confounders and diffusion parameters. The level of significance was set to alpha <0.05.

Effect size was determined using Cohen's *d* based on the means and the standard deviations of the DTI measures in the CST and SCP. Power was calculated based on an alpha error probability of 0.05 using G*Power3 software [53].

Results

Clinical and Behavioral Characteristics

All four groups, the patients altogether, the SQ^{abn}, and SQ^{norm} subgroups, and the controls, were well matched by age, gender, and handedness (Table 1). The patients altogether and the SQ^{abn} and SQ^{norm} subgroups did not differ in duration of illness, antipsychotic dose, extrapyramidal side effects (scores on BAS, AIMS, SAS), or any of the NSS subscales, except NSS-SQ, which served to divide the patient group (Table 2). The SQ^{abn} group had significantly more episodes than the SQ^{norm} group. Nearly 66 % of the patients expressed at least one minor movement sequencing abnormality (not reported

here), whereas 29 % of the patients, seven out of 24, had major deficits in NSS-SQ (score>2) and were classified as the SQ^{abn} subgroup.
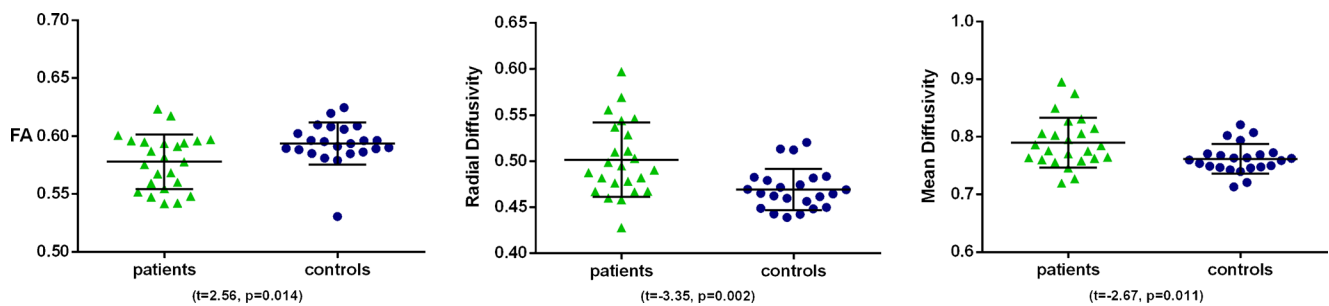
Group Differences in Tractography Measures

There were significant differences between healthy controls and patients with schizophrenia in the right hemisphere of the CST (Fig. 2). We found significantly lower FA (t=2.56, p=0.014) and higher MD (t=−2.67, p=0.011) and RD (t=−3.35, p=0.002) values in the patients compared with controls. No statistically significant group differences were found for the SCP.

The Effect of Movement Sequencing Abnormalities

ANOVA showed a significant effect of group in the CST on the right hemisphere for FA (F=4.89, p=0.012), MD (F=4.76, p=0.013), and RD (F=8.04, p=0.001) values (Fig. 3). Post hoc analysis revealed that only the SQ^{norm} group had significantly lower FA (p=0.003) values and higher MD (p=0.004) and RD (p=0.000) values than healthy controls, whereas SQ^{abn} patients did not differ statistically from the two other groups.

Conversely, for the SCP, ANOVA showed a statistical significance of group at trend levels for the effect of the fiber tract for MD (F=2.67, p=0.080) and RD (F=2.82, p=0.070) values (Fig. 4). Post hoc analysis revealed statistically significant differences between SQ^{abn} patients and healthy controls in the left SCP (MD, p=0.029; RD, p=0.023), whereas

Fig. 2 Results of tractography of the CST. Tractography shows significant group difference in DT-MRI parameters (FA, RD, MD) in the right CST between patients with schizophrenia and healthy controls. *CST* corticospinal tract, *FA* fractional anisotrophy, *RD* radial diffusivity, *MD* mean diffusivity. Unit of RD, MD values 10^{-3} mm²/s. The presentation of *scattered dots* is a graphical choice, so their distribution along the *x*-axis is not relevant

SQ^norm did not differ from the control group. Finally, SQ score correlated positively with the SCP RD ($r=0.42$, $p=0.042$) and MD ($r=0.41$, $p=0.045$) measures in the patient group (Fig. 5), supporting a link between the severity of the motor symptoms and the impairments of the SCP integrity.

Effect Size and Power Analysis

Because of the small numbers of subjects per group, we calculated the effect size and power. Power analysis indicated a chance higher than 80 % of detecting large effect sizes (defined by Cohen 1992) [54] in each individual tract between the groups compared, significant at the 0.05 level, one-tailed. The analysis for the right CST between healthy controls and patients with schizophrenia indicated a large effect (Cohen's $d=0.8$) and a power (1-β) of 84 %, for the right CST between healthy controls and SQ^norm patients indicated a large effect (Cohen's $d=1.1$) and a power of 96 %, for the left SCP between healthy controls and SQ^abn patients indicated a large effect (Cohen's $d=1.0$) and a power of 85 %.

Confounding Effects

There were no significant correlations between tractography measures and age, illness duration, number of previous psychotic episodes, or daily dose of antipsychotics in chlorpromazine equivalents. There was also no correlation with the measures of extrapyramidal symptoms: BAS, SAS, and AIMS score.

Discussion

The aim of this study was to investigate the integrity of WM tracts involved in the execution and planning of movement in patients with schizophrenia, with and without deficits in movement sequencing, and control subjects. We used MR postprocessing techniques to reconstruct the CST and the SCP from DT-MRI data in these subgroups. Patients with schizophrenia, as one group, showed significantly reduced FA and increased RD values in the right CST, which we
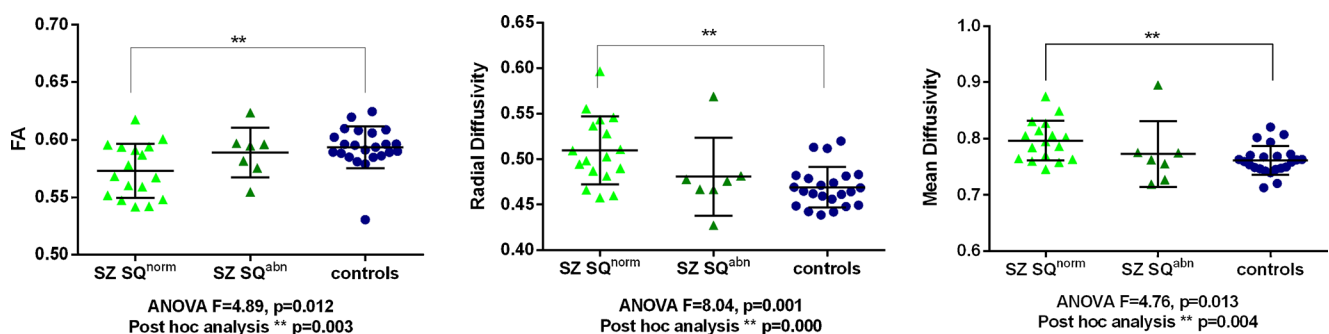
Fig. 3 Effect of movement sequencing abnormalities: CST. Tractography shows significant differences in DT-MRI parameters (FA, RD, MD) in the right CST between patients with and without movement sequencing abnormalities and healthy controls. Post hoc analysis revealed a significant difference among healthy controls and patients without movement sequencing abnormalities. *CST* corticospinal tract, *FA* fractional anisotrophy, *RD* radial diffusivity, *MD* mean diffusivity, *SZ SQ^norm* patients without movement sequencing abnormalities, *SZ SQ^abn* patients with movement sequencing abnormalities. Unit of RD, MD values 10^{-3} mm²/s. **Significant group differences at $p<0.01$
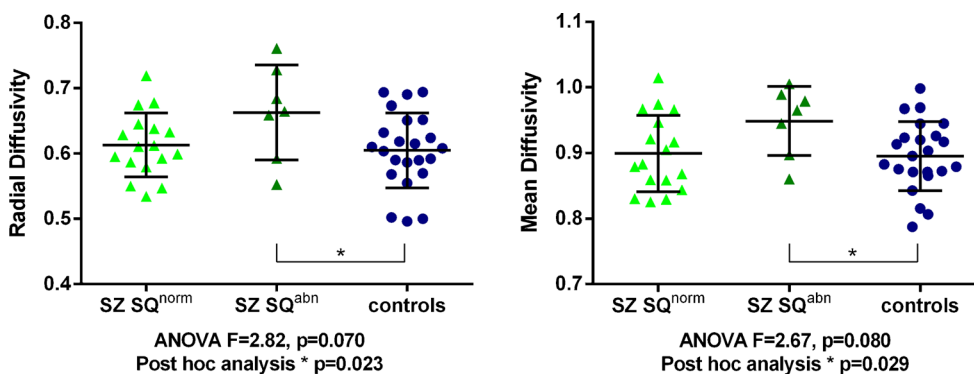
Fig. 4 Effect of movement sequencing abnormalities: SCP. Tractography shows significant differences in DT-MRI parameters (RD, MD) in the left SCP between patients with and without movement sequencing abnormalities and healthy controls. Post hoc analysis revealed significant differences among healthy controls and patients with movement sequencing abnormalities. *SCP* superior cerebellar peduncle, *RD* radial diffusivity, *MD* mean diffusivity, *SZ SQ[norm]* patients without movement sequencing abnormalities, *SZ SQ[abn]* patients with movement sequencing abnormalities. Unit of RD, MD values 10^{-3} mm^2/s. *Significant group differences at $p<0.05$

interpret as impaired integrity of the tract. When patients were divided into SQ[norm] and SQ[abn] subgroups and compared to controls, difference in the right CST were significant only in the SQ[norm] subgroup, whereas the SQ[abn] subgroup did not differ from the controls. Only the SQ[abn] subgroup showed changes in the left SCP in comparison to the control group, whereas the SCP measurements in SQ[norm] were the same as in the controls. The significant changes for SQ[norm] subjects were in the right CST and for SQ[abn] in the left CST. This suggests that schizophrenia patients represent distinct subgroups with neuroanatomical abnormalities in specific fiber tracts.

The CST is involved in the execution of discrete voluntary movement. The CST was previously delineated in healthy subjects [55], in gymnasts [56], and in several patient groups, including acute stroke [57] and amyotrophic lateral sclerosis [58], but not in schizophrenia. Our study is, to the best of our knowledge, the first to report the delineation of the CST in schizophrenic patients using a tractography approach. Nevertheless, previously published DTI studies in schizophrenia, which used whole brain WM analysis, such as tract-based spatial statistics (TBSS) or VBM have reported lower FA in the volume traversed by the CST in both first-episode schizophrenic patients [59, 60] and in patients with adolescent onset of schizophrenia [61, 62]. These reports are in accordance

with our findings. In this study, we went beyond reporting only FA and measured also RD and AD in order to explore microstructural changes in these tracts. To the best of our knowledge, this is the first report of reductions in FA and increases in RD, and no changes in AD reported for the CST in patients with schizophrenia and also in the patient subgroup with SQ[norm]. Similarly, we report increased RD of the SCP in SQ[abn] patients. Increases in RD in the absence of any changes to AD are increasingly being reported in WM in schizophrenia and are interpreted as demyelination of the axon [32–37]. Accordingly, the findings in our study suggest demyelination in the CST and SCP in schizophrenia patients.

The WM tracts of the cerebellum are of interest since the cerebellum is implicated in movement and also in processing and coordinating information as has been mentioned above. The SCP is a component of the cortico-ponto-cerebello-thalamo-cortical loop [17–20], which connects the neocortex and cerebellum. The SCP is the main cerebellar efferent fiber tract originating at the cerebellar dentate nucleus and projecting to the contralateral thalamus [19, 63, 64]. Several studies have found reduced FA values in the SCP of patients with schizophrenia, [65–68] and one study reported no changes [69]. Our study did not reveal any differences in FA or RD values for the SCP in the whole schizophrenia group, nor in

Fig. 5 Correlation between SQ score and MD and RD values in the left SCP in schizophrenia patients. *SCP* superior cerebellar peduncle, *RD* radial diffusivity, *MD* mean diffusivity. Unit of RD, MD values 10^{-3} mm^2/s
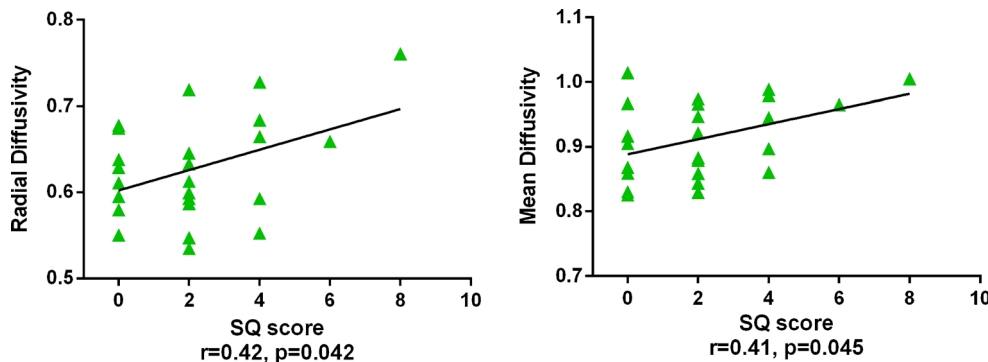
the SQ^{norm} subgroup, but it did reveal significant increases in MD and RD in the left SCP in the SQ^{abn} subgroup. Additionally, the RD and MD values of the SCP correlated positively with SQ score in the patient group, suggesting a relation between the demyelination of the axons of the SCP and the motor symptoms. Based on the findings of impaired integrity of the SCP, we assume deficits of the cortico-ponto-cerebello-thalamo-cortical loop in the SQ^{abn} subgroup. Deficits in the middle cerebellar peduncle, the corticopontine tract, and cortico-thalamic connections were reported in schizophrenia patients using TBSS, a whole brain analysis study [60, 70, 71]. It would be of interest to follow up with a future study to reconstruct the other fibers of the cortico-ponto-cerebello-thalamo-cortical loop in both the SQ^{abn} and the SQ^{norm} patient's group in order to explore whether only the SCP or whether additional fibers of the circuit are impaired.

There are several limitations of our study. First, all the patients were taking antipsychotic medication, and although we controlled for the effect of medication on anatomical connectivity, the approach may not rule out all possible long-term effects. Similarly, the effect of potential progression of the anatomical changes during the course of the illness may bias our results. We were, however, not able to find any correlations between the anatomical connectivity measures and illness duration, age, and the number of previous psychotic episodes. We analyzed only a selected part of the network that is presumably involved in the fine movement processing and timing. We have reconstructed the efferent fiber tract of the cerebellum, the SCP, but did not evaluate the thalamic or the tracts of basal ganglia, which are also involved in movement processing [72–77]. We were not able to explore the structural connectivity of the basal ganglia since our data does not allow the reconstruction of these fiber tracts based on insufficient resolution. Lastly, our study was based on a limited sample size. However, the effect size for our tractography findings suggests substantial differences between the cohorts, and thus, the power of our study is sufficient.

Conclusion

The goal of the present study was to explore whether patients diagnosed with schizophrenia can be subgrouped based on movement sequencing abnormalities assessed both functionally and neuroanatomically. We divided patients in two groups (SQ^{norm} and SQ^{abn}) according to their performance on movement sequencing tests. Tractography of DT-MRI data demonstrated that these two groups differ based on abnormalities of specific WM fiber tracts. When compared to the control group, both groups showed increases in RD and no changes in AD, which suggests demyelination of the tracts, but in the SQ^{norm} group, these changes were found in the right CST, whereas in the SQ^{abn} group, the changes were in the left SCP.

Abnormal SCP in SQ^{abn} subgroup is especially interesting as it demonstrates the involvement of the cerebellar fiber tract in movement sequencing and supports the hypothesis of cognitive dysmetria. The findings of this study may help to dissect schizophrenia, a clinically heterogeneous disorder, into neurobiologically defined subtypes and improve both diagnostics and treatment of individual cases in the future.

References

1. Bombin I, Arango C, Buchanan RW. Significance and meaning of neurological signs in schizophrenia: two decades later. Schizophr Bull. 2005;31(4):962–77.
2. Buchanan RW, Heinrichs DW. The neurological evaluation scale (NES): a structured instrument for the assessment of neurological signs in schizophrenia. Psychiatry Res. 1989;27(3):335–50.
3. Rosso I, Bearden C, Hollister J, Gasperoni T, Sanchez L, Hadley T, et al. Childhood neuromotor dysfunction in schizophrenia patients and their unaffected siblings: a prospective cohort study. Schizophr Bull. 2000;26(2):367–78.
4. Sanders RD, Joo YH, Almasy L, Wood J, Keshavan MS, Pogue-Geile MF, et al. Are neurologic examination abnormalities heritable? A preliminary study. Schizophr Res. 2006;86(1–3):172–80.
5. Cuesta MJ, Campos MS, García-Jalón E, Sánchez-Torres AM, Peralta V. Treatment response of neurological soft signs in drug-naïve patients with a first psychotic episode. Schizophr Res. 2012;139(1):144–50.
6. Madsen A, Vorstrup S, Rubin P, Larsen J, Hemmingsen R. Neurological abnormalities in schizophrenic patients: a prospective follow-up study 5 years after first admission. Acta Psychiatr Scand. 1999;100(2):119–25.
7. Shibre T, Kebede D, Alem A, Kebreab S, Melaku Z, Deyassa N, et al. Neurological soft signs (NSS) in 200 treatment-naive cases with schizophrenia: a community-based study in a rural setting. Nord J Psychiatry. 2002;56(6):425–31.
8. Scheffer RE. Abnormal neurological signs at the onset of psychosis. Schizophr Res. 2004;70(1):19–26.
9. Dazzan P, Murray RM. Neurological soft signs in first-episode psychosis: a systematic review. Br J Psychiatry Suppl. 2002;43:s50–7.
10. Chan R, Xu T, Heinrichs R, Yu Y, Wang Y. Neurological soft signs in schizophrenia: a meta-analysis. Schizophr Bull. 2010;36(6):1089–104.
11. Andreasen NC, Paradiso S, O'Leary DS. "Cognitive dysmetria" as an integrative theory of schizophrenia: a dysfunction in cortical-subcortical-cerebellar circuitry? Schizophr Bull. 1998;24(2):203–18.
12. Chan RC, Rao H, Chen EE, Ye B, Zhang C. The neural basis of motor sequencing: an fMRI study of healthy subjects. Neurosci Lett. 2006;398(3):189–94.
13. Kasparek T, Rehulova J, Kerkovsky M, Sprlakova A, Mechl M, Mikl M. Cortico-cerebellar functional connectivity and sequencing of

movements in schizophrenia. BMC Psychiatry C7 - 17. 2012;12(1): 1–9.

14. Tracy J, Madi S, Faro S, Mohamed P, DelVecchio N, Laskas J. A non-motor sequencing hypothesis for the cerebellum. NeuroImage. 2001;13(6):S1270.

15. Hoppenbrouwers S, Schutter D, Fitzgerald P, Chen R, Daskalakis Z. The role of the cerebellum in the pathophysiology and treatment of neuropsychiatric disorders: a review. Brain Res Rev. 2008;59(1): 185–200.

16. Picard H, Amado I, Mouchet-Mages S, Olie J, Krebs M. The role of the cerebellum in schizophrenia: an update of clinical, cognitive, and functional evidences. Schizophr Bull. 2008;34(1):155–72.

17. He SQ, Dum RP, Strick PL. Topographic organization of corticospinal projections from the frontal lobe: motor areas on the medial surface of the hemisphere. J Neurosci. 1995;15(5 Pt 1):3284–306.

18. Kamali A, Kramer LA, Frye RE, Butler IJ, Hasan KM. Diffusion tensor tractography of the human brain cortico-ponto-cerebellar pathways: a quantitative preliminary study. J Magn Reson Imaging. 2010;32(4):809–17.

19. Kitamura K, Nakayama K, Kosaka S, Yamada E, Shimada H, Miki T, et al. Diffusion tensor imaging of the cortico-ponto-cerebellar pathway in patients with adult-onset ataxic neurodegenerative disease. Neuroradiology. 2008;50(4):285–92.

20. Moritani T, Hiwatashi A, Wang HZ, Numaguchi Y, Ketonen L, Ekholm SE, et al. Anatomy and pathology of the cerebellar peduncle. Neurographics. 2003;2(1):1–9.

21. Nopoulos P, Ceilley J, Gailis E, Andreasen N. An MRI study of cerebellar vermis morphology in patients with schizophrenia: evidence in support of the cognitive dysmetria concept. Biol Psychiatry. 1999;46(5):703–11.

22. Ichimiya T, Okubo Y, Suhara T, Sudo Y. Reduced volume of the cerebellar vermis in neuroleptic-naive schizophrenia. Biol Psychiatry. 2001;49(1):20–7.

23. Thomann P, Roebel M, Dos Santos V, Bachmann S, Essig M, Schroder J. Cerebellar substructures and neurological soft signs in first-episode schizophrenia. Psychiatry Res Neuroimaging. 2009;173(2):83–7.

24. Deicken R, Feiwell R, Schuff N, Soher B. Evidence for altered cerebellar vermis neuronal integrity in schizophrenia. Psychiatry Res Neuroimaging. 2001;107(3):125–34.

25. Basser PJ, Pajevic S, Pierpaoli C, Duda J, Aldroubi A. In vivo fiber tractography using DT-MRI data. Magn Reson Med. 2000;44(4): 625–32.

26. Lebihan D, Breton E. {Imagerie de Diffusion In Vivo par Résonance Magnétique Nucléaire.}. XXX CR Acad Sci Paris. 1985;301:1109–12.

27. Mori S, Crain BJ, Chacko VP, van Zijl PC. Three-dimensional tracking of axonal projections in the brain by magnetic resonance imaging. Ann Neurol. 1999;45(2):265–9.

28. Basser PJ, Mattiello J, LeBihan D. MR diffusion tensor spectroscopy and imaging. Biophys J. 1994;66(1):259–67.

29. Beaulieu C. The basis of anisotropic water diffusion in the nervous system—a technical review. NMR Biomed. 2002;15(7–8):435–55.

30. Song SK, Sun SW, Ju WK, Lin SJ, Cross AH, Neufeld AH. Diffusion tensor imaging detects and differentiates axon and myelin degeneration in mouse optic nerve after retinal ischemia. NeuroImage. 2003;20(3):1714–22.

31. Song SK, Yoshino J, Le TQ, Lin SJ, Sun SW, Cross AH, et al. Demyelination increases radial diffusivity in corpus callosum of mouse brain. NeuroImage. 2005;26(1):132–40.

32. Abdul-Rahman MF, Qiu A, Sim K. Regionally specific white matter disruptions of fornix and cingulum in schizophrenia. PLoS One. 2011;6(4):e18652.

33. Ashtari M, Cottone J, Ardekani BA, Cervellione K, Szeszko PR, Wu J, et al. Disruption of white matter integrity in the inferior longitudinal

fasciculus in adolescents with schizophrenia as revealed by fiber tractography. Arch Gen Psychiatry. 2007;64(11):1270–80.

34. Carletti F, Woolley JB, Bhattacharyya S, Perez-Iglesias R, Fusar Poli P, Valmaggia L, et al. Alterations in white matter evident before the onset of psychosis. Schizophr Bull. 2012;38(6):1170–9.

35. Levitt JJ, Alvarado JL, Nestor PG, Rosow L, Pelavin PE, McCarley RW, et al. Fractional anisotropy and radial diffusivity: diffusion measures of white matter abnormalities in the anterior limb of the internal capsule in schizophrenia. Schizophr Res. 2012;136(1–3):55–62.

36. Seal ML, Yücel M, Fornito A, Wood SJ, Harrison BJ, Walterfang M, et al. Abnormal white matter microstructure in schizophrenia: a voxelwise analysis of axial and radial diffusivity. Schizophr Res. 2008;101(1–3):106–10.

37. Whitford TJ, Kubicki M, Schneiderman JS, O'Donnell LJ, King R, Alvarado JL, et al. Corpus callosum abnormalities and their association with psychotic symptoms in patients with schizophrenia. Biol Psychiatry. 2010;68(1):70–7.

38. Haroutunian V, Davis KL. Introduction to the special section: myelin and oligodendrocyte abnormalities in schizophrenia. Int J Neuropsychopharmacol. 2007;10(4):499–502.

39. Tkachev D, Mimmack ML, Ryan MM, Wayland M, Freeman T, Jones PB, et al. Oligodendrocyte dysfunction in schizophrenia and bipolar disorder. Lancet. 2003;362(9386):798–805.

40. Hakak Y, Walker JR, Li C, Wong WH, Davis KL, Buxbaum JD, et al. Genome-wide expression analysis reveals dysregulation of myelination-related genes in chronic schizophrenia. Proc Natl Acad Sci U S A. 2001;98(8):4746–51.

41. Dracheva S, Davis KL, Chin B, Woo DA, Schmeidler J, Haroutunian V. Myelin-associated mRNA and protein expression deficits in the anterior cingulate cortex and hippocampus in elderly schizophrenia patients. Neurobiol Dis. 2006;21(3):531–40.

42. Hof PR, Haroutunian V, Friedrich VL, Byne W, Buitron C, Perl DP, et al. Loss and altered spatial distribution of oligodendrocytes in the superior frontal gyrus in schizophrenia. Biol Psychiatry. 2003;53(12): 1075–85.

43. Uranova NA, Vostrikov VM, Orlovskaya DD, Rachmanova VI. Oligodendroglial density in the prefrontal cortex in schizophrenia and mood disorders: a study from the Stanley Neuropathology Consortium. Schizophr Res. 2004;67(2–3):269–75.

44. Sheehan DV, Lecrubier Y, Sheehan KH, Amorim P, Janavs J, Weiller E, et al. The Mini-International Neuropsychiatric Interview (M.I.N.I.): the development and validation of a structured diagnostic psychiatric interview for DSM-IV and ICD-10. J Clin Psychiatry. 1998;59 Suppl 20:22–33. quiz 4–57.

45. Barnes TR. A rating scale for drug-induced akathisia. Br J Psychiatry. 1989;154(5):672–6.

46. Simpson GM, Angus JWS. A rating scale for extrapyramidal side effects. Acta Psychiatr Scand. 1970;45(S212):11–9.

47. Guy WA. Abnormal involuntary movement scale (AIMS). ECDEU Assessment Manual for Psychopharmacology, U.S. Department of Health Education and Welfare, Washington, DC (1976) 1976. p. 534–7.

48. Tristán-Vega A, Westin C-F, Aja-Fernández S. Bias of least squares approaches for diffusion tensor estimation from array coils in DT–MRI. In: Yang G-Z, Hawkes D, Rueckert D, Noble A, Taylor C, editors. Medical Image Computing and Computer-Assisted Intervention – MICCAI 2009. Lecture Notes in Computer Science. 5761: Springer Berlin Heidelberg; 2009. p. 919–26.

49. Tristán-Vega A, Aja-Fernández S, Westin C-F. Least squares for diffusion tensor estimation revisited: propagation of uncertainty with Rician and non-Rician signals. NeuroImage. 2012;59(4):4032–43.

50. Pieper S, Halle M, Kikinis R, editors. 3D Slicer. Biomedical imaging: nano to macro, 2004 I.E. International Symposium on; 2004 15–18 April 2004.

51. Pieper S, Lorensen B, Schroeder W, Kikinis R, editors. The NA-MIC Kit: ITK, VTK, pipelines, grids and 3D slicer as an open platform for

the medical image computing community. Biomedical Imaging: Nano to Macro, 2006 3rd IEEE International Symposium on; 2006 6–9 April 2006.

52. Mori S, Wakana S, van Zijl PCM, Nagae-Poetscher LM. MRI atlas of human white matter. Amsterdam: Elsevier Science; 2005. 276 p.

53. Faul F, Erdfelder E, Buchner A, Lang AG. Statistical power analyses using G*Power 3.1: tests for correlation and regression analyses. Behav Res Methods. 2009;41(4):1149–60.

54. Cohen J. Statistical power analysis for the behavioral sciences. Hillsdale: L. Erlbaum Associates; 1988.

55. Kumar A, Juhasz C, Asano E, Sundaram SK, Makki MI, Chugani DC, et al. Diffusion tensor imaging study of the cortical origin and course of the corticospinal tract in healthy children. AJNR Am J Neuroradiol. 2009;30(10):1963–70.

56. Wang B, Fan Y, Lu M, Li S, Song Z, Peng X, et al. Brain anatomical networks in world class gymnasts: a DTI tractography study. NeuroImage. 2013;65:476–87.

57. Vargas P, Gaudron M, Valabrègue R, Bertasi E, Humbert F, Lehéricy S, et al. Assessment of corticospinal tract (CST) damage in acute stroke patients: comparison of tract-specific analysis versus segmentation of a CST template. J Magn Reson Imaging. 2012;37(4):836–45.

58. Ciccarelli O, Behrens TE, Altmann DR, Orrell RW, Howard RS, Johansen-Berg H, et al. Probabilistic diffusion tractography: a potential tool to assess the rate of disease progression in amyotrophic lateral sclerosis. Brain. 2006;129(Pt 7):1859–71.

59. Perez-Iglesias R, Tordesillas-Gutierrez D, Barker G, McGuire P, Roiz-Santianez R, Mata I, et al. White matter defects in first episode psychosis patients: a voxelwise analysis of diffusion tensor imaging. NeuroImage. 2010;49(1):199–204.

60. Ruef A, Curtis L, Moy G, Bessero S, Badan Bâ M, Lazeyras F, et al. Magnetic resonance imaging correlates of first-episode psychosis in young adult male patients: combined analysis of grey and white matter. J Psychiatry Neurosci. 2012;37(4):110057.

61. Douaud G, Mackay C, Andersson J, James S, Quested D, Ray MK, et al. Schizophrenia delays and alters maturation of the brain in adolescence. Brain. 2009;132(9):2437–48.

62. Kyriakopoulos M, Perez-Iglesias R, Woolley JB, Kanaan RAA, Vyas NS, Barker GJ, et al. Effect of age at onset of schizophrenia on white matter abnormalities. Br J Psychiatry. 2009;195(4):346–53.

63. Habas C, Cabanis E. Anatomical parcellation of the brainstem and cerebellar white matter: a preliminary probabilistic tractography study at 3 T. Neuroradiology. 2007;49(10):849–63.

64. Salamon N, Sicotte N, Drain A, Frew A, Alger JR, Jen J, et al. White matter fiber tractography and color mapping of the normal human cerebellum with diffusion tensor imaging. J Neuroradiol. 2007;34(2):115–28.

65. Kanaan R, Borgwardt S, McGuire P, Craig M, Murphy D, Picchioni M, et al. Microstructural organization of cerebellar tracts in schizophrenia. Biol Psychiatry. 2009;66(11):1067–9.

66. Liu H, Fan G, Xu K, Wang F. Changes in cerebellar functional connectivity and anatomical connectivity in schizophrenia: a combined resting-state functional MRI and diffusion tensor imaging study. J Magn Reson Imaging. 2011;34(6):1430–8.

67. Magnotta V, Adix M, Caprahan A, Lim K, Gollub R, Andreasen N. Investigating connectivity between the cerebellum and thalamus in schizophrenia using diffusion tensor tractography: a pilot study. Psychiatry Res Neuroimaging. 2008;163(3):193–200.

68. Okugawa G, Nobuhara K, Minami T, Takase K, Sugimoto T, Saito Y, et al. Neural disorganization in the superior cerebellar peduncle and cognitive abnormality in patients with schizophrenia: a diffusion tensor imaging study. Prog Neuro-Psychopharmacol Biol Psychiatry. 2006;30(8):1408–12.

69. Wang F, Sun Z, Du X, Wang X, Cong Z, Zhang H, et al. A diffusion tensor imaging study of middle and superior cerebellar peduncle in male patients with schizophrenia. Neurosci Lett. 2003;348(3):135–8.

70. Koch K, Wagner G, Dahnke R, Schachtzabel C, Schultz C, Roebel M, et al. Disrupted white matter integrity of corticopontine-cerebellar circuitry in schizophrenia. Eur Arch Psychiatry Clin Neurosci. 2010;260(5):419–26.

71. Okugawa G, Nobuhara K, Sugimoto T, Kinoshita T. Diffusion tensor imaging study of the middle cerebellar peduncles in patients with schizophrenia. Cerebellum. 2005;4(2):123–7.

72. Ivry RB, Spencer RMC. The neural representation of time. Curr Opin Neurobiol. 2004;14(2):225–32.

73. Harrington D, Boyd L, Mayer A, Sheltraw D, Lee R, Huang M, et al. Neural representation of interval encoding and decision making. Cogn Brain Res. 2004;21(2):193–205.

74. Bares M, Lungu O, Husarova I, Gescheidt T. Predictive motor timing performance dissociates between early diseases of the cerebellum and Parkinson's disease. Cerebellum. 2010;9(1):124–35.

75. Bares M, Lungu O, Liu T, Waechter T, Gomez C, Ashe J. The neural substrate of predictive motor timing in spinocerebellar ataxia. Cerebellum. 2011;10(2):233–44.

76. D'Angelo E, Mazzarello P, Prestori F, Mapelli J, Solinas S, Lombardo P, et al. The cerebellar network: from structure to function and dynamics. Brain Res Rev. 2011;66(1–2):5–15.

77. Husarova I, Mikl M, Lungu OV, Marecek R, Vanicek J, Bares M. Similar circuits but different connectivity patterns between the cerebellum, basal ganglia, and supplementary motor area in early Parkinson's disease patients and controls during predictive motor timing. J Neuroimaging. 2013;23(4):452–62.

NEURO

Structural and functional MRI correlates of T2 hyperintensities of brain white matter in young neurologically asymptomatic adults

Miloš Keřkovský[1] · Jakub Stulík[1] · Marek Dostál[1,2] · Matyáš Kuhn[3,4] · Jan Lošák[3] · Petra Praksová[5] · Monika Hulová[5] · Josef Bednařík[5] · Andrea Šprláková-Puková[1] · Marek Mechl[1]

Abstract

Objectives Although white matter hyperintensities (WMHs) are quite commonly found incidentally, their aetiology, structural characteristics, and functional consequences are not entirely known. The purpose of this study was to quantify WMHs in a sample of young, neurologically asymptomatic adults and evaluate the structural and functional correlations of lesion load with changes in brain volume, diffusivity, and functional connectivity.

Methods MRI brain scan using multimodal protocol was performed in 60 neurologically asymptomatic volunteers (21 men, 39 women, mean age 34.5 years). WMHs were manually segmented in 3D FLAIR images and counted automatically. The number and volume of WMHs were correlated with brain volume, resting-state functional MRI (rs-fMRI), and diffusion tensor imaging (DTI) data. Diffusion parameters measured within WMHs and normally appearing white matter (NAWM) were compared.

Results At least 1 lesion was found in 40 (67%) subjects, median incidence was 1 lesion (interquartile range [IQR] = 4.5), and median volume was 86.82 (IQR = 227.23) mm^3. Neither number nor volume of WMHs correlated significantly with total brain volume or volumes of white and grey matter. Mean diffusivity values within WMHs were significantly higher compared with those for NAWM, but none of the diffusion parameters of NAWM were significantly correlated with WMH load. Both the number and volume of WMHs were correlated with the changes of functional connectivity between several regions of the brain, mostly decreased connectivity of the cerebellum.

Conclusions WMHs are commonly found even in young, neurologically asymptomatic adults. Their presence is not associated with brain atrophy or global changes of diffusivity, but the increasing number and volume of these lesions correlate with changes of brain connectivity, and especially that of the cerebellum.

Key Points

• *White matter hyperintensities (WMHs) are commonly found in young, neurologically asymptomatic adults.*
• *The presence of WMHs is not associated with brain atrophy or global changes of white matter diffusivity.*
• *The increasing number and volume of WMHs correlate with changes of brain connectivity, and especially with that of the cerebellum.*

✉ Miloš Keřkovský
    Kerkovsky.Milos@fnbrno.cz

1   Department of Radiology and Nuclear Medicine, The University Hospital Brno and Masaryk University, Brno, Czech Republic

2   Department of Biophysics, Masaryk University, Brno, Czech Republic

3   Department of Psychiatry, The University Hospital Brno and Masaryk University, Brno, Czech Republic

4   Behavioural and Social Neuroscience, CEITEC MU, Brno, Czech Republic

5   Department of Neurology, The University Hospital Brno and Masaryk University, Brno, Czech Republic

Abbreviations

AD   Axial diffusivity
FA   Fractional anisotropy
FFE   Fast field echo
FLAIR   Fluid attenuation inversion recovery
ICC   Interclass correlation coefficient
IQR   Interquartile range
MD   Mean diffusivity
MS   Multiple sclerosis
NAWM   Normally appearing white matter
RD   Radial diffusivity
rs-fMRI   Resting-state functional MRI
TBSS   Tract-based spatial statistics
TE   Echo time
TR   Repetition time
TSE   Turbo spin echo
WM   White matter
WMHs   White matter hyperintensities

Introduction

White matter hyperintensities (WMHs) in T2-weighted MRI images are a common finding in neuroradiology. The prevalence of these lesions in neurologically asymptomatic individuals has been investigated by several authors with rather variable results ranging from 0.5% to more than 95% [1–4]. It is known that the prevalence of WMHs increases with age [5, 6]. Their presence is associated with several diseases or risk factors, such as hypertension [7], cognitive impairment [8, 9], and Parkinson's disease [10]. Comparatively few studies have focused on this finding in the populations under 40 years of age [4, 11]. This topic is interesting not only from the perspectives of aetiology, pathophysiology, and functional relationships of WMHs but also because WMHs constitute an important issue in differential diagnosis of several diseases. One of these is multiple sclerosis (MS), wherein the number and localisation of white matter (WM) lesions become crucial in terms of the McDonald criteria [12]. Because MS usually affects younger patients, investigating incidental WMHs in asymptomatic subjects of corresponding age may be beneficial.

Rapid development of MRI technology and data analysis techniques in recent years has opened up new possibilities for using such advanced methods as functional imaging (fMRI) or diffusion tensor imaging (DTI). The application of these modalities in relation to the presence of WMHs may contribute to knowledge about this topic, because the possible impact of incidentally found WMHs on structural and functional changes of the brain is not entirely known.

In this study, therefore, we set out to quantify the number and volume of WMHs in a sample of young, neurologically intact individuals and to evaluate the correlations between lesion load and changes in brain volume, diffusivity, and functional connectivity.

Methods

The study group included 60 neurologically asymptomatic individuals (21 men and 39 women) who had originally been recruited as a control group in another study concerning patients with demyelinating disease. Their mean age was 34.5 years (SD = 8.3 years) and ranged from 21.4 to 62.1 years. The exclusion criteria, as verified by questionnaire, included history of symptoms suggestive of MS lasting longer than 24 h, such as unilateral visual disturbance, diplopia, vertigo, facial nerve palsy, paresis, or abnormalities of skin sensitivity. Excluded also were those with history or suspicion of meningoencephalitis, stroke or transitory ischemic attack, epilepsy, and systemic inflammatory disease (e.g. systemic lupus erythematosus, rheumatic arthritis, or vasculitis), as well as subjects with known blood relatives suffering from MS. All participants entering the study signed an informed consent and the study was approved by an institutional ethical committee.

MRI brain scan on a 1.5-T scanner (Philips Achieva) was performed on all subjects. The protocol comprised sequences for structural imaging and subsequent volumetric analyses (T2, FLAIR 3D, and T1 3D), as well as DTI and resting-state functional MRI (rs-fMRI) sequences. The imaging protocol is detailed in Table 1. DTI was acquired with b factor 0 and 1000 s/mm^2 using 32 directions of the magnetic gradient; rs-fMRI data were measured at rest and awake for 7 min and 39 s in all subjects. A map of mean signal-to-noise ratio for rs-fMRI data is shown in the electronic supplementary material.

FLAIR images were evaluated in all subjects by two radiologists having more than 12 and 5 years of experience with MRI diagnostics (MK and JS, respectively). They searched for WHMs to differentiate the group of lesion-free individuals from those with at least 1 lesion. The two raters disagreed in four cases. Final decisions were then made by group consensus while including also the other co-authors (AŠ, MM). Both readers also recorded the presence of lesions in different zones of the WM (periventricular, paraventricular, and juxtacortical).

Furthermore, WMHs were segmented manually by MK in 3D FLAIR image using ITK SNAP v.3.4 (http://www.itksnap.org/pmwiki.php). The volume of segmented lesions was established in ITK SNAP and the number of segmented lesions was counted automatically using SPM toolbox function (spm_bwlabel). The latter labels connected areas by analysis of spatial relationships among 18 neighbouring voxels. A cluster of voxels was considered as one lesion if the voxels had mutual contact with at least one side or edge.

WMHs were segmented in ten randomly selected subjects independently by a second reader (JS) using the same methodology. The inter-observer variability as to the number and

Table 1   Parameters of MR imaging protocol

Sequence	Orientation	TR (ms)	TE (ms)	Acquisition voxel size (mm)	Reconstruction voxel size (mm)
T2 TSE	Transverse	4851	110	$0.9 \times 1.12 \times 5$	$0.9 \times 0.9 \times 6$
FLAIR 3D	Sagittal	8000	275	$1.2 \times 1.2 \times 1.4$	$0.7 \times 0.625 \times 0.625$
T1 3D FFE	Transverse	25	4.1	$0.9 \times 0.9 \times 1.6$	$0.84 \times 0.84 \times 0.80$
DTI	Transverse	21,000	62	$2 \times 2 \times 2$	$1.75 \times 1.75 \times 2$
rs-fMRI	Transverse	3000	50	$3.4 \times 3.5 \times 3.8$	$2.85 \times 2.85 \times 3.8$

TSE turbo spin echo, *TR* repetition time, *TE* echo time, *FLAIR* fluid attenuation inversion recovery, *FFE* fast field echo, *DTI* diffusion tensor imaging, *rs-fMRI* resting-state functional MRI

volume of WMHs between the two readers was evaluated by interclass correlation coefficient (ICC) analysis [13].

The number and volume of lesions were compared between males and females (Mann–Whitney U test) and correlated with the age of the subjects (Spearman's rank correlation coefficient).

The total brain volume and volumes of WM and grey matter were estimated with SienaX [14], which is part of FSL [15], using T1-weighted 3D images. The volumes were normalised using SienaX scaling factor to reduce head size–related variability between subjects. Pre-processing included also a lesion-filling procedure as described by Battaglini et al [16] to improve the accuracy of WM volume estimation. The number and volume of WMHs corrected for age and sex of the subjects were correlated with brain volumes using Spearman's rank correlation coefficient.

DTI data processing was done by FSL, starting with eddy current correction and calculation of maps of the following scalar parameters: fractional anisotropy (FA), mean diffusivity (MD), axial diffusivity (AD), and radial diffusivity (RD). The data were analysed by tract-based spatial statistics (TBSS) toolbox to find correlations of the scalar parameters with the number and volumes of lesions, while age and sex were set as further covariates. Furthermore, we registered FLAIR images to B0 images of DTI in individual subjects using linear registration (FSL toolbox FLIRT) and applied the transformation matrices to the segmentation masks of WMHs. We then registered atlas-based masks of WM (MNI 152 standard space) to T1 images in individual subjects using linear and non-linear registration (FSL toolboxes FLIRT and FNIRT) and subsequently registered the resulting WM masks to DTI space. Median values of the aforementioned diffusion parameters were calculated within the segmented lesions and normally appearing white matter (NAWM) in individual subjects and compared mutually using a paired t test. The median diffusion parameters measured within the entire NAWM were also correlated with the number and volume of WMHs using Spearman's rank correlation coefficient.

The rs-fMRI analysis was done using the MATLAB-based CONN toolbox [17]. One hundred twenty-eight regions of interest (ROIs) derived from the software's default brain parcellation atlas were used to extract rs-fMRI signals from various cortical and subcortical areas (average signals from 1-cm-diameter spheres centred at MNI coordinates described in the atlas). The signal denoising consisted in regressing out the movement parameters as well as the signals extracted from the cerebrospinal fluid and WM. This involved motion scrubbing and filtering using a 0.01–0.1-Hz band-pass filter. Using Pearson's correlation coefficient, 128×128 connectivity matrices were created among all the ROI signals. These matrices were used in subsequent analyses for calculating the main effect of the number and volume of WMHs on the connectivity values while correcting for age and sex of the subjects. FDR correction was used to control for the multiple comparisons problem, and thus, statistically significant connections correlating with the lesion load were identified.

Statistical analyses of rs-fMRI data and DTI TBSS analyses were performed using statistical modules of the aforementioned software tools. ICC estimates were calculated using R and irr software (https://CRAN.R-project.org/package=irr), and the remaining statistical tests were computed using Statistica 12 (StatSoft). The significance level for all statistical tests was set to $p < 0.05$.

Results

At least 1 lesion was found in 40 (67%) subjects, and median incidence in all subjects was 1 lesion (interquartile range [IQR] = 4.5) (Fig. 1). Separately in the group of subjects with WMHs, the median incidence was 3 lesions (IQR = 11.5). Results are detailed in Table 2.

At least 1 periventricular, paraventricular, or juxtacortical lesion was found in 11, 32, and 22 subjects, respectively, and in 5 (8.3%) subjects (3 women and 2 men of mean age 40.7 years), we observed simultaneous presence of at least 1 juxtacortical lesion and 1 periventricular lesion. Figure 2 presents a distribution map of the lesions.

ICC analysis of inter-observer variability of WMH segmentations found excellent reliability for the number of lesions (ICC, 0.985; 95% CI, 0.943–0.996), and moderate

a

b
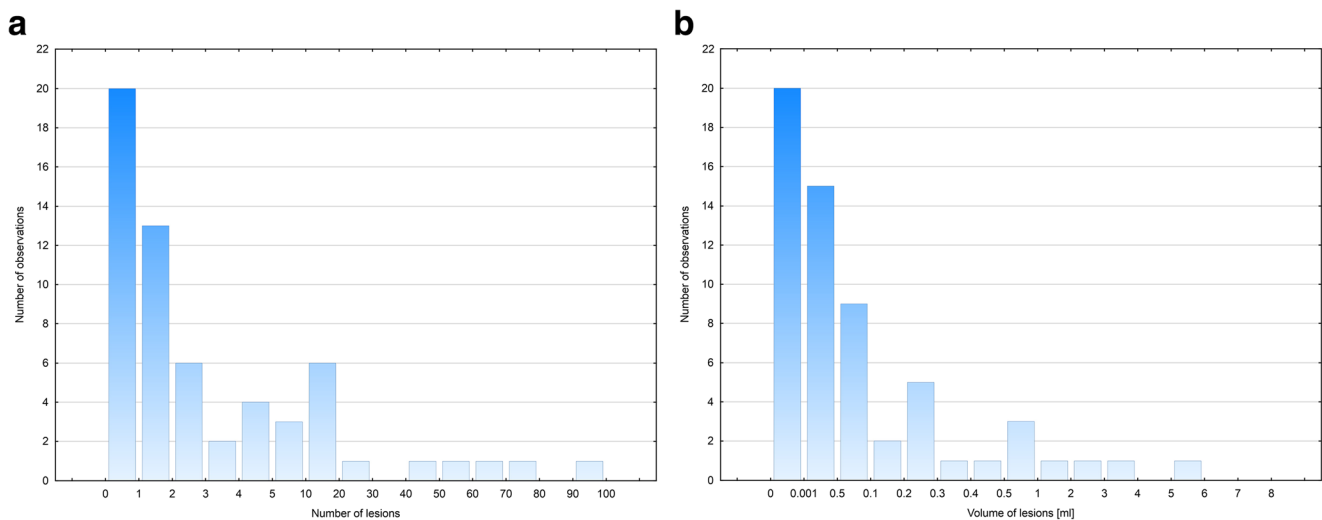
Fig. 1 Histograms demonstrating distribution of the number (**a**) and volume (**b**) of white matter hyperintensities in all subjects

reliability was observed concerning lesion volumes (ICC, 0.621; 59% CI, 0.087–0.887).

In the subgroup of subjects with WMHs, we revealed no statistically significant differences in the number or volume of the lesions or in the mean volume of 1 lesion between males and females. The parameters also did not correlate with the age of the subjects (Fig. 3).

Neither the number nor volume of WMHs correlated significantly with total brain volume or volumes of white and grey matter.

We also found no statistically significant correlation between lesion load and any of the DTI scalar parameters analysed by TBSS. There were no significant differences in diffusivity parameters between men and women; FA correlated negatively with the age of the subjects in extensive areas of WM (data shown in the electronic supplementary material).

Using analysis based upon region of interest, we found significantly higher MD values within WMHs (median 876.5×10^{-6}, IQR 143.5×10^{-6}) compared with all voxels of NAWM (median 745×10^{-6}, IQR 16.5×10^{-6}) by paired t test ($p < 0.0001$). The differences in other diffusion parameters (FA, AD, and RD) were not statistically significant (Fig. 4).

Also, the median values of all measured diffusion parameters of NAWM were not significantly correlated with WMH load.

By analysis of functional connectivity within a matrix of 128×128 connections, we revealed significantly decreased functional connectivity between the cerebellar vermis and right cerebellar hemisphere with the right supplementary motor area in correlation with the number of lesions. Increasing volume of lesions correlated significantly with decreased connectivity between the regions of the right and left cerebellar hemispheres, between the left cerebellum and right caudate nucleus, and between the left postcentral gyrus and right paracingulate gyrus. The connectivity of the left frontal operculum with the right pallidum was significantly increased in correlation with WMH volume (Fig. 5).

Discussion

In this study, we quantified WMHs found in a randomly selected sample of a normal young population and investigated their impacts on various advanced modalities of MRI.

Table 2 Number and volumes of white matter hyperintensities (WMHs) in the group of 40 subjects with at least 1 lesion

Group	Number of WMHs	Volume of WMHs (mm^3)	Mean volume of one lesion (mm^3)
All ($n = 40$)	3 (11.5; 1–96)	86.82 (227.23; 13.12–5920.74)	24.02 (21.53; 10.97–168.98)
Females ($n = 25$)	3 (8; 1–64)	85.59 (225.31; 13.4–5920.74)	21.4 (22.22; 10.97–168.98)
Males ($n = 15$)	2 (20; 1–96)	88.87 (394.02; 13.12–3394.18)	27.69 (17.67; 13.12–44.43)
≤30 (F = 5; M = 6)	2 (19; 1–74)	202.89 (559.86; 13.39–2929.33)	39.59 (25.3; 13.4–168.98)
31–40 (F = 12; M = 4)	4 (8.25; 1–64)	77.11 (93.11; 13.12–1581.28)	16.41 (7.29; 10.97–44.43)
≥41 (F = 8; M = 5)	2 (6; 1–96)	73.28 (235.16; 18.04–5920.74)	31.72 (15.31; 15.7–109.64)

The values are presented as medians along with interquartile range, minimum, and maximum values. The last three rows demonstrate the distribution of lesions across different age groups

WMHs white matter hyperintensities, *F* females, *M* males

**Fig. 2** Overlay of all co-registered segmentation masks of white matter hyperintensities (WMHs) over several axial images reformatted from 3D fluid attenuation inversion recovery. Different colours of the masks mark the areas with multiple occurrences of WMHs (blue = 1, green = 2, orange = 3, and red = 4 lesions)
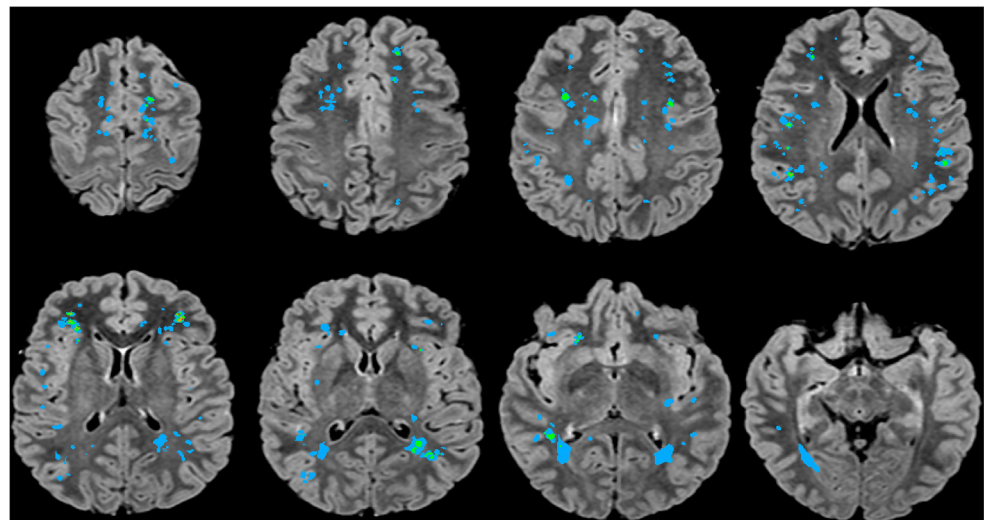

We found relatively high incidence of WMHs, as at least 1 lesion was found in almost 67% of subjects investigated. Although WMHs constitute a commonly reported finding in asymptomatic elderly individuals [5, 6, 18], relatively fewer studies have focused upon this finding in younger populations. Generally lower prevalence is reported among the young. In a retrospective study, Katzmann et al report incidence of WMHs in only 0.5% of 1000 subjects with mean age 30.6 years (range 3–83 years) [2]. Other authors have found WMHs in 5.3% of healthy individuals with mean age 36.95 years (range 16–65 years) [4]. A comparatively higher number of WMHs was reported from a study by Wen et al that had focused upon an asymptomatic population aged 44–48 years. They had used automated segmentation and classification methods to evaluate the presence and location of WMHs, finding these in 50.9% of those subjects investigated [19].

The higher incidence of WMHs in our study may be due to our employing 3D FLAIR imaging sequence or generally by differences in imaging protocols between this study and the previous studies cited. Katzmann et al have not used a standardised imaging protocol evaluating T1- and T2-weighted images, they provide no details about the spatial resolution of the sequences, and proton density images were available only occasionally [2]. Similarly, Hopkins et al evaluated sagittal T1-weighted scans and T2-weighted axial scans obtained with slice thickness of 5-mm and 2-mm interspace gap [4]. Wen et al, who reported considerably higher prevalence of WMHs compared with both aforementioned studies, used FLAIR images acquired on a 1.5-T MR device with slice thickness of 4 mm and fairly high in-plane resolution of 0.898×0.898 mm [19]. On that account, we believe that the imaging protocol may strongly influence the sensitivity for the detection of WMHs, because especially the absence of FLAIR sequence might underestimate the number of periventricular and subcortical lesions. Most other recent studies dealing with WMHs in normal subjects or under various pathological conditions use conventional 2D T2 or FLAIR sequences with slice thickness ranging usually from 3 to 5 mm [19–23]. Inasmuch as there are a few studies reporting higher sensitivity of 3D FLAIR sequences for detecting WM lesions in
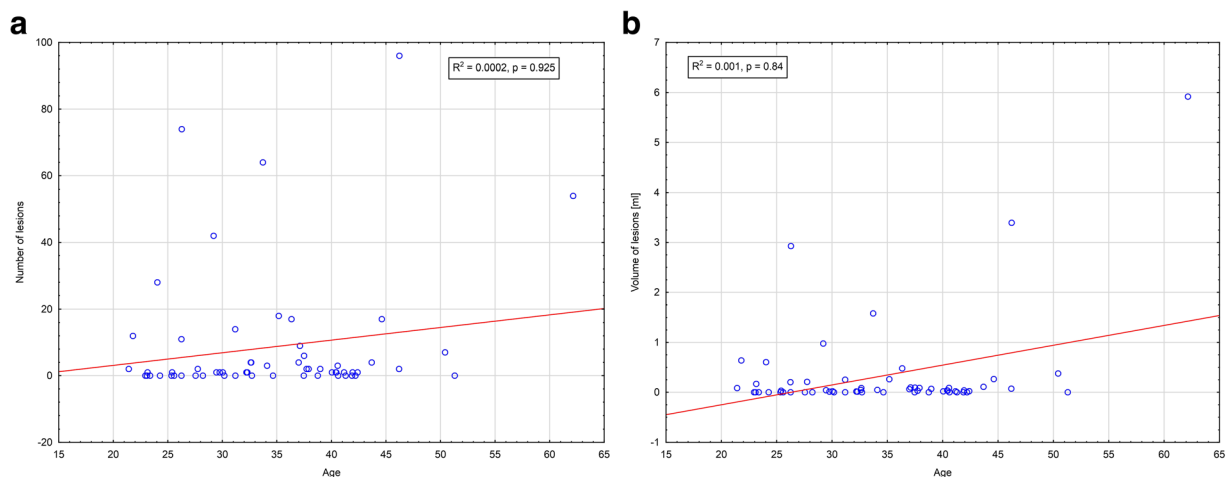
Fig. 3 Graphical representation of the number (**a**) and volume (**b**) of white matter hyperintensities as a function of age in all subjects
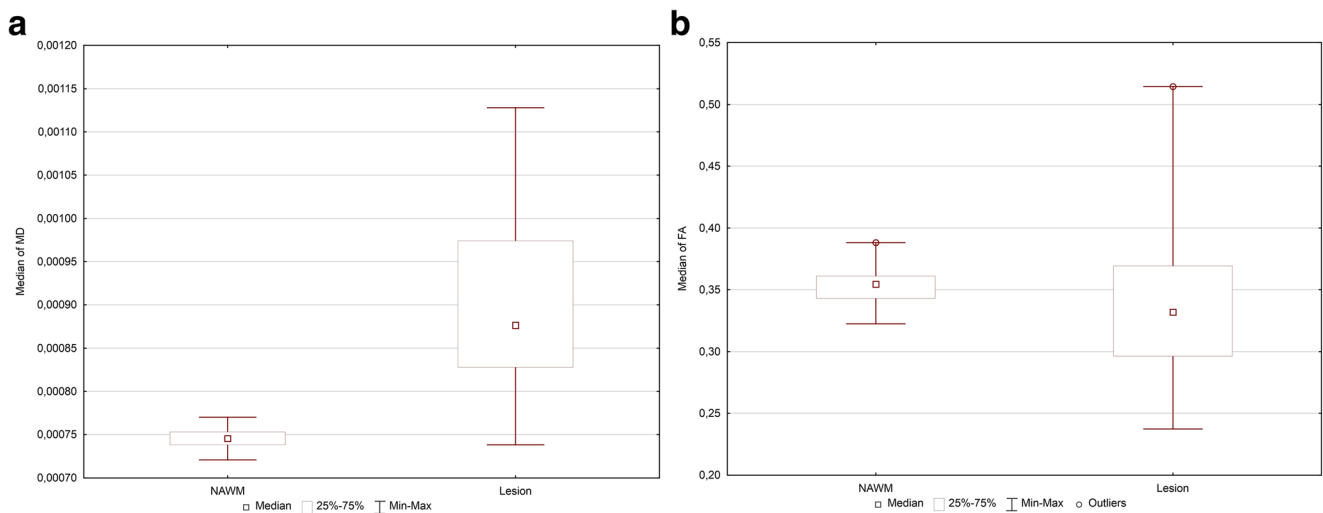
Fig. 4 Boxplot of mean diffusivity (**a**) and fractional anisotropy (**b**) values measured within the voxels of white matter hyperintensities and normally appearing white matter (NAWM). The differences in mean diffusivity values were statistically significant ($p < 0.0001$)

patients with MS [24–26] compared with conventional 2D techniques, we may analogously expect higher sensitivity also in the case of WMHs found incidentally in normal subjects. To our knowledge, however, no previous study has used 3D FLAIR technique in this field. Thus, a study directly

comparing sensitivity of 2D and 3D FLAIR imaging for the detection of WMHs in healthy subjects would be beneficial.

Data about WMH volumes found in healthy populations are not uniform and are less available in the literature, because many authors evaluate only the prevalence of the lesions or
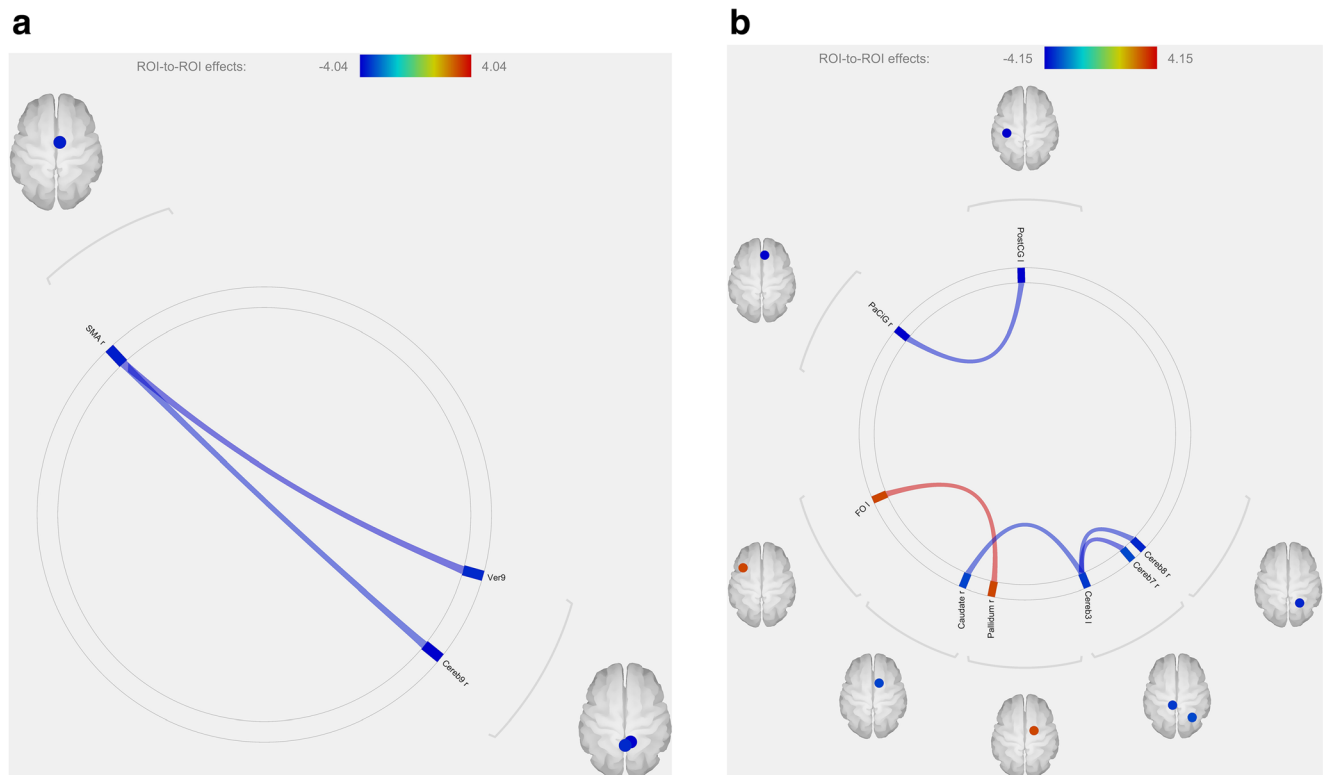
Fig. 5 Correlations of the number (**a**) and volume (**b**) of white matter hyperintensities with functional connectivity, corrected for the age and sex of the subjects. We found significantly decreased connectivity of the cerebellar vermis (Ver9) and right cerebellar hemisphere (Cereb9 r) with the right supplementary motor area (SMA r) in correlation with number of lesions. Increasing volume of lesions correlated significantly between the

regions of the right and left cerebellar hemispheres (Cereb8 r, Cereb7 r, Cereb3 l), between the left cerebellum and right caudate nucleus (Caudate r), and between the left postcentral gyrus (PostCG l) and right paracingulate gyrus (PaCiG r). The connectivity of the left frontal operculum (FO l) with the right pallidum (Pallidum r) was significantly increased in correlation with WMH volume

use various semi-quantitative scaling systems. One of the studies roughly comparable with ours reports WMH volume of 547.12 mm^3 in a subgroup of subjects with at least 1 lesion [19]. We have found comparatively smaller mean lesion load (86.82 mm^3) in a corresponding group. One possible explanation for this may be higher sensitivity in our study for detecting and segmenting very small lesions, as that would generally increase the prevalence of WMHs while reducing the mean volume of WMHs in lesion-positive subjects. In fact, the segmented WMHs were mostly dot-like and with relatively small mean volume (23.02 mm^3). Even higher lesion load (4773 mm^3) was reported in another paper from Wen et al [27], but they had investigated a study group between 60 and 64 years of age, and thus these results are not really comparable with our sample. Similarly, some other studies using WMH volumometry deal with subjects of higher age compared with those in our study [28, 29]. Our data indicate that WMHs can be found commonly in younger age categories but that both their numbers and mean total volume are low in most subjects.

In contrast to previous studies [5, 30], our study found no significant correlation for the number or volume of WMHs with age. Habes et al had proven significant correlation of WMH volume with age on a large cohort of volunteers, but their mean age was higher (55.6 years) compared with our study and the authors had observed that WMH volumes larger than 2000 mm^3 started to appear after the fifth decade of life [31]. The lower age of our study participants, who were mostly under 40 years of age, may be considered as a possible explanation for our results in view of the fact that ischaemic changes may not yet play a significant role within this age group. Also playing a certain role may be the thresholding performed by Habes et al, who segmented only lesions larger than 25 mm^3 [31]. If WMHs in young subjects would tend to be smaller compared with larger ischaemic lesions in elderly subjects, then they could be underestimated when considering volume only above the given threshold. Although we have not proven significant correlation between mean volume of 1 lesion with age in our study group, this factor might become important in studies encompassing a wider age distribution of the subjects. For this reason, and considering that even the small lesions were quite clearly distinguishable in 3D FLAIR images, which was verified by double reading, we have chosen not to threshold the segmentations by volume.

The lesions were distributed within all zones of the brain's WM. Although the subjects were free of symptoms suggestive of MS, we did record in 5 subjects simultaneous presence of juxtacortical and periventricular lesions. This finding would fulfil the McDonald criteria for dissemination in space and evokes the question of radiologically isolated syndrome, which was first introduced in 2009 to define a relevant cohort of individuals routinely encountered in clinical practice who are at risk for future demyelinating events [32]. Although data concerning the population-based incidence and prevalence of radiologically isolated syndrome are scarce, that data available does suggest this to be uncommon. Forslin et al indicate in their population-based study a cumulative incidence of 0.1% [33]. Our study group is not large enough to draw definitive conclusions about incidence of radiologically isolated syndrome, but our results do suggest that the measured incidence may be higher than reported previously if high-resolution FLAIR imaging technique is employed.

There is some data in the literature pointing to alteration in diffusivity of the brain's WM in association with WMHs. We measured significantly higher MD values within WMHs compared with NAWM, which finding was similar to that from the study of Meninenga et al [34]. This may be given by structural disintegration of the WM tissue within the lesions in correlation with prior neuropathological findings of neuronal loss, demyelination, or gliosis [35], which result in enlargement of the extracellular water component and increase in isotropic diffusivity of water molecules. The aforementioned study also proved the diffusivity changes within NAWM in correlation with increasing WMH score [34]. In contrast, we revealed no significant association between the diffusion scalar parameters of NAWM and lesion load. A possible explanation for this discrepancy is the lower age of the subjects in our study group, in whom the WM structural changes seem to be limited only to the WMHs themselves rather than to be associated with widespread changes within NAWM. This fact may imply also a different pathophysiological background for these lesions relative to those in elderly individuals. The age of the subjects was the only significant determinant of FA values, and these were negatively correlated with age in many WM areas. This is consistent with previous studies dealing with diffusivity changes in normal ageing [36].

The lesion load in our study group did not significantly influence the volume of brain white or grey matter. This finding may correspond to the DTI analyses, which do not indicate structural changes within NAWM and, considering the fact that the volume of WHMs in most of the subjects was relatively low, the lesions were not able to influence global brain volumes. On the other hand, we may expect atrophic changes of the brain to be correlated with WMH load in older individuals, as some authors have proven significant reduction of grey matter to be linked with increasing lesion load in subjects 60 years of age and older [27, 37].

Given the significant alterations in functional connectivity of the brain, and especially significantly reduced functional connectivity between the cerebellum and several supratentorial regions, the presence of WMHs may affect the function of the brain's neural networks. Because the lesions in all subjects were located within the WM of the brain hemispheres, we might assume disruption of the supratentorial segments of the neural loops connecting the cerebellum with supratentorial structures.

The cerebellum has long been known to be involved in the motor control system [38], but there are several reports about its relationship to such other specific functions as cognitive processing or executive functions [39, 40]. Inasmuch as we have no functional clinical data, we may only speculate about the functional impacts of these findings. One possible impact could be modest deficit in motor functions. Sachdev et al proved an association between WMH volumes and poorer motor functions [41], and this may generally concur with our findings of decreased connectivity of the cerebellum. Only by further studies using specific neuropsychological testing, however, could these hypotheses be confirmed.

Only very sparse data is available in the literature regarding the impact of WMHs on brain connectivity as measured by rs-fMRI, and such data as are available are not fully comparable with ours. Shi et al proved a significant correlation between regional WMH volumes and intrinsic connectivity contrast maps in various regions of the brain, including the left cuneus, right superior occipital cortex, right superior corona radiate, and left superior occipital cortex [42]. A study by De Marco et al [43] using independent component analysis of rs-fMRI data demonstrates correlations between WMH load within the anterior default mode network (namely the left medial temporal lobe) and the salience network (right parietal cortex). Those findings do not anatomically correspond to the changes in connectivity found in our study, but it is also the case that those authors used a different methodology in their data analysis and studied an older population (mean age 61.98 years). Further studies are needed to confirm these findings and to stratify the functional connectivity changes in different age groups.

A question may arise regarding the approach to statistical correlation of lesion load with the modalities investigated. Alternatively, a comparison might be made between lesion-free subjects and those having at least one lesion. We do not consider such approach to be appropriate, however, due to the relatively large proportion of subjects having just one or two lesions that are not likely to cause significant changes in brain volume or in structural or functional connectivity. On the other hand, we are not able to establish a hypothesis for an alternative threshold to distinguish between "normal" and "abnormal" subjects from the perspective of those advanced MRI modalities. For this reason, we have chosen to correlate the number and volume of WMHs as continuous variables.

In addition to the aforementioned lack of specific clinical data, this study has some other limitations. One of them may be seen in the use of a 1.5-T MR device, considering that 3 T is widely used today in neuroimaging studies. Higher magnetic field strength could provide better signal-to-noise ratio and spatial resolution, thereby leading to more precise segmentations as well as even more robust results in terms of correlations with advanced modalities, especially rs-fMRI. Another limitation is the relatively small number of subjects, in which

light this paper should not be regarded as an epidemiological study designed to reveal WMH prevalence. Our results nevertheless do suggest that the incidental finding of WMHs may be greater than previously reported when 3D FLAIR sequence is used. This fact may be especially important when evaluating examinations in patients suspected of having MS, for whom the 3D FLAIR imaging techniques are increasingly used. The topic thus deserves to be revisited from this perspective and analysed on larger study groups. Furthermore, although the exclusion criteria were set to filter out mainly those subjects with demyelinating or inflammatory CNS disease, we have no data about other comorbidities like diabetes, hypertension, or migraine that might also influence the load of WMHs. Thus, we are not able to discriminate the possible effect of these factors, and the subjects included in the study should be considered merely "neurologically intact" rather than completely "healthy". We believe, however, that in a vast majority of neuroimaging studies using cohorts of "healthy" subjects, the internal comorbidities are not set as exclusion criteria. Thus, one of the benefits of this study may be seen in its investigating impact of WMHs on the aforementioned MRI modalities in a population sample similar to those that are likely to be used in future neuroimaging studies comparing control subjects with patients.

In this regard, the question may arise as to whether the presence of incidentally found WMHs in cohorts of control subjects should be reflected in neuroimaging studies. According to our results, this is not the case for the global volumes of the brain, where we found no significant correlations with lesion load. Similarly, the impact of WMHs on the brain diffusivity seems to be relatively minor. Inasmuch as we have revealed significantly higher mean diffusivity within the lesions themselves compared with NAWM, some influence may become prominent in the case of ROI-based analyses in individual patients if ROI masks would be placed over the areas with high accumulation of WMHs. On the other hand, it seems that the lesion volume is too small compared with the overall WM volume to be able to affect global diffusivity changes, as revealed by our TBSS analysis. Thus, it appears that co-varying for the number or volume of WMHs in the studies using this methodology is not essential. Finally, according to our data, the load of WMHs seems significantly to affect functional connectivity of the brain, so the lesion load may be considered as a variable entering the rs-fMRI statistical analyses to eliminate this effect. Alternatively, those subjects with obviously high number of WMHs may be excluded. At this point, however, we are not able to differentiate whether the lesion load is really an independent predictor of connectivity changes or if the lesions are associated with, for example, cardiovascular risks or other internal comorbidities. In such a case, it would be advisable to reflect more carefully those factors so that they match within patient groups. Nevertheless, this hypothesis needs to be validated by further

studies. To conclude, WMHs constitute a common finding even in young, neurologically asymptomatic adults. The analyses of multimodal MRI data revealed no impact of WMH load on the global brain volumes, and the changes of diffusivity seem to be limited to the lesions themselves rather than to the entire NAWM. The lesion load correlates significantly with changes in brain functional connectivity, and especially that of the cerebellum.

Compliance with ethical standards

Guarantor The scientific guarantor of this publication is Assoc. Prof. Marek Mechl, M.D., Ph.D., MBA.

Conflict of interest The authors of this manuscript declare no relationships with any companies whose products or services may be related to the subject matter of the article.

Statistics and biometry No complex statistical methods were necessary for this paper.

Informed consent Written informed consent was obtained from all subjects in this study.

Ethical approval Institutional Review Board approval was obtained.

Methodology
• Prospective
• Cross-sectional study
• Performed at one institution

References

1. Longstreth WT Jr, Manolio TA, Arnold A et al (1996) Clinical correlates of white matter findings on cranial magnetic resonance imaging of 3301 elderly people. The Cardiovascular Health Study. Stroke 27:1274–1282

2. Katzman GL, Dagher AP, Patronas NJ (1999) Incidental findings on brain magnetic resonance imaging from 1000 asymptomatic volunteers. JAMA 282:36–39

3. de Groot JC, de Leeuw FE, Oudkerk M, Hofman A, Jolles J, Breteler MM (2001) Cerebral white matter lesions and subjective cognitive dysfunction: the Rotterdam Scan Study. Neurology 56:1539–1545

4. Hopkins RO, Beck CJ, Burnett DL, Weaver LK, Victoroff J, Bigler ED (2006) Prevalence of white matter hyperintensities in a young healthy population. J Neuroimaging 16:243–251

5. Fazekas F (1989) Magnetic resonance signal abnormalities in asymptomatic individuals: their incidence and functional correlates. Eur Neurol 29:164–168

6. Enzinger C, Smith S, Fazekas F et al (2006) Lesion probability maps of white matter hyperintensities in elderly individuals: results of the Austrian stroke prevention study. J Neurol 253:1064–1070

7. van Swieten JC, Geyskes GG, Derix MM et al (1991) Hypertension in the elderly is associated with white matter lesions and cognitive decline. Ann Neurol 30:825–830

8. Hirono N, Kitagaki H, Kazui H, Hashimoto M, Mori E (2000) Impact of white matter changes on clinical manifestation of Alzheimer's disease: a quantitative study. Stroke 31:2182–2188

9. van den Berg E, Geerlings MI, Biessels GJ, Nederkoorn PJ, Kloppenborg RP (2018) White matter hyperintensities and cognition in mild cognitive impairment and Alzheimer's disease: a domain-specific meta-analysis. J Alzheimers Dis. https://doi.org/10.3233/JAD-170573

10. Piccini P, Pavese N, Canapicchi R et al (1995) White matter hyperintensities in Parkinson's disease. Clinical correlations. Arch Neurol 52:191–194

11. Brown FW, Lewine RJ, Hudgins PA, Risch SC (1992) White matter hyperintensity signals in psychiatric and nonpsychiatric subjects. Am J Psychiatry 149:620–625

12. Thompson AJ, Banwell BL, Barkhof F et al (2017) Diagnosis of multiple sclerosis: 2017 revisions of the McDonald criteria. Lancet Neurol 17:162–173

13. Bartko JJ (1966) The intraclass correlation coefficient as a measure of reliability. Psychol Rep 19:3–11

14. Smith SM, Zhang Y, Jenkinson M et al (2002) Accurate, robust and automated longitudinal and cross-sectional brain change analysis. Neuroimage 17:479–489

15. Smith SM, Jenkinson M, Woolrich MW et al (2004) Advances in functional and structural MR image analysis and implementation as FSL. Neuroimage 23:S208–S219

16. Battaglini M, Jenkinson M, De Stefano N (2012) Evaluating and reducing the impact of white matter lesions on brain volume measurements. Hum Brain Mapp 33:2062–2071

17. Whitfield-Gabrieli S, Nieto-Castanon A (2012) Conn: a functional connectivity toolbox for correlated and anticorrelated brain networks. Brain Connect 2:125–141

18. de Leeuw FE, de Groot JC, Achten E et al (2001) Prevalence of cerebral white matter lesions in elderly people: a population based magnetic resonance imaging study. The Rotterdam Scan Study. J Neurol Neurosurg Psychiatry 70:9–14

19. Wen W, Sachdev PS, Li JJ, Chen X, Anstey KJ (2009) White matter hyperintensities in the forties: their prevalence and topography in an epidemiological sample aged 44–48. Hum Brain Mapp 30:1155–1167

20. Saba L, Lucatelli P, Anzidei M, di Martino M, Suri JS, Montisci R (2018) Volumetric distribution of the white matter hyper-intensities in subject with mild to severe carotid artery stenosis: does the side play a role? J Stroke Cerebrovasc Dis. https://doi.org/10.1016/j.jstrokecerebrovasdis.2018.02.065

21. Ataç Uçar C, Güneş HN, Sencer Demircan C, Çokal BG, Keskin Güler S, Yoldaş TK (2017) Cardiovascular risk factors and white matter hyperintensities in patients with migraine without aura. Agri 29:157–161

22. Boutet C, Rouffiange-Leclair L, Schneider F, Camdessanché JP, Antoine JC, Barral FG (2016) Visual assessment of age-related white matter hyperintensities using FLAIR images at 3 T: inter- and intra-rater agreement. Neurodegener Dis 16:279–283

23. Tully PJ, Qchiqach S, Pereira E, Debette S, Mazoyer B, Tzourio C (2017) Development and validation of a priori risk model for extensive white matter lesions in people age 65 years or older: the Dijon MRI study. BMJ Open 7:e018328

24. Gramsch C, Nensa F, Kastrup O et al (2015) Diagnostic value of 3D fluid attenuated inversion recovery sequence in multiple sclerosis. Acta Radiol 56:622–627

25. Patzig M, Burke M, Brückmann H, Fesl G (2014) Comparison of 3D cube FLAIR with 2D FLAIR for multiple sclerosis imaging at 3 Tesla. Rofo 186:484–488

26. Paniagua Bravo Á, Sánchez Hernández JJ, Ibáñez Sanz L, Alba de Cáceres I, Crespo San José JL, García-Castaño Gandariaga B (2014) A comparative MRI study for white matter hyperintensities detection: 2D-FLAIR, FSE PD 2D, 3D-FLAIR and FLAIR MIP. Br J Radiol 87:20130360

27. Wen W, Sachdev PS, Chen X, Anstey K (2006) Gray matter reduction is correlated with white matter hyperintensity volume: a voxel-based morphometric study in a large epidemiological sample. Neuroimage 29:1031–1039

28. Tiehuis AM, Vincken KL, Mali WP et al (2008) Automated and visual scoring methods of cerebral white matter hyperintensities: relation with age and cognitive function. Cerebrovasc Dis 25:59–66

29. Kim JH, Hwang KJ, Kim JH, Lee YH, Rhee HY, Park KC (2011) Regional white matter hyperintensities in normal aging, single domain amnestic mild cognitive impairment, and mild Alzheimer's disease. J Clin Neurosci 18:1101–1106

30. Awad IA, Spetzler RF, Hodak JA, Awad CA, Carey R (1986) Incidental subcortical lesions identified on magnetic resonance imaging in the elderly. I. Correlation with age and cerebrovascular risk factors. Stroke 17:1084–1089

31. Habes M, Erus G, Toledo JB et al (2016) White matter hyperintensities and imaging patterns of brain ageing in the general population. Brain 139:1164–1179

32. Okuda DT, Mowry EM, Beheshtian A et al (2009) Incidental MRI anomalies suggestive of multiple sclerosis: the radiologically isolated syndrome. Neurology 72:800–805

33. Forslin Y, Granberg T, Jumah AA et al (2016) Incidence of radiologically isolated syndrome: a population-based study. AJNR Am J Neuroradiol 37:1017–1022

34. Maniega SM, Valdés Hernández MC, Clayden JD et al (2015) White matter hyperintensities and normal-appearing white matter integrity in the aging brain. Neurobiol Aging 36:909–918

35. Fazekas F, Kleinert R, Offenbacher H et al (1993) Pathologic correlates of incidental MRI white matter signal hyperintensities. Neurology 43:1683–1689

36. Gunning-Dixon FM, Brickman AM, Cheng JC, Alexopoulos GS (2009) Aging of cerebral white matter: a review of MRI findings. Int J Geriatr Psychiatry 24:109–117

37. Godin O, Maillard P, Crivello F et al (2009) Association of white-matter lesions with brain atrophy markers: the three-city Dijon MRI study. Cerebrovasc Dis 28:177–184

38. Glickstein M (1992) The cerebellum and motor learning. Curr Opin Neurobiol 2:802–806

39. Daum I, Snitz BE, Ackermann H (2001) Neuropsychological deficits in cerebellar syndromes. Int Rev Psychiatry 13:268–275

40. Bellebaum C, Daum I (2007) Cerebellar involvement in executive control. Cerebellum 6:184–192

41. Sachdev PS, Wen W, Christensen H, Jorm AF (2005) White matter hyperintensities are related to physical disability and poor motor function. J Neurol Neurosurg Psychiatry 76:362–367

42. Shi L, Miao X, Lou W et al (2017) The spatial associations of cerebral blood flow and spontaneous brain activities with white matter hyperintensities-an exploratory study using multimodal magnetic resonance imaging. Front Neurol 8:593

43. De Marco M, Manca R, Mitolo M, Venneri A (2017) White matter hyperintensity load modulates brain morphometry and brain connectivity in healthy adults: a neuroplastic mechanism? Neural Plast 2017:4050536

Diffusion tensor imaging – současné možnosti MR zobrazení bílé hmoty mozku

Diffusion Tensor Imaging – Current Possibilities of Brain White Matter Magnetic Resonance Imaging

Souhrn

Zobrazení tenzorů difuze (diffusion tensor imaging, DTI) je poměrně nová technika vyšetření magnetickou rezonancí, která je v současné době jako jediná schopna zobrazit bližší strukturální detaily bílé hmoty mozku. Sofistikované softwarové zpracování základních dat umožňuje vizualizovat jednotlivé dráhy nebo měřit číselné hodnoty parametrů DTI, které dle dosavadních publikací citlivě reagují na strukturální poškození bílé hmoty. Autoři této práce si kladou za cíl přinést přehled současných aplikací DTI pro zobrazení bílé hmoty mozku. Probírány jsou základní technické aspekty, možnosti praktického využití této metody v běžné klinické praxi a v neposlední řadě i ryze výzkumné aplikace směřující k detekci a kvantifikaci diskrétní ultrastrukturální patologie u různých onemocnění bílé hmoty mozkové.

Abstract

Diffusion tensor imaging (DTI) is a relatively new magnetic resonance imaging technique that is capable of unique depiction of the structural detail in brain white matter. Its sophisticated software algorithms provide either three-dimensional reconstructions and visualizations of the particular tracts of the white matter or quantifications of various DTI parameters that appear, according to certain studies, to be highly sensitive to structural abnormalities in white matter. The aim of the present paper is to review the current applications of DTI for the depiction of brain white matter. Some basic technical remarks are made and clinical aspects are discussed, as well as purely research applications aimed at the detection and quantification of the subtle ultra-structural pathology of brain white matter.

M. Keřkovský[1],
A. Šprláková-Puková[1],
T. Kašpárek[2], P. Fadrus[3],
M. Mechl[1], V. Válek[1]

LF MU a FN Brno:
[1] Radiologická klinika
[2] Psychiatrická klinika
[3] Neurochirurgická klinika

✉

MUDr. Miloš Keřkovský
Radiologická klinika
LF MU a FN Brno
Jihlavská 20
625 00 Brno
e-mail: mkerkovsky@fnbrno.cz

Úvod

Zobrazení magnetickou rezonancí (MR) disponuje excelentním kontrastem měkkých tkání. Zejména pro tuto vlastnost je tato v současnosti již poměrně dobře dostupná zobrazovací modalita dnes a denně oceňována v běžné praxi. Z hlediska zobrazení mozku nabízí MR výborný kontrast mezi šedou a bílou hmotou a umožňuje přesnou diagnózu širokého spektra patologií. Nicméně ani tak technicky pokročilá zobrazovací technika, jakou MR je, není schopna při použití konvenčních sekvencí zobrazit bližší strukturální detaily bílé hmoty. Ta se na běžně používaných sekvencích jeví jako víceméně homogenní tkáň, která je hypointenzní oproti šedé hmotě mozkové v T2 váženém obraze a mírně hyperintenzní v T1 váženém obraze.

Zobrazení tenzorů difuze (diffusion tensor imaging, DTI) je poměrně nová metoda MR zobrazení, jejíž technické základy byly poprvé popsány v roce 1994 [1]. Jedná se v současné době o jedinou metodu schopnou zobrazit nervové dráhy bílé hmoty mozku a míchy, která zároveň dokáže detekovat jemné strukturální abnormality bílé hmoty disponující v tomto směru vyšší senzitivitou v porovnání s konvenčním MR zobrazením [2].

Tato práce si klade za cíl přinést přehled současných aplikací DTI pro MR zobrazení mozku v oblasti praktické neurodiagnostiky i výzkumných aplikací spolu se shrnutím základních technických principů této "mladé" zobrazovací metody.

Technické aspekty

DTI je metoda vycházející z principů difuzně váženého zobrazení (diffusion weighted imaging, DWI). Proces difuze představuje náhodný pohyb molekul vody ve tkáni, označuje se jako tzv. Brownův pohyb. Difuze je ovlivňována mnoha faktory, existují velké rozdíly v difuzivitě molekul vody v různých tkáních a v některých případech též mezi normální a patologicky změněnou tkání stejného druhu (obr. 1). Sekvence DWI umožňují zobrazení procesu difuze za pomoci použití zvláštních přídatných magnetických gradientů, které konvenční MR sekvence neobsahují. V okrscích tkáně, jež obsahují převážně stacionární protony vodíku vázané v molekulách vody, způsobí symetrické, opačně orientované magnetické gradienty rozfázování a opětovné sfázo-

vání spinů, a tudíž nedojde k žádnému úbytku signálu. Náhodný pohyb molekul vody v oblastech s vysokým stupněm difuze oproti tomu vede k nedokonalému sfázování spinů a následným fázovým posunům, což v konečném výsledku způsobuje pokles intenzity signálu [3]. Čím je tedy výraznější difuze ve tkáni, tím je nižší intenzita signálu výsledného DWI obrazu. Restrikce difuze naopak působí hyperintenzitu.

Kdyby zobrazovaná tkáň měla absolutně pravidelnou strukturu s nulovou směrovou závislostí (tzv. izotropní médium), výsledný obraz DWI by byl stále stejný bez ohledu na směr působícího přídatného magnetického gradientu. Ve skutečnosti reálné tkáně představují více či méně komplexně organizovanou strukturu, která proto vykazuje určitou míru anizotropie difuze. Intenzita signálu DWI obrazu je proto závislá na použitém směru přídatného magnetického gradientu; proces difuze je anizotropní (obr. 2) [4,5].

DTI technika využívá této zákonitosti aplikací přídatných gradientů opakovaně v mnoha různých směrech (typicky v 6 až 64). Výpočetní zpracování naměřených dat umožní stanovit směr, ve kterém difuze molekul vody probíhá nejsnadněji [6]. Bílá hmota mozku a míchy představuje z hlediska difuze vysoce anizotropní

prostředí vzhledem k paralelnímu průběhu axonů. Je nasnadě, že molekuly vody v tomto prostředí daleko snáze difundují podél dlouhé osy svazků než napříč. Dominantní směr difuze v bílé hmotě proto v zásadě odpovídá směru průběhu nervových drah.

Výsledky DTI vyšetření je možno vyjádřit graficky i číselně. Jedním ze základ-
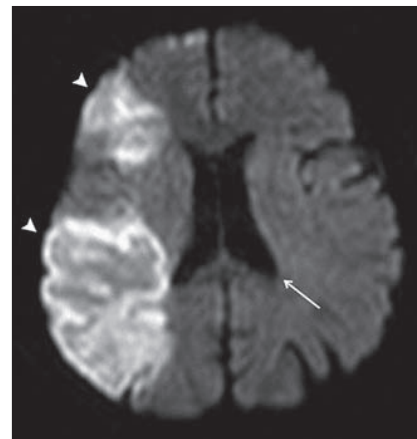
Obr. 1. DWI zobrazení mozku u pacienta s čerstvou ischemií v povodí a. cerebri media vpravo.

Hyperintenzita postižené oblasti značí restrikci difuze (plné šipky), s tím kontrastuje nízká intenzita signálu likvoru (šipka), kde je naopak difuze velmi výrazná.
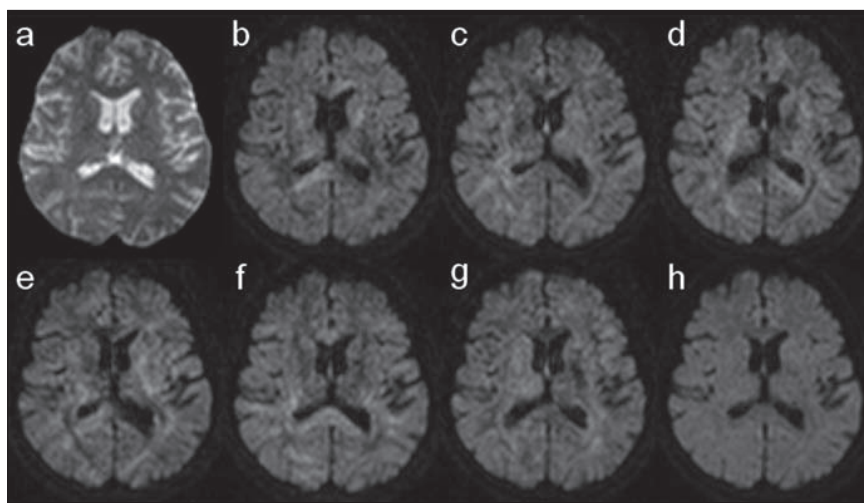
Obr. 2. Sada základních dat DTI vyšetření (b–g).

Difuzně vážené obrazy mozku s použitím šesti různých směrů přídatného magnetického gradientu (B), což je minimální počet potřebný k rekonstrukci mapy FA a barevné mapy směrové závislosti difuze. V závislosti na orientaci gradientu se mění intenzity signálu v jednotlivých oblastech.

a) B0 obraz nutný k výpočtu ADC mapy; jedná se o prostý T2 vážený obraz bez aplikace přídatného magnetického gradientu. h) Izotropní DWI obraz je průměrem obrazů b–g; spolu s B0 zobrazením slouží k výpočtu ADC mapy.
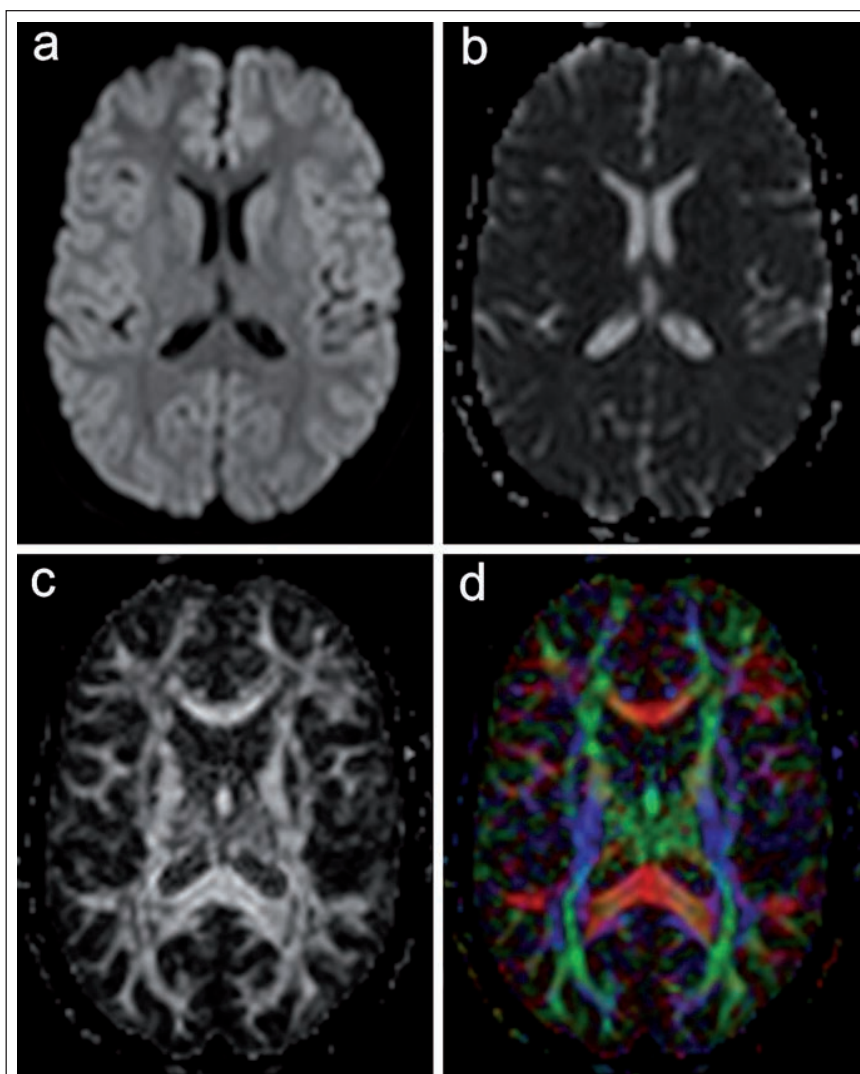
Obr. 3. Různé možnosti 2D prezentace DWI a DTI dat.

a) Izotropní DWI obraz vzniká zprůměrováním intenzity signálu z vícečetných (v tomto případě 32) opakovaných měření s různým směrem přídatného magnetického gradientu. Směrová závislost difuze zde proto nehraje roli.

b) ADC mapa kvantifikuje proces difuze ve tkáni též bez ohledu na izotropii. Pro výpočet je třeba izotropní DWI zobrazení s minimálně dvěma různými hodnotami přídatného gradientu (např. 0 a 1 000).

c) Mapa frakční anizotropie vyjadřuje míru směrové závislosti difuze v jednotlivých oblastech.

d) Směrová mapa difuze s barevným kódováním dominantního směru difuze, potažmo průběhu nervových drah.

Obr. 4. 3D rekonstrukce komisurálních traktů kalózního tělesa (modrá) a obou kortikospinálních drah (žlutá, červená).

z nich je prostá mapa FA, která vizualizuje hodnoty FA v jednotlivých oblastech bílé hmoty v černobílé škále. Další možností je rekonstrukce barevné mapy anizotropie. Základy této metody položili Pajevic a Pierpaoli, kteří v roce 1999 navrhli barevně kódovaná schémata za účelem zobrazení komplexní prostorové informace o architektonice bílé hmoty do dvoudimenzionálního obrazu [7]. Různé barvy představují dominantní směr průběhu nervových vláken (obr. 3).

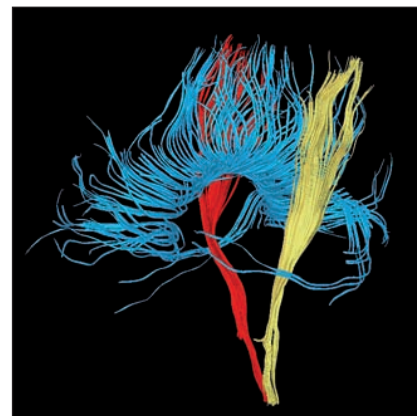Výpočetně nejnáročnější je 3D zpracování – tzv. traktografie (fiber-tracking), které je založeno na „stopování" převládajícího směru difuze za předpokladu, že tento odpovídá skutečnému směru průběhu nervových traktů [8,9]. Tato technika tak umožňuje rekonstrukci průběhu jednotlivých drah a jejich zobrazení ve 3D prostoru (obr. 4) nebo vytvoření jejich projekce do základních strukturálních obrazů konvenčních MR sekvencí.

Mluvíme-li o technických aspektech DTI vyšetření, nelze se nezmínit o několika významných technických problémech a limitacích, se kterými se tato metoda potýká. Jde především o nejrůznější artefakty základních obrazových dat (pohybové artefakty, distorze v důsledku „vířivých" proudů atd.), které v konečném důsledku snižují kvalitu rekonstrukcí. Při zpracování obrazu musíme též počítat s fenoménem „křížících se drah". V místech křížení z různých směrů probíhajících nervových drah může docházet k artificiálnímu snížení hodnot FA. Problém zde může nastat také u 3D rekonstrukcí, kde

ních dvou parametrů kvantifikace DTI dat je hodnota ADC (apparent diffusion coefficient) používaná i při DWI zobrazení, která vyjadřuje celkovou difuzivitu vody ve tkáni bez ohledu na směrovou závislost difuze. Pro DTI je specifickým parametrem tzv. frakční anizotropie (FA), jež vyjadřuje míru směrové závislosti procesu difuze. Jde o relativní veličinu nabývající

hodnot v rozmezí 0–1. Čím je tato hodnota vyšší, tím je vyšší anizotropie a směrové uspořádání struktury zobrazované tkáně. FA je v současnosti jeden z nejčastěji používaných parametrů ve výzkumu patologie bílé hmoty [2].

Softwarové zpracování DTI dat získaných vlastním měřením nabízí několik možností grafického znázornění. Jedním
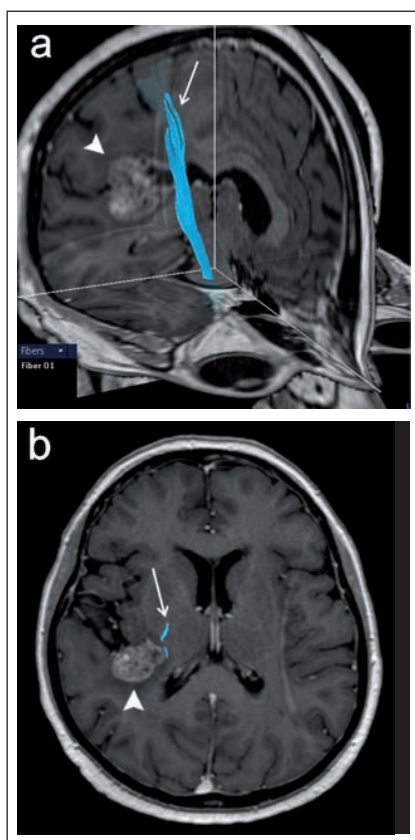
Obr. 5. DTI vyšetření u pacientky s metastázou adenokarcinomu vpravo temporálně (plná šipka) s rekonstrukcí kortikospinální dráhy (šipka).
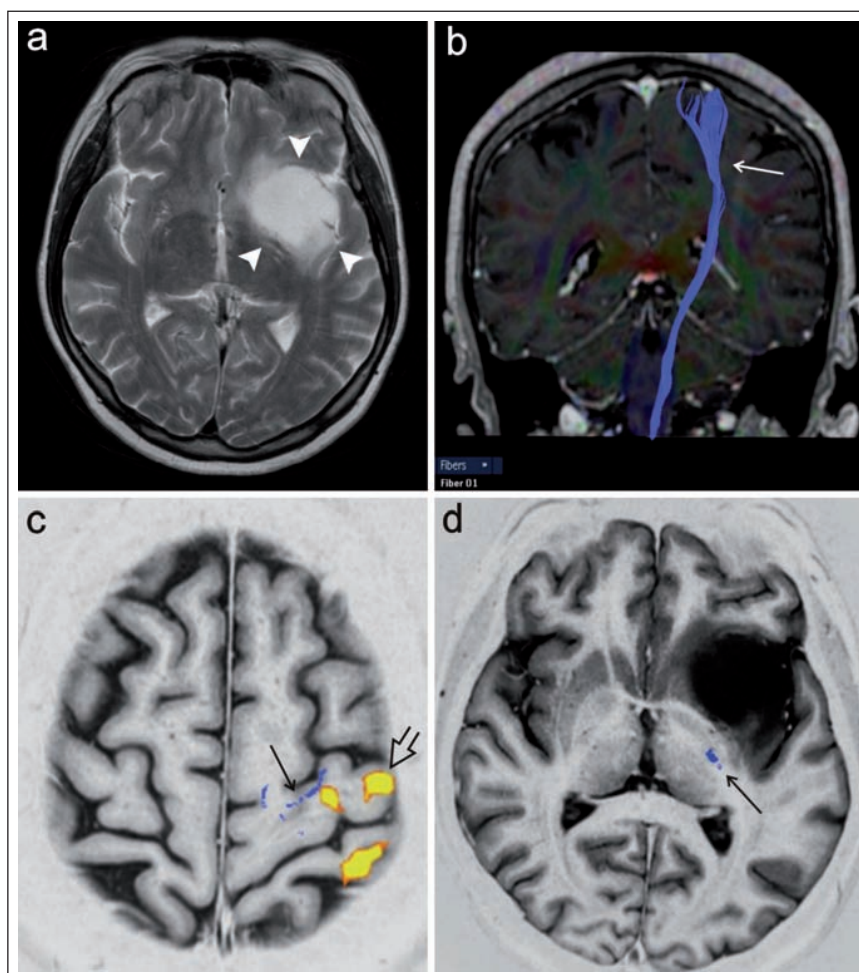
a) Přehledný 3D pohled.

b) Projekce do axiální roviny dobře znázorňuje těsný vztah dráhy k mediálnímu okraji tumoru.

Obr. 6. Předoperační fMR a DTI vyšetření pacientky s low-grade gliomem v oblasti levé inzuly.

a) Konvenční T2 vážené zobrazení, ložisko tumoru zde má vysokou intenzitu signálu (plné šipky). b) Projekce kortikospinální dráhy v koronární rovině.

c) Fúze fMR a DTI dat simultánně zobrazuje aktivaci primárního motorického kortexu (otevřená šipka) a průřezovou projekci kraniální části kortikospinálního traktu do axiální roviny (šipka).

d) Inversion recovery zobrazení se znázorněním prostorového vztahu průběhu kortikospinální dráhy k tumoru v axiální rovině.

výpočetní algoritmus může mylně stopovat průběh křížící dráhy [10,11].

DTI jako předoperační vyšetření

Současným trendem v neurochirurgii je maximální možná ochrana funkčně důležitých struktur mozku; předoperační MR vyšetření v tomto smyslu hraje důležitou roli [12]. Identifikaci kortikálních elokventních zón umožňuje v současné době mimo jiné funkční MR vyšetření (fMR), které pomáhá upřesnit strategii vlastní léčby a peroperačně usnadňuje provedení kortikální stimulace. Poranění kritických korových oblastí nicméně není jediným rizikem vzniku neurologického deficitu, k vážným důsledkům může vést také poškození subkortikálně probíhajících drah bílé hmoty.

Technika DTI byla v poslední době úspěšně použita pro předoperační vyšetření u pacientů s tumory a dalšími ložiskovými lézemi. Množství autorů potvrzuje spolehlivost DTI výsledků, když prokazují dobrou korelaci peroperační subkortikální stimulace motorických i jiných drah bílé hmoty s průběhem drah rekonstruovaných pomocí DTI [13,14]. Tato technika umožňuje zobrazení prostorového vztahu určité dráhy k patologické lézi, případně odlišení jejího odtlačení tumorem od přímé infiltrace a destrukce [15]. V některých pracích se popisují možnosti inte-

grace DTI dat do morfologických obrazů určených pro peroperační stereotaktickou navigaci [16].

Poměrně častým předmětem zájmu předoperačního DTI vyšetření je kortikospinální dráha, která je jedním z nejdůležitějších traktů z hlediska možného peroperačního poškození a následného vzniku funkčního neurologického deficitu (obr. 5). Při zpracování může být výhodou integrace dat fMR mapující motorický kortex pro správné a specifické umístění oblastí zájmu (ROI) použitých pro specifikaci rekonstrukce dráhy [17]. Kombinace

těchto dvou metod tak představuje pokročilé morfologicko-funkční předoperační zmapování motorického systému (obr. 6).

Dalším příkladem neméně funkčně významné dráhy je optická radiace, která vychází z talamického jádra corpus geniculatum lat., stáčí se laterálně a dorzálně ohybem označovaným jako Meyerova klička a dále směřuje dorzálně ke zrakovému kortexu okcipitálního laloku. V literatuře je popsána technika rekonstrukce této dráhy pomocí 3D traktografie, je zdůrazňována důležitost vizualizace této dráhy pro chirurgii spánkového laloku [18]. Resekce spánkového laloku např. u pacientů s epilepsií může představovat riziko poškození rostrální části Meyerovy kličky, které vede ke vzniku kontralaterálního defektu zorného pole. Autoři Nilsson et al (2007) a Yogarajah et al (2009) v této souvislosti poukazují na variabilitu uložení přední části Meyerovy kličky, což podtrhuje význam předoperačního DTI vyšetření pro posouzení rizika vzniku zrakového deficitu u pacientů s plánovanou resekcí spánkového laloku (obr. 7) [19,20].

DTI jako citlivý ukazatel patologie bílé hmoty

Jak bylo uvedeno výše, vysoce organizovaná mikrostruktura normální bílé hmoty mozku je příčinou výrazné anizotropie difuze v této tkáni. Ukazuje se, že různé patologické změny v bílé hmotě často vedou ke snížení anizotropie při patologickém nárůstu difuzivity molekul vody napříč nervovými trakty. Tato skutečnost je detekovatelná pomocí DTI, senzitivita této techniky byla v tomto smyslu mnohokráte potvrzena včetně experimentů na zvířecích modelech [21]. Zejména index FA je v současnosti považován za parametr senzitivní k narušení integrity bílé hmoty a je nyní jedním z nejčastěji sledovaných parametrů ve studiích využívajících DTI zobrazení [2].

Z pohledu histologa je lidská bílá hmota mozková velmi komplexní tkáň sestávající z uspořádaných neuronálních axonů s různou mírou myelinizace a z několika typů podpůrných buněk neuroglie. Veškeré mikrostrukturální abnormality, které vedou ke změnám FA, nejsou ještě v současné době do detailu známy. Integrita myelinových pochev axonů je jistě jedním ze zásadních faktorů zodpověd-
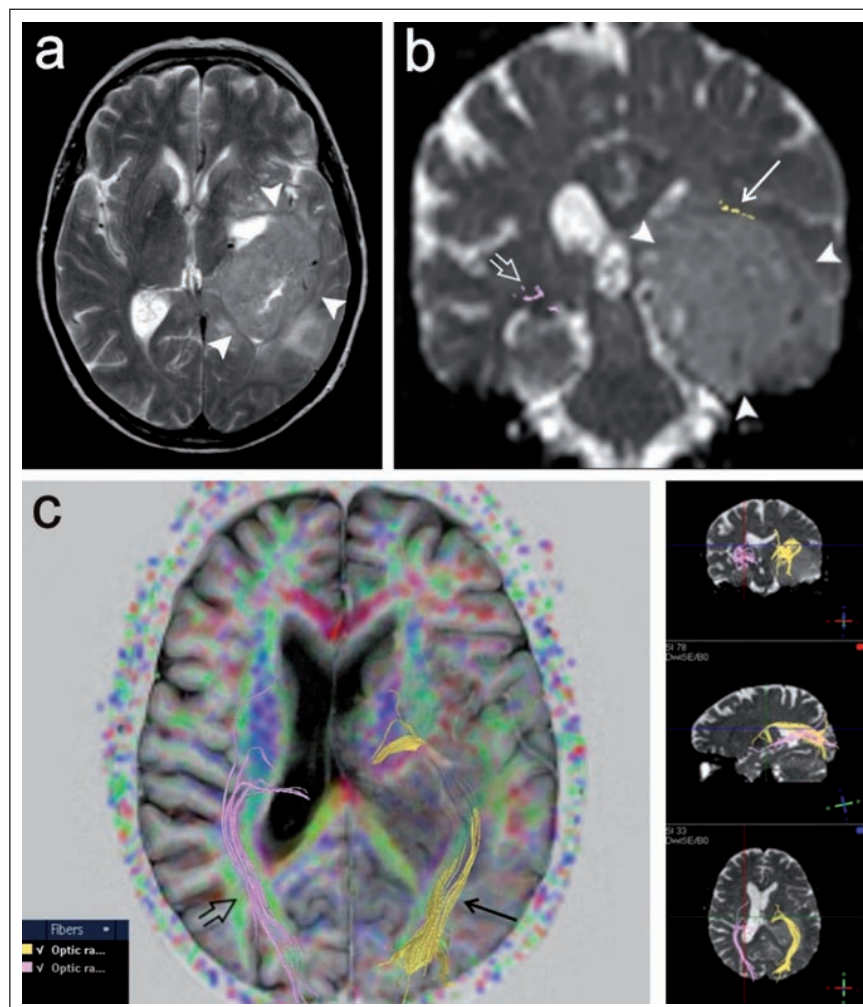
Obr. 7. Pacientka s tumorózní expanzí vlevo (gliom gr. III), u níž bylo provedeno předoperační DTI vyšetření za účelem posouzení průběhu levostranné optické dráhy.

a) T2 vážený obraz v axiální rovině, tumor má intenzity signálu blízké šedé hmotě mozku (plné šipky).

b) Rekonstrukce obou optických drah na průřezu v koronární rovině. Vlevo je dobře patrno odtlačení dráhy kraniálně (šipka), vpravo optická radiace v obvyklém průběhu (otevřená šipka).

c) Projekce obou optických drah v různých rovinách, vlevo je zřetelné odtlačení dráhy.

ných za anizotropii difuze; tento fakt dokládají mimo jiné četné odkazy na signifikantní změny FA u inkompletně myelinizované bílé hmoty v průběhu pre- i postnatálního zrání centrálního nervového systému [22,23].

V posledních letech se objevuje mnoho prací zaměřených na problematiku DTI vyšetření u pacientů trpících roztroušenou sklerózou (RS). Z dosavadních výsledků je zřejmé, že patologický proces demyelinizace způsobuje prokazatelné změny v parametrech DTI měření. Jednotliví autoři se

vesměs shodují ve zjištění poklesu hodnot FA v demyelinizačních plakách a v blízké zóně okolní bílé hmoty (obr. 8). Prokázány byly dokonce i významné odchylky FA v oblastech normálně vyhlížející bílé hmoty u pacientů s RS v porovnání s kontrolní skupinou zdravých subjektů [24,25]. Bester et al (2008) ve své práci analyzují FA bílé hmoty bez viditelného postižení na konvenčních sekvencích u pacientů s klinicky izolovaným syndromem manifestujícím se jako optická neuritida. U skupiny těchto pacientů byl zjištěn signifikantní
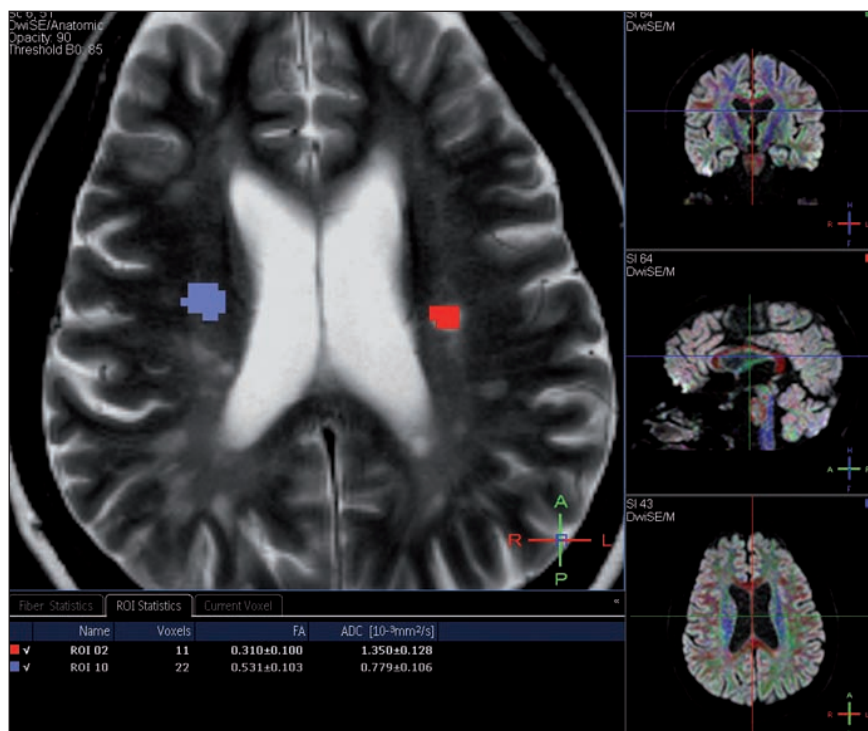
Obr. 8. Měření hodnot ADC a FA v rámci DTI vyšetření u pacientky s roztroušenou sklerózou.

Oblast zájmu (ROI) umístěna vlevo do místa demyelinizační plaky (červená), kde je zjištěn pokles hodnoty FA (0,31) a elevace hodnoty ADC (1,350). Vpravo měření provedeno v bílé hmotě bez viditelného postižení v T2 váženém obraze (modrá); hodnota FA je zde vyšší (0,531), ADC hodnota naopak nižší (0,779).

pokles hodnot FA v oblasti splenia kalózního tělesa v porovnání s kontrolní skupinou zdravých dobrovolníků [26]. Uvedené skutečnosti potvrzují vysokou senzitivitu DTI v detekci patologie bílé hmoty v porovnání s konvenčním MR zobrazením a do budoucna mohou být příslibem praktického využití DTI u pacientů s RS.

RS nicméně není zdaleka jediným onemocněním, kde bylo DTI zobrazení použito pro hodnocení diskrétnějších strukturálních změn bílé hmoty. Jako další příklady této aplikace lze uvést studie zaměřující se na využití DTI v diagnostice amyotrofické laterální sklerózy, kde byly prokázány signifikantní abnormality FA v průběhu kortikospinálního traktu v porovnání s kontrolní skupinou [27]. U pacientů s multisystémovou atrofií (MSA) se dle výsledků dosavadních studií jeví patologie bílé hmoty jako jeden z důležitých atributů tohoto neurodegenerativního onemocnění [28]. Autoři Prakash et al (2009) ve své poslední práci dokonce zmiňují možnost odlišení různých typů ataktických syndromů pomocí DTI [29].

DTI se v současné době též stále častěji uplatňuje jako výzkumný nástroj na poli psychiatrických onemocnění, a to zejména u pacientů se schizofrenií. Diagnostika této choroby v současnosti představuje výzvu pro zobrazovací diagnostické metody, neboť konvenční MR vyšetření, které je považováno za špičku v nynějších možnostech zobrazení mozku, obvykle při klasickém vizuálním hodnocení neprokáže viditelné patologické změny u pacientů trpících schizofrenií. Mluvíme-li stále o diagnostice pomocí konvenčních MR sekvencí, je pro detekci jemných strukturálních abnormalit mozku třeba podrobnější analýzy obrazu se zapojením sofistikovaných metod výpočetního zpracování na bázi volumometrie a „voxel-based" analýzy. Již dříve byly popsány méně nápadné změny gyrifikace prokazatelné pomocí měření abnormálních hodnot gyrifikačních indexů [30,31] nebo změny objemu šedé hmoty mozku v nejrůznějších oblastech kortexu [32]. Bylo dále zjištěno, že uvedené změny ve funkční organizaci a strukturálním vývoji

mozkového kortexu jsou úzce spjaty s konektivitou jednotlivých kortikálních oblastí [33]. Tato asociace kortikální organizace s funkční i anatomickou konektivitou je zčásti vysvětlena v současnosti přijímanou patofyziologickou hypotézou funkční dyskonektivity mozku u pacientů se schizofrenií [34].

DTI se v této souvislosti pro svoji známou citlivost k ultrastrukturální patologii bílé hmoty nabízí jako vhodný nástroj pro bližší výzkum patologické konektivity u schizofrenických pacientů. Na toto téma bylo provedeno množství prací, které vesměs porovnávají skupiny pacientů se schizofrenií se skupinami zdravých dobrovolníků. Pro zpracování dat jednotliví autoři používají buď ROI (region of interest) analýzu, kdy jsou měřeny parametry ADC a FA v konkrétních oblastech bílé hmoty, nebo složitější „voxel-based" zpracování. Jako potvrzení výše uvedených tezí byly prokázány signifikantní změny FA v mnoha různých oblastech bílé hmoty mozku u pacientů se schizofrenií, a to zejména v průběhu asociačních drah propojujících frontální, temporální a parietální kortex, v oblasti cingula a kalózního tělesa [35]. Několik málo autorů se zaměřuje též na korelaci mezi klinickou symptomatikou a měřením DTI parametrů s vesměs negativními výsledky [36]. Autoři Shin et al (2006) nicméně ve své práci prokazují pozitivní korelaci ADC hodnot bílé hmoty pravé inzuly se subskóre negativní symptomatiky v rámci škály pozitivních a negativních příznaků (PANSS) [37]. DTI nám na tomto poli poskytuje nový náhled na patofyziologii schizofrenie a podporuje teorii rozsáhlé ultrastrukturální abnormality bílé hmoty mozkové jako jeden z významných faktorů pro vznik tohoto onemocnění.

Závěr

Lze říci, že MR-DTI je unikátní metoda, která jako jediná prozatím umožňuje podrobnější strukturální zobrazení bílé hmoty mozkové s vizualizací jednotlivých nervových drah. Nalézá praktické uplatnění jako předoperační vyšetření u pacientů s plánovaným neurochirurgickým výkonem, kdy umožňuje zobrazit vztah patologické léze k jednotlivým drahám, čímž pomáhá při stanovení celkové strategie léčby a umožňuje vhodně modifikovat operační postup za účelem minimalizace pooperačního neurologického deficitu.

Zároveň jde o metodu, která je výrazně citlivá k ultrastrukturální patologii bílé hmoty s novými možnostmi kvantifikace, což je skutečnost v posledních letech hojně využívaná pro výzkum nejrůznějších onemocnění bílé hmoty mozku.

Technika DTI prochází neustálým vývojem z hlediska základních parametrů sekvencí i výpočetního zpracování. Současná metodika DTI traktografie založená na Gaussovském modelu procesu difuze může selhávat v případě jeho komplexnější distribuce, jako např. v místech křížení vláken. Tento problém řeší nové techniky, jako např. „q-ball imaging", kde se používá větší počet směrů přídatných gradientů o vyšší síle, než je tomu v případě konvenčního DTI zobrazení [38,39]. Při kombinaci těchto technik s potenciálem doposud experimentálních MR přístrojů disponujících velmi vysokým statickým magnetickým polem (7T) se můžeme dočkat dalších překvapivých výsledků a výhledově snad i implementace DTI vyšetření do standardního diagnostického protokolu u některých onemocnění postihujících bílou hmotu mozku či míchy.

Literatura

1. Basser PJ, Mattiello J, LeBihan D. MR diffusion tensor spectroscopy and imaging. Biophys J 1994; 66(1): 259–267.
2. Assaf Y, Pasternak O. Diffusion tensor imaging (DTI)-based white matter mapping in brain research: a review. J Mol Neurosci 2008; 34(1): 51–61.
3. Le Bihan D. Molecular diffusion, tissue microdynamics and microstructure. NMR Biomed 1995; 8(7–8): 375–386.
4. Pierpaoli C, Basser PJ. Toward a quantitative assessment of diffusion anisotropy. Magn Reson Med 1996; 36(6): 893–906.
5. Basser PJ. Inferring microstructural features and the physiological state of tissues from diffusion-weighted images. NMR Biomed 1995; 8(7–8): 333–344.
6. Basser PJ, Pajevic S, Pierpaoli C, Duda J, Aldroubi A. In vivo fiber tractography using DT-MRI data. Magn Reson Med 2000; 44(4): 625–632.
7. Pajevic S, Pierpaoli C. Color schemes to represent the orientation of anisotropic tissues from diffusion tensor data: application to white matter fiber tract mapping in the human brain. Magn Reson Med 1999; 42(3): 526–540.
8. Conturo TE, Lori NF, Cull TS, Akbudak E, Snyder AZ, Shimony JS et al. Tracking neuronal fiber pathways in the living human brain. Proc Natl Acad Sci U S A 1999; 96(18): 10422–10427.
9. Mori S, Crain BJ, Chacko VP, van Zijl PC. Three-dimensional tracking of axonal projections in the brain

by magnetic resonance imaging. Ann Neurol 1999; 45(2): 265–269.
10. Mukherjee P, Chung SW, Berman JI, Hess CP, Henry RG. Diffusion tensor MR imaging and fiber tractography: technical considerations. AJNR Am J Neuroradiol 2008; 29(5): 843–852.
11. Tournier JD, Yeh CH, Calamante F, Cho KH, Connelly A, Lin CP. Resolving crossing fibres using constrained spherical deconvolution: validation using diffusion-weighted imaging phantom data. Neuroimage 2008; 42(2): 617–625.
12. Berman JI. Diffusion MR tractography as a tool for surgical planning. Magn Reson Imaging Clin N Am 2009; 17(2): 205–214.
13. Bello L, Gambini A, Castellano A, Carrabba G, Acerbi F, Fava E et al. Motor and language DTI Fiber Tracking combined with intraoperative subcortical mapping for surgical removal of gliomas. Neuroimage 2008; 39(1): 369–382.
14. Berman JI, Berger MS, Chung SW, Nagarajan SS, Henry RG. Accuracy of diffusion tensor magnetic resonance imaging tractography assessed using intraoperative subcortical stimulation mapping and magnetic source imaging. J Neurosurg 2007; 107(3): 488–494.
15. Wei CW, Guo G, Mikulis DJ. Tumor effects on cerebral white matter as characterized by diffusion tensor tractography. Can J Neurol Sci 2007; 34(1): 62–68.
16. Zolal A, Sameš M, Vachata P, Bartoš R, Nováková M, Derner M. Použití DTI traktografie v neuronavigaci při operacích mozkových nádorů: kazuistiky. Cesk Slov Neurol N 2008; 71/104(3): 352–357.
17. Smits M, Vernooij MW, Wielopolski PA, Vincent AJ, Houston GC, van der Lugt A. Incorporating functional MR imaging into diffusion tensor tractography in the preoperative assessment of the corticospinal tract in patients with brain tumors. AJNR Am J Neuroradiol 2007; 28(7): 1354–1361.
18. Sherbondy AJ, Dougherty RF, Napel S, Wandell BA. Identifying the human optic radiation using diffusion imaging and fiber tractography. J Vis 2008; 8(10): 1–11.
19. Nilsson D, Starck G, Ljungberg M, Ribbelin S, Jönsson L, Malmgren K et al. Intersubject variability in the anterior extent of the optic radiation assessed by tractography. Epilepsy Res 2007; 77(1): 11–16.
20. Yogarajah M, Focke NK, Bonelli S, Cercignani M, Acheson J, Parker GJ et el. Defining Meyer's loop-temporal lobe resections, visual field deficits and diffusion tensor tractography. Brain 2009; 132(6): 1656–1668.
21. Harsan LA, Poulet P, Guignard B, Steibel J, Parizel N, de Sousa PL et al. Brain dysmyelination and recovery assessment by noninvasive in vivo diffusion tensor magnetic resonance imaging. J Neurosci Res 2006; 83(3): 392–402.
22. Mukherjee P, Miller JH, Shimony JS, Conturo TE, Lee BC, Almli CR et al. Normal brain maturation during childhood: developmental trends characterized with diffusion-tensor MR imaging. Radiology 2001; 221(2): 349–358.
23. Mukherjee P, Miller JH, Shimony JS, Philip JV, Nehra D, Snyder AZ et al. Diffusion-tensor MR imaging of gray and white matter development during normal human brain maturation. AJNR Am J Neuroradiol 2002; 23(9): 1445–1456.

24. Guo AC, MacFall JR, Provenzale JM. Multiple sclerosis: diffusion tensor MR imaging for evaluation of normal-appearing white matter. Radiology 2002; 222(3): 729–736.
25. Andrade RE, Gasparetto EL, Cruz LC jr, Ferreira FB, Domingues RC, Marchiori E et al. Evaluation of white matter in patients with multiple sclerosis through diffusion tensor magnetic resonance imaging. Arq Neuropsiquiatr 2007; 65(3A): 561–564.
26. Bester M, Heesen C, Schippling S, Martin R, Ding XQ, Holst B et al. Early anisotropy changes in the corpus callosum of patients with optic neuritis. Neuroradiology 2008; 50(7): 549–557.
27. Hong YH, Sung JJ, Kim SM, Park KS, Lee KW, Chang KH et al. Diffusion tensor tractography-based analysis of the pyramidal tract in patients with amyotrophic lateral sclerosis. J Neuroimaging 2008; 18(3): 282–287.
28. Shiga K, Yamada K, Yoshikawa K, Mizuno T, Nishimura T, Nakagawa M. Local tissue anisotropy decreases in cerebellopetal fibers and pyramidal tract in multiple system atrophy. J Neurol 2005; 252(5): 589–596.
29. Prakash N, Hageman N, Hua X, Toga AW, Perlman SL, Salamon N. Patterns of fractional anisotropy changes in white matter of cerebellar peduncles distinguish spinocerebellar ataxia-1 from multiple system atrophy and other ataxia syndromes. Neuroimage 2009; 47 (Suppl 2): T72–T81.
30. Falkai P, Honer WG, Kamer T, Dustert S, Vogeley K, Schneider-Axmann T et al. Disturbed frontal gyrification within families affected with schizophrenia. J Psychiatr Res 2007; 41(10): 805–813.
31. Harris JM, Yates S, Miller P, Best JJ, Johnstone EC, Lawrie SM. Gyrification in first-episode schizophrenia: a morphometric study. Biol Psychiatry 2004; 55(2): 141–147.
32. Honea R, Crow TJ, Passingham D, Mackay CE. Regional deficits in brain volume in schizophrenia: a meta-analysis of voxel-based morphometry studies . Am J Psychiatry 2005; 162(12): 2233–2245
33. Van Essen DC. A tension-based theory of morphogenesis and compact wiring in the central nervous system. Nature 1997; 385(6614): 313–318.
34. Stephan KE, Baldeweg T, Friston KJ. Synaptic plasticity and dysconnection in schizophrenia. Biol Psychiatry 2006; 59(10): 929–939.
35. Kubicki, M, McCarley R, Westin CF, Park HJ, Maier S, Kikinis R et al. A review of diffusion tensor imaging studies in schizophrenia. J Psychiatr Res 2007; 41(1–2): 15–30.
36. Kyriakopoulos M, Bargiotas T, Barker GJ, Frangou S. Diffusion tensor imaging in schizophrenia. Eur Psychiatry 2008; 23(4): 255–273.
37. Shin YW, Kwon JS, Ha TH, Park HJ, Kim DJ, Hong SB et al. Increased water diffusivity in the frontal and temporal cortices of schizophrenic patients. Neuroimage 2006; 30(4): 1285–1291.
38. Mukherjee P, Hess CP, Xu D, Han ET, Kelley DA, Vigneron DB. Development and initial evaluation of 7-T q-ball imaging of the human brain. Magn Reson Imaging 2008; 26(2): 171–180.
39. Hess CP, Mukherjee P, Han ET, Xu D, Vigneron DB. Q-ball reconstruction of multimodal fiber orientations using the spherical harmonic basis. Magn Reson Med 2006; 56(1): 104–117.

Význam MR zobrazení difuze míchy v diferenciální diagnostice míšních lézí

The Role of MR Diffusion Weighted Imaging in the Differential Diagnosis of Spinal Cord Lesions

Souhrn

Úvod: Zobrazení difuze pomocí magnetické rezonance (DWI) a zobrazení tenzorů difuze (DTI) jsou metody poměrně často využívané při MR diagnostice mozku. Využití těchto metod pro zobrazení míchy je technicky náročnější a méně časté. Cílem této pilotní práce je shrnutí zkušeností autorů s technikou DWI a DTI z hlediska možného přínosu pro diferenciální diagnostiku míšních lézí. *Metodika:* Retrospektivně jsme hodnotili DWI/DTI nálezy u 11 pacientů s patologickým nálezem míchy při konvenčním MR zobrazení. Spektrum diagnóz zahrnovalo míšní ischemii, demyelinizaci, ependymom, myelitidu, radiační myelopatii a cévní malformaci. Měřili jsme hodnoty ADC (Apparent Diffusion Coefficient) a v případě DTI i frakční anizotropie (FA) míchy, dále byly hodnoceny nálezy deterministické DTI traktografie. *Výsledky:* U čtyř pacientů s míšní ischemií byl pozorován pokles ADC hodnoty v místě léze oproti nepostiženému úseku o 36–61 %. Okrsky restrikce difuze byly patrné i u pacienta s radiační myelopatií. U dvou pacientů s ependymomem bylo patrné roztlačení míšních traktů a výrazné snížení hodnoty FA (0,247 a 0,299). U ostatních pacientů nebyla patrná patologie na traktografii, u pacientů s demyelinizací jsme pozorovali středně výrazný pokles hodnoty FA (0,494 a 0,471). *Závěr:* DWI/DTI míchy může dle našich zkušeností přispět ke správnému nasměrování diferenciálnědiagnostické rozvahy zejména průkazem restrikce difuze u míšních ischemií a zhodnocením obrazu traktografie u míšních tumorů. Další výzkum na větších souborech pacientů by mohl otevřít možnosti diferenciace jednotlivých patologií pomocí kvantifikace DTI parametrů.

Abstract

Introduction: Diffusion weighted imaging (DWI) and diffusion tensor imaging (DTI) are magnetic resonance imaging methods, nowadays commonly used to depict the brain. Application of these methods for the spinal cord imaging is technically more demanding and less frequent. The aim of this pilot study was to summarize authors' current experience with DWI and DTI of the spinal cord, considering the potential value for the differential diagnosis of the spinal cord lesions. *Methods:* We retrospectively evaluated DWI/DTI findings in a group of 11 patients with pathological findings of the spinal cord on conventional MRI examination. The diagnosis comprised spinal cord ischemia, multiple sclerosis, myelitis, radiation myelopathy and arteriovenous malformations. We measured apparent diffusion coefficient (ADC) in all patients and, of the DTI data, we also measured fractional anisotropy (FA) values and evaluated the deterministic tractography reconstructions. *Results:* In four patients with spinal cord ischemia, we observed a decrease of the ADC values of the spinal cord lesions compared to the normal-appearing segment within a range 36–61%. Small areas of restricted diffusion of the spinal cord were found also in a patient with radiation myelopathy. In two patients with spinal cord tumors, DTI tractography showed displacement and/or disruption of the spinal cord tracts and marked decrease of the FA values (0.247 and 0.299). No abnormalities were observed on tractography in the rest of the patients, moderate decrease of the FA values was found in patients within demyelinating lesions of the spinal cord (0.494 and 0.471). *Conclusion:* DWI/DTI of the spinal cord may contribute to the correct direction of the differential diagnostic considerations through depiction of restricted diffusion within the spinal cord ischemia and evaluation of tractography in patients with spinal cord tumors. Further research with larger numbers of patients might enable differentiation of the spinal cord lesions based on quantification of DTI parameters.

M. Keřkovský[1,2], A. Šprláková-Puková[1], J. Bednařík[2,3], M. Smrčka[4], M. Mechl[1]

[1] Radiologická klinika LF MU a FN Brno
[2] CEITEC – Středoevropský technologický institut, MU, Brno
[3] Neurologická klinika LF MU a FN Brno
[4] Neurochirurgická klinika LF MU a FN Brno

✉
MUDr. Miloš Keřkovský, Ph.D.
Radiologická klinika
LF MU a FN Brno
Jihlavská 20
625 00 Brno
e-mail: mkerkovsky@fnbrno.cz

Úvod

Vyšetření magnetickou rezonancí (MR) je v současnosti standardní diagnostická metoda u pacientů s klinickou manifestací míšní léze [1]. Problémy však mohou nastat při stanovení diferenciální diagnostiky míšních lézí, kdy se někdy nevyhneme neurčitým závěrům, které neumožňují v daném časovém okamžiku zahájení specifické léčby [2].

MR diagnostika v současnosti disponuje metodami zobrazení, které svým způsobem opouštějí rámec konvenční zobrazovací diagnostiky a začínají poskytovat informace o mikrostrukturální patologii a patofyziologii nejrůznějších onemocnění. Mezi tyto metody se mimo jiné řadí MR zobrazení difuze (Diffusion Weighted Imaging, DWI) a zobrazení tenzorů difuze (Diffusion Tensor Imaging, DTI), metody v současnosti hojně využívané pro zobrazení mozku. V případě zobrazení míchy je jejich využití z různých důvodů méně časté, byť technicky proveditelné [3].

Míru difuzivity molekul vody ve tkáni lze v rámci DWI kvantifikovat pomocí měření tzv. hodnoty ADC (Apparent Diffusion Coeficient). Technicky můžeme vyšetření DTI chápat jako určitou nadstavbu DWI přinášející však zcela nový druh informací. Využíváme zde opakovaného měření s mnoha různými směry gradientu magnetického pole, který slouží k měření difuze. Velikost a trvání tohoto gradientu definuje změny měřeného signálu v závislosti na difuzi – tzv. b-faktor –, což platí i pro prosté DWI vyšetření. Opakovaná směrová aplikace gradientu nám však umožní zhodnocení tzv. anizotropie zkoumané tkáně, která je výrazná u vysoce strukturálně uspořádaných tkání, jakou je např. bílá hmota mozku či míchy [4]. Pro kvantifikaci můžeme využít parametr frakční anizotropie (FA), který odráží míru směrové závislosti procesu difuze ve zkoumané tkáni. Ze získaných obrazových dat DTI je také možno provést rekonstrukci průběhu míšních drah.

Obsahem této pilotní práce je retrospektivní analýza vyšetření DWI a DTI u pacientů s nálezem míšní patologie při konvenčním MR zobrazení s cílem zhodnocení přínosu těchto metod pro diferenciální diagnostiku míšních lézí.

Metodika

Zkoumaný soubor tvoří 11 pacientů s klinickými projevy míšní léze a s nálezem míšního postižení na konvenčním zobrazení MR, u kterých bylo provedeno též DWI či DTI vyšetření míchy. U všech pacientů šlo o obraz zvýšeného signálu míchy na T2 vážených obrazech v rozsahu minimálně jednoho spinálního segmentu s variabilní mírou postkontrastního sycení nebo projevů expanzivity. Spektrum patologií zahrnuje míšní ischemii, ependymom, demyelinizační postižení míchy v rámci roztroušené sklerózy (RS), myelitidu, arteriovenózní malformaci a radiační myelopatii (tab. 1). Uvedená finální diagnóza byla u všech pacientů stanovena na základě klinických a laboratorních nálezů, sledováním vývoje klinického obrazu a nálezů zobrazovacích metod v čase a v případě tumorů též histologickou verifikací.

U všech pacientů byly provedeny standardní základní sekvence pro zobrazení páteřního kanálu – T1, T2 vážený obraz a STIR (Short-Tau Inversion Recovery) v sagitální rovině, dále T2 FFE (Fast Field Echo) v axiální rovině a krčním úseku nebo bTFE (balanced Turbo Field Echo) v axiální rovině v hrudním úseku.

U čtyř pacientů s míšní ischemií bylo provedeno DWI vyšetření technikou echo-planárního zobrazení v prove-

Tab. 1. Klinická data pacientů.

Iniciály	Pohlaví	Věk	Patologie	Etáž	Interval	Klinické příznaky
ZŠ	Ž	81	ischemie	Th3–6	1 den	syndrom transverzální míšní léze v úrovni Th5–6, paraplegie, porucha sfinkterových funkcí
PK	M	58	ischemie	C4–6	7 dnů	kvadruparéza, hranice čití distálně od Th10, sfinkterová dysfunkce
MR	Ž	13	ischemie	Th11–12	1 den	těžká paraparéza, hranice čití distálně od Th7
JC	M	76	ischemie	Th2–5	11 dnů	paraparéza LDK, plegie PDK, hypestezie od Th12, sfinkterová dysfunkce
AŠ	Ž	68	ependymom	C7–Th4	více než rok	těžká paraparéza akcentována vpravo
HD	Ž	60	ependymom	C4–Th1	3 měsíce	porucha citlivosti DKK, paraparéza, mírná porucha sfinkterových funkcí
EM	Ž	44	RS	C5–6	9 měsíců	paraparéza, sfinkterová dysfunkce
MP	Ž	25	RS	C3–7	3 měsíce	centrální triparéza lehkého stupně na PHK a DKK
MM	M	26	myelitida	C2–7	7 dnů	parestezie na LHK a LDK, paréza na obou HK, bolesti hlavy, dysartrie
ŠS	Ž	44	AVM	C1–7	9 dnů	kvadruparéza s levostrannou akcentací, hypestezie na končetinách
JD	M	58	radiační myelopatie	C1–5	2 týdny	paraparéza DKK, v úvodu parestezie DKK

Ž – žena, M – muž, interval – doba mezi vznikem klinických příznaků a MR vyšetřením, LDK – levá dolní končetina, PDK – pravá horní končetina, DKK – dolní končetiny, PHK – pravá horní končetina, LHK levá horní končetina, RS – roztroušená skleróza, AVM – arteriovenózní malformace

dení „single-shot" EPI SSh (tloušťka řezu 4 mm, repetition time – TR 2 000 ms, echo time – TE 75 ms, sklápěcí úhel 90°, matrix 112 × 137) v sagitální a transverzální rovině s dvěma hodnotami b-faktoru přídatného magnetického gradientu (0 a 400 s/mm²). Ze získaných dat byl proveden výpočet mapy ADC na pracovní stanici MR extended workplace (release 2.6.3, Philips Medical Systems, Holandsko). ADC hodnoty byly vypočteny dle vzorce $S/S_0 = \exp(-b \times ADC)$, kde S odpovídá signálu naměřenému při zapnutém gradientu difuze, S_0 signálu bez aplikace gradientu. Následně bylo provedeno měření ADC hodnoty na axiálních řezech míchou pomocí ručního vymezení oblastí zájmu (Region Of Interest, ROI). Měření byla provedena v místě míšní léze s patologicky zvýšeným signálem v T2 obraze a kraniálněji od postižené oblasti v místě bez viditelného postižení míchy. U těchto čtyř pacientů jsme v rámci akutních vyšetření neprováděli DTI zobrazení z časových důvodů a zejména kvůli převažující lokalizace postižení do oblasti hrudní míchy, kde při nutnosti použití cívky SPINE není DTI v našich podmínkách realizovatelné v dostatečné obrazové kvalitě a při zachování únosné doby akvizice.

U ostatních pacientů bylo provedeno vyšetření DTI pomocí 16kanálové hlavové a krční cívky s použitím sekvence EPI SSh v axiální rovině (tloušťka řezu 4 mm, TR 3 549 ms, TE 83 ms, sklápěcí úhel 90°, matrix 136 × 136, velikost voxelu 1,25 × 1,25 × 4 mm) s opakovaným měřením s 15 různými směry přídatného magnetického gradientu o síle 900 s/mm². Získaná data byla softwarově zpracována pomocí aplikace FiberTrak, která je součástí výše uvedené platformy MR extended workplace. Po provedení registrace DTI dat s korekcí pohybu a artefaktů vířivých proudů jsme rekonstruovali mapy ADC a FA, následně jsme měřili hodnoty FA a ADC na axiálním průřezu míchou v místě míšní léze a v místě bez viditelného postižení při konvenčním MR zobrazení. V případě ADC hodnot získaných pomocí DTI zobrazení šlo o izotropní difuzivitu, jež byla v rámci výpočetního zpracování stanovena jako průměr anizotropní difuzivity odvozené z vícečetných zdrojových nekolineárních měření s různými směry magnetického gradientu. Dále jsme provedli rekonstrukci drah míchy pomocí aplikace FiberTrak, která využívá principů
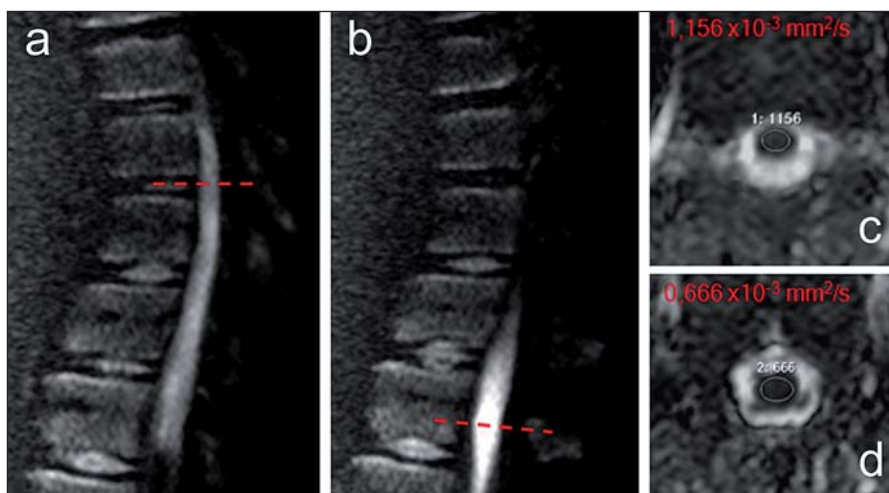
Obr. 1. Difuzně vážené zobrazení u 13leté pacientky s míšní ischemií.
Sagitální difuzně vážené skeny s hodnotou b-faktoru 400 s/mm²; v oblasti míšního konu je zřetelná hyperintenzita (a, b). Přerušované čáry označují místa měření na mapách ADC (Apparent Diffusion Coeficient) v axiální rovině v místě ischemie (d) a kraniálněji v místě bez postižení (c) s nálezem abnormálního poklesu ADC hodnoty v místě ischemické léze.

deterministické traktografie, s umístěním jedné výchozí oblasti zájmu (technika „single-ROI") do oblasti míšní léze případně do sousedních nepostižených segmentů. Pro rekonstrukce traktografie byly nastaveny parametry trasování minimální FA 0,15, maximální změna úhlu 27° a minimální délka vláken 10 mm.

Výsledky

U pacientů s míšní ischemií jsme pozorovali lokální zvýšení T2 signálu míchy v rozsahu 2–4 segmentů s jejím lehkým rozšířením, v DWI obraze bylo v místě postižení patrné zvýšení intenzity signálu (obr. 1). Při kvantifikaci míry difuze jsme zaznamenali pokles ADC hodnot v místě T2 hyperintenzní míšní léze v porovnání s kraniálnějším nepostiženým segmentem, a to v rozmezí 36–61 % (tab. 2).

U všech pacientů vyšetřených pomocí DTI jsme provedli rekonstrukci míšních drah; u obou pacientů s míšním tumorem výsledný obraz svědčil pro hrubší strukturální abnormitu míšních traktů a měl charakter odtlačení a místy také možného přerušení míšních drah působením expanzivní léze. Při umístění ROI přímo do oblasti tkáně tumoru nebyly nalezeny žádné dráhy při daném nastavení trasovacích parametrů. Naopak bylo možné stopovat vlákna míšních drah ve tkáni míchy roztlačené tumorem do periferie. U ostatních pacientů jsme při prostém vizuálním hod-

nocení nepozorovali zřetelnou abnormalitu průběhu míšních traktů v místě patologické léze (obr. 2).

Při hodnocení hodnoty FA jsme u pacientů s míšním tumorem pozorovali výrazný pokles hodnoty FA, a to o 48 a 68 %. U pacientů s diagnózou RS byl patrný středně výrazný pokles hodnoty FA o 16 a 27 %. U pacienta s myelopatií vzniklou za sedm měsíců po radioterapii s frakcionovanou dávkou 30 Gy na oblast krční páteře jsme pozorovali okrsky restrikce difuze míchy s vysokým signálem na DWI a s poklesem ADC hodnoty cca o 30 %.

Diskuze

Onemocnění míchy tvoří heterogenní skupinu postižení etiologie demyelinizační, zánětlivé, vaskulární či tumorózní. Jde často o závažná postižení s hrozbou výrazného funkčního deficitu, v mnoha případech trvalého. Lze říci, že klinické symptomy myelopatie jsou variabilní a z hlediska etiologie poměrně nespecifické.

K hlavním úkolům MR zobrazení u těchto pacientů patří detekce patologické míšní léze a odlišení tumorózní a netumorózní etiologie postižení [1]. V praxi se však občas setkáváme s případy, kdy MR diagnostika selhává například z pohledu nemožnosti přesného stanovení etiologie postižení při nespecifickém obraze [2] nebo z důvodu nedostatečné senzitivity konvenčních sek-

Tab. 2. Měření hodnot ADC a FA (v případě DTI vyšetření) u všech pacientů s různým typem míšní léze.

Iniciály	Patologie	Metoda	ADC norm.	ADC abnorm.	Změna ADC (%)	FA norm.	FA abnorm.	Změna FA (%)
ZŠ	ischemie	DWI	1,233	0,474	−61,6	x	x	x
PK	ischemie	DWI	1,194	0,765	−35,9	x	x	x
MR	ischemie	DWI	1,156	0,666	−42,4	x	x	x
JC	ischemie	DWI	1,235	0,788	−36,2	x	x	x
AŠ	ependymom	DTI	1,129	1,275	12,9	0,574	0,299	−47,9
HD	ependymom	DTI	1,669	1,696	1,6	0,775	0,247	−68,1
EM	SM	DTI	1,04	0,973	−6,4	0,682	0,494	−27,6
MP	SM	DTI	1,309	1,263	−3,5	0,562	0,471	−16,2
MM	myelitida	DTI	1,322	1,187	−10,2	0,624	0,613	−1,8
ŠS	AVM	DTI	1,237	1,038	−16,1	0,567	0,558	−1,6
JD	rad. myelopatie	DTI	1,13	0,797	−29,5	0,623	0,634	1,8

DWI – Diffusion Weighted Imaging (difuzně vážené zobrazení), DTI – Diffusion Tensor Imaging (zobrazení tenzorů difuze), ADC – Apparent Diffusion Coefficient, FA – frakční anizotropie
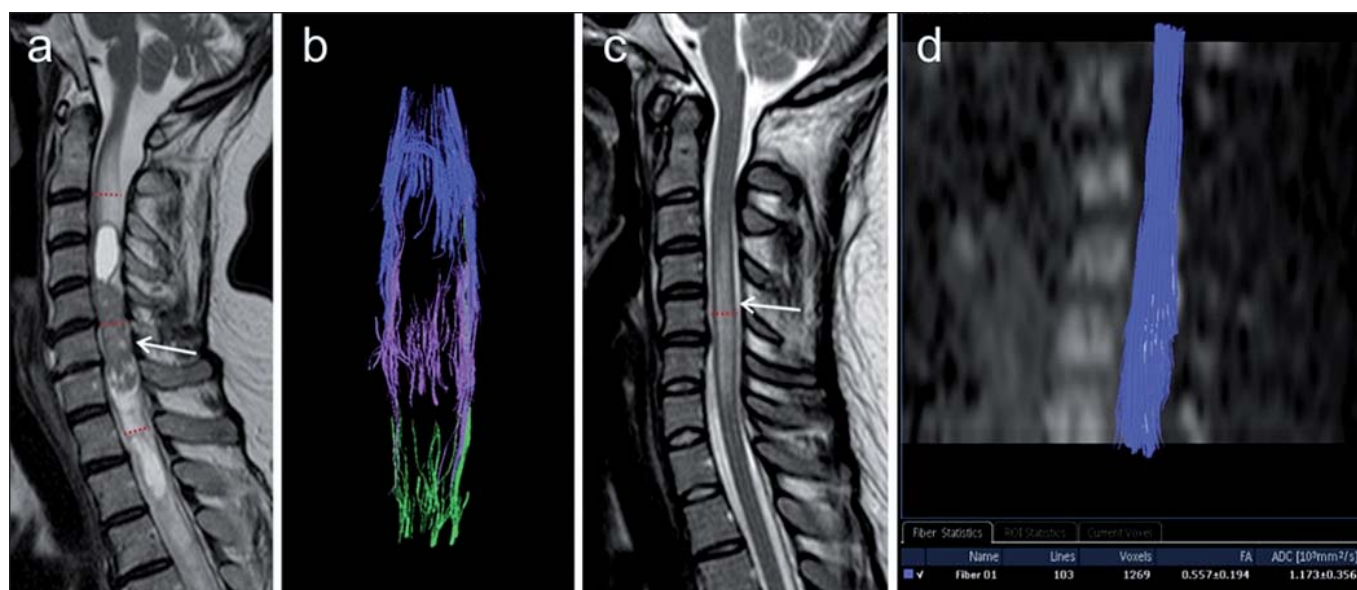
Obr. 2. 3D traktografie u dvou pacientů s postižením míchy různé etiologie.

Obr. 2a, b) Pacientka s míšním tumorem. a) T2 vážený obraz v sagitální rovině, šipka znázorňuje vlastní tumorózní ložisko, v okolí patrný edém a známky hydrosyringomyelie. Červené linie značí úroveň umístění tří různých oblastí zájmu pro traktografii – jedna uprostřed vlastního tumorózního ložiska, další dvě kraniálněji, resp. kaudálněji. b) Traktografie za použití tří oblastí zájmu demonstruje zřetelné roztlačení a přerušení míšních drah (projekce v koronární rovině). Ze žádné ze zvolených oblastí zájmu nebylo možné vystopovat souvislé dráhy probíhající přes celou oblast tumoru, jedná se zde o opakované rekonstrukce technikou „single-ROI".

Obr. 2c, d) Pacientka s dg. roztroušené sklerózy. c) T2 vážený obraz v sagitální rovině, patrna je hyperintenzní míšní léze (šipka). Červená linie značí umístění jedné oblasti zájmu pro traktografii přibližně uprostřed postižené oblasti. d) Traktografie míšních drah na podkladě izotropního DWI obrazu (sagitální rekonstrukce), není zde patrna abnormalita průběhu míšních traktů, které byly spojitě rekonstruovány z jediné oblasti zájmu umístěné do oblasti léze.

vencí, jako je tomu třeba v časném stadiu míšní ischemie [5]. Přitom v případě zobrazení míšních lézí je zvláště důležitá přesná diferenciální diagnostika, neboť možnosti biopsie míchy jsou velmi omezené a zejména u pacientů s míšní lézí potenciálně netumorózní etiologie může vést ke zbytečnému iatrogennímu poškození [2].

Za této situace se pro zobrazení míchy jeví nadějným použití „nových" technik, jakými jsou DWI a DTI. Jejich využití pro diagnostiku míšních lézí je podstatně méně

časté, než je tomu u zobrazení mozku; důvod je možno spatřovat zejména v technických problémech daných mimo jiné nehomogenitou magnetického pole v zobrazované oblasti páteře, která je příčinou zvýšené míry distorzí obrazu a susceptibilních artefaktů, kvalitu zobrazení snižují též pohybové artefakty vzniklé v důsledku pulzací míchy. Problémem může být také dostupnost vhodných sekvencí, které navíc vyžadují velkou míru optimalizace [5]. Přesto je však technika DWI a DTI pro zobrazení míchy prakticky použitelná, což dokládá vícero prací popisujících možnosti využití těchto metod v klinické diagnostice či výzkumných aplikacích [6,7].

Cílem této pilotní práce je shrnutí dosavadních zkušeností autorů s technikou DWI/DTI u pacientů s míšní lézí z pohledu praktické neurodiagnostiky. Těžiště významu DWI vyšetření je možné spatřovat v diagnostice míšní ischemie. U čtyř pacientů s míšní ischemií jsme pozorovali známky restrikce difuze dokumentované výrazným poklesem hodnot ADC, což je ve shodě se závěry několika dalších autorů zabývajících se tímto tématem [5,8]. U lézí zánětlivé, demyelinizační či tumorózní etiologie jsme oproti tomu pozorovali jen malý pokles či naopak vzestup ADC hodnot, v čemž lze proto spatřovat hlavní význam DWI pro diferenciální diagnostiku. Ačkoliv možnosti terapeutického ovlivnění míšní ischemie jsou v současnosti poměrně malé, nasměrování diferenciálnědiagnostické rozvahy směrem k ischemické etiologii může celkově přispět k racionalizaci další diagnostiky. Při standardizaci techniky DWI vyšetření míchy by snad tato metoda v budoucnu mohla přispět i k zahájení účinné včasné terapie.

U pacienta s proběhlou radioterapií na oblast krční páteře byla v diferenciální diagnostice kromě radiační myelopatie zvažována možnost sekundárního míšního tumoru nebo koincidence zánětlivého postižení míchy. V tomto případě jsme pozorovali drobné okrsky restrikce difuze míchy, čímž vznikl obraz charakteru edému v kombinaci s drobnými fokálními ischemiemi. Na základě této skutečnosti jsme označili radiační myelopatii jako nejpravděpodobnější etiologii postižení.

Stejně jako je tomu u vyšetření mozku, i v případě DTI zobrazení míchy se u nej-

různějších patologií ukazuje, že zejména kvantifikace hodnot FA umožňuje citlivější detekci ultrastrukturální patologie míchy v porovnání s konvenčním zobrazením [9]. Autoři Ducreux et al ve své práci poukazují na možnost bližší charakterizace míšních tumorů pomocí kvantifikace hodnot FA [6]. Autoři Vargas et al v nedávné publikaci popisují DTI nálezy u skupiny 14 pacientů s různými typy míšních lézí tumorózní i netumorózní etiologie [10]. U pomalu progredujících patologických procesů, jako je např. ependymom, je popisováno roztlačení nervových traktů míchy, zatímco u akutně vzniklých změn, jako je ischemie či trauma, bylo pozorováno převážně přerušení a defigurace vláken. Dle našich prvotních zkušeností hrubší patologie míchy, jakou je míšní tumor, působí obraz zřetelného roztlačení či eventuálně přerušení míšních traktů na rekonstrukcích traktografie spolu s výrazným snížením hodnoty FA v místě patologické léze. Oproti tomu u patologií, kde je možné očekávat relativně méně výrazné strukturální abnormity míchy, jako je např. demyelinizace či myelitida, bylo snížení hodnot FA méně výrazné a při rekonstrukci míšních drah nebyla patrná abnormalita jejich průběhu. Tímto způsobem by kvantifikace parametrů DTI spolu s hodnocením obrazů traktografie v budoucnu mohla být přínosem pro vzájemnou diferenciaci míšních lézí.

Zřejmým limitem této pilotní práce je malý počet pacientů neumožňující komplexnější statistické vyhodnocení. Jde nicméně o obecný problém prací publikovaných na toto téma, neboť s postižením míchy typu ischemie či tumoru se setkáváme podstatně méně často, než je tomu u onemocnění mozku, situaci navíc dále komplikuje omezená možnost bioptické verifikace; ucelené zhodnocení přínosu DWI/DTI pro diagnostiku míšních lézí lze tedy očekávat spíše v delším časovém horizontu nejpravděpodobněji cestou multicentrických studií či metaanalýz.

S výše uvedeným souvisí též větší heterogenita struktury souboru pacientů z hlediska etiologie onemocnění míchy. Společným jmenovatelem našeho souboru byl nález patologické míšní léze při konvenčním MR zobrazení, který u většiny z těchto pacientů vzbuzoval dia-

gnostické rozpaky. Za této situace bylo využití techniky DWI/DTI přínosné z hlediska poměrně jednoznačného odlišení míšní ischemie od ostatních lézí a správné nasměrování diferenciálnědiagnostické rozvahy mezi tumorózní a netumorózní etiologií, což je stěžejní pro plánování další laboratorní i zobrazovací diagnostiky a v konečném důsledku i zvolení vhodné terapie.

Dle našich prvotních zkušeností tedy technika DWI a DTI může sehrát pozitivní roli v rámci diferenciální diagnostiky myelopatií různé etiologie, byť komplexní zhodnocení této problematiky bude vyžadovat další práce s většími soubory pacientů. Již dnes lze však využití těchto metod doporučit jako součást rozšířeného protokolu MR vyšetření míchy pro jejich neinvazivitu a časovou nenáročnost, neboť u pacientů s míšní lézí nejasné etiologie je jakákoliv nová informace přínosem.

Literatura

1. Do-Dai DD, Brooks MK, Goldkamp A, Erbay S, Bhadelia RA. Magnetic resonance imaging of intramedullary spinal cord lesions: a pictorial review. Curr Probl Diagn Radiol 2010; 39(4): 160–185.
2. Smrčka M, Šprláková A, Smrčka V, Keřkovský M. Problematika indikace operační léčby u intramedulárních lézí. Cesk Slov Neurol N 2010; 73/106(4): 393–397.
3. Holder CA, Muthupillai R, Mukundan S jr, Eastwood JD, Hudgins PA. Diffusion-weighted MR imaging of the normal human spinal cord in vivo. AJNR Am J Neuroradiol 2000; 21(10): 1799–1806.
4. Pierpaoli C, Basser PJ. Toward a quantitative assessment of diffusion anisotropy. Magn Reson Med 1996; 36(6): 893–906.
5. Thurnher MM, Bammer R. Diffusion-weighted MR imaging (DWI) in spinal cord ischemia. Neuroradiology 2006; 48(11): 795–801.
6. Ducreux D, Fillard P, Facon D, Ozanne A, Lepeintre JF, Renoux J et al. Diffusion tensor magnetic resonance imaging and fiber tracking in spinal cord lesions: current and future indications. Neuroimaging Clin N Am 2007; 17(1): 137–147.
7. Thurnher MM, Law M. Diffusion-weighted imaging, diffusion-tensor imaging, and fiber tractography of the spinal cord. Magn Reson Imaging Clin N Am 2009; 17(2): 225–244.
8. Loher TJ, Bassetti CL, Lövblad KO, Stepper FP, Sturzenegger M, Kiefer C et al. Diffusion-weighted MRI in acute spinal cord ischaemia. Neuroradiology. 2003; 45(8): 557–617.
9. Keřkovský M, Šprláková-Puková A, Kašpárek T, Fadrus P, Mechl M, Válek V. Diffusion tensor imaging – současné možnosti MR zobrazení bílé hmoty mozku. Cesk Slov Neurol N 2010; 73/106(2): 136–142.
10. Vargas MI, Delavelle J, Jlassi H, Rilliet B, Viallon M, Becker CD et al. Clinical applications of diffusion tensor tractography of the spinal cord. Neuroradiology 2008; 50(1): 25–29.

Case Report

Diffusion Tensor Imaging in Radiation-Induced Myelopathy

Miloš Keřkovský, PhD, Jana Zitterbartová, MD, Luděk Pour, PhD, Andrea Šprláková-Puková, PhD, Marek Mechl, MD, PhD, MBA

From the University Hospital Brno and Masaryk University, Department of Radiology, Central European Institute of Technology, Multimodal and Functional Imaging Laboratory (MK); Masaryk Memorial Cancer Institute, Department of Radiation Oncology (JZ); University Hospital Brno and Masaryk University, Department of Internal Medicine, Hematology, and Oncology (LP); and Department of Radiology (ASP, MM).

ABSTRACT

Radiation myelopathy (RM) is a rare complication of spinal cord irradiation. Diagnosis is based on the history of radiotherapy, laboratory tests, and magnetic resonance imaging of the spinal cord. The MRI findings may nevertheless be quite unspecific. In this paper, we describe the findings of diffusion tensor imaging in a case of the delayed form of RM. We observed areas of restricted diffusion within the spinal cord which probably corresponded to the ischemic changes. This would concur with the currently accepted pathogenetic theory concerning RM.

Introduction

Radiation myelopathy (RM) is a rare complication of radiotherapy occurring when the radiation dose to the spinal cord has exceeded a certain threshold value. The condition develops after a latent period, which is usually longer than 6 months and may range up to several years.[1]

Diagnosis of RM is based upon the history of irradiation with spinal cord inclusion into the radiation field. The main neurological lesion must be explained by the pathology's affecting those spinal cord segments exposed to the radiation, and other causes of the neurological dysfunction must be excluded.[2] Although magnetic resonance imaging (MRI) is usually used to depict the pathological changes of the spinal cord, the findings may be unspecific and differentiation of the tumor lesion from pathology of a different origin may be problematic.[3]

In this paper, we describe a case involving a patient with delayed-form RM which developed after cervical spine irradiation. Soon after the onset of clinical symptoms, MRI was performed of the cervical spinal cord and diffusion tensor imaging (DTI) was part of the imaging protocol. Thus, we had an opportunity for in vivo observation of the diffusion properties within the spinal cord affected by RM. According to our best knowledge, no other case of DTI application in RM has been described in the literature.

Case Report

A male patient 55 years of age had undergone a CT examination of the cervical spine for severe neck pain with a finding of osteolysis of the first cervical vertebra. This had been subsequently confirmed by MRI (Fig 1). The CT-guided biopsy had revealed plasmocytoma, and further testing had confirmed the diagnosis of multiple myeloma (stage IA according to the Durie-Salmon system). The patient was then treated with chemotherapy (cyclophosphamide, thalidomide, and dexamethasone) and radiotherapy (12×3 Gy/36 Gy) targeted to the affected first cervical vertebra. The treatment technique was based on 2-dimensional conventional planning with 2 laterolateral opposing fields. The local dose to the spinal cord was calculated by planning algorithm and corresponds to the total dose. Autologous transplantation of stem cells was performed 5 months later after high-dose chemotherapy.

Seven months after cessation of radiotherapy, the patient complained of 2 weeks of progressing paresthesia and hypesthesia of the lower limbs and a central paraparesis developed. Conventional MRI examination performed on a 1.5T device discovered cervical spinal cord myelopathy, and DTI revealed small areas of restricted diffusion within the affected spinal cord segment at C2 level with decrease of apparent diffusion coefficient (ADC) values ($.797 \times 10^{-3}$ mm^2/s) compared to the
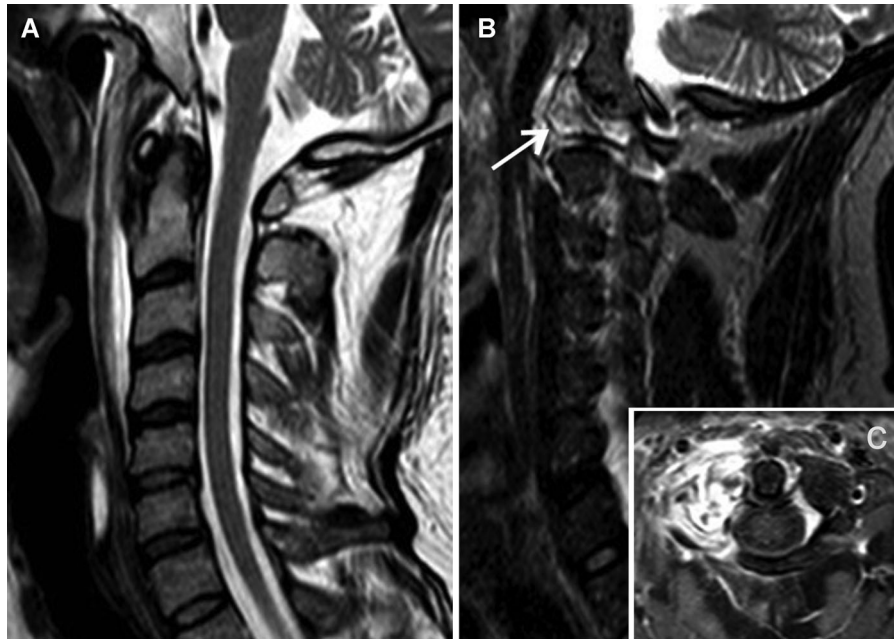
Fig 1. Plasmocytoma infiltration of the first cervical vertebra. (A) A sagittal T2-weighted image depicts normal cervical spinal cord. (B) A short-tau inversion recovery image in sagittal plane. The right part of the atlas has increased signal intensity (arrow). (C) An axial, T1-weighted image with fat saturation after application of contrast agent depicts marked enhancement of the tumor infiltration.

normally appearing spinal cord segment measured at C6 level $(1.13 \times 10^{-3}$ mm^2/s). Fractional anisotropy (FA) values measured in this area were slightly increased (.63) compared to the unaffected spinal cord (.623). The FA values measured within the T2-hyperintense area more caudally (at C3 level) were moderately lower (.587) compared to the normally appearing spinal cord, and ADC value was 1.172×10^{-3} mm^2/s. The FA and ADC values measured at C4 level were .604 and 1.130×10^{-3} mm^2/s, respectively.

Using tractography, we were able to reconstruct the spinal cord fibers without substantial deviation or disruption (Fig 2). For the DTI sequence, we used a single-shot echo planar technique (repetition time 4,438 ms, echo time 83 ms) with 4 mm slice thickness and in-plane resolution 1.25 mm $\times$ 1.25 mm in the axial plane, applying 15 directions of diffusion sensitizing gradient with 900 s/mm^2 as the b value setting. For data analysis, we used the FiberTrak software package that is a part of the MR extended workplace software (Release 2.6.3, Philips Medical Systems, The Netherlands).

At this time, RM was stated as the most probable diagnosis, particularly as cerebrospinal fluid (CSF) analysis did not prove the presence of malignant cells. The follow-up MRI examination showed significant regression of the spinal cord's pathological changes (Fig 3). The patient was treated symptomatically and his clinical state progressively developed to that of persistent quadriparesis.

Discussion

The differential diagnosis of RM may be difficult, because clinical and radiological findings in these patients are unspecific.[4] Differentiation from a tumor's infiltration may be difficult. That

is especially the case when RM is at a fully developed stage, at which time conventional MRI usually reveals the swollen spinal cord with hyperintensity in a T2-weighted image and variable contrast enhancement.[5]

In the case of our patient, we found small areas of the restricted diffusion in the posterior part of the spinal cord, which probably represented the areas of ischemic necrosis. This finding corresponds with the conclusions of other authors previously analyzing MRI diffusion findings in spinal cord ischemia of a different origin and who had reported ADC values for the ischemic spinal cord areas in the range .23-.9 $\times 10^{-3}$ mm^2/s.[6] The inference that these areas of restricted diffusion are indicative of RM is also supported by the pathology of RM itself, as the vascular changes leading to ischemic necrosis of the spinal cord are thought to be among those pathogenic factors responsible for the development of RM.[1] The findings at the other affected segments of the spinal cord (C3 and C4) were not specific as the FA and ADC values measured here were not considerably different from the normally appearing spinal cord.

Blood-brain barrier dysfunction and related brain edema lead to various neurological symptoms. The blocking of leakage from brain capillary endothelium by angiogenesis inhibitor (bevacizumab) seems to be a logical treatment strategy and one that improves clinical outcome.[7] These new therapeutic options make the early diagnosis of RM even more important.

According to a few papers describing DTI findings in spinal cord tumors, restricted diffusion is not characteristically found within the tumors. Liu et al report significantly higher ADC values for tumors compared to tumor-like lesions.[8] Nevertheless, the finding of areas with some level of diffusion restriction may occur also for other types of spinal cord conditions. For
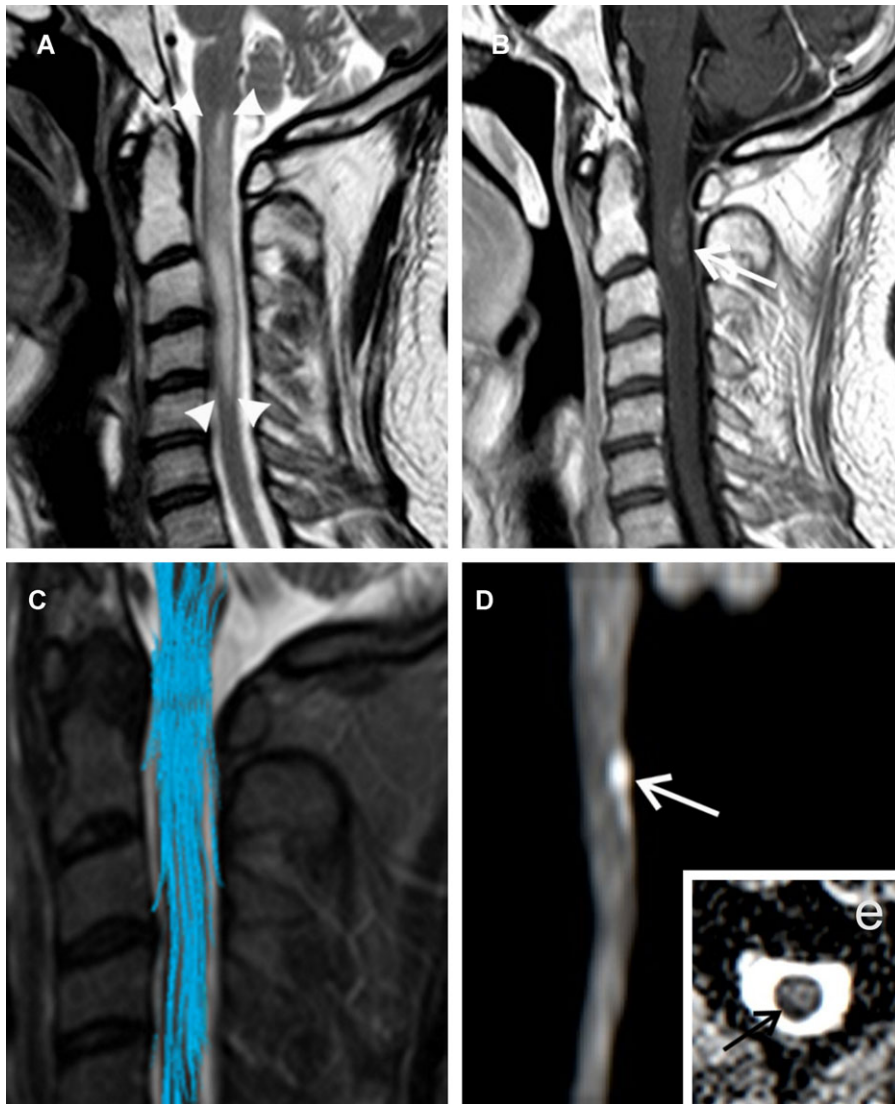
Fig 2. MRI examination performed 7 months after radiotherapy of the C1 infiltration depicts myelopathy with high signal intensity in a T2-weighted image (marked with arrowheads; A), with enhancing lesion after contrast agent's application at C2 level (arrow; B). Tractography reconstruction of the continuous spinal cord fibers without substantial distortions (C). The sagittal reconstruction of the isotropic diffusion image of the spinal cord revealed small areas of high signal intensity in the dorsal part of the spinal cord (arrow) corresponding to the site of the contrast enhancement depicted above (D). The diffusion restriction is confirmed by the small hypointense area in the right dorsolateral part of the spinal cord at the axial image of the ADC map (arrow; E).

example, Zecca et al report a restricted diffusion pattern for acute spinal cord demyelinating lesions.[9] Acute myelitis is also one of the differential diagnostic possibilities in our case. There are only a few reports about the DTI findings in myelitis. Lee et al report decreased FA values of the spinal cord in acute transverse myelitis that was in correlation with clinical outcome;[10] ADC values had not been measured in that case. In comparison to the findings from that report, the FA changes in our case of RM do not seem to be substantial. Renoux et al also report mostly decreased FA values of the spinal cord in patients with myelitis of different etiology.[11] Decrease of the ADC values is in that paper indicated in part of the patients having multiple sclerosis, but the ADC values in cases of acute transverse myelitis were near normal. An inflammatory or demyelinating origin

of the myelopathy also was not likely in the case of our patient, considering his normal values for CSF white cells, that his age was not typical for multiple sclerosis, and that he had no history of demyelinating attacks.

The question may arise whether the diffusion properties of brain radiation necrosis are similar to those of RM. Several authors have used diffusion-weighted imaging or DTI to differentiate between recurrence of high-grade glioma and radiation-induced changes of the brain. Hein et al report significantly higher ADC values within the radiation necrosis compared to the glioma recurrence, and, according to their normalized ADC values, both of the values were higher than those measured in normally appearing contralateral white matter.[12] As it is known that ADC values of ischemic brain tissue
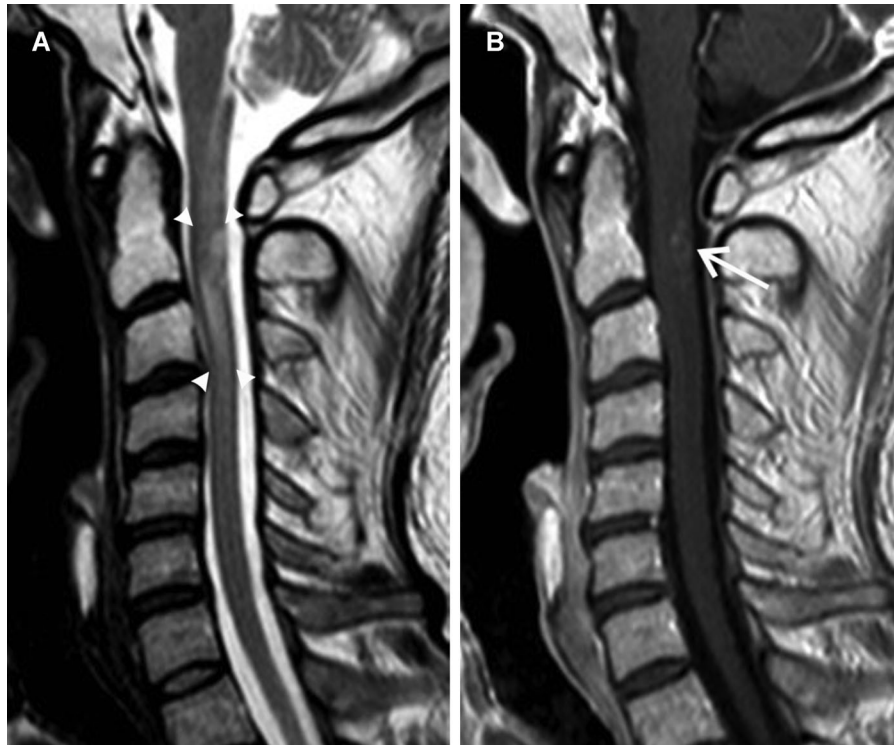
Fig 3. The follow-up MR examination of the cervical spinal cord 1 week after the initial MR. (A) A sagittal T2-weighted image depicts partial regression of the T2-hyperintense area (arrowheads). Also, enhancement of the lesion at C2 level is weaker (arrow) after contrast agent's application (B).

increase over time,[13] the absence of diffusion restriction within the brain radiation necrosis that is in contrast to our observation in RM may be explained by different timing of the brain imaging. A functionally critical spinal cord lesion may lead to earlier indication of the MR imaging, and thus the chance to detect areas with restricted diffusion could be greater. An important role may play also differences in vascular supply of the brain compared to the vascular supply of the spinal cord.

The tractography findings in most of the previously reported cases had suggested severe abnormalities caused by the tumor with displacement or disruption of the fibers.[14] In our case, by contrast, we observed no gross abnormalities of the spinal tract to suggest a mass effect from the spinal cord affection. On the other hand, the true structural damage of the spinal cord pathways was probably underestimated by the tractography because of the spinal cord neurological symptomology present at the time of the DTI examination. Similarly, the FA values measured within the RM affection did not differ substantially from those for the normally appearing spinal cord segment. Despite partial regression in the extent of pathologic signal depicted by the conventional follow-up MR examination, the severe final neurological deficit may be seen as resulting from evolution of destructive changes within the spinal cord.

The diagnosis of RM itself was in this case based on the anamnestic data, lab tests, and repeated MRI scans. The radiation dose for the spinal cord in this patient had been within the currently accepted safe limits, but radiosensitivity of the spinal cord might have been heightened due to the chemotherapy.[15]

Although the described DTI findings should not be considered entirely specific for RM, this technique provided us some additional information and supported the diagnosis of RM. Thus, we were able to choose a "watch-and-wait" strategy that finally led to confirming the RM diagnosis in time enough to avoid spinal cord biopsy.

References

1. Okada S, Okeda R. Pathology of radiation myelopathy. *Neuropathology* 2001;21:247-265.
2. Pallis CA, Louis S, Morgan RL. Radiation myelopathy. *Brain* 1961;84:460-479.
3. Smrčka M, Šprláková A, Smrčka V, et al. Problematika indikace operační léčby u intramedulárních lézí. *Cesk Slov Neurol N* 2010;73(106):393-397.
4. Kadir T, Sarica FB, Ozgur K, et al. Delayed radiation myelopathy: differential diagnosis with positron emission tomography/computed tomography examination. *Asian J Neurosurg* 2012;7:206-209.
5. Alfonso ER, De Gregorio MA, Mateo P, et al. Radiation myelopathy in over-irradiated patients: MR imaging findings. *Eur Radiol* 1997;7:400-404.
6. Thurnher MM, Bammer R. Diffusion-weighted MR imaging (DWI) in spinal cord ischemia. *Neuroradiology* 2006;48:795-801.
7. Levin VA, Bidaut L, Hou P, et al. Randomized double-blind placebo-controlled trial of bevacizumab therapy for radiation necrosis of the CNS. *Int J Radiat Oncol Biol Phys* 2011;79:1487-1495.
8. Liu X, Tian W, Kolar B, et al. Advanced MR diffusion tensor imaging and perfusion weighted imaging of intramedullary tumors

and tumor like lesions in the cervicomedullary junction region and the cervical spinal cord. *J Neurooncol* 2014;116:559-566.

9. Zecca C, Cereda C, Wetzel S, et al. Diffusion-weighted imaging in acute demyelinating myelopathy. *Neuroradiology* 2012;54:573-578.

10. Lee JW, Park KS, Kim JH, et al. Diffusion tensor imaging in idiopathic acute transverse myelitis. *AJR Am J Roentgenol* 2008;191:W52-W57.

11. Renoux J, Facon D, Fillard P, et al. MR diffusion tensor imaging and fiber tracking in inflammatory diseases of the spinal cord. *AJNR Am J Neuroradiol* 2006;27:1947-1951.

12. Hein PA, Eskey CJ, Dunn JF, et al. Diffusion-weighted imaging in the follow-up of treated high-grade gliomas: tumor recurrence versus radiation injury. *AJNR Am J Neuroradiol* 2004;25:201-209.

13. Eastwood JD, Engelter ST, MacFall JF, et al. Quantitative assessment of the time course of infarct signal intensity on diffusion-weighted images. *AJNR Am J Neuroradiol* 2003;24:680-687.

14. Vargas MI, Delavelle J, Jlassi H, Rilliet B, et al. Clinical applications of diffusion tensor tractography of the spinal cord. *Neuroradiology* 2008;50:25-29.

15. Gatcombe H, Lawson J, Phuphanich S, et al. Treatment related myelitis in Hodgkin's lymphoma following stem cell transplant, chemotherapy and radiation: a case report and review of the literature. *J Neurooncol* 2006;79:293-298.

Spine

DIAGNOSTICS

Magnetic Resonance Diffusion Tensor Imaging in Patients With Cervical Spondylotic Spinal Cord Compression

Correlations Between Clinical and Electrophysiological Findings

Miloš Keřkovský, MD,* Josef Bednařík, Prof.,† Ladislav Dušek, Assoc. Prof.,‡ Andrea Šprláková-Puková, MD,*
Igor Urbánek, MD,† Marek Mechl, PhD, MBA,* Vlastimil Válek, Prof.,* and Zdeněk Kadaňka, Prof.†

Study Design. A prospective study evaluating a cohort of patients with spondylotic cervical spine compression.

Objective. To analyze the potential of diffusion tensor imaging (DTI) of the cervical spinal cord in the detection of changes associated with spondylotic myelopathy, with particular reference to clinical and electrophysiological findings.

Summary of Background Data. Conventional magnetic resonance imaging (MRI) may provide confusing findings because of a frequent disproportion between the degree of the spinal cord compression and clinical symptoms. The DTI is known to be more sensitive to subtle pathological changes of the spinal cord compared with conventional MRI.

Methods. The DTI of the cervical spinal cord was performed within a group of 52 patients with spondylotic spinal cord compression and 13 healthy volunteers on a 1.5-T MRI scanner. All patients underwent clinical examination that differentiated between asymptomatic and symptomatic myelopathy subgroups, and 45 patients underwent electrophysiological examination. We measured the apparent diffusion coefficient and fractional anisotropy of the spinal cord at C2/C3 level without compression and at the maximal compression level (MCL). Sagittal spinal canal diameter, cross-sectional spinal cord area, and presence of T2 hyperintensity at the MCL were also recorded. Nonparametric statistical testing was used for comparison of controls with subgroups of patients.

Results. Significant differences in both the DTI parameters measured at the MCL, between patients with compression and control group, were found, while no difference was observed at the noncompression level. Moreover, fractional anisotropy values were lower and apparent diffusion coefficient values were higher at the MCL in the symptomatic patients than in the asymptomatic patients. The DTI showed higher potential to discriminate between clinical subgroups in comparison with standard MRI parameters and electrophysiological findings.

Conclusion. The DTI appears to be a promising imaging modality in patients with spondylotic spinal cord compression. It reflects the presence of symptomatic myelopathy and shows considerable potential for discriminating between symptomatic and asymptomatic patients.

Key words: cervical spondylotic myelopathy, diffusion tensor imaging, magnetic resonance imaging. **Spine 2012;37:48–56**

Diffusion tensor imaging (DTI) is a relatively new technique based on magnetic resonance (MR), capable of depicting structural detail in the brain and spinal cord white matter.[1–5] The DTI parameters, especially fractional anisotropy (FA), have been described as disclosing subtle pathological changes in white matter integrity[1,6,7] and have been of use in various spinal cord disorders.[4,8]

The DTI is a diagnostic approach employing the basic principles of diffusion magnetic resonance imaging (MRI).[9,10] However, in contrast with diffusion-weighted imaging, which images just the rate of water diffusion at a given site, the DTI relies on differences in the rate of water diffusion dictated by various intrinsic alignments within the tissue structures, analogous to the anisotropy of certain crystals.[11,12] The DTI exploits such structural regularity by applying a special diffusion-sensitizing gradient repeatedly in many different directions. Computer analysis of the acquired data set enables the determination of the dominant direction of diffusion of water molecules.[13] The results of the DTI examination may be quantified by 2 main parameters. The first is the apparent diffusion coefficient (ADC) value, which refers to the overall diffusivity of the tissue irrespective of directional

dependence.[14,15] The second parameter, known as the FA, reflects the directional dependence of the diffusion process.[16] This is a relative number in a range from 0 to 1 and increasing in relation to the diffusion anisotropy of the tissue being evaluated.

The issue of clinical aspects and diagnostic imaging becomes particularly important in cervical spondylotic myelopathy (CSM), because the incidence of this disorder is high and has the potential to lead to severe neurological disability. The CSM is considered the most common cause of spinal cord dysfunction in elderly patients.[17]

MRI facilitates precise depiction of spinal canal stenosis and spinal cord compression.[18] However, individual tolerance to compression of the spinal cord may be somewhat variable.[19] MRI findings can thus lead to confusion, arising out of a frequent disproportion between the degree of spinal cord compression and the clinical symptomatology.[20–22]

Considering these data, we hypothesized that DTI parameters might be more sensitive in the detection of myelopathic changes resulting from spinal cord compression and show a better relationship to actual clinical signs of myelopathy in comparison with standard MRI and electrophysiological investigations and parameters.

MATERIALS AND METHODS

Study Design
The study evaluated MR-DTI data in a consecutive series of patients with both symptomatic and asymptomatic degenerative spondylotic cervical cord compression with respect to clinical and electrophysiological findings and in comparison with healthy volunteers.

Patients with cervical spinal cord compression were recruited from consecutive patients examined clinically in the Centre for Spondylogenic Myelopathy of the University Hospital between June 2008 and December 2009, with signs and symptoms of either cervical myelopathy, radiculopathy, or chronic cervical pain, and in whom MRI detected signs of spondylotic cervical spinal cord compression. MRI signs of cervical cord compression were defined as impingement on the cervical cord (i.e., a concave defect in the spinal cord adjacent to the site of disc bulging or osteophyte) and/or compression of the cervical cord (compression ratio of <0.4).[21] DTI was part of the standard imaging protocol in these patients.

Excluded were patients with previous spinal cord injury, with cervical compression of other than degenerative origin or those with documented or suspected significant spinal cord or brain disorder that could mimic CSM. Those who agreed were examined electrophysiologically within 3 months of documentation of cervical cord compression.

The control group was recruited between January 2010 and March 2010 from healthy volunteers—employees of the University Hospital. Originally, 15 age-matched participants without a history of any significant neurological disease (including cervical spine or spinal cord lesion) agreed to take part in the experiment. All were examined clinically (with no signs of cervical spinal cord lesion found), and then the MRI + MR-DTI were performed. Data from 13 participants without signs of cervical cord compression were finally included into the analysis, while 2 participants with asymptomatic spondylotic cervical cord compression detected on MRI were excluded from the analysis.

Participants
The study group comprised a total of 52 patients with MR signs of spondylotic cervical spinal cord compression—33 men and 19 women, average age 58 years, age range 39 to 78 years. Patients with clinical signs and symptoms of cervical myelopathy, who displayed decreased modified Japanese Orthopedic Association scale (<18),[23] made up the symptomatic CSM subgroup (A) and comprised 20 patients (13 men and 7 women, average age 59 years, age range 45 to 78 years). Thirty-two patients with cervical pain and/or symptoms/signs of cervical radiculopathy, but without symptoms/signs of CSM, formed the asymptomatic spondylotic cervical cord encroachment (SCCE) subgroup (B), made up of 20 men and 12 women, average age 57 years, age range 39 to 71 years.

The control group consisted of a group of 13 healthy, age-matched volunteers—9 men and 4 women, average age 57 years, age range 47 to 67 years—with neither evident brain or spinal cord disease nor spondylotic cervical spinal cord compression. Informed consent was obtained from both patients and healthy participants. The study was approved by the institutional ethics board.

Electrophysiological Evaluation
Short-latency somatosensory evoked potentials (SEPs), from the median- and the tibial nerves (SEP), and motor-evoked potentials (MEPs), elicited by means of transcranial and root magnetic stimulation, were taken from 45 patients; 7 patients did not consent to such examination. Central conduction abnormalities attributed to possible cervical spinal cord lesion were defined and recorded. More details on the methodology of evoked potential examination have been given in a previous publication.[22]

Imaging Procedures
All examinations were performed in the 2008 to 2010 period on a 1.5-T MR scanner (Philips Achieva, Philips Medical Systems, Eindhoven, The Netherlands) by using a 16-channel head-and-neck coil. The protocol involved conventional sequences for the evaluation of the spine and spinal cord morphology, including T1, T2, and short-tau inversion recovery images in the sagittal plane and axial T2 fast-field echo scans coherently covering 5 segments of cervical spine from C2/C3 to C6/C7 levels. The DTI scans were acquired in the axial plane with 4-mm slice thickness, using the same geometry settings as for the axial T2 fast-field echo images. Single-shot echo planar imaging was employed for the DTI sequence (repetition time 3549 ms, echo time 83 ms, flip angle 25°), applying 15 directions of diffusion-sensitizing gradient with

900 mT/s as *b* value setting. A parallel acquisition technique of sensitivity encoding (SENSE) was used with a reduction factor of $P = 2$. The T2-weighted single-shot ($b = 0$) image was also acquired to calculate ADC maps (Figure 1).

Image Analysis

For the ADC and FA map calculations and measurements, a FiberTrak software package (Release 2.6.3, Philips Medical Systems, Eindhoven, The Netherlands), which is a part of the MR extended workplace software, was used. Motion coregistration of the diffusion data was performed before the actual analysis. Region-of-interest analysis was applied to the measurements. The regions of interest were placed on a template of the axial isotropic diffusion-weighted images covering the whole cross-sectional area of the spinal cord (Figure 2). Special attention was given to avoiding the surrounding cerebrospinal fluid and contamination through susceptible artifacts. The measurements were performed at the C2/C3 level, both where the spinal canal was wide enough in all patients and no compression of the spinal cord had been recorded (no compression level, NCL), and at the level of maximal spinal cord compression caused by the degenerative spinal canal narrowing (maximal compression level, MCL). This level was identified by the degree of spinal canal narrowing as represented by the reduction of anteroposterior (AP) spinal canal diameter. In patients with multisegmental involvement and similar degrees of spinal canal stenosis, the level with the smallest spinal cord area was chosen. Measurements included mean FA and ADC values of the spinal cord cross section at both levels, as well as the FA and ADC ratios (FA or ADC value at MCL divided by the value at NCL). On the T2–fast-field echo axial scans, we evaluated selected basic morphological parameters (sagittal spinal canal diameter and spinal cord cross-sectional area [CSA]) (Figure 3). Any presence of abnormal T2 hyperintensity of the spinal cord was also recorded.

Data Analysis

Univariate robust statistical techniques were used to test differences in continuous variables between groups of patients. Standard Mann-Whitney *U* test and the Kruskal-Wallis test were applied for mutual comparison of different subgroups of
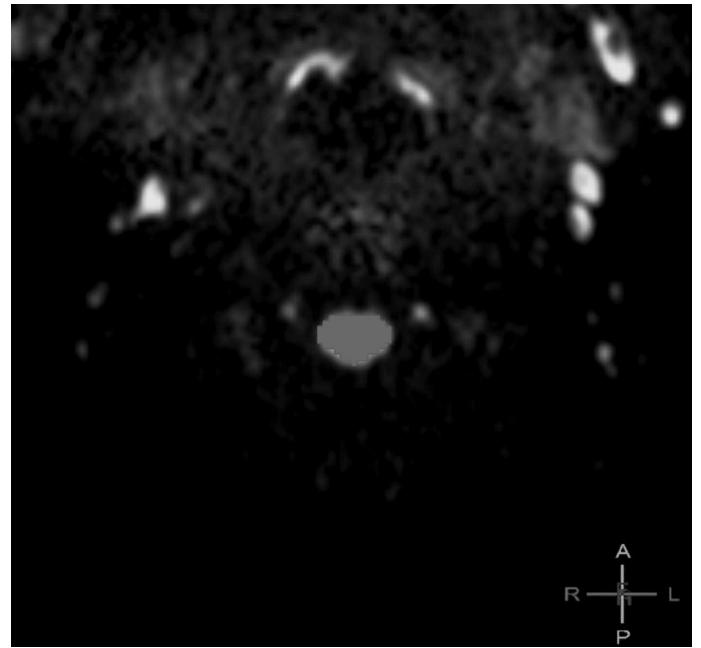
Figure 2. Measurement of the fractional anisotropy and apparent diffusion coefficient values using FiberTrak software. Region of interest is placed over the spinal cord cross section, using an axial isotropic diffusion-weighted image as a template.

patients and controls. Both univariate and multivariate analytical strategies were adopted to quantify the discriminative power of the binary-coded variables and discriminate between symptomatic and asymptomatic clinical subgroups. The odds ratio with 95% confidence limits was estimated on the basis of logistic regression models and tested in the
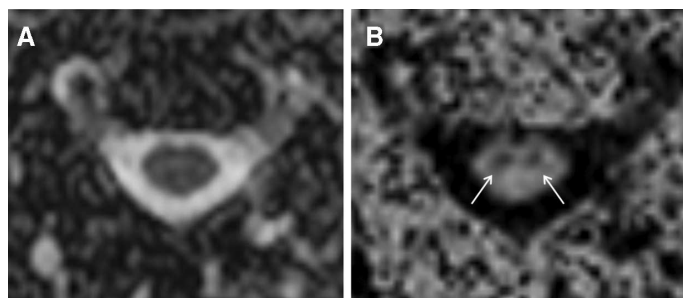
Figure 1. (**A**) Apparent diffusion coefficient map of the spinal cord (axial plane). (**B**) Fractional anisotropy map in axial plane showing structural details of the spinal cord cross section. The gray matter generates a lower signal intensity because of its lower fractional anisotropy values than the white matter (arrows).
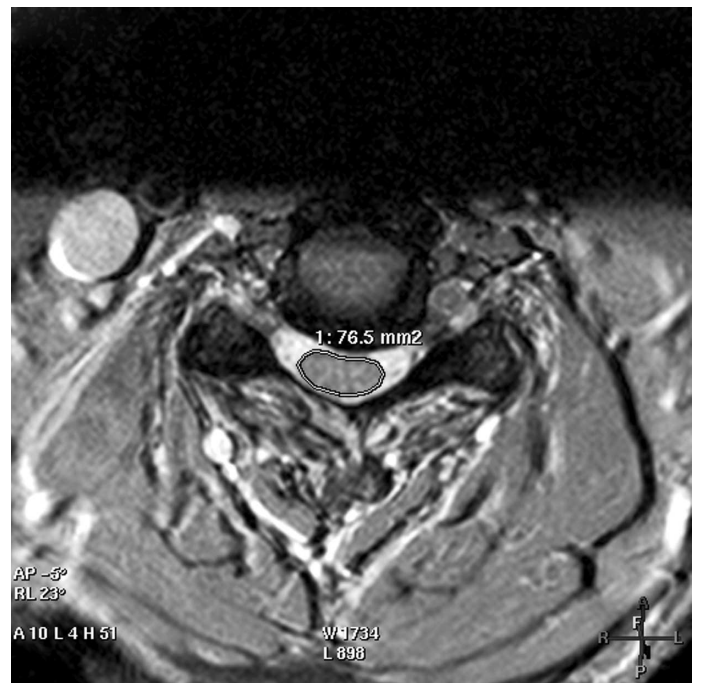
Figure 3. Axial, T2-gradient echo image with measurement of spinal cord cross-sectional area, using manual placement of polygonal region of interest.

Wald test. Parameters with sufficient discrimination power ($P < 0.10$) were then examined for mutual correlation, and interaction terms were coded for significantly correlated pairs of variables. The final set of potential discriminative factors and interaction terms (all as binary code) was subjected to backward stepwise selection algorithm in multivariate logistic regression. The best maximum-likelihood estimates for cutoff values with optimal sensitivity and specificity of the parameters chosen were obtained from computer-assisted receiver-operating characteristic curve analysis. Correlation analyses were carried out using Spearman rank correlation coefficient. $P < 0.05$ was taken as the universal limit for significance for any given statistical test.

To assess the interobserver variability of 4 selected MR-DTI parameters (FA NCL, FA MCL, ADC NCL, and ADC MCL), 2 repeated evaluations of 18 randomly selected patients were performed blindly by 2 different observers (M.K. and A.S.), and the reproducibility was evaluated according to the methodology proposed by Bland and Altman,[24,25] which is based on the standard deviation of the differences between pairs of repeated measurements(SD_{diff}). The test-retest reproducibility assessed by this method was expressed as confidence limits of agreement calculated from SD_{diff} (coefficient of repeatability). The Bland-Altman plot was used to assess a relationship between the differences in order to look for systematic bias and to identify possible outliers. In addition, a standard analysis of variance was employed to assess the proportion of total variability of the selected measures related to the differences between repeated measurements (Table 1).

RESULTS

Both statistical methods employed (based on SD_{diff} and analysis of variance) confirmed a sufficient level of reproducibility of all evaluated imaging parameters (Table 1). The 95% confidence limits for differences between pairs of measurement (based on evaluation of SD_{diff}) varied in the range ±0.100 units for FA NCL (*i.e.*, ±16.7% of mean of primary values), ±0.031 units for FA MCL (±5.7%), ±0.284 units for ADC NCL (±21.3%), and ±0.090 units for ADC MCL (±7.5%). Considering the suggested cutoff values, such results for reproducibility are acceptable. Using standard analysis of variance, the variability of repeated measurements represented up to 17.6% of the total variability of the values, which again shows a good reproducibility of all the parameters tested (data not shown).

Comparison of FA values for controls and patients displayed no significant difference at the C2/C3 level, while at the MCL level (compared with C5/C6 level in controls) the FA values showed significant decreases in both clinical subgroups: symptomatic CSM subgroup ($P = 0.001$) and asymptomatic SCCE ($P = 0.04$) compared with those of the controls.

The ADC values were significantly higher in symptomatic CSM subgroup patients at both NCL and MCL than with the control group (C5/C6 level was used as a counterpart to MCL in the control group; $P = 0.048$ and 0.044, respectively), while they did not differ significantly in the asymptomatic SCCE subgroup (data not shown).

The DTI parameters in symptomatic CSM patients measured at MCL differed significantly from values found in asymptomatic SCCE patients: FA values were significantly lower and ADC values significantly higher in the symptomatic CSM subgroup (Table 2). Moreover, the FA ratio was significantly lower in the symptomatic CSM subgroup.

No differences between symptomatic and asymptomatic patients were detected in terms of the spinal canal area and AP canal diameter (Table 2).

The potential of DTI, other MRI, and electrophysiological parameters transformed to binary form, for discrimination between subsets of spondylotic cervical cord compression patients with and without clinically symptomatic myelopathy are compared in Table 3. The DTI parameters showed higher discrimination power, supported by significantly higher sensitivity and specificity, in comparison with standard MRI parameters (MRI spinal cord hyperintensity, spinal cord CSA), while spinal canal AP diameter and EP abnormalities were not able to discriminate between clinical subgroups (Figure 4).

The EP abnormalities were more frequent in symptomatic CSM patients than in asymptomatic SCCE cases, without statistical significance (Table 4). Furthermore, there was no difference in any of the DTI parameters for subsets of patients with and without EP abnormality (Table 5).

Table 6 shows a multivariate statistical model utilizing an FA ratio less than 0.84, ADC at MCL more than 1.20, and spinal cord CSA less than 65.9, to discriminate asymptomatic SCCE and symptomatic CSM patients with a sensitivity of 70% and a specificity of 78.1%.

DISCUSSION

The study disclosed that MR-DTI parameters were able to discriminate the patients with spondylotic cervical cord compression with respect to the presence of clinically symptomatic myelopathy. The DTI parameters proved superior in this respect compared with the standard MRI parameters used to detect or predict symptomatic myelopathy and to the evoked potential abnormalities that have previously been shown to be capable of predicting the development of clinically symptomatic myelopathy in patients with spondylotic SCCE.[21,22]

The basic motivation for this study was a common clinical-to-imaging mismatch arising out of variable individual tolerance of the spinal cord to the compression caused by degenerative spinal canal narrowing. It has been demonstrated by animal-model experiments that spinal cord function may be surprisingly resistant to compression.[19] This is also manifest in the relatively common "accidental" finding of asymptomatic spondylotic cervical spinal cord compression. Thorpe *et al*[26] described degenerative changes of the cervical spine in 64% of a target group of asymptomatic individuals at ages between 18 and 72 years, and spinal cord compression was noted in 11% of the group. In another study within a group of asymptomatic individuals aged more than 64 years, disc protrusions were described in 57% and spinal cord impingement in 26%.[27] This clinical entity is usually described as asymptomatic SCCE[28,29] or presymptomatic CSM.[21,22]

Parameter	Mean Difference (SD)*	95% CI for Mean Difference†	Limits of Agreement‡	Interobserver Variability,§ %
FA NCL	0.006 (0.051)	−0.018; 0.030	−0.093; 0.106	17.6
FA MCL	0.003 (0.016)	−0.004; 0.011	−0.028; 0.035	1.7
ADC NCL	−0.030 (0.145)	−0.097; 0.037	−0.313; 0.254	11.8
ADC MCL	0.020 (0.046)	−0.002; 0.042	−0.070; 0.110	3.0

TABLE 1. Description of the Interobserver Variability

*Mean and SD_{diff} of interobserver differences.

†95% confidence interval for average interobserver difference (mean ± 1.96 *standard error).

‡Limits of agreement are computed as mean ± 1.96 * SD.

§Computed using repeated-measures analysis of variance as proportion of total variability of the selected measures related to the differences between repeated measurements.

ADC indicates apparent diffusion coefficient; FA, fractional anisotropy; MCL, maximal compression level; NCL, no compression level (C2/C3).

The AP spinal canal diameter and spinal cord cross-sectional area have been reported as correlating with clinical manifestation of CSM, but considerable overlap of measurements recorded in symptomatic and asymptomatic populations has been noted.[30,31] In another recent study,[20] we found a critical interval of 50 to 60 mm² for the development of myelopathy, measured on axial MR images within a subgroup of patients with T2 hyperintensities at the level of spinal cord compression. Severe compression may lead to development of focal areas of increased spinal cord signal intensity on T2-weighted MR images; the exact pathophysiology, however, remains unclear.[32] Moreover, there exists only limited consensus about the clinical value of T2 hyperintensities with respect to clinical manifestation of the disorder and response to its treatment.[33–36]

TABLE 2. Comparison Between DTI and Selected MRI Parameters for Patients With Symptomatic CSM and Asymptomatic SCCE

MRI Parameter	Group	Level	Median (5th–95th Percentile Range)	P (Mann-Whitney U Test)
FA	SCCE	NCL	0.60 (0.51; 0.75)	0.446
	CSM	NCL	0.58 (0.51; 0.64)	
	SCCE	MCL	0.54 (0.44; 0.69)	0.029
	CSM	MCL	0.48 (0.35; 0.61)	
FA ratio*	SCCE	MCL/NCL	0.89 (0.69; 1.12)	0.034
	CSM	MCL/NCL	0.81 (0.61; 1.03)	
ADC, 10^{-3}mm²/s	SCCE	NCL	1.28 (0.90; 1.52)	0.430
	CSM	NCL	1.33 (0.97; 1.58)	
	SCCE	MCL	1.13 (0.85; 1.37)	0.022
	CSM	MCL	1.26 (0.90; 1.57)	
ADC ratio*	SCCE	MCL/NCL	0.88 (0.69; 1.13)	0.164
	CSM	MCL/NCL	0.94 (0.66; 1.30)	
Spinal canal AP diameter, mm	SCCE	MCL	7.9 (5.3; 10.3)	0.402
	CSM	MCL	7.7 (3.8; 9.6)	
Spinal cord CSA, mm²	SCCE	MCL	66.9 (48.5; 75.8)	0.201
	CSM	MCL	63.7 (37.4; 77.8)	

*Ratio: Value at MCL divided by value at NCL.

ADC indicates apparent diffusion coefficient; CSA, cross-sectional area; CSM, (symptomatic) cervical spondylotic myelopathy; DTI, diffusion tensor imaging; FA, fractional anisotropy; MCL, maximal compression level; MRI, magnetic resonance imaging; NCL, no compression level (C2/3); SCCE, (asymptomatic) spondylotic cervical cord encroachment.

TABLE 3. Potential of Binary-Coded Parameters to Discriminate Between Patients With Asymptomatic SCCE and Those With Symptomatic CSM

Parameters*	Univariate Logistic Models		ROC Analysis			
	P†	Odds Ratio (95% CI)	AUC (95% CI)	P	Sensitivity	Specificity
ADC MCL > 1.20	0.002	7.00 (2.01; 24.36)	0.73 (0.58; 0.87)	0.007	70.0%	75.0%
FA ratio‡ ≤ 0.84	0.006	5.57 (1.65; 18.84)	0.70 (0.55; 0.85)	0.016	65.0%	75.0%
FA MCL ≤ 0.50	0.011	4.75 (1.43; 15.75)	0.68 (0.53; 0.84)	0.026	65.0%	71.9%
Spinal cord CSA < 65.9	0.015	4.46 (1.34; 14.83)	0.68 (0.53; 0.83)	0.032	70.0%	65.6%
Hyperintensity: yes	0.018	4.37 (1.29; 14.73)	0.67 (0.51; 0.82)	0.046	55.0%	78.1%
ADC ratio‡ >1.00	0.084	2.92 (0.87; 9.86)	-	-	-	-
EP abnormality	0.098	2.91 (0.84; 10.10)	-	-	-	-
Spinal canal AP diameter ≤7.9	0.358	1.70 (0.55; 5.28)	-	-	-	-

*All quantitative parameters were coded as binary predictors on the basis of cutoff points leading to maximum sensitivity and specificity.

†Wald test.

‡Ratio: value at MCL divided by value at NCL (C2/C3).

ADC indicates apparent diffusion coefficient; AP, anteroposterior; AUC, area under the ROC curve; CI, confidence interval; CSA, cross-sectional area; CSM, (symptomatic) cervical spondylotic myelopathy; EP, evoked potentials; FA, fractional anisotropy; MCL, maximal compression level; NCL, no compression level (C2/C3); ROC, receiver operating characteristic; SCCE, (asymptomatic) spondylotic cervical cord encroachment.

DTI is believed to have great potential for the detection of pathological ultrastructural changes of the brain white matter.[5] Considerably fewer studies of spinal cord DTI have been published, but there are several reports of superior sensitivity for DTI measurements in terms of subtle pathological changes in the spinal cord as compared with conventional MRI.[4,37,38] A few authors[39–43] have also mentioned significant changes in the FA and/or ADC values of the spinal cord, arising out of compression; the results, however, are not entirely uniform. Demir et al[38] described an increase of ADC values in 34 patients with spinal cord compression. Facon et al[41] do not refer to changes in ADC values caused by spinal cord compression but emphasize the high sensitivity of FA. In agreement with previous studies[41,43] quantitatively evaluating changes of diffusivity in compressed spinal cord, we found a significant decrease of FA at MCL not only in both subgroups of patients in comparison with controls without compression but also in symptomatic cases compared with the asymptomatic cases. This fact may be partially explained by gray matter "contamination" of

Figure 4. Two patients with similar degrees of spinal cord compression on conventional magnetic resonance examination, compared to demonstrate the possible application of diffusion tensor imaging. (**A** and **D**) A patient with clinical symptoms of myelopathy with a fairly low fractional anisotropy value (0.426) at the level of maximal compression. (**B** and **C**) A patient with evident spinal cord compression due to disc herniation, with no clinical signs of myelopathy. The fractional anisotropy value was higher in this case (0.707). The arrows on the sagittal scans (**A** and **C**) indicate the level of measurements (**B** and **D**).
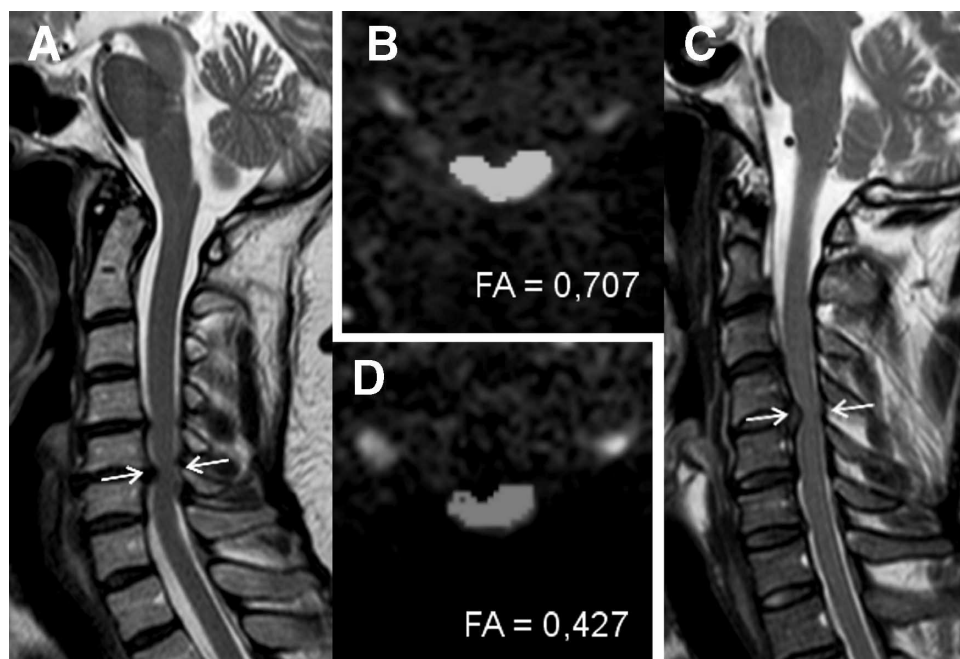
TABLE 4. Frequency of EPs–Abnormalities in Clinical Subsets of Patients With Spondylotic Cervical Cord Compression

Clinical Subgroup	No. of Patients With Abnormal Finding/%		
	Motor EP	Somatosensory EP	Overall EP*
Symptomatic CSM (n = 18)	9/50.0	10/55	12/66.6
Asymptomatic SCCE (n = 27)	7/25.9	8/29.6	10/40.7

*Abnormal motor EP and/or somatosensory EP.

CSM indicates cervical spondylotic myelopathy; EP, evoked potential; SCCE, spondylotic cervical cord encroachment.

measured regions of interest, covering the entire cross section of the spinal cord. Spinal cord gray matter exhibits lower anisotropy than the white matter,[44] and therefore gray matter contamination could be increased in proportion to the degree of lowering the spinal cord CSA. Another reason may

be sought in true damage to the spinal cord white matter, represented by demyelization or axonal disintegration leading to increased diffusivity across the neural tracts. This has been described by several authors[7,45,46] investigating experimental spinal cord damage in animal models. Similarly, we found higher ADC values at the MCL level in symptomatic CSM cases compared with the controls and asymptomatic SCCE patients. The ADC value changes dependent on clinical manifestation may arise partly out of extracellular water content,[47] in analogous fashion to the course of changes in diffusivity observed in spinal cord ischemia.[48,49]

The sensitivity and specificity of both FA and ADC values as predictors of symptomatic myelopathy were higher in our study than in the presence of spinal cord T2 hyperintensity or reduction of the spinal cord area. Evoked potential abnormalities have been reported as predicting the development of symptomatic CSM in cases with asymptomatic SCCE.[21,22] Frequency and degree of EP abnormalities have been shown to be higher in symptomatic CSM than with the controls and asymptomatic compression cases,[50] but discriminating power was not sufficient to separate symptomatic and asymptomatic subgroups in our comparatively small sample of patients. Moreover, spondylotic cervical cord compression subgroups with normal and abnormal

TABLE 5. Comparison of Selected MR-DTI and Conventional MR Parameters in Subsets of Spondylotic Cervical Cord Compression Cases With Normal Versus Abnormal EPs

Parameter	Group	Level	Median (5th–95th percentile)	P (Mann-Whitney U Test)
FA	EP normal	NCL	0.618 (0.530; 0.678)	0.192
	EP abnormal	NCL	0.602 (0.495; 0.652)	
	EP normal	MCL	0.557 (0.455; 0.646)	0.220
	EP abnormal	MCL	0.544 (0.393; 0.638)	
FA ratio*	EP normal	MCL/NCL	0.922 (0.756; 1.065)	0.586
	EP abnormal	MCL/NCL	0.931 (0.663; 1.142)	
ADC	EP normal	NCL	1.286 (1.159; 1.495)	0.115
	EP abnormal	NCL	1.224 (1.030; 1.433)	
	EP normal	MCL	1.095 (0.918; 1.419)	0.820
	EP abnormal	MCL	1.119 (0.885; 1.543)	
ADC ratio*	EP normal	MCL/NCL	0.864 (0.709; 1.061)	0.180
	EP abnormal	MCL/NCL	0.909 (0.714; 1.366)	
Spinal canal AP diameter	EP normal	MCL	7.8 (6.4; 10.3)	0.725
	EP abnormal	MCL	7.7 (5.3; 10.1)	
CSA	EP normal	MCL	65.2 (50.6; 72.9)	0.601
	EP abnormal	MCL	66.9 (44.7; 77.8)	

*Ratio: value at MCL divided by value at NCL (C2/C3).

ADC indicates apparent diffusion coefficient; AP, anteroposterior; CSA, cross-sectional area; DTI, diffusion tensor imaging; EP, evoked potentials; FA, fractional anisotropy; MCL, maximal compression level; MR, magnetic resonance; NCL, no compression level (C2/C3).

TABLE 6. Multivariate Logistic Model Discriminating Asymptomatic SCCE and Symptomatic CSM Patients and Validation of Multivariate Score in ROC Analysis

Predictors in Multivariate Logistic Model	P*	Odds Ratio (95% CI)†
FA ratio‡ ≤ 0.84	0.046	4.293 (1.026–17.967)
ADC MCL > 1.20	0.006	7.647 (1.817–32.194)
Spinal cord CSA ≤ 65.9	0.048	3.781 (1.017–14.058)
ROC analysis of multivariate model		
AUC (95% CI)	0.841 (0.734–0.947)	
P	<0.001	
Sensitivity	70.0%	
Specificity	78.1%	

*Wald test.

†Multivariate adjusted odds ratio.

‡Ratio: value at MCL divided by value at NCL (no compression level, C2/3).

ADC indicates apparent diffusion coefficient; AUC, area under the ROC curve; CI, confidence interval; CSA, cross-sectional area; CSM, (symptomatic) cervical spondylotic myelopathy; FA, fractional anisotropy; MCL, maximal compression level; ROC, receiver operating characteristic; SCCE, (asymptomatic) spondylotic cervical cord encroachment.

➤ **Key Points**

❑ In the current article, the potential of diffusion tensor imaging (DTI) in the detection of spondylotic myelopathy changes, in relation to clinical and electrophysiological findings, is analyzed.

❑ The DTI parameters of the compressed spinal cord differ significantly between patients and controls as well as between subgroups with and without symptomatic myelopathy.

❑ The accuracy of the DTI in discrimination between clinical subgroups of patients is higher than those of the attributes of conventional magnetic resonance imaging.

evoked potentials showed no differences in DTI parameters, suggesting different pathogenic mechanisms for EP abnormalities and changes of spinal cord tissue diffusivity.

The interpretation of the measurements in individual patients may be brought into question through variability in the absolute values of the parameters measured. Both ADC and FA values of the normal spinal cord appear to be age dependent.[43] Moreover, the FA values are significantly dependent on the number of directions of the diffusion-sensitizing gradient and also on voxel size.[51] In this context, it might be helpful to use the relative FA index (MCL/NCL), which, according to our data, significantly decreases in symptomatic patients.

To conclude, DTI appears to be a promising imaging modality in patients with spondylotic spinal cord compression. It reflects the presence of symptomatic myelopathy and shows diagnostically acceptable validity in discrimination between symptomatic and asymptomatic cases when compared with the conventional MR and electrophysiological parameters. A relatively simple measurement procedure using a standard "built-in" software package might facilitate possible future practical application of the method. The value of the DTI parameters in predicting further spontaneous course and the effects of surgical decompression awaits further investigation.

References

1. Assaf Y, Pasternak O. Diffusion tensor imaging (DTI)–based white matter mapping in brain research: a review. *J Mol Neurosci* 2008;34:51–61.
2. Bello L, Gambini A, Castellano A, et al. Motor and language DTI fiber tracking combined with intraoperative subcortical mapping for surgical removal of gliomas. *Neuroimage* 2008;39:369–82.
3. Berman JI, Berger MS, Chung SW, et al. Accuracy of diffusion tensor magnetic resonance imaging tractography assessed using intraoperative subcortical stimulation mapping and magnetic source imaging. *J Neurosurg* 2007;107:488–94.
4. Ducreux D, Fillard P, Facon D, et al. Diffusion tensor magnetic resonance imaging and fiber tracking in spinal cord lesions: current and future indications. *Neuroimaging Clin N Am* 2007;17:137–47.
5. Kerkovsky M, Sprláková-Pukova A, Kasparek T, et al. Diffusion tensor imaging—current possibilities of brain white matter magnetic resonance imaging. *Cesk Slov Neurol N* 2010;73/106;136–42.
6. Harsan LA, Poulet P, Guignard B, et al. Brain dysmyelination and recovery assessment by noninvasive *in vivo* diffusion tensor magnetic resonance imaging. *J Neurosci Res* 2006;83:392–402.
7. Kozlowski P, Raj D, Liu J, et al. Characterizing white matter damage in rat spinal cord with quantitative MRI and histology. *J Neurotrauma* 2008;25:653–76.
8. Vargas MI, Delavelle J, Jlassi H, et al. Clinical applications of diffusion tensor tractography of the spinal cord. *Neuroradiology* 2008;50:25–9.
9. Basser PJ, Mattiello J, LeBihan D. MR diffusion tensor spectroscopy and imaging. *Biophys J* 1994;66:259–67.
10. Mukherjee P, Chung SW, Berman JI, et al. Diffusion tensor MR imaging and fiber tractography: technical considerations. *AJNR Am J Neuroradiol* 2008;29:843–52.
11. Pierpaoli C, Basser PJ. Toward a quantitative assessment of diffusion anisotropy. *Magn Reson Med* 1996;36:893–906.
12. Basser PJ. Inferring microstructural features and the physiological state of tissues from diffusion-weighted images. *NMR Biomed* 1995;8:333–44.
13. Basser PJ, Pajevic S, Pierpaoli C, et al. *In vivo* fiber tractography using DT-MRI data. *Magn Reson Med* 2000;44:625–32.
14. Patel MR, Siewert B, Warach S, et al. Diffusion and perfusion imaging techniques. *Magn Reson Imaging Clin N Am* 1995;3:425–38.
15. Mascalchi M, Filippi M, Floris R, et al. Diffusion-weighted MR of the brain: methodology and clinical application. *Radiol Med* 2005;109:155–97.
16. Basser PJ, Pierpaoli C. Microstructural and physiological features of tissues elucidated by quantitative-diffusion-tensor MRI. *J Magn Reson B* 1996;111:209–19.
17. Young WF. Cervical spondylotic myelopathy: a common cause of spinal cord dysfunction in older persons. *Am Fam Physician* 2000;62:1064–70.

18. Alexander JT. Natural history and nonoperative management of cervical spondylosis. In: Menezes AH, ed. *Principles of Spinal Surgery*. New York, NY: McGraw-Hill; 1996:547–57.

19. Al-Mefty O, Harkey HL, Marawi I, et al. Experimental chronic compressive cervical myelopathy. *J Neurosurg* 1993;79:550–61.

20. Kadanka Z, Kerkovsky M, Bednarik J, et al. Cross-sectional transverse area and hyperintensities on magnetic resonance imaging in relation to the clinical picture in cervical spondylotic myelopathy. *Spine* 2007;32:2573–7.

21. Bednarik J, Kadanka Z, Dusek L, et al. Presymptomatic spondylotic cervical myelopathy—an updated predictive model. *Eur Spine J* 2008;17:421–31.

22. Bednarik J, Kadanka Z, Dusek L, et al. Presymptomatic spondylotic cervical cord compression. *Spine* 2004;29:2260–9.

23. Benzel EC, Lancon J, Kesterson L, et al. Cervical laminectomy and dentate ligament section for cervical spondylotic myelopathy. *J Spinal Disord* 1991;4:286–95.

24. Bland JM, Altman DG. Statistical methods for assessing agreement between two methods of clinical measurement. *Lancet* 1986;1:307–10.

25. Bland JM, Altman DG. Measuring agreement in method comparison studies. *Stat Methods Med Res* 1999;8:135–60.

26. Thorpe JW, Kidd D, Kendall BE, et al. Spinal cord MRI using multiarray coils and fast-spin echo. I. Technical aspects and findings in healthy adults. *Neurology* 1993;43:2625–31.

27. Teresi LM, Lufkin RB, Reicher MA, et al. Asymptomatic degenerative disk disease and spondylosis of the cervical spine: MR imaging. *Radiology* 1987;164:83–8.

28. Murphy DR, Coulis CHM, Gerrard JK. Cervical spondylosis with spinal cord encroachment: should preventive surgery be recommended? *Chiropractic Osteopathy* 2009;17:8.

29. Bednařík J, Sládková D, Kadaňka Z, et al. Are subjects with spondylotic cervical cord encroachment at increased risk of cervical spinal cord injury after minor trauma? *J Neurol Neurosurg Psychiatry* 2011;82:779–81.

30. Nurick S. The pathogenesis of the spinal cord disorder associated with cervical spondylosis. *Brain* 1972;95:87–100.

31. Penning L, Wilmink JT, van Woerden HH, et al. CT myelographic findings in degenerative disorders of the cervical spine: clinical significance. *AJR Am J Roentgenol* 1986;146:793–801.

32. Ratliff J, Voorhies R. Increased MRI signal intensity in association with myelopathy and cervical instability: case report and review of the literature. *Surg Neurol* 2000;53:8–13.

33. Kohno K, Kumon Y, Oka Y, et al. Evaluation of prognostic factors following expansive laminoplasty for cervical spinal stenotic myelopathy. *Surg Neurol* 1997;48:237–45.

34. Matsuda Y, Miyazaki K, Tada K, et al. Increased MR signal intensity due to cervical myelopathy. Analysis of 29 surgical cases. *J Neurosurg* 1991;74:887–92.

35. Wada E, Ohmura M, Yonenobu K. Intramedullary changes of the spinal cord in cervical spondylotic myelopathy. *Spine* 1995;20:2226–32.

36. Yone K, Sakou T, Yanase M, et al. Preoperative and postoperative magnetic resonance image evaluations of the spinal cord in cervical myelopathy. *Spine* 1992;17:388–92.

37. Lee JW, Park KS, Kim JH, et al. Diffusion tensor imaging in idiopathic acute transverse myelitis. *AJR Am J Roentgenol* 2008;191:W52–7.

38. Ohgiya Y, Oka M, Hiwatashi A, et al. Diffusion tensor MR imaging of the cervical spinal cord in patients with multiple sclerosis. *Eur Radiol* 2007;17:2499–504.

39. Ries M, Jones RA, Dousset V, et al. Diffusion tensor MRI of the spinal cord. *Magn Reson Med* 2000;44:884–92.

40. Demir A, Ries M, Moonen CT, et al. Diffusion-weighted MR imaging with apparent diffusion coefficient and apparent diffusion tensor maps in cervical spondylotic myelopathy. *Radiology* 2003;229:37–43.

41. Facon D, Ozanne A, Fillard P, et al. MR diffusion tensor imaging and fiber tracking in spinal cord compression. *AJNR Am J Neuroradiol* 2005;26:1587–94.

42. Aota Y, Niwa T, Uesugi M, et al. The correlation of diffusion-weighted magnetic resonance imaging in cervical compression myelopathy with neurologic and radiologic severity. *Spine* 2008;33:814–20.

43. Mamata H, Jolesz FA, Maier SE. Apparent diffusion coefficient and fractional anisotropy in spinal cord: age and cervical spondylosis-related changes. *J Magn Reson Imaging* 2005;22:38–43.

44. Mamata H, Jolesz FA, Maier SE. Characterization of central nervous system structures by magnetic resonance diffusion anisotropy. *Neurochem Int* 2004;45:553–60.

45. Herrera JJ, Chacko T, Narayana PA. Histological correlation of diffusion tensor imaging metrics in experimental spinal cord injury. *J Neurosci Res* 2008;86:443–7.

46. Cheung MM, Li DT, Hui ES, et al. *In vivo* diffusion tensor imaging of chronic spinal cord compression in rat model. *Conf Proc IEEE Eng Med Biol Soc* 2009;2009:2715–8.

47. Le Bihan D. Molecular diffusion, tissue microdynamics, and microstructure. *NMR Biomed* 1995;8:375–86.

48. Loher TJ, Bassetti CL, Lövblad KO, et al. Diffusion-weighted MRI in acute spinal cord ischaemia. *Neuroradiology* 2003;45:557–61.

49. Küker W, Weller M, Klose U, et al. Diffusion-weighted MRI of spinal cord infarction—high resolution imaging and time course of diffusion abnormality. *J Neurol* 2004;251:818–24.

50. Bednařík J, Kadaňka Z, Voháňka S, et al. The value of somatosensory and motor-evoked potentials in predicting and monitoring the effect of therapy in spondylotic cervical myelopathy (prospective randomised study). *Spine* 1999;24:1593–8.

51. Santarelli X, Garbin G, Ukmar M, et al. Dependence of the fractional anisotropy in cervical spine from the number of diffusion gradients, repeated acquisition, and voxel size. *Magn Reson Imaging* 2010;28:70–6.

ORIGINAL RESEARCH

WILEY Brain and Behavior
Open Access

Predictors of symptomatic myelopathy in degenerative cervical spinal cord compression

Zdenek Kadanka Jr[1] | Blanka Adamova[1,2] | Milos Kerkovsky[3] | Zdenek Kadanka[1] |
Ladislav Dusek[4] | Barbora Jurova[3] | Eva Vlckova[1,2] (iD) | Josef Bednarik[1,2] (iD)

[1]Department of Neurology, University Hospital Brno, Brno, Czech Republic

[2]Applied Neurosciences Research Group, Central European Institute of Technology, Masaryk University Brno, Brno, Czech Republic

[3]Department of Radiology, University Hospital Brno, Brno, Czech Republic

[4]Institute of Biostatistics and Analyses, Faculty of Medicine, Masaryk University Brno, Brno, Czech Republic

Correspondence
Josef Bednarik, Department of Neurology, University Hospital, Brno, Czech Republic.
Email: bednarik.josef@fnbrno.cz

Funding information
This study was funded by grant project NT-13449-4 of the Internal Grant Agency of the Ministry of Health of the Czech Republic and by the Ministry of Health of the Czech Republic project for conceptual development in research organizations, ref. 65269705 (University Hospital, Brno, Czech Republic)

Abstract

Objectives: To update a previously established list of predictors for neurological cervical cord dysfunction in nonmyelopathic degenerative cervical cord compression (NMDCCC).

Material and Methods: A prospective observational follow-up study was performed in a cohort of 112 consecutive NMDCCC subjects (55 women and 57 men; median age 59 years, range 40–79 years), either asymptomatic (40 subjects) or presenting with cervical radiculopathy or cervical pain (72 subjects), who had completed a follow-up of at least 2 years (median duration 3 years). Development of clinical signs of degenerative cervical myelopathy (DCM) as the main outcome was monitored and correlated with a large number of demographic, clinical, electrophysiological, and MRI parameters including diffusion tensor imaging characteristics (DTI) established at entry.

Results: Clinical evidence of the first signs and symptoms of DCM were found in 15 patients (13.4%). Development of DCM was associated with several parameters, including the clinical (radiculopathy, prolonged gait and run-time), electrophysiological (SEP, MEP and EMG signs of cervical cord dysfunction), and MRI (anteroposterior diameter of the cervical cord and cervical canal, cross-sectional area, compression ratio, type of compression, T2 hyperintensity). DTI parameters showed no significant predictive power. Multivariate analysis showed that radiculopathy, cross-sectional area (CSA) ≤ 70.1 mm^2, and compression ratio (CR) ≤ 0.4 were the only independent significant predictors for progression into symptomatic myelopathy.

Conclusions: In addition to previously described independent predictors of DCM development (radiculopathy and electrophysiological dysfunction of cervical cord), MRI parameters, namely CSA and CR, should also be considered as significant predictors for development of DCM.

KEYWORDS
cervical radiculopathy, degenerative cervical myelopathy, magnetic resonance imaging, nonmyelopathic degenerative cervical cord compression, predictive model

1 | INTRODUCTION

Degenerative cervical cord compression detected by imaging methods, mostly magnetic resonance imaging (MRI), is a prerequisite for the clinical diagnosis of degenerative cervical myelopathy (DCM). This overarching term is preferred to describe the various degenerative conditions of the cervical spine that cause myelopathy, including most frequent cervical spondylotic myelopathy, but also degenerative disc disease and ossification of the posterior longitudinal ligament and of the ligamentum flavum (Nouri, Tetreault, Singh, Karadimas, & Fehlings, 2015). There is a considerable body of current research related to various aspects of DCM, including prognostic factors (Tetreault, Karpova, & Fehlings, 2015; Tetreault, Nouri, Singh, Fawcett, & Fehlings, 2014). In recent years, studies have demonstrated that asymptomatic degenerative cervical cord compression detected on MRI (Boden et al., 1990; Matsumoto et al., 1998; Teresi et al., 1987) may be of a prevalence that exceeds that of symptomatic myelopathy (Bednarik et al., 2004, 2008; Bednařík et al., 1998; Kovalova et al., 2016; Wilson et al., 2013). Knowledge of the prevalence, as well as the frequency, of myelopathy development, and of risk factors influencing this progression, however, is sparse (Wilson et al., 2013). Such knowledge would be of crucial importance to the practical management of asymptomatic degenerative cervical cord compression, and bear upon the important issue of indications for preventive surgical decompression.

In other studies, we have established that the presence of symptomatic cervical radiculopathy and central conduction deficit in the cervical cord, disclosed by electrophysiological methods—somatosensory (SEP) and/or motor-evoked potentials (MEP)—were independent predictors for the development of symptomatic DCM (Bednarik et al., 2004, 2008; Bednařík et al., 1998). These results tally, in part, with those of an international survey undertaken by the spine care community (Wilson et al., 2013) that identified the presence of radiculopathy together with MRI evidence of intramedullar T2 hyperintensity as important factors influencing the decision to perform preventive decompressive surgery in nonmyelopathic patients with degenerative cervical cord compression.

Our previous study (Bednarik et al., 2008), although extensive, had several limitations. Most importantly, the patients, although lacking any clear myelopathic symptoms and/or signs (i.e., "nonmyelopathic"), were in fact not completely asymptomatic, as our cohort was recruited from consecutive patients referred for radiculopathy and/or cervical axial pain. The term "asymptomatic" degenerative cervical cord compression should be reserved for completely asymptomatic cases, while nonmyelopathic subjects with or without signs/symptoms of radiculopathy or cervical pain should be referred to in terms of "nonmyelopathic degenerative cervical cord compression" (NMDCCC). As one of two alternative criteria for MRI-detected cervical cord compression, we used compression ratio (CR) < 0.4 that might preclude less severe diffuse compression to be included into the study.

Further, spinal cord T2 hyperintensity is considered an important risk factor by the spine care community (Wilson et al., 2013), and diffusion tensor imaging (DTI) parameters have shown the capacity to differentiate cervical myelopathy patients not only from normal individuals (Chen et al., 2016; Guan et al., 2015; Lee et al., 2015) but also from nonmyelopathic cervical cord compression cases (Kerkovsky et al., 2012), and further to correlate with severity of myelopathy (Rajasekaran et al., 2014), the segments of the cervical cord involved (Suetomi et al., 2016), and to predict postsurgical outcome (Arima et al., 2015). A re-evaluation of the predictive model describing the risk of progression of NMDCCC to symptomatic myelopathy (Bednarik et al., 2008) was thus indicated, in a sample also including completely asymptomatic subjects with less severe stages of degenerative cervical cord compression and with the use of DTI parameters to validate the previous model.

2 | MATERIAL & METHODS

The sample size calculation, about 120 patients, was based on an anticipated frequency of DCM development of about 18% over the course of 3 years (derived from the previous study, Bednarik et al., 2008) and the number of evaluated predictors (20).

The study sample here consisted of a cohort of consecutive subjects who had been referred to the Department of Neurology between January 2012 and December 2013 with clinical signs and symptoms of cervical radiculopathy, moderate-to-severe chronic or intermittent axial cervical pain, and volunteers in whom MRI signs of degenerative cervical cord compression had previously been detected during an epidemiological study focusing on the prevalence of degenerative cervical cord compression in the population of the province of South Moravia (Kovalova et al., 2016). The inclusion of volunteers from the epidemiological study, complying with the criteria for the current study into prospective evaluation, had been planned beforehand.

All subjects in the study had to comply with the following inclusion criteria:

- MR signs of degenerative compression of the cervical spinal cord with or without concomitant change in signal intensity from the cervical cord on T2/T1 images (see "Imaging" below)
- Absence of any current myelopathic clinical signs and symptoms that could probably be attributed to cervical cord involvement, from the following list.

  Symptoms:

- Gait disturbance
- Numb and/or clumsy hands
- Lhermitte's phenomenon
- Bilateral arm paresthesias
- Weakness of lower or upper extremities
- Urinary urgency, frequency, or incontinence.

Signs:

- Corticospinal tract signs:
  o Hyperreflexia/clonus
  o Spasticity
  o Pyramidal signs (Babinski's or Hoffman's sign)
  o spastic paresis of any of the extremities (most frequently lower spastic paraparesis)
- Flaccid paresis of one or two upper extremities in the plurisegmental distribution
- Atrophy of hand muscles
- Sensory involvement in various distributions in upper or lower extremities (always plurisegmental)
- Gait ataxia with positive Romberg sign.

Originally, 137 NMDCCC subjects were included into the prospective evaluation. Twenty-five subjects were lost during follow-up and the follow-up of at least 2 years was completed by a group of 112 subjects (55 women and 57 men; median age 59 years, range 34–79 years): 72 subjects had nonmyelopathic signs or symptoms probably related to degenerative changes of the cervical spine (namely axial pain and/or symptoms or signs of upper extremity monoradiculopathy), while 40 subjects were completely asymptomatic. The whole study cohort was a completely new sample, and none of these subjects had been included in a previously published prospective study on this topic (Bednarik et al., 2004).

Ethical approval for the study was granted by the Ethical Committee of the University Hospital, Brno.

2.1 | Clinical evaluation

A detailed clinical examination was carried out at the beginning of the study and every 6 months thereafter. Patients were instructed about possible signs and symptoms that might indicate newly developed DCM and encouraged to arrange a consultation with a neurologist from the study group if they suspected a progression to myelopathy. The minimum follow-up period was 24 months (median 30 months; range 24–48 years).

A standardized, timed 10-m walk and run (as quickly as possible) was evaluated, in terms of time taken and number of steps required.

The primary end-point of the study was the detection of development of symptomatic DCM based on the occurrence of at least one symptom and one sign (from the list used as exclusionary criteria—see above), which were probably attributed to degenerative cervical cord compression, were not present at the beginning of the follow-up and had no other topical or etiological explanation.

Clinical evaluation focused on the determination of development of symptomatic myelopathy (as primary outcome) was performed by neurology specialists experienced in the diagnosis and practical management of myelopathic cases (ZK, ZKJ, MN) and the final decision on meeting the outcome, that is, development of symptomatic DCM, was approved by ZK, a senior neurologist with a long-term experience in clinical studies on cervical myelopathy.

2.2 | Imaging

Plain anteroposterior, oblique, and lateral radiograms were obtained in all patients. Their Torg–Pavlov ratio (TPR) at C5 level was calculated from lateral radiograms as the anteroposterior diameter of the spinal canal divided by the anteroposterior diameter of the vertebral body. All subjects underwent MRI examination of the cervical spine on a 1.5 T MR device with a 16-channel head and neck coil. The standardized imaging protocol included conventional pulse sequences in sagittal-T1, T2 and short-tau inversion recovery (STIR) and axial planes (gradient-echo T2) for the purpose of morphological evaluation and a DTI sequence in the axial plane coherently covering five segments of the cervical spine from levels C2/3 to C6/7. The DTI scans were acquired at a slice thickness of 4 mm, with the same geometry settings as those employed for the axial T2 images. The clinical status of patients/volunteers was blinded to the neuroradiologists who examined the cervical spine MRIs. The MRI of every subject was evaluated by two neuroradiologists, who agreed on the assessment of the compression in the majority of cases. Where disagreement existed—seldom—the final decision was based on a cooperative decision.

The imaging criterion for cervical cord compression was defined as a change in spinal cord contour or shape at the level of an intervertebral disc on axial or sagittal MRI scan compared to that at midpoint level of neighboring vertebrae.

Spinal cord compression was further graded as:

- Impingement, that is focal concave, usually anterior, defect of spinal cord contour and with preservation of a major part of subarachnoid space outside of the compression—type I (Figure 1a)
- Flat or circular compression with partially preserved subarachnoid space—type IIa (Figure 1b)—or with lost subarachnoid space—type IIb (Figure 1c).

The following conventional MRI parameters were also measured: Cross-sectional spinal cord area (CSA), anteroposterior (AP) and laterolateral (LL) spinal cord diameter, compression ratio considered in terms of anteroposterior/laterolateral spinal cord diameter (CR) (Arima et al., 2015; Wilson et al., 2013), circumference of spinal cord (CSC), and anteroposterior diameter of cervical canal (APo). These measurements were taken at the level of maximum spinal cord compression (MCL) identified as maximum reduction of AP spinal canal diameter in comparison with other segments. In patients with multisegmental involvement and a similar degree of spinal canal stenosis, the level with the smallest spinal cord area was chosen. The presence of T2 hyperintensity was also noted.

FiberTrak, Extended MR WorkSpace (release 2.6.3.5, Philips Medical Systems) was used for DTI data analysis. Diffusion data were processed and fractional anisotropy (FA) and apparent diffusion coefficient (ADC) values calculated. Measurements were subjected to region-of-interest (ROI) analysis by placing the ROIs at the level of intervertebral disks over the entire spinal cord area depicted on the axial images of isotropic diffusion. Mean FA and ADC values of the spinal cord cross-sections were recorded at maximum
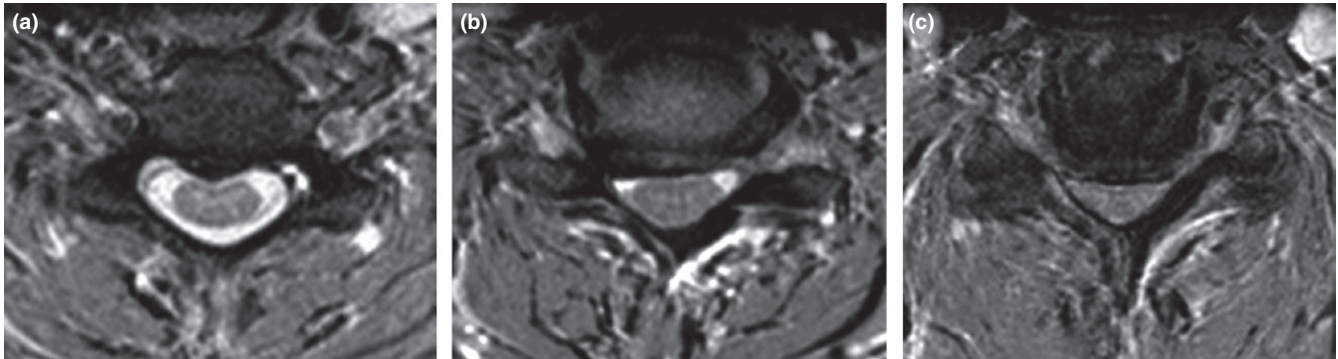
FIGURE 1 (a) Example of the "impingement" type of spondylotic cervical cord compression (type I): focal concave anterior defect of spinal cord contour and with preserved subarachnoid space. (b) Example of a flat compression with partially preserved subarachnoid space (type IIa). (c) Example of a flat compression with lost subarachnoid space (type IIb)

compression level (MCL) in all NMDCCC subjects. FA (ADC) ratios were calculated as FA (ADC) at MCL levels divided by FA (ADC) at C2/3 level.

2.3 | Electrophysiological evaluation

Short-latency SEPs from the median and the tibial nerves were elicited at the beginning of the study by electrical stimulation of mixed nerves at the wrist and the ankle. Similarly, MEPs were elicited by means of transcranial and root magnetic stimulation and recorded from abductor digiti minimi and abductor hallucis muscles on both sides. Details on the methodology of electrophysiological examination and evaluation of results with definition of central conduction abnormality attributable to possible cervical spinal cord lesion are described in previous publications (Bednarik et al., 2004, 2008; Bednařík et al., 1998).

Motor and sensory conduction studies were performed on six motor nerves (median, ulnar, and tibial nerves bilaterally) and four sensory (ulnar and sural nerves bilaterally) using conventional techniques. Needle EMG from four muscles (deltoid, biceps brachii, triceps brachii, and first dorsal interosseous) was performed bilaterally with assessment of spontaneous activity, motor unit potential parameters, and interference patterns. EMG signs of acute motor axonal neuropathy in one myotome (C5–Th1) corresponding with radicular signs and symptoms were classified as radicular. EMG signs of acute, subacute, or chronic motor axonal neuropathy, established in more than one myotome (C5–Th1) unilaterally or bilaterally, were classified as signs of anterior horn cell lesion resulting from degenerative cervical myelopathy.

The following variables were recorded at the entry examination and their association with the predefined end-points (i.e., development of clinically symptomatic DCM and time taken for it) were analyzed.

2.4 | Demographic and clinical data

- Age
- Sex
- Baseline clinical status:

  o Presence of clinical symptoms and signs of cervical radiculopathy (with corresponding CT and/or MR findings and, in the case of motor deficit with corresponding EMG findings, of motor axonal neuropathy in one myotome)
  o Cervical pain
  o Randomly recruited asymptomatic subjects
- 10-m timed walk (time and number of steps)
- 10-m timed run (time and number of steps).

2.5 | Electrophysiological data

- Abnormal SEP interpreted as lesion in either segmental dorsal horn or dorsal column
- Abnormal MEP interpreted as lesion of corticospinal tract
- Abnormal EMG signs of plurisegmental anterior horn cell lesion.

2.6 | Imaging data

- TPR
- AP, LL, CR, CSC, CSA
- FA and ADC at MCL level
- FA and ADC ratios
- T2 hyperintensity
- Type of MRI-detected cervical cord compression
- Maximum stenotic level and number of stenotic levels

2.7 | Statistical analysis

Standard univariate statistical techniques were used to test differences between the chosen subgroups of patients and association between the parameters examined: Fisher's exact test for binary outcomes (or its extension—Fisher–Freeman–Halton exact test for contingency tables larger than 2 × 2) and Mann–Whitney U test for continuous variables.

The power of parameters to discriminate between NMDCCC subjects who developed symptomatic DCM and those who remained asymptomatic was evaluated by receiver operating curve (ROC)

analysis and expressed as area under curve (AUC), with sensitivity and specificity based on established cut-off values. The power of parameters to predict development of DCM was calculated using univariate logistic regression. All continuous parameters were also coded as binary predictors on the basis of cut-off points defined in ROC analysis.

Finally, multivariate model—adjusted logistic regression—was used to seek independent predictors for the development of symptomatic DCM. The variables were selected using a forward step-wise selection algorithm.

3 | RESULTS

Clinical evidence of the first signs and symptoms of DCM within the entire follow-up period was found in 15 patients (13.4%): the DCM+ subgroup. DCM developed in seven cases (6.3%) during the first 12 months of the follow-up period. The frequency of myelopathic symptoms and signs in our cohort are summarized in Table 1. Gait disturbance was the most frequent symptom, followed by numb or clumsy hands, while corticospinal tract signs represented dominant initial clinical presentation on neurological examination.

Baseline characteristics for the development of symptomatic cervical myelopathy are summarized in Table 2. Demographic factors (age, sex), maximum compression level, Torg–Pavlov ratio and DTI parameters showed no difference in distribution between DCM+ subgroup and those who did not develop symptomatic DCM (DCM− subgroup). Several clinical (baseline clinical symptoms or signs, parameters of gait and run), electrophysiological (SEP, MEP, EMG), and imaging parameters (type of compression, T2 hyperintensity, APo, AP, CSA, CR), however, displayed differences between DCM+ and DCM− subgroups.

TABLE 1 Frequency of myelopathic symptoms and signs in 15 patients with newly developed DCM

	Frequency (no of patients)
Symptoms	
Gait disturbance	9
Numb and/or clumsy hands	7
Weakness of lower extremity	3
Bilateral arm paresthesias	2
Lhermitte's phenomenon	1
Signs	
Hyperreflexia/clonus	5
Pyramidal signs (Babinski's or Hoffman's sign)	4
Sensory involvement (plurisegmental)	3
Gate ataxia	3
Flaccid paresis of upper extremity (plurisegmental)	3
Spastic paresis of lower extremity, spastic gate	2

Some of these parameters were able to discriminate significantly NMDCCC subjects who developed symptomatic DCM (n = 15) from those who remained asymptomatic (n = 97) (Table 3). Furthermore, the predictive value of parameters to forecast development of DCM using univariate logistic regression and Cox proportional hazard models was evaluated (Table 4). Among significant predictors were the presence of radiculopathy, quantitative gait and run parameters, electrophysiological signs of cervical cord dysfunction detected by SEP, MEP and EMG, and several radiological parameters: type IIB of MRI compression, APo, AP, CSA, CR, and the presence of T2 hyperintensity. DTI parameters showed no significant predictive power.

Multivariate analysis using multivariate-adjusted logistic regression model, however, disclosed radiculopathy, CSA ≤ 70.1 mm^2, and CR ≤ 4.0 as being the only independent predictors (Table 5).

4 | DISCUSSION

This contribution reports the results of a validation study on the predictors for neurological dysfunction in the nonmyelopathic patient with degenerative cervical spinal cord compression. In a sample of subjects with NMDCC that included individuals with no signs and symptoms related to degeneration of the cervical spine, it emerged that cervical radiculopathy is the most important independent predictor for development of DCM. In addition, it established the independent predictive power of certain MRI parameters: CSA < 70.1 mm^2 and CR < 0.4.

In a previous study, with a cohort of 199 NMDCCC individuals followed for 48 months, the authors documented the predictive value of cervical radiculopathy and electrophysiological signs of cervical cord dysfunction detected with SEP and MEP. This cohort, however, included nonmyelopathic but not completely asymptomatic cases, referred to a neurologist for radiculopathy or cervical pain. In this study, 37.5% of nonmyelopathic subjects had the least severe type of compression (type I) and 20.5% the most severe, type IIb. The data from the previous study (Bednařík et al., 1998) were re-evaluated, and the proportions of types I and IIb proved different, with a lower proportion of type I (25.6%) and a higher proportion of type IIb (36.2%). Similarly, CSA < 70 mm^2 was present in 22.3% of individuals in this study compared with 39.7% in the previous one. Thus, subjects in the former study were largely more severe, although still myelopathy-free cases compared with this study, and this probably accounts for the partial discrepancy between the lists of independent predictors in the two studies and for why CSA and CR were disclosed as independent predictors for DCM development. These parameters have been shown to have high reliability in the assessment of cervical cord compression (Karpova et al., 2013; Kovalová, Bednařík, Keřkovský, Adamová, & Kadaňka, 2015). It is not surprising that adding completely asymptomatic subjects to our study group led to a lower proportion of NMDCCC individuals developing DCM in comparison with the former study (13.4% over 3 years and 7.3% during the first year in comparison with 22.6% over 48.4 months and 8.0 during the first year).

TABLE 2 Baseline characteristics in relation to the development of symptomatic cervical myelopathy

Parameter[a]	Total (n = 112)	DCM+ (n = 15)	DCM− (n = 97)	p[b]
Sex (male)	57 (50.9%)	8 (53.3%)	49 (50.5%)	.999
Age	59.0 (34.0; 79.0)	58.0 (42.0; 77.0)	59.0 (34.0; 79.0)	.898
Baseline clinical status				
Asymptomatic	40 (35.7%)	2 (13.3%)	38 (39.2%)	.015
Cervical pain	50 (44.6%)	6 (40.0%)	44 (45.4%)	
Radiculopathy	22 (19.6%)	7 (46.7%)	15 (15.5%)	
Gait: time (s)	6.0 (3.8; 19.7)	8.8 (4.0; 19.7)	6.0 (3.8; 16.0)	.015
Gait: steps	13.0 (6.0; 29.0)	18.0 (10.0; 29.0)	13.0 (6.0; 21.0)	.002
Run: time (s)	4.0 (2.2; 13.0)	5.1 (3.0; 13.0)	4.0 (2.2; 8.0)	.003
Run: steps	11.0 (7.0; 23.0)	12.0 (8.0; 23.0)	11.0 (7.0; 19.0)	.143
EMG signs of myelopathy	7 (6.3%)	3 (20.0%)	4 (4.1%)	.049
Abnormal MEP	10 (8.9%)	5 (33.3%)	5 (5.2%)	.004
Abnormal SEP	17 (15.2%)	6 (40.0%)	11 (11.3%)	.011
Torg–Pavlov ratio	0.9 (0.5; 1.5)	0.9 (0.6; 1.2)	0.9 (0.5; 1.5)	.187
Maximum compression level				
C3/4	15 (13.4%)	2 (13.3%)	13 (13.4%)	.668
C4/5	25 (22.3%)	4 (26.7%)	21 (21.6%)	
C5/6	61 (54.5%)	9 (60.0%)	52 (53.6%)	
C6/7	11 (9.8%)	0 (0.0%)	11 (11.3%)	
Type of compression				
I	42 (37.5%)	1 (6.7%)	41 (42.3%)	.005
IIA	47 (42.0%)	7 (46.7%)	40 (41.2%)	
IIB	23 (20.5%)	7 (46.7%)	16 (16.5%)	
APo (mm)	8.0 (4.7; 12.6)	7.5 (5.1; 9.8)	8.3 (4.7; 12.6)	.015
AP (mm)	6.7 (4.7; 8.7)	6.1 (4.7; 7.5)	6.7 (4.8; 8.7)	.015
LL (mm)	14.6 (12.3; 17.3)	14.6 (13.0; 15.8)	14.6 (12.3; 17.3)	.966
SCC (mm)	36.4 (31.0; 42.9)	35.7 (33.4; 39.0)	36.5 (31.0; 42.9)	.356
CSA (mm^2)	78.7 (53.0; 103.7)	67.1 (53.0; 88.4)	79.4 (54.4; 103.7)	.001
CR	0.5 (0.3; 0.6)	0.4 (0.3; 0.5)	0.5 (0.3; 0.6)	.004
T2 hyperintensity	11 (9.8%)	5 (33.3%)	6 (6.2%)	.006
FA MCL	0.5 (0.3; 0.7)	0.5 (0.4; 0.6)	0.5 (0.3; 0.7)	.620
ADC MCL	1.2 (0.6; 1.6)	1.2 (1.0; 1.4)	1.1 (0.6; 1.6)	.093
FA ratio	0.9 (0.5; 1.6)	0.9 (0.6; 1.1)	0.9 (0.5; 1.6)	.513
ADC ratio	0.9 (0.6; 1.5)	0.9 (0.7; 1.1)	0.9 (0.6; 1.5)	.522

ADC, apparent diffusion coefficient; ADC ratio, ADC at MCL level/C2/3 level; AP, anteroposterior spinal cord diameter; APo, anteroposterior cervical canal diameter; CR, compression ratio; CSA, cross-sectional spinal cord area; DCM, degenerative cervical myelopathy; EMG, electromyography; FA, fractional anisotropy; FA ratio, FA at MCL level/C2/3 level; LL, laterolateral spinal cord diameter; MCL, maximum compression level; MEP, motor-evoked potentials; SCC, spinal cord circumference; SEP, somatosensory-evoked potentials.

[a]Median (minimum–maximum) values were used for continuous variables; absolute and relative frequencies were used for categorical variables. Statistically significant differences are expressed in bold type (p < .05).

[b]Mann–Whitney U test was used for continuous variables; Fisher's exact test or Fisher–Freeman–Halton exact test was used for categorical variables.

The main limitation of this study is the low number of outcome events in relation to the high number of potential predictors, which weakened the statistical evaluation. In contrast to radiculopathy, which proved a significant predictor in both the current and the previous study (Bednarik et al., 2008) and is generally accepted as such (Wilson et al., 2013), MRI parameters

TABLE 3 Discrimination power of parameters to distinguish between NMDCCC subjects who developed symptomatic DCM (n = 15) and those that remained asymptomatic (n = 97)

Parameter	AUC (95% CI)[a]	p	Cut-off	Sensitivity (%)	Specificity (%)
Sex (male)	0.514 (0.357; 0.672)	.861	—	53.3	49.5
Age	0.510 (0.358; 0.662)	.898	≤59.5	66.7	49.5
Gait: time (s)	0.696 (0.534; 0.858)	**.015**	≥7.35	80.0	66.0
Gait: steps	0.754 (0.601; 0.906)	**.002**	≥17.5	53.3	90.7
Run: time (s)	0.743 (0.584; 0.901)	**.004**	≥4.95	71.4	72.2
Run: steps	0.621 (0.457; 0.784)	.148	≥12.5	50.0	74.4
EMG signs of myelopathy	0.579 (0.410; 0.748)	.324	—	20.0	95.9
Abnormal MEP	0.641 (0.470; 0.812)	.080	—	33.3	94.8
Abnormal SEP	0.643 (0.476; 0.810)	.075	—	40.0	88.7
Torg–Pavlov ratio	0.606 (0.455; 0.757)	.188	≤0.925	73.3	51.5
APo (mm)	0.695 (0.553; 0.838)	**.015**	≤8.4	93.3	42.3
AP (mm)	0.694 (0.546; 0.842)	**.016**	≤5.75	46.7	89.7
LL (mm)	0.503 (0.346; 0.661)	.966	≤15.95	100.0	10.3
SCC (mm)	0.574 (0.431; 0.718)	.356	≤34.35	33.3	84.5
CSA (mm^2)	0.760 (0.624; 0.897)	**.001**	≤70.1	66.7	82.5
CR	0.733 (0.588; 0.877)	**.004**	≤0.40	60.0	89.7
T2 hyperintensity	0.636 (0.466; 0.806)	.092	—	33.3	93.8
FA MCL	0.540 (0.407; 0.673)	.620	≤0.5975	93.3	24.7
ADC MCL	0.635 (0.522; 0.748)	.093	≥1.089	93.3	42.3
FA ratio	0.553 (0.424; 0.681)	.513	≤1.0205	93.3	30.9
ADC ratio	0.552 (0.401; 0.702)	.522	≥0.938	53.3	64.9

ADC, apparent diffusion coefficient; ADC ratio, ADC at MCL level/C2/3 level; AP, anteroposterior spinal cord diameter; APo, anteroposterior cervical canal diameter; CR, compression ratio; CSA, cross-sectional spinal cord area; DCM, degenerative cervical myelopathy; EMG, electromyography; FA, fractional anisotropy; FA ratio, FA at MCL level/C2/3 level; LL, laterolateral spinal cord diameter; MCL, maximum compression level; MEP, motor-evoked potentials; SCC, spinal cord circumference; NMDCCC, nonmyelopathic degenerative cervical cord compression; SEP, somatosensory-evoked potentials.
[a]Area under the curve (95% CI) and its statistical significance, based on ROC analysis. Statistically significant discriminating powers are expressed in bold type (p < .05).

should be considered as preliminary predictors awaiting further confirmation.

Reliable detection of especially early stages of symptomatic DCM is a crucial point of the study. Although previously used diagnostic criteria for DCM were neither standardized nor consistent across published studies, recent and current studies have defined DCM by the presence of at least one neurological sign and at least one neurological symptom in addition to a positive MRI for compression of the cord (Amenta et al., 2014; Kalsi-Ryan, Karamidas, & Fehlings, 2013).

Definition of MRI criteria for degenerative cervical cord compression is essential for reliable and reproducible diagnosis of DCM. In general, spinal cord compression can be described based on the appearance or by measuring a ratio between the anteroposterior diameter at the compressed site and that of a noncompressed site, a ratio between the anteroposterior diameter and the transverse diameter (i.e., CR), or CSA at the region of compression (Nouri, Martin, Mikulis, & Fehlings, 2016). MRI T1/T2 signal changes, although frequently detected in DCM, are neither sensitive nor specific for degenerative cervical cord compression and are invaluable to the diagnosis of DCM (Kalsi-Ryan et al., 2013; Wilson et al., 2013). Regardless of the method

used, the objective of especially quantitative measurements is to determine the severity of spinal cord compression rather than to detect especially subtle focal compressions.

The used MRI criterion for cervical cord compression based on subjective evaluation of a spinal cord contour or shape might be considered controversial. In our previous studies on that topic (Bednarik et al., 2004, 2008), we used the presence of impingement (i.e., focal change of contour) and/or CR < 0.4 as MRI criteria for cervical cord compression. However, using these criteria might have prevented less severe circular compressions from inclusion into the study and the compression ratio from showing off its predictive value.

We addressed the issue of an optimal quantitative imaging criterion for cervical cord compression in a recent cross-sectional study of a large cohort of randomly recruited individuals (Kovalova et al., 2016). We used the same qualitative criterion (a change in spinal cord contour) as a gold standard and validated several quantitative MRI parameters for their sensitivity and specificity to discriminate between nonmyelopathic compression and no compression. An anteroposterior diameter of the cervical spinal canal of <9.9 mm was associated with the highest probability of MRI-detected nonmyelopathic cervical cord compression

TABLE 4 Predictive power of parameters to distinguish between NMDCCC subjects who developed symptomatic DCM (n = 15) and those that remained asymptomatic (n = 97) using univariate analysis

Parameter	Univariate logistic regression models		Univariate Cox proportional hazard models	
	Odds ratio (95% CI)	p	Hazard ratio (95% CI)	p
Sex (male)	1.120 (0.377; 3.329)	.839	1.102 (0.400; 3.039)	.851
Age	1.004 (0.949; 1.063)	.888	1.005 (0.952; 1.061)	.858
≤59.5	1.959 (0.624; 6.156)	.250	1.791 (0.612; 5.243)	.287
Clinical status at entry				
Asymptomatic	ref.		ref.	
Cervical pain	2.591 (0.494; 13.601)	.260	2.353 (0.000; 0.000)	.296
Radiculopathy	8.867 (1.650; 47.635)	**.011**	6.177 (0.000; 0.000)	**.024**
Gait: time (s)	1.324 (1.112; 1.576)	**.002**	1.235 (1.099; 1.388)	**<.001**
≥7.35	7.758 (2.045; 29.422)	**.003**	6.425 (1.811; 22.796)	**.004**
Gait: steps	1.359 (1.145; 1.613)	**<.001**	1.253 (1.132; 1.388)	**<.001**
≥17.5	11.175 (3.284; 38.022)	**<.001**	7.610 (2.749; 21.067)	**<.001**
Run: time (s)	1.802 (1.249; 2.601)	**.002**	1.368 (1.161; 1.613)	**<.001**
≥4.95	5.760 (1.795; 18.484)	**.003**	4.625 (1.578; 13.553)	**.005**
Run: steps	1.206 (1.017; 1.430)	**.032**	1.154 (1.010; 1.318)	**.035**
≥12.5	2.815 (0.921; 8.603)	.069	2.515 (0.912; 6.939)	.075
EMG signs of myelopathy	5.812 (1.158; 29.171)	**.032**	4.084 (1.151; 14.491)	**.029**
Abnormal MEP	9.200 (2.267; 37.341)	**.002**	6.130 (2.084; 18.030)	**.001**
Abnormal SEP	5.212 (1.556; 17.456)	**.007**	4.114 (1.462; 11.571)	**.007**
Torg–Pavlov ratio	0.084 (0.002; 3.522)	.194	0.105 (0.003; 3.356)	.203
≤0.925	2.926 (0.871; 9.827)	.082	2.623 (0.834; 8.249)	.099
Maximum compression level				
C3/4	ref.		ref.	
C4/5	1.238 (0.198; 7.741)	.819	1.177 (0.215; 6.459)	.851
C5/6	1.125 (0.216; 5.848)	.889	1.049 (0.226; 4.870)	.952
C6/7	—		—	
Type of compression				
I	ref.		ref.	
IIA	7.175 (0.844; 60.989)	.071	6.363 (0.783; 51.715)	.083
IIB	17.937 (2.041; 157.650)	**.009**	14.520 (1.784; 118.149)	**.012**
APo (mm)	0.540 (0.338; 0.864)	**.010**	0.581 (0.390; 0.865)	**.008**
≤8.4	10.250 (1.296; 81.097)	**.027**	9.251 (1.216; 70.398)	**.032**
AP (mm)	0.398 (0.190; 0.835)	**.015**	0.450 (0.238; 0.852)	**.014**
≤5.75	7.612 (2.276; 25.456)	**.001**	5.683 (2.053; 15.730)	**.001**
LL (mm)	0.974 (0.564; 1.680)	.923	0.989 (0.595; 1.645)	.967
≤15.95	—		—	
SCC (mm)	0.912 (0.723; 1.150)	.436	0.928 (0.751; 1.147)	.491
≤34.35	2.733 (0.818; 9.133)	.102	2.310 (0.789; 6.766)	.127
CSA (mm^2)	0.911 (0.859; 0.966)	**.002**	0.925 (0.882; 0.971)	**.002**
≤70.1	9.412 (2.851; 31.071)	**<.001**	7.002 (2.388; 20.529)	**<.001**
CR (0.1 increase)	0.157 (0.051; 0.481)	**.001**	0.217 (0.089; 0.529)	**.001**
≤0.40	13.050 (3.842; 44.329)	**<.001**	8.504 (3.018; 23.962)	**<.001**
T2 hyperintensity	7.583 (1.957; 29.387)	**.003**	5.105 (1.737; 15.000)	**.003**
FA MCL	0.280 (0.000; 320.502)	.723	0.369 (0.001; 254.941)	.765
≤0.5975	4.603 (0.575; 36.861)	.150	4.135 (0.543; 31.474)	.170

(Continues)

TABLE 4 (Continued)

Parameter	Univariate logistic regression models		Univariate Cox proportional hazard models	
	Odds ratio (95% CI)	p	Hazard ratio (95% CI)	p
ADC MCL	8.197 (0.348; 193.260)	.192	6.195 (0.369; 104.003)	.205
≥1.089	10.250 (1.296; 81.097)	**.027**	9.038 (1.188; 68.753)	**.033**
FA ratio	0.334 (0.015; 7.428)	.488	0.392 (0.023; 6.715)	.518
≤1.0205	6.269 (0.788; 49.874)	.083	5.657 (0.744; 43.030)	.094
ADC ratio	2.555 (0.054; 119.886)	.633	2.547 (0.077; 84.577)	.601
≥0.938	2.118 (0.707; 6.341)	.180	2.031 (0.736; 5.606)	.171

ADC, apparent diffusion coefficient; ADC ratio, ADC at MCL level/C2/3 level; AP, anteroposterior spinal cord diameter; APo, anteroposterior cervical canal diameter; CR, compression ratio; CSA, cross-sectional spinal cord area; DCM, degenerative cervical myelopathy; EMG, electromyography; FA, fractional anisotropy, FA ratio, FA at MCL level/C2/3 level; LL, laterolateral spinal cord diameter; MCL, maximum compression level; MEP, motor-evoked potentials; NMDCCC, nonmyelopathic degenerative cervical cord compression; SCC, spinal cord circumference; SEP, somatosensory-evoked potentials.
All continuous parameters were also coded as binary predictors on the basis of cut-off points defined in ROC analysis. Statistically significant predictive powers are expressed in bold type ($p < .05$).

TABLE 5 Predictive power of parameters to distinguish between NMDCC subjects who developed symptomatic DCM ($n = 15$) and those that remained asymptomatic ($n = 97$): multivariate model based on step-wise analysis of data

Parameter	Multivariate-adjusted logistic regression models	
	Odds ratio (95% CI)	p
Radiculopathy	5.208 (1.288; 21.057)	**.021**
CR ≤ 4.0	5.613 (1.451; 21.708)	**.012**
CSA (mm^2) ≤ 70.1	6.176 (1.608; 23.719)	**.008**

CR, compression ratio; CSA, cross-sectional spinal cord area; EMG, electromyography; NMDCCC, nonmyelopathic degenerative cervical cord compression. Significant independent predictors are expressed in bold type.

in comparison with CR or CSA, which represent more severe circular compressions and are, on the contrary, more valuable in discrimination between nonmyelopathic compression and symptomatic DCM (Kovalova et al., 2016). We, thus, believe that the use of subjective evaluation of a change in the spinal cord contour or shape compared to that of the neighboring segment and based on agreement of two neuro-radiologist is a legitimate criterion for definition of MRI signs of degenerative cervical cord compression in this study. Quantitative MRI parameters—CR and CSA—proved that especially more severe compressions increase the risk for development of symptomatic DCM and established cut-offs might be used for stratification of a practical management of NMDCCC cases in addition to already known risk factors.

In NMDCCC cases with already detected MRI signs of cervical cord compression, progression into symptomatic myelopathy is based on clinical presentation. Symptoms, especially gait disturbance and loss of sensation, are the most commonly identified presenting symptoms (Kalsi-Ryan et al., 2013), and our findings are similar. Myelopathic signs, although necessary for confirmation of myelopathic origin of otherwise unspecific symptoms, such as gait disturbance, are usually a hallmark of more advanced stage of myelopathy. Assessment tools to better define and document impairment and function quantitatively will be useful in identifying the actual clinical presentation and the impact on independence for these individuals (Kalsi-Ryan et al., 2013). Quantified walk and run are definitely among those assessment tools. Gait or run impairment, however, can have quite a broad range of clinical presentations. We used quantified gait and run not for definition of symptomatic DCM, but as another possible predictor for progression of the disease. Prolonged gait or run proved to be able to discriminate/predict those patients with higher risk of developing symptomatic myelopathy. Lower statistical power of our study due to low number of outcome events in relation to the high number of potential predictors might be the reason why these functional tests, as well as some other predictors, did not prove to be an independent predictors using multivariate analysis. They are, however, promising and worthy further evaluation.

The degenerative compression is certainly a continuum with increased severity of compression and concomitant dysfunction/impairment of spinal cord. As it is not possible to differentiate reliably between symptomatic and nonmyelopathic cervical cord compression cases exclusively on clinical grounds, this limitation could lead to some confusion in terminology. One might speculate whether patients with MRI signs of cervical cord compression and abnormal conduction across spinal cord tracts proved by SEPs or MEP, those with MRI intramedullar signal changes, or those with prolonged time on quantified walk are really nonmyelopathic. Nevertheless, the current concept of symptomatic DCM is based on the presence of clear clinical symptoms and signs, and those "abnormal" or "subclinical" parameters increasing the risk for development of symptomatic myelopathy might define a subgroup of degenerative compressions that might be labeled as high-risk NMDCCC or "presymptomatic myelopathy."

In conclusion, previously and recently identified predictors of DCM development in NMDCCC individuals could help the decision-making process for preventive surgical decompression and, more importantly, in defining a subgroup of NMDCCC individuals at higher risk of DCM, among whom a randomized trial evaluating the benefit of such decompression would be justifiable.

ACKNOWLEDGMENT

CONFLICT OF INTEREST

The authors declare no conflict of interest.

REFERENCES

Amenta, P. S., Ghobrial, G. M., Krespan, K., Nguyen, P., Ali, M., & Harrop, J. S. (2014). Cervical spondylotic myelopathy in the young adult: A review of the literature and clinical diagnostic criteria in an uncommon demographic. *Clinical Neurology and Neurosurgery*, *120*, 68–72.

Arima, H., Sakamoto, S., Naito, K., Yamagata, T., Uda, T., Ohata, K., & Takami, T. (2015). Prediction of the efficacy of surgical intervention in patients with cervical myelopathy by using diffusion tensor 3T-magnetic resonance imaging parameters. *Journal of Craniovertebral Junction & Spin*, *6*, 120–124.

Bednarik, J., Kadanka, Z., Dusek, L. I., Novotny, O., Surelova, D., Urbanek, I., & Prokes, B. (2004). Pre-symptomatic spondylotic cervical cord compression. *Spine*, *29*, 2260–2269.

Bednarik, J., Kadanka, Z., Dusek, L., Kerkovsky, M., Vohanka, S., Novotny, O., … Kratochvilova, D. (2008). Presymptomatic spondylotic cervical myelopathy – An updated predictive model. *European Spine Journal*, *17*(3), 421–431.

Bednařík, J., Kadaňka, Z., Voháňka, S., Kerkovsky, M., Vohanka, S., Novotny, O., … Kratochvilova, D. (1998). The value of somatosensory and motor evoked potentials in pre-clinical spondylotic cervical cord compression. *European Spine Journal*, *7*, 493–500.

Boden, S. D., McCowin, P. R., Davis, D. O., Dina, T. S., Mark, A. S., & Wiesel, S. (1990). Abnormal magnetic-resonance scans of the cervical spine in asymptomatic subjects. *Journal of Bone and Joint Surgery. American Volume*, *72*, 1178–1184.

Chen, X., Kong, C., Feng, S., Guan, H., Yu, Z., Cui, L., & Wang, Y. (2016). Magnetic resonance diffusion tensor imaging of cervical spinal cord and lumbosacral enlargement in patients with cervical spondylotic myelopathy. *Journal of Magnetic Resonance Imaging*, *43*(6), 1484–1491.

Guan, X., Fan, G., Wu, X., Gu, G., Gu, X., Zhang, H., & He, S. (2015). Diffusion tensor imaging studies of cervical spondylotic myelopathy: A systemic review and meta-analysis. *PLoS ONE*, *10*(2), e0117707. https://doi.org/10.1371/journal.pone.0117707

Kalsi-Ryan, S., Karamidas, S. K., & Fehlings, M. G. (2013). Cervical spondylotic myelopathy: The clinical phenomenon and the current pathobiolog of an increasingly prevalent and devastating disorder. *Neuroscientist*, *19*(4), 409–421.

Karpova, A., Arun, R., Davis, A. M., Kulkarni, A. V., Mikulis, D. J., Sooyong, C., … Fehlings, M. G. (2013). Reliability of quantitative magnetic resonance imaging methods in the assessment of spinal canal stenosis and cord compression in cervical myelopathy. *Spine*, *38*(3), 245–252.

Kerkovsky, M., Bednarik, J., Dusek, L., Sprláková-Puková, A., Urbánek, I., Mechl, M., … Kadanka, Z. (2012). Magnetic resonance diffusion tensor imaging in patients with cervical spondylotic spinal cord compression: Correlations between clinical and electrophysiological findings. *Spine*, *37*(1), 48–56.

Kovalová, I., Bednařík, J., Keřkovský, M., Adamová, B., & Kadaňka, Z. (2015). Asymptomatic spondylotic cervical cord compression. *Ceska a Slovenska Neurologie a Neurochirurgie*, *78*(1), 24–33.

Kovalova, I., Kerkovsky, M., Kadanka, Z., Kadanka, Z. Jr., Nemec, M., Jurova, B., … Bednarik, J. (2016). Prevalence and imaging characteristics of asymptomatic and symptomatic spondylotic cervical spinal cord compression. *Spine*, *41*(24), 1908–1916.

Lee, S., Lee, Y. H., Chung, T. S., Jeong, E. K., Kim, S., Yoo, Y. H., … Park, J. H. (2015). Accuracy of diffusion tensor imaging for diagnosing cervical spondylotic myelopathy in patients showing spinal cord compression. *Korean Journal of Radiology*, *16*(6), 1303–1312.

Matsumoto, M., Fujimura, Y., Suzuki, N., Nishi, Y., Nakamura, M., Yabe, Y., & Shiga, H. (1998). MRI and cervical intervertebral discs in asymptomatic subjects. *Journal of Bone and Joint Surgery. British Volume*, *80*, 19–24.

Nouri, A., Martin, A. R., Mikulis, D., & Fehlings, M. G. (2016). Magnetic resonance imaging assessment of degenerative cervical myelopathy: A review of structural changes and measurement techniques. *Neurosurgical Focus*, *40*(6), E5.

Nouri, A., Tetreault, L., Singh, A., Karadimas, S. K., & Fehlings, M. G. (2015). Degenerative cervical myelopathy: Epidemiology, genetics, and pathogenesis. *Spine*, *40*, E675–E693.

Rajasekaran, S., Yerramshetty, J. S., Chittode, V. S., Kanna, R. M., Balamurali, G., & Shetty, A. P. (2014). The assessment of neuronal status in normal and cervical spondylotic myelopathy using diffusion tensor imaging. *Spine*, *39*, 1183–1189.

Suetomi, Y., Kanchiku, T., Nishijima, S., Imajo, Y., Suzuki, H., Yoshida, Y., … Taguchi, T. (2016). Application of diffusion tensor imaging for the diagnosis of segmental level of dysfunction in cervical spondylotic myelopathy. *Spinal Cord*, *54*(5), 390–395.

Teresi, L. M., Lufkin, R. B., Reicher, M. A., Moffit, B. J., Vinuela, F. V., Wilson, G. M., … Hanafee, W. N. (1987). Asymptomatic degenerative disc disease and spondylosis of the cervical spine: MR imaging. *Radiology*, *164*, 83–88.

Tetreault, L. A., Karpova, A., & Fehlings, M. G. (2015). Predictors of outcome in patients with degenerative cervical spondylotic myelopathy undergoing surgical treatment: Results of a systematic review. *European Spine Journal*, *24*(Suppl 2), 236–251.

Tetreault, L. A., Nouri, A., Singh, A., Fawcett, M., & Fehlings, M. G.. (2014). Predictors of outcome in patients with cervical spondylotic myelopathy undergoing surgical treatment: A survey of members from AOSpine International. *World Neurosurgery*, *81*, 623–633.

Wilson, J. R., Barry, S., Fischer, D. J., Skelly, A. C., Arnold, P. M., Riew, K. D., … Fehlings, M. G. (2013). Frequency, timing, and predictors of neurological dysfunction in the nonmyelopathic patient with cervical spinal cord compression, canal stenosis, and/or ossification of the posterior longitudinal ligament. *Spine*, *38*, S37–S53.

Spinal Cord MR Diffusion Properties in Patients with Degenerative Cervical Cord Compression

Miloš Keřkovský, Josef Bednařík, Barbora Jurová, Ladislav Dušek, Zdeněk Kadaňka, Zdeněk Kadaňka Jr, Martin Němec, Ivana Kovaľová, Andrea Šprláková-Puková, Marek Mechl

From the Department of Radiology (MK, BJ, AŠ-P, MM), University Hospital Brno, Czech Republic; Faculty of Medicine (MK, AŠ-P, MM), Masaryk University, Brno, Czech Republic; Department of Neurology, University Hospital Brno, Czech Republic (JB, ZK, ZKJ, MN, IK); Applied Neurosciences Research Group, Central European Institute of Technology, Masaryk University, Brno, Czech Republic (JB, IK); and Institute of Biostatistics and Analyses, Masaryk University Brno, Czech Republic (LD).

ABSTRACT

BACKGROUND AND PURPOSE: Diffusion tensor imaging (DTI) has previously been used as a biomarker of myelopathy in patients with degenerative cervical cord compression (DCCC). However, many factors may affect the diffusion properties of the spinal cord. This prospective study seeks to identify sources of variability in spinal cord DTI parameters in both DCCC patients and healthy subjects.

METHODS: The study group included 130 patients with DCCC confirmed by magnetic resonance imaging and 71 control subjects without signs of DCCC. DTI data of the cervical spine were acquired in all subjects. Fractional anisotropy (FA) and apparent diffusion coefficient (ADC) values were measured at different levels of the spinal cord (SCLs). Statistical data analysis was then used to determine diffusion parameters in terms of age, sex, SCL, and spinal cord compression.

RESULTS: Significant variations in FA and ADC values emerged when several spinal cord levels were mutually compared in the control group. FA values correlated significantly with age in the DCCC group and sex had a significant influence on ADC values in both groups. The two diffusion parameters in the DCCC group differed significantly between patients with clinical signs of mild-to-moderate myelopathy compared with asymptomatic patients, and correlated with measurements of spinal canal morphology.

CONCLUSIONS: Diffusion parameters of the cervical spinal cord were thus shown to respond significantly to spinal cord compression, but were subject to interaction with several other factors including sex, age, and SCL. These findings may be important to the interpretation of DTI measurements in individual patients.

Introduction

Diffusion tensor imaging (DTI) has recently emerged as a sensitive marker of structural abnormalities of the brain and spinal cord, enabled by measurements of the scalar parameters that characterize the diffusion properties of tissue.[1] The prospects for its application to degenerative cervical myelopathy (DCM) appear promising, since asymptomatic spinal cord compression is frequent,[2] and in some patients, it appears difficult to link the clinical manifestation with the finding of cervical cord compression. Thus, a reliable diagnostic tool capable of sensitive detection and quantification of the spinal cord structural abnormality is desirable.

Several authors have described significant changes in DTI parameters in patients with degenerative cervical cord compression (DCCC).[3–5] However, certain recent reports indicate an apparent physiological variability in scalar diffusion parameters between cervical spinal cord levels (SCLs)[6,7] and these parameters may also correlate significantly with age.[8] It has become relevant to investigate the extent to which DTI parameters may relate to such physiological variables and to establish the real contribution of spinal cord compression in patients with DCCC, because it may be important for evaluation of cervical cord abnormalities by means of DTI analysis in patients suspected of having DCM. The main purpose of this prospective study is therefore to evaluate the influences of age, sex, level within the spinal cord (SCL), and the presence of spinal cord compression, together with clinically manifest myelopathy, on the diffusion characteristics of the cervical spinal cord in a group of patients with DCCC. Furthermore, analysis of DTI data in a group of controls without signs of spinal cord compression provides normative data and enables study of physiological variability in diffusion parameters.

Materials and methods
Subjects

DCCC group

The group consisted of 130 prospectively examined patients (77 men, 53 women, and mean age 62 years) with various clinical signs of cervical spine degenerative disease (cervical

Table 1. Demographic Features of the Study Subjects

		N	Mean Age	SD	Range
DCCC group	Total	130	62.2	9.5	39-82
	Male	77	63.3	8.9	39-82
	Female	53	60.6	10.2	40-78
Control group	Total	71	62.6	10.4	43-87
	Male	31	62.4	12.0	43-87
	Female	40	62.7	9.2	44-83

N = number of subjects; SD = standard deviation; DCCC = degenerative cervical cord compression.

pain, radiculopathy, or myelopathy). Detailed demographic data of the study group appear in Table 1. The inclusion criterion was the finding of spinal cord compression arising out of intervertebral disc herniation and/or osteophytes confirmed by magnetic resonance imaging (MRI). Spinal cord compression was defined as a change of spinal cord contour visible on axial and sagittal MRI scans at the level of the intervertebral disc. The MRI of every subject was evaluated by two radiologists who agreed on the assessment of the compression in the majority of cases. In debatable cases, the final decision was based on group discussion. Signs of DCM were sought by standardized clinical examination in all subjects in the DCCC group and 37 patients with symptoms and signs of DCM (20 men, 17 women, mean age 59 years) were identified, with decreased modified Japanese Orthopaedic Association scale (mJOA)[9] of <18 (mean score 15, SD 1.7, range 12–17)–the DCM subgroup. The remaining 93 individuals (57 men, 36 women, mean age 63 years) formed the asymptomatic DCCC (ADCCC) subgroup. Clinical signs of radiculopathy were observed in 4 patients (3 from the DCM subgroup and 1 from the ADCCC subgroup). Patients with other confirmed or suspected neurological disease that might mimic DCM were not included in the study.

Control group

The control group consisted of 71 subjects (31 men, 40 women, mean age 63 years) without cervical spinal cord compression and with no history of significant neurological disorder. They were recruited from a prospectively examined cohort of volunteers, selecting only those who were free of MRI signs of DCCC according to the criteria described above. For more information about the demographic features of the subjects, see Table 1.

Informed consent was obtained from all patients and volunteers and the study was approved by the institutional ethics board.

MRI Examination and Image Analysis

All subjects enrolled into the study underwent MRI examination of the cervical spine on a 1.5 T MR device with a 16-channel head and neck coil (Philips Achieva, Best, the Netherlands). The standardized imaging protocol included conventional pulse sequences in sagittal (T1-weighted, T2-weighted, and short tau inversion recovery (STIR) images) and axial planes (T2-weighted gradient-echo) for the purpose of morphological evaluation and a DTI sequence in the axial plane giving comprehensive coverage of spinal cord segments C2/3-C6/7 (Figs 1 and 2). The DTI scans were acquired with a slice thickness of 4 mm, with the same geometry settings as those employed for the axial

T2 images. Single-shot echo planar imaging was used for the DTI sequence (TR 3549 ms, TE 83 ms, flip angle 25°, in-plane resolution 1.25×1.25 mm), applying 15 directions of diffusion-sensitizing gradient with 900 s/mm^2 as the value of *b*-factor.

In the DCCC group, morphological parameters measured on axial T2 scans included anteroposterior (AP) spinal canal diameter, spinal cord cross-sectional area and compression ratio (AP divided by laterolateral diameter of the spinal canal), using Impax software (release 6.6.0.145, Agfa HealthCare, Mortsel, Belgium). These measurements were taken at the level of maximum spinal cord compression (MCL), which was identified by maximum reduction of AP spinal canal diameter in comparison with other segments. In patients with multisegmental involvement and a similar degree of spinal canal stenosis, the level with the smallest spinal cord area was chosen.

A diffusion registration tool (Philips Medical Systems, Best, the Netherlands) was employed to remove misalignments and distortions arising out of head motion and eddy currents. FiberTrak application, Extended MR WorkSpace (release 2.6.3.5, Philips Medical Systems) was used for DTI data analysis. The diffusion data were processed and fractional anisotropy (FA) and apparent diffusion coefficient (ADC) values calculated. Measurements were subjected to region-of-interest (ROI) analysis by placing the ROIs at the level of intervertebral disks over the entire spinal cord area depicted on the axial images of isotropic diffusion. Special care was taken to avoid the surrounding cerebrospinal fluid and data contamination by susceptible artifacts, by avoiding the borderline zone at the margins of the spinal cord cross sections, and abnormal signal intensities from susceptible artifacts at the spinal cord margins, if visible on the isotropic diffusion images. Mean FA and ADC values of the spinal cord cross sections were recorded at MCL in the DCCC group and at all cervical levels (C2/3 to C6/7) in the control group. Interobserver variability of FA and ADC values had already been tested in a previous study of ours, where the same technique of DTI data analysis had been used; the reproducibility of all parameters tested proved acceptable.[3]

Data Analysis

DCCC group. Subjects from the DCCC group were classified into subgroups according to level of maximum spinal cord compression. Comparisons were made up of FA values between different SCLs, and the same done for ADC. The statistical significance of differences in paired measurements between SCLs was assessed by repeated application of the ANOVA model. ADC and FA values were compared between subgroups defined by sex, presence, or absence of T2 hyperintensity and clinical manifestation of myelopathy using the *t*-test for independent samples. Both diffusion parameters were correlated with age and morphological measurement by means of Pearson correlation coefficient. ADC and FA values at individual SCLs were also mutually compared between the control group and DCCC group using Mann-Whitney U test.

The repeated-measures ANOVA model was applied to identify and quantify sources of interindividual variability in ADC and FA values; particular factors (age, sex, SCL, morphological parameters, presence of myelopathy, and spinal cord T2 hyperintensity) were assessed using the relative sum of squares related to the total experimental sum of the square.
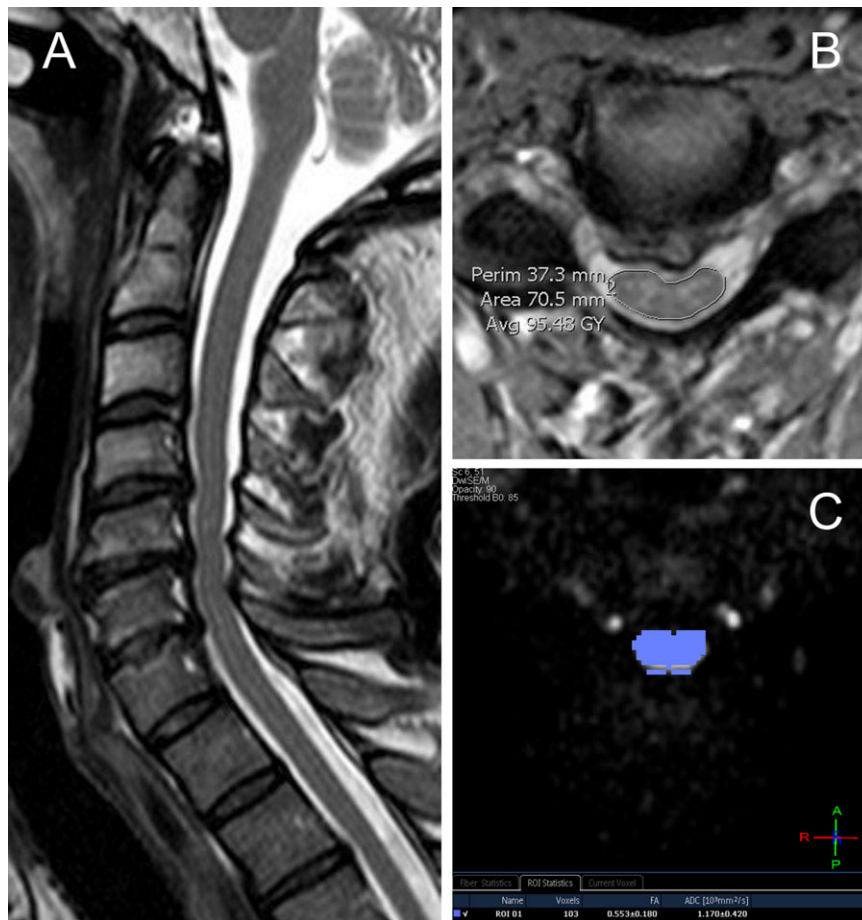
Fig 1. Conventional and DTI MR examination of a patient with multisegmental narrowing of the spinal canal. (A) T2-weighted image in sagittal plane. (B) T2-weighted image in axial plane at C4/5 level depicting spinal cord impingement by intervertebral disk herniation; an example of spinal cord area measurement is also shown. (C) Isotropic diffusion-weighted image at the same level calculated from multidirectional diffusion data in FiberTrak application, diffusion parameters measured within the region-of-interest placed over the spinal cord cross section.

Control group. ADC and FA values were compared between different SCLs using the repeated measures ANOVA model and the Tukey HSD post hoc test. Both diffusion parameters were compared between males and females using the *t*-test for independent samples and correlated with age by means of Pearson correlation coefficient.

The repeated-measures ANOVA model was applied to identify and quantify sources of interindividual variability in ADC and FA values; age, sex, SCL, and their mutual interactions were evaluated using the relative sum of squares related to the total experimental sum of the square.

Finally, post hoc analysis was performed to disclose potential relations between spinal cord area, sex, and ADC values. Thus, the spinal cord area was compared between males and females at individual SCLs using Mann-Whitney U test and the interactions of spinal cord area and sex with ADC values were addressed by univariate and multivariate linear regression models.

The statistical analyses were performed with SPSS 22 (IBM Corporation, Armonk, New York, United States 2014) and Statistica 12 (Statsoft Inc., Tulsa, OK, USA 2014)

Results
Control Group

A summary of morphological parameters measured at different SCLs appears in Table 2. Significant differences of FA and ADC values were found between SCLs, with a decrease of FA values from C2/3 level to C6/7 level. The ADC values decreased from level C2/3 to C5/6, while at C6/7, they were comparatively higher. ADC values differed significantly between men and women in most of the SCLs (except C2/3 level), with higher values in women (Table 3); the FA values were not significantly different (data not shown). Neither ADC nor FA values correlated significantly with age.

The interindividual variability in ANOVA analysis was relatively high and only partially explained by the factors investigated. The most important predictor was SCL, which emerged as by far the strongest source of variability of FA values, less conspicuously of ADC values. Sex contributed significantly to ADC values (Table 4).

The spinal cord area was significantly lower in women compared to men at most SCLs (Table 5). Sex of subject emerged as a significant predictor of ADC values independent of spinal cord area according to multivariate regression analysis at SCLs C4/5, C6/7, and C6/7 (Table 6). Significant interactions between sex and ADC also appeared in the univariate regression model at the above-mentioned SCLs; however, interactions with spinal cord area were not significant (data not shown). Both spinal cord area and sex significantly predicted ADC values at C3/4 level according to the univariate regression model ($P = .033$ and .018, respectively), but these interactions in the

Fig 2. Example of MR examination of a cervical spine in a subject without spinal cord compression and in a patient with present spinal cord compression. (A)-(F) Subject without spinal cord compression. (G)-(L) Patient with present spinal cord compression. (A,G) T2-weighted images in sagittal plane. (B)-(F) and (H)-(L) T2-weighted gradient echo images in axial plane at spinal cord levels C2/3 to C6/7, respectively. Mild disk protrusions can be seen in a control subject at the levels C5/6 and C6/7 without any signs of cord compression. Conversely, severe degenerative changes are present in a patient with flat spinal cord compression at the level of maximal spinal canal stenosis C4/5 (J).

multivariate model were not significant. No significant interactions between spinal cord area, sex, and ADC values were found at C2/3 level.

DCCC Group

Maximum spinal cord compression appeared most often at C5/6 level (67 subjects, 51.5%). Maximum spinal cord compression did not occur at C2/3 level in any of the subjects. Mean AP spinal canal diameter measured for all patients with spinal cord compression at all MCLs was 8 mm (SD 1.7 mm), spinal cord area 74 mm^2 (SD 14.3 mm^2), and compression ratio .45 (SD .081). The morphological measurements at individual SCLs appear in Table 2.

Analysis of DTI parameters revealed a statistically significant decrease in FA values and an increase in ADC values in the DCM subgroup compared with the ADCCC subgroup. Significant differences were also found in comparison of FA and ADC values in the subgroup of patients with T2 hyperintensity (mean values .45 and 1.33, respectively) compared with those with normal spinal cord T2 signal (.54 and 1.15, respectively). FA values correlated significantly with age according to analysis of continuous predictors ($r = -.227$, $P = .009$). ADC values were significantly lower in men compared to women, although differences in FA values were not significant here. Details of DTI parameters and comparisons between selected subgroups appear in Tables 7A and 7B.

Table 2. Morphological Measurements of the Spinal Canal and Spinal Cord in Control Group and DCCC Group

Group	SCL	N	AP (mm)	CR	CSA (mm²)
Control group	C2/3	71	13.1 (1.4)	.67 (.07)	85.4 (9.1)
	C3/4	71	12.3 (1.2)	.59 (.06)	88.5 (9.1)
	C4/5	71	11.8 (1.8)	.54 (.05)	90.1 (9.4)
	C5/6	71	11.6 (1.5)	.54 (.05)	87.3 (10.1)
	C6/7	71	12.2 (2.1)	.59 (.07)	83.0 (12.3)
DCCC group	C3/4	16	8.3 (1.3)	.46 (.08)	73.3 (11.9)
	C4/5	35	8.4 (2.0)	.43 (.09)	75.8 (15.2)
	C5/6	67	8.3 (1.8)	.44 (.08)	74.7 (15.0)
	C6/7	12	8.5 (.7)	.5 (.04)	70.1 (9.7)

The values of measurements are given as mean and standard deviation. SCL = spinal cord level; N = number of subjects; AP = anteroposterior diameter of the spinal canal; CR = compression ratio; CSA = cross-sectional area of the spinal cord; DCCC = degenerative cervical cord compression.

When all MCLs were analyzed altogether, significant positive correlations of FA values were found in all the morphological parameters measured (AP canal diameter, spinal cord area, and compression ratio). Such correlations were also found separately at C3/4 level and FA correlated positively with AP canal diameter at C4/5 level. For ADC values, there was a significant negative correlation with AP canal diameter and spinal cord area in overall analysis of all MCLs. Analysis at individual SCLs revealed significant negative correlations of ADC values with

Table 3. FA and ADC According to Age, Sex, and Spinal Cord Level in Control Group

Group[1]	N	FA C2/3	FA C3/4	FA C4/5	FA C5/6	FA C6/7	P[2]
Total	71	0.58 (.57; .60)[a]	0.59 (.57; .60)[a]	0.56 (.55; .57)[b]	0.54 (.53; .56)[b]	0.51 (.50; .53)[c]	<.001

Group[1]	N	ADC C2/3	ADC C3/4	ADC C4/5	ADC C5/6	ADC C6/7	P[2]
Total	71	1.29 (1.25; 1.33)[a]	1.24 (1.21; 1.28)[ab]	1.23 (1.20; .26)[b]	1.17 (1.13; 1.21)[c]	1.24 (1.19; 1.29)[ab]	<.001
female	40	1.31 (1.25; 1.36)[a]	1.28 (1.23; 33)[ab]	1.28 (1.24; .32)[ab]	1.21 (1.16; 1.27)[b]	1.3 (1.23; 1.36)[ab]	0.035
Sex male	31	1.27 (1.20; 1.34)[a]	1.19 (1.15; 1.24)[ab]	1.17 (1.13; 1.21)[bc]	1.1 (1.05; 1.15)[c]	1.17 (1.11; 1.23)[bc]	<.001
P[3]		0.44	0.018	<.001	0.005	0.011	

[1]Mean and 95% confidence interval. N = number of subjects; FA = fractional anisotropy; ADC = apparent diffusion coefficient; P = statistical significance. [2]Repeated measures ANOVA. [3]t-test for two independent samples. [a, b, c, d]mark statistical significance of differences within rows–categories marked with the same letter are not mutually significantly different (tested by Tukey HSD post hoc test; P < .05).

Table 4. Sources of FA and ADC Variability in the Control Group

Model parameters[a]	FA Explained variance (%)	P	ADC Explained variance (%)	P
Sex	.03%	.796	6.21%	.004
Age	.07%	.712	.14%	.646
Sex × Age	.00%	.960	.65%	.332
SCL	17.03%	<.001	5.06%	<.001
SCL × Sex	.81%	.321	.53%	.457
SCL × Age	1.26%	.124	.99%	.153
SCL × Sex × Age	.75%	.367	1.84%	.015
Interindividual variability (error)	80.05%		84.58%	

[a]Based on repeated measures ANOVA. SCL = spinal cord level; FA = fractional anisotropy; ADC = apparent diffusion coefficient; P = statistical significance.

Table 5. Comparison of Cross-Sectional Area of the Spinal Cord Values between Men and Women in Control Group

Spinal Cord Level	Men (N = 31) CSA Mean ± SD (mm²)	Women (N = 40) CSA Mean ± SD (mm²)	P
C2/3	88.7 ± 8.6	82.9 ± 8.7	.015
C3/4	92.1 ± 8.8	85.7 ± 8.4	.009
C4/5	94.2 ± 9.3	86.9 ± 8.2	.002
C5/6	90.9 ± 10.5	84.5 ± 9.0	.007
C6/7	86.1 ± 12.5	80.5 ± 11.7	.083

Statistical significance (P) was tested by Mann-Whitney U test. CSA = cross-sectional area of the spinal cord.

spinal cord area at C3/4 and C4/5 levels. No significant correlations of morphological parameters with either FA or ADC values were found at C5/6 and C6/7 levels.

There were no significant differences in ADC and FA between MCLs (Tables 7A and 7B), but SCL explained some of the variability of ADC in ANOVA analysis. Other significant predictors were sex and T2 hyperintensity for ADC values and age, T2 hyperintensity, and AP spinal canal diameter for FA values (Table 8). The presence of clinical manifestation of myelopathy had a borderline significant influence on both FA and ADC values.

Comparison of the diffusion parameters between the DCCC group and the control group revealed significant decreases of FA values at C3/4 and C5/6 levels in the DCCC group compared with the control group (P = .004 and .030, respectively). At C4/5 level, the ADC values were significantly lower in the DCCC group compared to the control group (P = .041). No significant differences in diffusion parameters were found at C6/7 level.

Discussion

This study systematically analyzes the influence of several factors (age, sex, and segmental level) upon DTI parameters (ADC and FA values) of the cervical cord in patients with asymptomatic and symptomatic DCCC and a control group.

A number of studies have investigated the influence of age on cervical spinal cord diffusion parameters; their findings have, however, been somewhat variable. Mamata et al[10] report a significant positive correlation of ADC values and a negative correlation of FA with age, both measured at only the upper spinal cord in groups of patients with cervical spondylosis. A recent study by Wang et al[8] reported significant age-dependent changes in both ADC and FA values in a group of healthy volunteers by measuring those parameters selectively in spinal cord gray matter and in various white-matter funiculi. A further study found significant age-dependent FA and mean diffusivity (MD) changes using novel automatic segmentation methods.[11] Agosta et al[12] performed a study analyzing a comparatively large group of 96 healthy subjects, and reported a significant decrease of cervical cord mean FA associated with age, but nothing similar for MD values. Brandner et al,[13] in a recent study, found no correlation between DTI metrics and age.

This study reveals no significant relation between diffusion parameters and age in the control group. Contrasting and variable results elsewhere may be explained in part by differences in modes of measurement and approaches to data analysis employed in particular studies, eg, ROI analysis versus tractography-based segmentation[11] or histogram analysis.[12] Further, this study did not include subjects younger than 43 years. Thus, the findings herein do not actually contest a general dependency of spinal cord DTI parameters on age; however, it does appear that the a priori age-related modification of DTI parameters is not substantial in individuals between approximately 40 and 80 years of age. On the other hand, age was identified as the most important predictor of FA values in the DCCC group. As it may be assumed that the period of spinal cord compression is longer in elderly patients, we may hypothesize that the duration of spinal cord

Table 6. Prediction of ADC Values by Multivariate Linear Regression Model in Control Group

SCL		β (95% CI)	P	R²
C2/3	Constant	1.427 (.953; 1.902)		
	Spinal cord area (mm²)	−.002 (−.007; .004)	.508	1.5%
	Women	.025 (−.071; .121)	.606	
C3/4	Constant	1.470 (1.084; 1.856)		
	Spinal cord area (mm²)	−.003 (−.007; .001)	.153	10.6%
	Women	.067 (−.008; .143)	.079	
C4/5	Constant	1.223 (.905; 1.540)		
	Spinal cord area (mm²)	−.001 (−.004; .003)	.739	17.2%
	Women	.104 (.042; .167)	.001	
C5/6	Constant	1.244 (.867; 1.622)		
	Spinal cord area (mm²)	−.002 (−.006; .003)	.447	11.4%
	Women	.103 (.020; .187)	.016	
C6/7	Constant	1.231 (.873; 1.590)		
	Spinal cord area (mm²)	−.001 (−.005; .003)	.726	9.2%
	Women	.123 (.023; .223)	.017	

β (95% CI) = regression coefficient and 95% confidence interval; P = statistical significance; R^2 = coefficient of determination; SCL = spinal cord level; ADC = apparent diffusion coefficient.

Table 7A. FA at Maximum Compression Level According to Level of Compression and Presence of Clinically Manifest Myelopathy in the DCCC Group

Group[1]	FA Total	FA C3/4	FA C4/5	FA C5/6	FA C6/7	P[2]
Total	N = 130; .52 (.51; .53)	N = 16; .52 (.48; .56)	N = 35; .54 (.52; .57)	N = 67; .52 (.50; .54)	N = 12; .49 (.44; .53)	0.18
Myelopathy						
no	N = 93; .54 (.52; .55)	N = 12; .54 (.50; .58)	N = 27; .56 (.53; .59)	N = 45; .53 (.51; .55)	N = 9; .50 (.46; .55)	0.15
yes	N = 37; .48 (.46; .51)	N = 4; .47 (.38; .56)	N = 8; .48 (.44; .52)	N = 22; .50 (.46; .53)	N = 3; .44 (.32; .55)	0.627
P[3]	<.001	0.109	0.009	0.087	0.227	

DCCC = degenerative cervical cord compression. [1]Sample size; mean supplemented by 95% confidence interval. FA = fractional anisotropy; ADC = apparent diffusion coefficient; P = statistical significance. [2]ANOVA. [3]Independent samples t-test.

Table 7B. ADC at Maximum Compression Level According to Level of Compression, Sex, and Presence of Clinically Manifest Myelopathy in the DCCC Group

Group[1]	ADC total	ADC C3/4	ADC C4/5	ADC C5/6	ADC C6/7	P[2]
Total	N = 130; 1.18 (1.14; 1.21)	N = 16; 1.27 (1.18; 1.36)	N = 35; 1.17 (1.11; 1.22)	N = 67; 1.16 (1.11; 1.21)	N = 12; 1.18 (1.06; 1.30)	0.217
Sex						
female	N = 53; 1.24 (1.19; 1.28)	N = 2; 1.43 (1.15; 1.70)	N = 10; 1.24 (1.16; 1.33)	N = 35; 1.22 (1.17; 1.27)	N = 6; 1.27 (1.14; 1.40)	0.255
male	N = 77; 1.14 (1.09; 1.18)	N = 14; 1.25 (1.15; 1.34)	N = 25; 1.14 (1.07; 1.20)	N = 32; 1.10 (1.02; 1.17)	N = 6; 1.09 (.91; 1.27)	0.129
P[3]	0.003	0.215	0.046	0.011	0.143	
Myelopathy						
no	N = 93; 1.14 (1.10; 1.17)	N = 12; 1.23 (1.13; 1.32)	N = 27; 1.14 (1.08; 1.19)	N = 45; 1.12 (1.07; 1.17)	N = 9; 1.13 (1.00; 1.27)	0.291
yes	N = 37; 1.27 (1.21; 1.34)	N = 4; 1.40 (1.19; 1.60)	N = 8; 1.26 (1.14; 1.39)	N = 22; 1.24 (1.15; 1.33)	N = 3; 1.33 (1.16; 1.50)	0.531
P[3]	<.001	0.118	0.06	0.013	0.162	

DCCC = degenerative cervical cord compression. [1]Sample size; mean supplemented by 95% confidence interval. FA = fractional anisotropy; ADC = apparent diffusion coefficient; P = statistical significance. [2]ANOVA. [3]Independent samples t-test.

compression could be a more important determinant of FA values than the age of the subjects themselves. However, in the light of the assumption that at least a substantial proportion of compressions remain asymptomatic at onset, it was not possible to establish retrospectively the duration of spinal cord compression in our study group. Further data provided by long-term prospective studies would be required to quantify the matter accurately.

The influence of sex on DTI parameters may be assumed to parallel DTI studies of the brain; some authors indicate significant differences in FA values between men and women within certain areas of brain white matter.[14,15] Nevertheless, Takao et al[15] suggest that the differences in FA may be partly related to the fact that total brain volume is different in men and women. There are only few reports of sex-related changes in DTI parameters of the cervical spinal cord, and no significant

Table 8. Sources of FA and ADC Variability in DCCC Group

Model Parameters[1]	FA Explained		ADC Explained	
	Variance (%)	P	Variance (%)	P
SCL	4.23%	.082	5.66%	.039
Sex	1.42%	.131	10.63%	<.001
Age	9.62%	<.001	.24%	.548
Myelopathy	2.09%	.068	2.08%	.078
T2 hyperintensity	5.07%	.005	3.13%	.031
Channel diameter	3.35%	.021	.01%	.920
Spinal cord area	.24%	.532	.11%	.687
Compression ratio	.66%	.301	.00%	.959
Error	73.31%		78.15%	

DCCC = degenerative cervical cord compression. [1]Based on ANOVA model. SCL = spinal cord level; FA = fractional anisotropy; ADC = apparent diffusion coefficient; P = statistical significance.

correlations have emerged.[13,16] This study, with a comparatively large population of healthy volunteers, demonstrated no differences in FA values between males and females, but such differences in ADC values were significant in both the DCCC group and in the control group. The association of these differences with spinal cord volume may raise questions similar to those generated by Takao's brain study.[15] Papinutto et al[17] reported sex-related differences in the total cross-sectional and gray matter area at upper cervical level, while this study found lower values of total cord area at most SCLs in women compared to men. However, sex was identified as a significant predictor of ADC values at C4/5-C6/7 SCLs independent of spinal cord area, the influence of which upon ADC values was not significant here. Although the measurement of cross-sectional area is not equivalent to volumometry of the spinal cord calculated from isotropic data, a relation between spinal cord volume and diffusivity appears improbable. Interestingly, the independent influence of sex on ADC values was observed below C4/5 level, which corresponds approximately with the location of the cervical enlargement that is characterized by a greater amount of gray matter.[18] The sex-related changes of ADC may therefore arise largely out of differences in gray-matter diffusivity. Further studies using separate gray and white matter segmentations based on DTI data with higher image resolution may provide important data to support such a hypothesis.

Brain structural sex dimorphisms have been linked to hormonal differences between the sexes. Herting et al[19] reported differences in FA and MD in various regions of the brain white matter and demonstrated significant correlations between diffusion parameters and sex hormones. Menzies et al[20] found a significant decrease in MD values (not FA values) of the brain white matter in adolescent boys correlating with salivary testosterone levels. Although these conclusions may not easily be applied to the entire central nervous system, it can be assumed that sex hormones have a certain influence on spinal cord diffusivity. Our findings of significant differences in ADC without changes of FA suggest changes in the directionally independent magnitude of diffusion within the spinal cord tissue. This may be related, in part, to differences in the extracellular water content or in overall tissue density, quite apart from differences in directional structure; further studies are necessary to explain these findings in relation to the spinal cord microstructure. To the best of our knowledge, this is the first study to report sex-

related differences in diffusion parameters measured within the cervical spinal cord.

The findings of this study indicate that in the group of subjects without spinal cord compression, DTI parameters depend strongly on the level at which measurements are taken. Previously published data on this topic are not consistent; Song et al,[7] in agreement with our findings, found differences in FA values between cranial and caudal spinal cord segments, but observed no differences in ADC values. Their group of volunteers was comparatively small. Brandner et al[13] report a decrease in FA and increase in ADC in a craniocaudal direction from C2 to C7, results similar to those that appear here. Conversely, other authors have reported no significant differences in DTI parameters in a group of healthy controls.[21] The variation in diffusion properties between levels of the spinal cord may be related to differences in the anatomical structure of the cervical spine. Wheeler-Kingshott et al[18] suggested that a decline in FA values in the lower SCL may be due to the brachial plexus nerve roots entering and leaving the lower cervical spinal cord, something that leads to a degree of disruption of the directional coherence of the fibers at voxel scales. Another reason may lie in the relatively higher volume of spinal cord gray matter within the ROIs at segments of cervical enlargement,[18] since it is established that diffusion parameters within gray matter are different from those measured in white matter.[8,16]

Technical considerations and variable image quality of the diffusion data may also be responsible for SCL-dependent differences. Vedentam et al[16] have demonstrated a decrease in the signal-to-noise ratio (SNR) in the lower spinal cord segments (C4-Th1) compared with the upper segments (C1-3). It is known that low SNR may lead to overestimation of FA values at b-factors approaching 1,000 s/mm[2,22,23] so signal quality may influence DTI metrics. Although this alone does not explain the decrease of FA in a craniocaudal direction, some influence of SNR variation on measurements is possible. Further experimental studies, using multiple acquisitions with different acquisition settings and SNR, would be required to evaluate reliably the influence of SNR, and other technical aspects, on diffusion measurements.

Spinal cord compression in patients with cervical spondylosis is important to any determination of DTI parameters. This study disclosed significant differences in both FA and ADC values between patients with clinical findings of symptomatic myelopathy compared with ADCCC patients. These findings are in agreement with existing reports[6,24] and with our own previously published data.[3] Some authors stress the role of DTI as a more sensitive biomarker of myelopathy than conventional T2-weighted images.[3,25] From this perspective, it is not surprising that the finding of spinal cord T2 hyperintensity had a significant influence on both FA and ADC values.

According to the findings herein, the reactivity of diffusion parameters to spinal cord compression is greater at the upper cervical levels (C3/4 and C4/5), as FA and ADC values measured at these segments correlated well with the degree of spinal canal stenosis, in contrast to segments C5/6 and C6/7. The explanation for this phenomenon is not straightforward, although it may be related to the above-described level-dependent differences in anatomical structure of the spinal cord or technical aspects, mainly differences in SNR. Nevertheless, sensitivity of DTI to clinically manifest myelopathy is preserved even at lower cervical segments, where this study found significant

changes of ADC values measured at C5/6 level. On the other hand, the general influence of myelopathy findings (mostly mild-to-moderate represented in this study group) on the diffusion parameters was comparatively low among other variables considering the influence of the particular factors investigated through variability of ADC and FA values. Thus, the potential of DTI to discriminate myelopathy at the early stage seems to be reduced by the influence of physiological or technical factors that contribute to variability of diffusion parameters.

Variations in diffusion parameters between SCLs were not significant in the DCCC group. This is probably due to the modification of the values measured near the spinal cord compression itself, and also to the varying reactivity of parameters measured at different SCLs.

Direct comparison of the two diffusion parameters between the DCCC group and the control group revealed significant differences in either ADC or FA values at several SCLs. These results are not fully consistent with the aforementioned correlation analyses of diffusion and morphological parameters within the individual groups. At C4/5 level, there was a mild but statistically significant decrease in ADC values in the DCCC group compared to the control group, which contrasts with the finding of increasing ADC values in correlation with the reduction of spinal cord area. It can be surmised that a certain degree of spinal cord compression may generally lead to mild decrease of ADC values by reduction of the extracellular compartment and increase in relative cellularity. Increasing compression of the spinal cord documented by the reduction of the spinal cord area, which would cause structural damage to the spinal cord tissue, may then be reflected in an increase of ADC values.

A limitation of this study may lie in the selection of the scalar parameters available for the quantification of diffusion within ROIs in FiberTrak software, which is limited to ADC and FA. There are other scalar parameters, eg, axial diffusivity (AD) and radial diffusivity (RD), which may be used in the investigation of diffusivity characteristics. All these parameters may be calculated from the eigenvectors that represent the magnitude of the three main axes of the ellipsoid characterizing diffusion anisotropy.[26] Some studies use MD instead of ADC for the quantification of total diffusivity; however, both of these parameters represent measures of total direction-independent diffusivity.[24]

ADC and FA are the most commonly employed parameters in studies using DTI in CSM research.[24] This study therefore centered around them, with consequent effects upon the extent of the study and its main objective, which was to discriminate those factors that might have some general influence upon the diffusivity of the spinal cord in terms of DCCC. More specific analysis of other parameters may provide additional information, as it is known that AD and RD may be helpful in differentiation between axonal injury and demyelination.[27] AD, RD, and particular eigenvalues of the ellipsoid have been evaluated by only a few studies of patients with CSM.[5,28,29] Changes in their values were more or less followed by changes in ADC or FA values. Rajasekaran et al[5] have recorded a significant increase of all three eigenvalues in a myelopathy group compared to healthy volunteers, together with an increase in ADC and a decrease in FA. Other authors report increases in AD, RD, and FA in CSM patients, but they point out that regional differences between spinal cord tracts exist; while AD and RD

changed in similar fashion in all spinal columns, a decrease in FA was more pronounced in the lateral and dorsal columns.[28,29] Rajasekaran et al[5] considered the FA pattern of the myelopathic cord more compatible with histopathological features appearing in previously published studies than AD and RD. Thus, the evaluation of AD and RD in terms of CSM currently seems to play comparatively minor role.

It should be noted that the analyses indicating level-specific results in the DCCC group may have been influenced by the different numbers of subjects in the subgroups, which were classified according to MCL, thus modifying the power of the statistical analyses. Another possible source of bias may lie in the selection of MCL. Li et al[30] correlated DTI measurements with detailed neurological examination in patients with multilevel DCM and found the capacity of DTI to identify the level of spinal cord pathology higher than that of conventional morphological measurements. As dynamic factors may play an important role in this matter,[31] it may be assumed that diffusivity changes might correlate better with clinical presentation at other SCLs than at MCL identified at rest position if the spinal cord is compressed and damaged, eg, by a shear mechanism at these levels more markedly than at MCL. Thus, further investigation combining DTI with dynamic studies may prove productive.

To conclude, DTI is a valuable tool for the evaluation of structural abnormalities of the cervical spinal cord caused by the degenerative compression, correlating with clinical manifestation of myelopathy and with degree of spinal canal stenosis. However, it appears that the diffusion properties of the cervical spinal cord are dictated by the interaction of several other factors beyond the cord compression itself, mainly sex of the patient and segmental level of measurement. These may not have a substantial effect on the results of various group studies, if males and females and various stenotic levels are represented proportionally throughout the study groups, but may be highly important for evaluation of the diffusion parameters in individual patients with DCCC in clinical settings. Such interpretations require robust, normative data reflecting the aforementioned variables.

References

1. Harsan LA, Poulet P, Guignard B, et al. Brain dysmyelination and recovery assessment by noninvasive in vivo diffusion tensor magnetic resonance imaging. J Neurosci Res 2006;83:392-402.
2. Teresi LM, Lufkin RB, Reicher MA, et al. Asymptomatic degenerative disk disease and spondylosis of the cervical spine: MR imaging. Radiology 1987;164:83-8.
3. Keřkovský M, Bednařík J, Dušek L, et al. Magnetic resonance diffusion tensor imaging in patients with cervical spondylotic spinal cord compression: correlations between clinical and electrophysiological findings. Spine (Phila Pa 1976) 2012;37:48-56.
4. Banaszek A, Bladowska J, Szewczyk P, et al. Usefulness of diffusion tensor MR imaging in the assessment of intramedullary changes of the cervical spinal cord in different stages of degenerative spine disease. Eur Spine J 2014;23:1523-30.
5. Rajasekaran S, Yerramshetty JS, Chittode VS, et al. The assessment of neuronal status in normal and cervical spondylotic myelopathy using diffusion tensor imaging. Spine (Phila Pa 1976) 2014;39:1183-9.
6. Uda T, Takami T, Tsuyuguchi N, et al. Assessment of cervical spondylotic myelopathy using diffusion tensor magnetic resonance imaging parameter at 3.0 tesla. Spine (Phila Pa 1976) 2013;38:407-14.

7. Song T, Chen WJ, Yang B, et al. Diffusion tensor imaging in the cervical spinal cord. Eur Spine J 2011;20:422-8.

8. Wang K, Song Q, Zhang F, et al. Age-related changes of the diffusion tensor imaging parameters of the normal cervical spinal cord. Eur J Radiol 2014;83:2196-202.

9. Benzel EC, Lancon J, Kesterson L, et al. Cervical laminectomy and dentate ligament section for cervical spondylotic myelopathy. J Spinal Disord 1991;4:286-95.

10. Mamata H, Jolesz FA, Maier SE. Apparent diffusion coefficient and fractional anisotropy in spinal cord: age and cervical spondylosis-related changes. J Magn Reson Imaging 2005;22:38-43.

11. Van Hecke W, Leemans A, Sijbers J, et al. A tracking-based diffusion tensor imaging segmentation method for the detection of diffusion-related changes of the cervical spinal cord with aging. J Magn Reson Imaging 2008;27:978-91.

12. Agosta F, Laganà M, Valsasina P, et al. Evidence for cervical cord tissue disorganisation with aging by diffusion tensor MRI. Neuroimage 2007;36:728-35.

13. Brander A, Koskinen E, Luoto TM, et al. Diffusion tensor imaging of the cervical spinal cord in healthy adult population: normative values and measurement reproducibility at 3T MRI. Acta Radiol 2014;55:478-85.

14. Hsu JL, Leemans A, Bai CH, et al. Gender differences and age-related white matter changes of the human brain: a diffusion tensor imaging study. Neuroimage 2008;39:566-77.

15. Takao H, Hayashi N, Ohtomo K. Sex dimorphism in the white matter: fractional anisotropy and brain size. J Magn Reson Imaging 2014;39:917-23.

16. Vedantam A, Jirjis MB, Schmit BD, et al. Characterization and limitations of diffusion tensor imaging metrics in the cervical spinal cord in neurologically intact subjects. J Magn Reson Imaging 2013;38:861-7.

17. Papinutto N, Schlaeger R, Panara V, et al. Age, gender and normalization covariates for spinal cord gray matter and total cross-sectional areas at cervical and thoracic levels: a 2D phase sensitive inversion recovery imaging study. PLoS One 2015;10:e0118576.

18. Wheeler-Kingshott CA, Hickman SJ, Parker GJ, et al. Investigating cervical spinal cord structure using axial diffusion tensor imaging. Neuroimage 2002;16:93-102.

19. Herting MM, Maxwell EC, Irvine C, et al. The impact of sex, puberty, and hormones on white matter microstructure in adolescents. Cereb Cortex 2012;22:1979-92.

20. Menzies L, Goddings AL, Whitaker KJ, et al. The effects of puberty on white matter development in boys. Dev Cogn Neurosci 2015;11:116-28.

21. Wang W, Qin W, Hao N, et al. Diffusion tensor imaging in spinal cord compression. Acta Radiol 2012;53:921-8.

22. Jones DK, Basser PJ. "Squashing peanuts and smashing pumpkins": how noise distorts diffusion-weighted MR data. Magn Reson Med 2004;52:979-93.

23. Pierpaoli C, Basser PJ. Toward a quantitative assessment of diffusion anisotropy. Magn Reson Med 1996;36:893-906.

24. Guan X, Fan G, Wu X, et al. Diffusion tensor imaging studies of cervical spondylotic myelopathy: a systemic review and meta-analysis. PLoS One 2015;10:e0117707.

25. Demir A, Ries M, Moonen CT, et al. Diffusion-weighted MR imaging with apparent diffusion coefficient and apparent diffusion tensor maps in cervical spondylotic myelopathy. Radiology 2003;229:37-43.

26. Le Bihan D, Mangin JF, Poupon C, et al. Diffusion tensor imaging: concepts and applications. J Magn Reson Imaging 2001;13:534-46.

27. Song SK, Sun SW, Ju WK, et al. Diffusion tensor imaging detects and differentiates axon and myelin degeneration in mouse optic nerve after retinal ischemia. Neuroimage 2003;20:1714-22.

28. Wen CY, Cui JL, Mak KC, et al. Diffusion tensor imaging of somatosensory tract in cervical spondylotic myelopathy and its link with electrophysiological evaluation. Spine J 2014;14:1493-500.

29. Cui JL, Li X, Chan TY, et al. Quantitative assessment of column-specific degeneration in cervical spondylotic myelopathy based on diffusion tensor tractography. Eur Spine J 2015;24:41-7.

30. Li X, Cui JL, Mak KC, et al. Potential use of diffusion tensor imaging in level diagnosis of multilevel cervical spondylotic myelopathy. Spine (Phila Pa 1976) 2014;39:E615-22.

31. Muhle C, Metzner J, Weinert D, et al. Classification system based on kinematic MR imaging in cervical spondylitic myelopathy. AJNR Am J Neuroradiol 1998;19:1763-71.